

---

**Unusual Non-covalent Interactions in Biomolecules: A Combined  
High Resolution Laser Spectroscopy, NMR Spectroscopy and  
Benchmark Quantum Chemical Calculations**

*BY*

**VENKATESWARA RAO MUNDLAPATI  
CHEM11201204009**

**National Institute of Science Education and Research Bhubaneswar  
Jatni, Khurda, Odisha - 752050**

*A thesis submitted to the  
Board of Studies in Chemical Sciences  
In partial fulfilment of requirements  
For the degree of*

**DOCTOR OF PHILOSOPHY  
of  
HOMI BHABHA NATIONAL INSTITUTE**



**May, 2018**

---

# Homi Bhabha National Institute

## Recommendations of the Viva Voce Committee

As members of the Viva Voce Committee, we certify that we have read the dissertation prepared by Venkateswara Rao Mundlapati entitled " Unusual Non-covalent Interactions in Biomolecules: A combined High Resolution Laser Spectroscopy, NMR Spectroscopy and Benchmark Quantum Chemical Calculations " and recommend that it may be accepted as fulfilling the thesis requirement for the award of Degree of Doctor of Philosophy.

Chairman – Prof. A. Srinivasan



Date: 13.9.18

Guide / Convener – Dr. Himansu Sekhar Biswal



Date: 13/09/2018

Examiner – Prof. Elangannan Arunan



Date:

13/09/2018

Member 1 – Dr. Subhadip Ghosh



Date:

13/09/2018

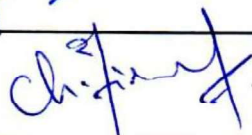
Member 2 – Dr. Arindam Ghosh



Date:

13/9/18

Member 3 – Dr. Tirumala Kumar Chowdary



Date:

13/09/2018

Final approval and acceptance of this thesis is contingent upon the candidate's submission of the final copies of the thesis to HBNI.

I hereby certify that I have read this thesis prepared under my direction and recommend that it may be accepted as fulfilling the thesis requirement.

Date: 13/09/2018

Place: NISER.

Guide 

Dr. Himansu Sekhar Biswal

---

## **STATEMENT BY AUTHOR**

This dissertation has been submitted in partial fulfilment of requirements for an advanced degree at Homi Bhabha National Institute (HBNI) and is deposited in the Library to be made available to borrowers under rules of the HBNI.

Brief quotations from this dissertation are allowable without special permission, provided that accurate acknowledgement of source is made. Requests for permission for extended quotation from or reproduction of this manuscript in whole or in part may be granted by the Competent Authority of HBNI when in his or her judgment the proposed use of the material is in the interests of scholarship. In all other instances, however, permission must be obtained from the author.

**VENKATESWARA RAO MUNDLAPATI**

---

## **DECLARATION**

I, hereby declare that the investigation presented in the thesis has been carried out by me. The work is original and has not been submitted earlier as a whole or in part for a degree / diploma at this or any other Institution / University.

**VENKATESWARA RAO MUNDLAPATI**

---

## List of Publications

### a. Published

1. <sup>§</sup>**V. Rao Mundlapati**, Sanat Ghosh, Aditi Bhattacharjee, Prince Tiwari, and Himansu S. Biswal\*; Critical Assessment of the Strength of Hydrogen Bonds between the Sulfur Atom of Methionine/Cysteine and Backbone Amides in Proteins. *The Journal of Physical Chemistry Letters* **2015**, 6 (8), 1385-1389.
2. <sup>§</sup>Arun Anand Gagrai<sup>#</sup>, **V. Rao Mundlapati**<sup>#</sup>, Dipak Kumar Sahoo, H. Satapathy\*, Himansu S. Biswal\*; The Role of Molecular Polarizability in Designing Organic Piezoelectric Materials. *ChemistrySelect* **2016**, 1 (14), 4326-4331.  
# equal contribution
3. <sup>§</sup>**V. Rao Mundlapati**, Sanjeev Gautam, Dipak Kumar Sahoo, Arindam Ghosh, and Himansu S. Biswal\*; Spectroscopic Evidences for Strong Hydrogen Bonds with Selenomethionine in Proteins. *The Journal of Physical Chemistry Letters* **2017**, 8(4), 794-800.
4. <sup>§</sup>**V. Rao Mundlapati**, Dipak Kumar Sahoo, Sanat Ghosh, Umesh Kumar Purame, Shubhant Pandey, Rudresh Acharya, Nitish Pal, Prince Tiwari, and Himansu S. Biswal\*; Thioamide, a Hydrogen Bond Acceptor in Proteins and Nucleic Acids. *The Journal of Physical Chemistry Letters* **2017**, 8 (18), 4573-4579.
5. Ashim Baishya, **V. Rao Mundlapati**, Sharanappa Nembenna, Himansu S. Biswal\*; Structure, bonding and energetics of N-heterocyclic carbene (NHC) stabilized low oxidation state group 2 (Be, Mg, Ca, Sr and Ba) metal complexes: A theoretical study. *Journal of Chemical Sciences* **2014**, 126 (6), 1781-1788.
6. Akshaya K. Kar, Achyut N. Acharya, **V. Rao Mundlapati**, Guru C. Pradhan, Himansu S. Biswal\*; Anadi C. Dash\*; Ligand substitution and electron transfer reactions of trans-(diaqua)(salen)manganese(III) with oxalate: an experimental and computational study. *RSC Advances* **2014**, 4 (102), 58867-58879.
7. **V. Rao Mundlapati**; Jena, P.; Achyut N. Acharya, Akshaya K. Kar, Anadi C. Dash, Himansu S. Biswal\*; Water exchange reaction of a manganese catalase mimic: oxygen-17 NMR relaxometry study on (aqua)manganese(III) in a salen scaffold and its reactions in a mildly basic medium. *RSC Advances* **2016**, 6 (113), 111739-111746.
8. Dipak Kumar Sahoo, **V. Rao Mundlapati**, Arun Anand Gagrai, Himansu S. Biswal\*; Efficient SO<sub>2</sub> Capture through Multiple Chalcogen Bonds, Sulfur-Centered Hydrogen Bonds and S•••π Interactions: A Computational Study. *ChemistrySelect* **2016**, 1 (8), 1688-1694.
9. Jena, P.; Acharya, A. N.; **Mundlapati, V. R.**; Dash, A. C.; Biswal, H. S. Kinetics and mechanistic study of the reduction of Mn(III) by oxalate in Salophen scaffold: relevance to oxalate oxidase. *Journal of Chemical Sciences* **2018**, 130, 123.

### b. Communicated:

10. <sup>§</sup>**V. Rao Mundlapati**, Dipak Kumar Sahoo, Suman Bhaumik, Subhrakant Jena, , Amol Chandrakar, Himansu S. Biswal\*; Critical Assessment of the Occurrence, Strength and Importance of Carbon Bonds in Proteins
11. <sup>§</sup>**V. Rao Mundlapati**; Himansu S. Biswal\*; Computational Assessment of N-Oxide, N-Sulfide Organic Molecules as Potential Carbon Bond Acceptors

§ Pertaining to thesis

---

## List of conferences attended

1. Presented poster in **Spectroscopy and Dynamics of Molecules and Clusters (SDMC)**, organized by **NISER, BHUBANESWAR** (20-23 FEB 2014). Title: Tautomerism of Uracil, Thiouracil and Phosphouracil: Interplay between intramolecular interactions and  $\pi$ -electron delocalization, Authors: **V. Rao Mundlapati**, Nitish Pal and Himansu S. Biswal\*.
2. Presented poster in **Spectroscopy and Dynamics of Molecules and Clusters (SDMC)**, organized by **IIT Kanpur and IISER Mohali at Nainital** (19-22 FEB 2015). Title: IR Spectroscopy and CCSD(T) Energetics Unveils the Strength of amide-N-H...S Hydrogen Bonds in Biological Molecules; Authors: **V. Rao Mundlapati**, Sanat Ghosh, Aditi Bhattacharjee, Prince Tiwari, Dipak Sahoo and Himansu S. Biswal\*.
3. Presented poster in **Spectroscopy and Dynamics of Molecules and Clusters (SDMC)**, organized by **IISER Pune and NCL, Pune at Mahabaleswar** (18-21 FEB 2016); Computational Assessment of Sulfur Center Hydrogen Bonded Systems as Promising Organic Piezoelectric Materials; Authors: **V. Rao Mundlapati**, Arun Anand Gagrai, Dipak Kumar Sahu and Himansu S. Biswal\*.
4. Presented poster in **the 30th Annual Conference of Orissa Chemical Society**, organized by **KIIT University, Bhubaneswar** (24-25 DEC 2016); Title: Sulfur Centered Hydrogen Bond (SCHB): Its Strength and Application; Authors: **V. Rao Mundlapati**, Dipak Kumar Sahoo, Subhrakant Jena and Himansu S. Biswal\*.
5. Presented poster in **Spectroscopy and Dynamics of Molecules and Clusters (SDMC)**, organized by **IISc, Bangalore at Pondicherry** (16-19 FEB 2017); Spectroscopic Evidences for Strong Hydrogen Bonds with Selenomethionine in Proteins; Authors: **V. Rao Mundlapati**, Dipak Kumar Sahoo, Sanat Ghosh, and Himansu S. Biswal\*

### Oral Presentation

6. **INTER IISER & NISER CHEMISTRY MEET**, Organized by NISER, Bhubaneswar (22-24 DEC 2017); Title: Revealing the Strength of Hydrogen Bond in Sulfur/Selenium Containing Biomolecules.

Venkateswara Rao Mundlapati

---

*Dedicated to*  
*My Parents*

---

## Acknowledgements

I feel privileged to acknowledge all the people who have actively or passively contributed to accomplish this thesis. Reaching this far would not have been possible without the guidance and help of many individuals during the course of the work.

I would like to extend my first and foremost heartfelt gratitude to my supervisor, Dr. Himansu Sekhar Biswal. His constant support and encouragement have played a vital role in the success of much of the work carried as a part of this thesis. Working with him has been a wonderful learning experience from both personal and professional point of view. I believe that his patience, especially in allowing me to make my own set of mistakes and learn from them has helped me develop as an individual and shaped many of the ideas presented here. His unique way of training Ph.D. students is really appreciable.

I would also like to express my sincere thanks to Prof. Sanjay Wategaonkar for his constant support and encouragement to perform gas phase experiments in his lab. I would also like to express my heartfelt gratitude to our collaborators Prof. Anadi C. Dash and Dr. Arindam Ghosh for their continuous help, motivation and valuable advice.

I wish to thank Prof. Sudhakar Panda (Director, NISER), Prof. V. Chandrasekhar (Former Director, NISER), Prof. T. K. Chandrashekar (Founder Director, NISER) for their help and support. I would like to thank my Thesis Monitoring Committee members Prof. A. Srinivasan, Dr. Subhadip Ghosh, Dr. Arindam Ghosh and Dr. Tirumala K. Chowdary, for their valuable guidance. It is my privilege to thank Prof. A. Srinivasan, the Chairperson and Dr. Moloy Sarkar, the former Chairperson of School of Chemical Sciences, and Dr. N. K. Sharma (PGCS, School of Chemical Sciences) for their suggestions and help in the hours of need. I would like to thank

---

Prof. T. K. Chandrashekar, Dr. Arindam Ghosh, Dr. Moloy Sarkar, Dr. Sudip Barman, Dr. P. Mal and Dr. Bhargava B.L. for teaching me in my course work, which had uplifted my understanding of Chemistry. I am sincerely thankful to all other faculty members of School of Chemical Sciences for their timely help in various aspects.

I sincerely thank Dr. Arun Kumar for helping me in purchasing chemicals and his support for handling the instruments in central facility lab. I sincerely thank Mr. Sanjaya Mishra for recording the NMR spectra of my samples and Mr. Amit and Mr. Raj for recording mass spectra of my samples. I would also like to thank Bhawani and Ashutosh for helping me by providing chemicals in need. I thank all the non-academic staffs of School of Chemical Sciences and the Institute.

I would also like to express my gratitude to our collaborators at TIFR, Mumbai, Dr. Aditi Bhattacharjee, and Dr. Sanat Ghosh for training me on Laser Spectroscopy experiments. I would also like to thank to Viola for her constant support while doing experiments in TIFR. My very special thanks go to Ajay who has been always ready to help with any kind of technical issues while performing experiments in TIFR.

I would like to express my special thanks to Dr. Rudresh Acharya for his collaboration work on writing code in one of my project. I am thankful to Dr. Sharanappa Nembenna for involved me for collaboration work and discussion in his one of project. I am also thankful to Dr. Yatendra S. Chaudhary for allowing me to work in his lab for IR experiments. My sincere thanks go to Mr. A. Ananda Raman for his continuous help for software installation issues in our lab server.

---

I am obliged to the infrastructural facilities and financial assistance of NISER, Bhubaneswar and express my sincere thanks for the same. I would like to thank the Department of Atomic Energy, Government of India for the financial support.

I would also like to express my gratitude to juniors and coworkers, Dipak, Subhrakant, Juhi, Kiran, Shubhranshu, Nitish, Prince, Arun, Sanjeev, Ankit, Srikant, Kalyani, Suman, Amol Chandrakar, Rana and Shubransu for their constant support and high degree of co-operation throughout the years.

I extend my heartily gratitude to my friends Dr. Manoj, Dr. Subba Reddy, Dr. Giri Teja Illa, Dr. Tapas, Dr. Adi, Dr. Ashim, Peddarao, Dr. Dhanu, Dr. Chandu, Dr. Mukund, Dr. Ramesh and my batchmates Tirupathi, Amarnath, Dr. Sourav, Nayan, Manas, Dr. A. Ghosh and Tanmay for extending their helping hands whenever it was needed the most and with whom I spent a lot of time during my stay at NISER, Bhubaneswar. I really enjoyed their company.

My deepest gratitude goes to my family members, my parents (amma, Purnamma and nanna, Naraiiah) for their constant support, encouragement and love through all these years. I specially thank my wife, Triveni for inspiring me a lot over the years to reach at this level. My sincere thanks goes to my brothers (Srinivasarao, Venkateswarlu, Saidaiah), sister-in-laws, nephews and brother-in-law for their inspiration, encouraged and supported to achieve this prestigious degree.

---

# Contents

Synopsis.....	I-XIV
List of Figures .....	XV-XXI
List of Tables .....	XXII-XXIII
List of abbreviations .....	XXIV-XXV
<b>Chapter 1. Introduction.....</b>	<b>1</b>
1.1 Hydrogen bond and their classifications.....	2
1.1.1 Sulfur centered hydrogen bond (SBHB).....	4
1.1.1a Sulfur as H-bond donor .....	5
1.1.1b Sulfur as Hydrogen bond acceptor.....	7
1.1.2 Selenium center Hydrogen bond (SeCHB).....	11
1.1.3 Application of Hydrogen bond system as Piezoelectric Materials .....	13
1.2 Carbon Bonding .....	15
1.2.1 Carbon forms a proper non-covalent interactions.....	15
1.2.2 N-oxide acts as C-acceptors .....	18
1.3 Objectives of the thesis .....	19
1.4 Structure of the thesis .....	20
References.....	22
<b>Chapter 2. Experimental and Computational Methods .....</b>	<b>39</b>
2.1. Experimental methods .....	40
2.1.1 Supersonic expansion method .....	41
2.1.2 Electronic excitation spectra of monomers and complexes .....	47
2.1.2.1 Laser induced fluorescence (LIF) Spectroscopy .....	48
2.1.2.2 Resonance enhanced multiphoton ionization (REMPI) or 1-colour (2-colour) resonant two photon ionization (1c or 2c-R2PI) .....	50
2.1.2.3 Time of flight mass spectrometry .....	52
2.1.2.4 IR–UV double resonance spectroscopy–Fluorescence depletion by infrared (FDIR)/ Resonant ion depletion by infrared (RIDIR) .....	54
2.1.3 Spectroscopic Techniques in Solution phase .....	56
2.1.3.1 Nuclear Magnetic Resonance Spectroscopy .....	56
2.1.3.2 Horizontal Attenuated Total Reflectance Fourier Infrared Spectroscopy (HATR).....	59
2.2 Computational Methods .....	61
2.2.1 Geometry optimization and frequency calculations: .....	62
2.2.2 Stabilization energy estimation .....	63
2.2.3 Electron density topology and Natural bond orbital analysis of non-covalent interactions: .....	66
Reference .....	69
<b>Chapter 3. Sulfur Centered Hydrogen Bond .....</b>	<b>73</b>
3.1. The Strength of Sulfur Centered Hydrogen Bond (SCHB) in Model Systems of Biomolecules in Isolated Condition.....	74
3.1.1 Introduction.....	74
3.1.1.1 The small molecules as model compounds of proteins and nucleic acids .....	75
3.1.2. Experimental and Computational Results.....	77
3.1.2.1. Electronic and IR spectra of monomer and H-bond complexes of model compounds .....	77
3.1.2.2. Quantum Chemical Calculations .....	82

3.1.2.3 Comparison with Backbone-amide N-H...S H-Bonds in Peptides and Proteins.....	87
3.1.3 Conclusions .....	89
3.2. Sulfur Centered H-bond Enthalpy in Solution: Thioamides as H-bond Acceptors in Proteins and Nucleic acids .....	91
3.2.1 Introduction .....	91
3.2.2. Experimental and Computational Results .....	93
3.2.2.1. Computational investigation of strength of SCHB as thioamide H-bond acceptor in proteins and nucleic acids and its model compounds .....	93
3.2.2.2. Experimental investigation of strength of SCHB as thioamide H-bond acceptor in model compounds of proteins and nucleic acids .....	99
3.2.3 Conclusions.....	112
References .....	113
<b>Chapter 4. Selenium Centered Hydrogen Bond (SeCHB) in Selenomethionine Containing Peptides and Proteins .....</b>	<b>119</b>
4.1. Introduction: .....	119
4.2. Existence of amide-N-H...Se H-bonds in proteins: PDB analysis .....	120
4.3. Experimental and Computational studies for -N-H...Se H-bonds in Model Compounds of Biomolecules .....	126
4.3.1. High-Resolution Laser Spectroscopy: .....	126
4.3.2 Quantum Chemical Calculations at CCSD-T level: .....	132
4.3.3. Contribution of Electronegativity, Atomic Charge and Local Polarizability to the strength of H-bond: .....	137
4.4. Conclusions: .....	139
References: .....	141
<b>Chapter 5. Applications of SCHBs and SeCHBs in designing Organic Piezoelectric Materials ....</b>	<b>145</b>
5.1 Introduction .....	145
5.2 Characterization of Hydrogen bond and binding energies of different H-bond complexes .....	148
5.3 Computational Methods to Calculate the Piezoelectric Coefficients ( $d_{33}$ ) .....	149
5.3.1 Method-A (Estimated Method) .....	150
5.3.2 Method-B (Calculated Method) .....	153
5.3.3 Method-C: Effect of Polarizability on piezoelectric coefficient ( $d_{33}$ ).....	156
5.4 Substituent effect on $d_{33}$ and Mimicking Crystal Structure .....	160
5.5 Conclusions .....	166
References .....	168
<b>Chapter 6. Carbon Bonding (C-Bonding) in Proteins and Small Organic Molecules .....</b>	<b>171</b>
6. Introduction.....	171
6.1 Carbon bonding in proteins: NMR, IR Spectroscopy and Quantum Chemical Calculations .....	171
6.1.1 Motivation.....	171
6.1.2 Protein data base analysis for existence of C-bond in proteins.....	173
6.1.3 Experimental evidences and strength of C-bond in model compounds and proteins .....	183
6.1.4 Nature of C-bond interaction in model compounds and proteins .....	200
6.1.5 Significant role of C-bonds in structural and functional analysis in proteins .....	202
6.1.6 Conclusions.....	205

---

6.2 Computational Assessment of the strength of Carbon bonding: N-Oxide, N-Sulfide Compounds as C-Bond Acceptors.....	207
6.2.1 Introduction.....	207
6.2.2 Computational Calculations for evidence of C-bond formation with N-Oxides/N-sulfides....	209
6.2.2.1 Computational methods .....	210
6.2.2.2 Geometrical parameters and Stabilization energies for C-bond complexes .....	210
6.2.2.3 Confirmation of C-bond formation between N-oxides/N-Sulfides and C atom of methyl group with topological analyses .....	212
6.2.3 Conclusions.....	222
References.....	223
<b>Chapter 7. Concluding Remarks and Future prospective .....</b>	<b>228</b>
7.1 Concluding Remarks .....	228
7.2 Future prospective .....	238

---

## SYNOPSIS

Non-covalent interactions are the attractive forces between atoms and molecules that lead to formation of atomic clusters or molecular aggregations. These are set of strong to weak interactions such as hydrogen bonds (H-Bonds), halogen bonds, carbon bonds (C-Bonds), van der Waals forces, etc. These interactions play crucial roles in catalysis<sup>1-2</sup>, molecular recognition<sup>3-4</sup>, solvation<sup>5-6</sup> and self assembly<sup>7-9</sup> etc. The inter- and intra-molecular non-covalent interactions between the monomer units with the solvents, control the conformational landscape of folded and unfolded structures of biopolymers such as proteins, DNA, RNA, carbohydrates, etc.<sup>10-11</sup>. In most of the cases, the observed non-covalent interactions in biomolecules are hydrogen bonds, viz. O-H $\cdots$ O, N-H $\cdots$ O, N-H $\cdots$ O=C, N-H $\cdots$  $\pi$  interactions, and  $\pi$ -stacking. This thesis consists of two parts. The first part describes the strength of H-bonds between the S/Se of methionine/selenomethionine with the backbone amide-N-H. The second part of the thesis deals with the “Carbon bond” in proteins. The carbon bond is, represented by C=O $\cdots$ C-X, the interaction between C=O of backbone/side chain of peptides with the hydrophobic alkyl and aryl groups.

### **Objectives of thesis:**

- I. To assess the strength of N-H $\cdots$ Y (Y=S, Se and Te) H-bonds using mass selective and conformer specific high resolution IR-UV double resonance spectroscopy in isolated jet-cooled condition
- II. To determine the N-H $\cdots$ S H-bond enthalpy in solution with NMR spectroscopy and quantum chemical calculations
- III. To investigate the nature and strength of -C=O $\cdots$ C C-bonds in proteins.

---

## Structure of the Thesis

The thesis is divided into six chapters

- 1) Introduction
- 2) Experimental and computational methods
- 3) (A) The Strength of Sulfur Centered Hydrogen Bond (SCHB) in Model Systems of Biomolecules in Isolated Condition  
(B) Sulfur Centered Hydrogen Bond Enthalpy in Solution: Thioamides as H-Bond Acceptors in Proteins and Nucleic Acids
- 4) Selenium Centered Hydrogen Bond (SeCHB) in Selenomethionine Containing Peptides and Proteins
- 5) The Applications of SCHBs and SeCHBs in designing Organic Piezoelectric Materials
- 6) (A) Carbon bonding in proteins: NMR, IR Spectroscopy and Quantum Chemical Calculations  
(B) Computational Assessment of the strength of Carbon bonding: N-Oxide, N-Sulfide Compounds as C-Bond Acceptors

**1. Introduction:** This chapter deals with the problems investigated and discussion on previous literature relevant to the thesis<sup>13-15</sup>. It also describes the concept of piezoelectric effect and use of hydrogen bonded systems in designing piezoelectric materials. The origin of another new type of non-covalent interaction namely Carbon bond and its previous studies were also discussed. At the end of this chapter, the objectives and the scope of the present work have been discussed.

**2. Experimental and computational methods:** The intermolecular 1:1 complexes and corresponding monomers studied in this thesis were prepared in cold state (typical temperature ~5K) and collision free condition using supersonic jet expansion and were probed by various

---

laser based spectroscopic techniques. This chapter briefly describes the spectroscopic techniques such as Laser Induced Fluorescence (LIF) Spectroscopy, Resonance-Enhanced Multiphoton Ionization (REMPI) Spectroscopy to obtain the electronic spectra, and IR-UV Double Resonance Spectroscopy that were employed to obtain vibrational spectra in gas phase.

Solution NMR spectroscopy was used to investigate the H-bond/C-bond complexes. The  $^1\text{H}$  NMR and  $^{13}\text{C}$  NMR spectra show downfield/upfield chemical shifts due to formation of the complexes in solution. The chemical shifts are monitored as a function of concentration and temperature to get the thermodynamic parameters of complexation. The diffusion-ordered spectroscopy ( $^1\text{H}$  DOSY) was used to get diffusion coefficient of monomers and complexes at different concentrations. We also performed the deuterium exchange studies to measure the rate of H/D exchange.

The results of the aforementioned experiments were directly compared with ab initio calculations. The monomers and different conformers of the complexes were optimized at the Density Functional Theory (DFT) such as B3LYP, PBE0, B97-D functionals using both Pople and Dunning type basis sets with diffuse and polarization functions (def2-TZVPP). The solvent effect was considered by using self-consistent reaction field (SCRF) method such as Solvent Model based on Density (SMD) model to obtain the solvation free energies of non-covalently bonded (H-Bond/C-Bond) complexes. Computations were also carried out at MP2/aug-cc-pVDZ and CCSD-T/aug-cc-pVDZ level of theory to calculate the binding energies of complexes investigated in this work. All the calculations were carried out using Gaussian 09 and Turbomole 6.5<sup>16</sup>. Quantum theory of atoms in molecules (QTAIM)<sup>17</sup>, natural bond orbital (NBO)<sup>18-19</sup>, localized molecular orbital energy decomposition analysis (LMOEDA) and non-covalent

---

interaction (NCI) plot analysis were also carried out to investigate the nature of the H-bond and C-bond interactions.

**3. Sulfur Centered Hydrogen Bond (SCHB):** This chapter is divided into two sections. The first section describes the assessment of the strength of N-H $\cdots$ S hydrogen bond in isolated and jet-cooled condition. The second section deals with the H-bond enthalpy for amide/thioamide N-H $\cdots$ S=C-thioamide H-bond in a non-polar solvent.

**3A. The Strength of Sulfur Centered Hydrogen Bond (SCHB) in Model Systems of Biomolecules in Isolated Condition:** This chapter focuses on the determination of the strength of SCHB in biomolecules without environmental and conformational effects. The model compounds N-phenylacetamide (NPAA), N-methylformamide (NMFA) and 2-pyridone (2-PY) were chosen as H-bond donors, consist of both trans and cis amides, representing the amides in peptides and nucleobases, respectively. DME (dimethylether), DMS (dimethylsulfide), DMF (dimethylformamide) and benzene (Bz) were chosen as H-bond acceptors which represents H-bond acceptor such as in the side chain of serine (O-), methionine/cysteine (S-), backbone/side chain (-C=O) and side chain aromatic groups ( $\pi$ -acceptors). The H-bond donor-acceptor combinations give rise to N-H $\cdots$ S, N-H $\cdots$ O=C, N-H $\cdots$ O, and N-H $\cdots$  $\pi$  H-bonds. The 1:1 hydrogen bond complexes of NPAA and 2-PY were prepared by co-expansion of NPAA/2-PY vapor with pre-mixtures of different solvents (DME, DMF, DMS, Bz) using Helium as a buffer gas in a supersonic jet. The monomer and hydrogen bonded complexes of NPAA and 2-PY were identified by their electronic spectra obtained via REMPI and LIF spectroscopy. In the electronic spectra of NPAA complexes with DME, DMS, DMF and Bz, new transition peaks were observed which are red shifted by 275, 259, 420, and 401  $\text{cm}^{-1}$ . However, in the case of 2-PY

---

complexes with DMS and DMF new transition peaks are obtained at 202 and 251  $\text{cm}^{-1}$  blue shifted to monomer band origin of 2-PY.

The IR spectra of the NPAA and 2-PY monomers and their complexes were recorded in the NH stretching region (2900-3600  $\text{cm}^{-1}$ ) by IR-UV double resonance spectroscopy. The IR spectra of NPAA and 2-PY complexes with DME, DMS, DMF and Bz were red shifted with respect to their monomers. The observed red shift ( $\Delta\nu_{\text{NH}}$ ) values for N-H $\cdots$ S H-bond complexes of NPAA and 2-PY are 96, 291  $\text{cm}^{-1}$ , respectively, and which are higher than that of N-H $\cdots$  $\pi$  H-bond (12, 56  $\text{cm}^{-1}$ ). The  $\Delta\nu_{\text{NH}}$  values of N-H $\cdots$ S H-bond of NPAA and 2-PY are similar to the conventional H-bonds N-H $\cdots$ O (99, 250  $\text{cm}^{-1}$ ) and N-H $\cdots$ O=C H-bond (73, 311  $\text{cm}^{-1}$ ). The experimental frequencies were assigned with the help of computational calculations. The obtained results of model compound complexes were in good agreement with results of methionine/cysteine containing peptides and proteins. The donor-acceptor interaction energies ( $E_{\text{DA}}$ ) for amide N-H $\cdots$ S-methionine and amide N-H $\cdots$ S-cysteine H-bonds in proteins were calculated at MP2/aug-cc-pVDZ level that are 53.9 and 37.5 kJ/mol, respectively. These results that N-H $\cdots$ S H-bonds in proteins are similar to those observed for simple model compounds of peptides.

**3B. Sulfur Centered H-bond Enthalpy in solution: Thioamides as H-bond Acceptors in Proteins and Nucleic acids:** The results from above section revealed that the sulfur centered hydrogen bond N-H $\cdots$ S strength is as strong as conventional hydrogen bonds in gas phase without conformational and solvent effects. The studies in this section are motivated from the above results and recent review<sup>20</sup> by J. Schneider et al. that enlisted the experimental binding energies for almost all types of hydrogen bonds except SCHB in solution. It shows that there is no experimental determination of the strength of SCHBs in solution till date. We first carried out

---

DFT studies to compare the strength of N-H $\cdots$ S=C-thioamide H-bonds with the other conventional (N-H $\cdots$ O, N-H $\cdots$ O=C) H-bonds that are simultaneously observed in peptide and nucleobase (PDB: 1QX5, 1KBM and 5LPG). The PDB structures were optimized by adding hydrogen to 10-15 residues around the amide-N-H $\cdots$ S=C H-bonds while freezing all other atomic positions and then the donor-acceptor interaction energy ( $E_{DA}$ ) was calculated using NBO formalism. The interaction energies ( $E_{DA}$ ) of N-H $\cdots$ S=C-thioamide in different protein structures are in the range of 21 to 77 kJ/mol. The variation of interaction energies of N-H $\cdots$ S=C-thioamide H-bond in different protein structures are because of conformational constraints imposed by other residues. However, the N-H $\cdots$ S=C H-bond strengths were comparable to those of the N-H $\cdots$ O=C and N-H $\cdots$ N H-bonds in proteins and nucleic acids. Then, 23 model complexes, representing H-bond systems in proteins and nucleobases without having any conformational constraints were chosen to estimate the H-bond enthalpy computationally. The calculated hydrogen bond enthalpy of amide-N-H $\cdots$ O=C H-bonds are similar to thioamide-N-H $\cdots$ S=C H-bonds. The maximum H-bond enthalpy is  $\sim$ 30 kJ/mol for 2-pyridone (2-PY) and 2-thiopyridone (2-TPY) dimers. Then 2-TPY and 2-PY model compounds were chosen to measure the strength of N-H $\cdots$ S=C and N-H $\cdots$ O=C in solution. We carried out concentration and temperature dependent NMR experiments to measure the strength of N-H $\cdots$ O=C, N-H $\cdots$ S=C hydrogen bonds. The dimerization of 2-PY and 2-TPY were confirmed at higher concentration with the diffusion ordered spectroscopy. The concentration dependent experimental H-bond enthalpies are  $\sim$ 31 kJ/mol for (2-PY) $_2$  and  $\sim$ 30 kJ/mol for (2-TPY) $_2$ . We also performed deuterium exchange NMR experiments to measure the rate of deuterium exchange in 2-PY and 2-TPY dimers that is in the range of  $3 \times 10^{-2}$  to  $4 \times 10^{-2}$  min $^{-1}$ . Concentration and deuterium exchange experiments results confirm that the N-H $\cdots$ S=C H-bonds are as strong as the classical

---

N-H $\cdots$ O/N-H $\cdots$ O=C H-bonds. The experimental results obtained are corroborated by the benchmark quantum chemical calculations at CCSD(T)-SMD/aug-cc-pVDZ//B97D-SMD/aug-cc-pVDZ level of theory

#### **4. Selenium Centered Hydrogen Bond (SeCHB) in Selenomethionine Containing Proteins:**

The results described in chapter 3A and 3B revealed that low electronegative element (S) has potential to form strong hydrogen bonds as conventional hydrogen bonds. The other objective is to explore the existence of selenium centered hydrogen bond (SeCHB) between the Selenium (which is less electronegative atom than sulfur) in the side chain of selenomethionine/selenocysteine and backbone amide-NH in proteins. At first, the protein data bank (PDB) analysis was carried out to get structural and geometrical evidences for the SeCHB in proteins. The protein structure coordinates were retrieved from RCSB website and to find the N-H $\cdots$ Se H-bonds we have used in-house program written in C-language. About 52% of total interactions were found within the sum of van der Waals radii of Se and H atom, conforming the formation of N-H $\cdots$ Se H-bonds. The donor-acceptor interaction energy ( $E_{DA}$ ) of N-H $\cdots$ Se H-bond is found to be 175 kJ/mol in one of the proteins (PDB: 1W2F) and that is comparable with any conventional H-bond. Further, the strength of N-H $\cdots$ Se H-bond was determined experimentally by using mass selected IR/UV double resonance spectroscopy in model compounds.

N-phenyl acetamide (NPAA), N-methyl formamide (NMFA) and 2-pyridone (2PY) were chosen as H-bond donors which representing as trans amide-NH of peptides and cis amide-NH of nucleobases, respectively. Dimethylselenide (DMSe) as side chains of selenomethionine and dimethylsulfide (DMS) as constituent of and methionine were chosen as H-bond acceptors. Resonant ion depletion infrared (RIDIR) spectroscopy was used to get IR spectra

---

of NPAA and 2-PY monomer and their respective 1:1 H-bond complexes with DMSe and DMS. In case of NPAA (trans amide) the  $\Delta\nu_{\text{NH}}$  values for N-H $\cdots$ Se and N-H $\cdots$ S H-bond complexes are 91 and 96  $\text{cm}^{-1}$ , respectively while in case of 2-PY (cis amide) the  $\Delta\nu_{\text{NH}}$  is 262  $\text{cm}^{-1}$  for N-H $\cdots$ Se H-bond complex and 291  $\text{cm}^{-1}$  for N-H $\cdots$ S H-bond complex. The red shifts in NPAA (trans amide) and 2-PY(cis amide) amide-N-H $\cdots$ Se H-bond complexes confirm Se as a potential H-bond acceptors in proteins and nucleobases. The experimental frequencies of NPAA (trans)/ 2-PY (cis amide) monomer and complexes were comparable to the vibrational frequencies calculated at the B97-D/def2-TZVPP level of theory. These results stimulated us to investigate N-H $\cdots$ Te H-bond. The electronegativity of Te is very similar to H. We could not perform the experiments for N-H $\cdots$ Te H-bond due to unavailability of dimethylteluride (DMTe). So computational frequencies of N-H $\cdots$ Te H-bond complexes of both cis (2-PY-DMTe) and trans (NPAA-DMTe) amide systems were calculated at the B97-D/def2-TZVPP level of theory. We found out the scaling factor from available experimental and DFT vibrational frequencies and used it to estimate amide-NH stretching frequency for amide-NH $\cdots$ Te H-bond. The  $\Delta\nu_{\text{NH}}$  value of amide-N-H $\cdots$ Te H-bond complexes is found to be 80  $\text{cm}^{-1}$  for NPAA and 241  $\text{cm}^{-1}$  for 2-PY that are close to amide-N-H $\cdots$ Se/S H-Bonds. The experimental and computational results revealed that S, Se and Te can form hydrogen bond and their strengths are similar to the conventional hydrogen bond acceptors (N and O). To know the reason why S, Se, and Te form strong hydrogen bonds although they have less electronegativities, we calculated the charges ( $q$ ) and polarizabilities ( $\alpha$ ) of hydrogen bond acceptors. A linear correlation was observed between  $\sqrt{|q\sqrt{\alpha}|}$  and computed  $E_{\text{DA}}$  interaction energies/ $\Delta\nu_{\text{NH}}$  values of complexes. This can be concluded that the strength of amide-NH $\cdots$ Y (Y=O, S, Se and Te) H-bonds are not only

---

governed by the electronegativities and charges of the acceptor atoms (Y) but also by their polarizabilities.

### **5. The Applications of SCHBs and SeCHBs in designing Organic Piezoelectric Materials:**

The piezoelectricity is the ability of certain material to convert mechanical energy to electrical energy. The criteria for a material to be piezoelectric are (a) it should have ionic or partly ionic bonds and (b) it should be non-centrosymmetric. The hydrogen bond is highly directional and polar. The results in the previous chapter explored that the SCHB, SeCHB H-bond are as strong as the conventional H-bonds. The aim of this chapter is to use SCHB, SeCHB complexes in designing piezoelectric material. We used nitrobenzene (NBz) as hydrogen bond acceptor, whereas phenol (PH), thiophenol (SPH) and selenophenol (SePH) were chosen as hydrogen bond donors. Quantum chemical calculations were carried out at the DFT using B3LYP, PBE0 as functionals and 6-31G\*, aug-cc-pVDZ as basis sets. The geometry optimization and the piezoelectric coefficients ( $d_{33}$ ) of H-bond systems were carried out at the same level of theory. The piezoelectric coefficients ( $d_{33}$ ) for different hydrogen bonded complexes were calculated using three methods proposed by Daniel S. Lambrecht and co-workers work<sup>21</sup>. The piezoelectric coefficients of SPH-NBz, SePH-NBz are 25.57 pm/V, 26.90 pm/V, respectively, that are higher than that of the conventional hydrogen bond system (PH-NBz) i.e.18.89 pm/V. These are also larger than experimentally determined piezoelectric coefficients of 2-methyl-4-nitroaniline (14 pm/V)<sup>22</sup> and the computationally obtained value for Aniline-NBz (23 pm/V<sup>21</sup>) at B3LYP/6-31G\*. To know the reason for higher piezoelectric coefficients for SCHB and SeCHB we have calculated the polarizability and dipole moment and their derivatives and found linear correlation with piezoelectric coefficients. The low force constant and less dipole moment of H-bond of

---

SeCHB, SCHB systems with the change in bond length are responsible for the higher piezoelectric response.

## **6A. Carbon Bond in Proteins: NMR, IR Spectroscopy and Quantum Chemical**

**Calculations:** This chapter focuses on a new type of non-covalent interaction, i.e. ‘carbon bond’ where the  $\sigma$ -hole on carbon atom participates in the interaction. In recent years, E. Arunan and other groups computationally showed that C-bond could be possible between carbon and an electron rich group or atom. The  $X-C\cdots Y$  ( $X, Y = O, N, F, \pi$ , etc), C-bonds have very similar characteristics as observed in  $X-H\cdots Y$  hydrogen bond and could play significant role in numerous biological and chemical processes. Alkyl and aromatic side chains of amino acids in proteins reside in the hydrophobic cores. Therefore, the possibility of formation of C-bond with backbone or side chain electron rich groups such as carbonyl groups cannot be belittled. In this chapter, the experimental evidence for the existence of the carbon bond and the strength of  $X-C\cdots Y$  carbon bond interaction in proteins and model compounds are discussed. We have done the protein data bank (PDB) analysis to know the existences of the C-bonds in proteins using the inbuilt python 2.7 language program and found 5738 interactions. This analysis provides the detailed information of engaged amino acid, secondary structure, type of bond and different atoms involved in the carbon bond. The PDB analysis shows that C-bond exists between alkyl and aromatic side chain amino acids and backbone  $-C=O$  in proteins. We have chosen several model compounds to study the strength of  $C=O\cdots C-X$  C-bond interaction with the help of NMR Spectroscopy, IR spectroscopy and quantum chemical calculations. The model compounds are N,N-dimethylacetamide (NNDMA) as C-bond acceptor and acetonitrile, nitromethane, acetic acid, alanine, acetyl chloride and trifluoroacetone as C-bond donors respectively. The FTNMR, FTIR spectroscopic techniques were used to determine the strength of  $C=O\cdots C-C$  C-bond in

---

model compounds. The binding energies were calculated at CCSD-T/aug-cc-pVDZ level of theory. We derived an expression to estimate the binding energies and nature of C-bond in proteins just by knowing the distance between O and C ( $d_{O\cdots C}$ ) from model compounds. The estimated binding energies are in the range of ~2 to 20 kJ/mol. The nature of C-bond depends on  $d_{O\cdots C}$  distance, shorter the  $d_{O\cdots C}$ , more electrostatic is the C-bond and longer  $d_{O\cdots C}$ , more dispersive is the C-bond.

**6B. Computational Assessment of the strength of Carbon bonding: N-Oxide, N-Sulfide Compounds as C-Bond Acceptors:** N-Oxides/sulfides or amine oxides/sulfides are useful in pharmaceutical, agriculture, supramolecular chemistry and biology because of its large dipole moment, less basicity and high solubility in water. These have also an inherent property to act as hydrogen bond and halogen bond acceptors. N-Methylenemethanamine oxide/sulfide, 1-H-Imidazole-3-oxide/sulfide and pyridine N-oxide/sulfide as C-bond acceptors and acetonitrile and nitromethane as carbon bond donors were taken for computational study. The C-bond complexes were optimized at B97D/aug-cc-pVDZ and binding energy calculations were performed at MP2, CCSD-T and CCSD-T/CBS level of theory. The carbon bond formation was confirmed by quantum theory of atoms in molecule (QTAIM), non-covalent interaction (NCI) analysis, natural bond orbital analysis and molecular electrostatic potential analysis. These results show that N-Oxides and N-Sulfides are strong carbon bond acceptor like hydrogen bond acceptor and halogen bond acceptor and their binding energies are ~20 kJ/mol.

## 7. Concluding remarks and future directions:

a. The strength of N-H $\cdots$ S H-bond in the model compounds is as strong as conventional N-H $\cdots$ O and N-H $\cdots$ O=C H-bonds, but stronger than N-H $\cdots$  $\pi$  H-bonds. They are very similar to those observed in peptides and proteins.

---

b. For the first time we provided the spectroscopic evidences of N-H $\cdots$ S H-bond in solution phase and estimated H-bond enthalpy is  $\sim 30$ kJ/mol. The concentration dependent experiment gives accurate H-bond enthalpy, which is in agreement with the benchmark quantum chemical calculations at CCSD(T)-SMD/aug-cc-pVDZ level of theory.

c. The PDB structure analysis gives structural evidences for the existences of N-H $\cdots$ Se H-bonds in proteins. The high-resolution vibrational spectroscopy confirms the N-H $\cdots$ Se H-bonds in model compounds of biomolecules. The benchmark quantum chemical calculations, PDB structure experimental data firmly suggest that amide-N-H $\cdots$ Se/Te H-bonds are as strong as classical amide-N-H $\cdots$ O and amide-N-H $\cdots$ O=C H-bonds. These results of SCHB and SeCHBs in the gas phase and SCHB in solution phase helps in designing new force fields for the protein structure simulation.

d. In this thesis, we have shown the application of SCHB and SeCHBs in designing piezoelectric materials. The higher piezoelectric coefficients were observed for SCHB and SeCHB organic systems than their oxygen counter part, namely organic crystal (2-methyl-4-nitroaniline) with the largest known piezoelectric response.

e. The analysis of the PDB confirmed the existences of Carbon bonds (C-bond) in proteins as amide-C=O $\cdots$ C-X C-bond. By using FTNMR and FTIR spectroscopy, for the first time we have given experimental evidence of carbon bond as C=O $\cdots$ C-C in model compounds of proteins. With the combination of experimental and computational studies, we estimated the C=O $\cdots$ C-X C-bond binding energies and that can be in the range of 2-22 kJ/mol. The nature of the carbon bond in proteins depends on the distance between O and C ( $d_{O\cdots C}$ ). The C-bond is more electrostatic in nature at shorter  $d_{O\cdots C}$  and at longer  $d_{O\cdots C}$  it is more dispersive in nature.

---

Computationally we have shown that N-oxides and N-sulfides form the C-bonds. They are strong C-bond acceptor like H-bond acceptor and halogen bond acceptor.

**References:**

1. Knowles, R. R.; Jacobsen, E. N. *Proc. Natl. Acad. Sci. U.S.A.* **2010**, *107* (48), 20678-20685.
2. Wheeler, S. E.; Seguin, T. J.; Guan, Y.; Doney, A. C. *Acc. Chem. Res.* **2016**, *49* (5), 1061-1069.
3. Lehn, J.-M., *Chem. Soc. Rev.* **2007**, *36* (2), 151-160.
4. Sessler, J. L.; Lawrence, C. M.; Jayawickramarajah, J., *Chem. Soc. Rev.* **2007**, *36* (2), 314-325.
5. Impellizzeri, G.; Bonomo, R. P.; Calì, R.; Cucinotta, V.; Rizzarelli, E., *Thermochimica Acta* **1984**, *80* (2), 275-279.
6. Rinaudo, M., *Macromol. Biosci.* **2006**, *6* (8), 590-610.
7. Spolar, R. S.; Ha, J. H.; Record, M. T., *Proc. Natl. Acad. Sci. U.S.A.* **1989**, *86* (21), 8382-8385.
8. Sherrington, D. C.; Taskinen, K. A., *Chem. Soc. Rev.* **2001**, *30* (2), 83-93.
9. Whitesides, G. M.; Grzybowski, B., *Science* **2002**, *295* (5564), 2418-2421.
10. Pace, C. N.; Fu, H.; Fryar, K. L.; Landua, J.; Trevino, S. R.; Shirley, B. A.; Hendricks, M. M.; Iimura, S.; Gajiwala, K.; Scholtz, J. M.; Grimsley, G. R., *J. Mol. Biol.* **2011**, *408* (3), 514-528.

- 
11. Rose, G. D.; Fleming, P. J.; Banavar, J. R.; Maritan, A., *Proc. Natl. Acad. Sci. U.S.A* **2006**, *103* (45), 16623-16633.
  12. Zhou, P.; Tian, F.; Lv, F.; Shang, Z., *Proteins: Struct., Funct., Bioinf.* **2009**, *76* (1), 151-163.
  13. Biswal, H. S.; Wategaonkar, S., *J. Phys. Chem. A* **2009**, *113* (46), 12763-12773.
  14. Biswal, H. S.; Gloaguen, E.; Loquais, Y.; Tardivel, B.; Mons, M., *J. Phys. Chem. Lett.* **2012**, *3* (6), 755-759.
  15. Alauddin, M.; Biswal, H. S.; Gloaguen, E.; Mons, M., *Phys. Chem. Chem. Phys.* **2015**, *17* (3), 2169-2178.
  16. Furche, F.; Ahlrichs, R.; Hättig, C.; Klopper, W.; Sierka, M.; Weigend, F. *Wiley Interdiscip. Rev. Comput. Mol. Sci.* **2014**, *4* (2), 91-100.
  17. Bader, R. F. W., *Chem. Rev.* **1991**, *91* (5), 893-928.
  18. Reed, A. E.; Curtiss, L. A.; Weinhold, F., *Chem. Rev.* **1988**, *88* (6), 899-926.
  19. Weinhold, F.; Landis, C. R., *Valency and Bonding: A Natural Bond Orbital Donor-Acceptor Perspective*, *Cambridge University Press: Cambridge*, 2005.
  20. Biedermann, F.; Schneider, H. J., *Chem. Rev.* **2016**, *116* (9), 5216-5300.
  21. Werling, K. A.; Griffin, M.; Hutchison, G. R.; Lambrecht, D. S. *J. Phys. Chem. A* **2014**, *118* (35), 7404-7410.
  22. Paturle, A.; Graafsma, H.; Sheu, H. S.; Coppens, P.; Becker, P. *Phys. Rev. B* **1991**, *43*, 1468

## List of Figures

<b>Figure 1.1</b> (a) Piezoelectric effect: applying mechanical stress on material to generate electricity (b) inverse piezoelectric effect: applying electric field on material and its displacement in the direction of applied electric field .....	13
<b>Figure 2.1:</b> A comparison of the excitation spectra of phthalocyanine measured under static gas room temperature conditions .....	42
<b>Figure 2.2:</b> A supersonic jet expansion formed by expansion Set up.....	45
<b>Figure 2.3:</b> Velocity distributions of monoatomic gases in supersonic jet at different M values.	46
<b>Figure 2.4:</b> Schematic experimental set-up of High resolution spectroscopy (LIF and REMPI spectroscopy). .....	47
<b>Figure 2.5:</b> Schematic of a) LIF spectroscopy and b) total fluorescence detection in LIF spectroscopy.....	49
<b>Figure 2.6:</b> Schematic diagram of the REMPI spectroscopy. The ion signal is plotted against the excitation laser energy .....	51
<b>Figure 2.7:</b> A schematic diagram of the TOF mass spectrometer used for the experiment.....	53
<b>Figure 2.8:</b> Schematic of the IR-UV double resonance spectroscopy .....	55
<b>Figure 2.9:</b> (a) Brownian motion of the solute molecule, (b) Stejskal–Tanner plot .....	59
<b>Figure 2.10:</b> A Horizontal Attenuated Total Reflectance (HATR) experimental setup .....	61
<b>Figure 2.11:</b> PES of a non-covalent interaction complex (X---Y).....	64
<b>Figure 3.1.1</b> Top: Representative Model compounds .....	76
<b>Figure 3.1.2</b> The electronic spectrum of monomer (NPAA) and its H-bond complexes .....	78
<b>Figure 3.1.3</b> Gas phase vibrational spectra of monomer (NPAA) and its H-bond complexes ....	80
<b>Figure 3.1.4</b> The electronic spectra of monomer (2-PY) and its H-bond complexes .....	81
<b>Figure 3.1.5</b> Gas phase vibrational spectra of monomer (2PY) and its H-bond complexes.....	82
<b>Figure 3.1.6</b> The global minimum optimized complexes of NPAA, NMFA and 2-PY with DMS, DME, DMF and Bz obtained at RIB97-D3/def2-TZVPP level.....	83

<b>Figure 3.1.7</b> The orbital overlap between the lone pair (lp) electrons of S/O and the antibonding $\sigma^*$ N-H orbital ( $\sigma^*_{\text{N-H}}$ ) of trans/cis amides .....	85
<b>Figure 3.1.8</b> Primary N-H $\cdots$ S/O/O=C/ $\pi$ H-bonds and secondary C-H $\cdots$ S/O/ $\pi$ H-bonds in (a) NPAA, (b) 2-PY, (c) NMFA with DMS/DME/DMF/BZ complexes as revealed by colored isosurfaces of the reduced electron density gradient (3D-NCI-plot), following the NCI-plot topological analysis of the electron density at the MP2/aug-cc-pVDZ .....	86
<b>Figure 3.1.9</b> Linear correlation plot between donor-acceptor interaction energies and red shift of N-H stretching frequencies .....	87
<b>Figure 3.1.10</b> NBO 3D overlap diagrams for $n_{\text{S}} \rightarrow \sigma^*_{\text{NH}}$ donor-acceptor interaction in methionine and cysteine containing peptides .....	88
<b>Figure 3.1.11</b> (a) Left: Amide-N-H $\cdots$ S hydrogen bond in methionine containing protein, Right NBO 3D overlap diagram for $n_{\text{S}} \rightarrow \sigma^*_{\text{NH}}$ donor-acceptor interaction of same protein (b) Left: Amide-N-H $\cdots$ S hydrogen bond in cysteine containing protein, Right NBO 3D overlap diagram for $n_{\text{S}} \rightarrow \sigma^*_{\text{NH}}$ donor-acceptor interaction of same protein.....	89
<b>Figure 3.2.1</b> Protein and nucleic acid examples of amide-N-H $\cdots$ S=C hydrogen bonds .....	94
<b>Figure 3.2.2</b> Model molecular complexes used to study amide-N-H $\cdots$ S and N-H $\cdots$ O H-bonds in biomolecules .....	97
<b>Figure 3.2.3</b> 1D $^1\text{H}$ NMR Spectra of 2-Pyridone at Higher concentration in $\text{CDCl}_3$ solvent ....	100
<b>Figure 3.2.4</b> 1D $^1\text{H}$ NMR Spectra of 2-thiopyridone at Higher concentration in $\text{CDCl}_3$ solvent .....	101
<b>Figure 3.2.5</b> $^1\text{H}$ NMR Spectra of 2-Pyridone with increasing the concentration.....	101
<b>Figure 3.2.6</b> $^1\text{H}$ NMR Spectra of 2-thiopyridone with increasing the concentration.....	102
<b>Figure 3.2.7</b> $^1\text{H}$ -DOSY Plot of (a)2-PY,(b)2-TPY fitting of Stejskal–Tanner equation to the decay of a spectral peak (NH) of 2-PY at lower concentration and higher concentration .....	104
<b>Figure 3.2.8</b> (a) 1:1 binding isotherm fitting in concentration dependent NMR experiment for 2-PY (b) for 2-TPY in $\text{CDCl}_3$ solvent.....	106
<b>Figure 3.2.9</b> (a) Temperature dependent plot of 2-PY and (b) of 2-TPY .....	110

<b>Figure 3.2.10</b> (a) Integration of amide (NH) $^1\text{H}$ NMR peaks of 2-PY with reference of aromatic CH $^1\text{H}$ NMR peak at 5 <sup>th</sup> position and (b) at 3 <sup>rd</sup> position in $\text{CDCl}_3$ over time following the addition of $\text{D}_2\text{O}$ .....	111
<b>Figure 3.2.11</b> (a) Integration of amide (NH) $^1\text{H}$ NMR peaks of 2-TPY with reference of aromatic CH $^1\text{H}$ NMR peak at 5 <sup>th</sup> position and (b) at 3 <sup>rd</sup> position in $\text{CDCl}_3$ over time following the addition of $\text{D}_2\text{O}$ .....	111
<b>Figure 4.1</b> Complete H-bond distance ( $d_{\text{N-H}\cdots\text{Se}}$ ) distribution in Selenomethionine (MSe) containing proteins.....	121
<b>Figure 4.2</b> Two representative examples of amide-N-H $\text{H}\cdots\text{Se}$ hydrogen bonds in proteins .....	122
<b>Figure 4.3:</b> NBO 3D overlap diagram for selenomethionine containing proteins (a) 1W2F (b) 4KRG. ....	124
<b>Figure 4.4:</b> The plots of the reduced density gradient ( $s$ ) versus the sign of the second eigen value of the electron-density Hessian matrix ( $\lambda_2$ ) times electron density ( $\text{sign}(\lambda_2)\rho$ ) for (a) 1w2f and (b) 4krG with the bond critical point (BCP) of amide-N-H $\cdots$ Se hydrogen bond. ....	124
<b>Figure 4.5:</b> Model compounds of biomolecules.....	127
<b>Figure 4.6:</b> LIF spectra of bare 2-PY and 2-PY in presence of DMSe .....	128
<b>Figure 4.7:</b> The mass spectra of NPAA-DMSe and 2c-R2PI spectra of NPAA and NPAA in presence of DMS and DMSe. ....	129
<b>Figure 4.8:</b> Gas phase vibrational spectra of monomer N-phenylacetamide (NPAA) and its H-bond complexes with Selenium and Sulfur. ....	130
<b>Figure 4.9:</b> Gas phase vibrational spectra of monomer 2-pyridone (2-PY) and its H-bond complexes with Selenium and Sulfur acceptors .....	132
<b>Figure 4.10:</b> Optimized structures of N-H $\cdots$ Se and N-H $\cdots$ Te H-bond complexes at RI-B97-D/def2-TZVPP level of theory.....	134
<b>Figure 4.11:</b> Linear correlation plot between vibrational frequencies estimated by DFT and experimental N-H stretching frequencies .....	135
<b>Figure 4.12</b> (a) Left panel: 3D-NCI plot, colored isosurfaces of the reduced electron density gradient and Right panel: Orbital overlap of s- and p-type Se/Te lone pair and N-H $\sigma^*$ orbitals in N-H $\cdots$ Se and N-H $\cdots$ Te H-bonded complexes of 2-PY, NMFA and (b) NPAA at MP2-aug-cc-pVDZ level of theory. ....	136

<b>Figure 4.13</b> Linear correlation plot between donor-acceptor interaction energies ( $E_{DA}$ ) and red shift of N-H stretching frequencies. ....	137
<b>Figure 4.14</b> Linear correlation plot between donor-acceptor interaction energies ( $E_{DA}$ ) and red shift of N-H stretching frequencies ( $\Delta\nu_{NH}$ ) with the geometric mean of atomic charges ( $q$ ) and spherically averaged static square root of polarizability ( $\alpha_{avg}$ ) ( $\sqrt{ q\sqrt{\alpha_{avg}} }$ ) of H-bond acceptor atoms. ....	138
<b>Figure 5.1</b> Piezoelectric materials used in different devices Examples.....	146
<b>Figure 5.2</b> H-bond donors and H-bond acceptors chosen to design Piezoelectric Materials through hydrogen bond .....	147
<b>Figure 5.3</b> (a, d, g) Optimized geometries, (b, e, h) natural bond orbital overlapping and (c, f, i) electron density topologies for PH $\cdots$ NBz, SPH $\cdots$ NBz and SePH $\cdots$ NBz respectively. Bond critical points are shown in red. ....	149
<b>Figure 5.4.</b> Schematic representation for align H-bond vector with the direction of electric field (a) absence of applied electric field and (b) applying the electric field in direction of H-bond vector used in Method B. ....	151
<b>Figure 5.5</b> Linear plots applied electric field vs equilibrium H-bond distance (a)PH-NBz dimer, (b) SPH-NBz dimer, (c) SePH-NBz dimer at B3LYP/6-31G* level of theory. ....	154
<b>Figure 5.6</b> Comparison of piezoelectric coefficients of different hydrogen bonded systems at (a) 6-31G* (b) aug-cc-pVDZ basis sets using B3LYP and PBE0 functionals in both the methods. ....	155
<b>Figure 5.7</b> Correlation between piezoelectric coefficients obtained from different methods. Red dots and line indicates method-C vs method-A, black squares and line indicates: method-B vs method-A; 1-PH-NBz dimer, 2-SPH-NBz dimer, 3-SePH-NBz dimer.....	158
<b>Figure 5.8</b> Correlation graphs (a) the linear correlation between piezoelectric coefficient and dipole moment and (b) dipole moment derivative with respect to geometric displacement.1-PH-NBz, 2-SPH-NBz, 3-SePH-NBz dimers. ....	159
<b>Figure 5.9</b> Correlation graphs (a) the linear correlation between piezoelectric coefficient and isotropic polarizability and (b)polarizability derivative with respect to geometric displacement.1-PH-NBz, 2-SPH-NBz, 3-SePH-NBz dimers. ....	159

<b>Figure 5.10</b> Optimized structure of left panel: Cl-SPH, middle panel: CN-SPH, right panel: CH <sub>3</sub> -SPH with different substituents at para position of NBz dimers at B3LYP/6-31G* level of theory. ....	162
<b>Figure 5.11</b> Optimized structure of left panel: MeO-SPH, right panel: SPH with different substituents at para position of NBz dimers at B3LYP/6-31G* level of theory. ....	163
<b>Figure 5.12</b> Plot showing dependence of calculated piezo-coefficients, $d_{33}$ (pm/V) on binding energy (kJ/mol) for (1) PH-NBz, (2) SPH-NBz, (3) SePH-NBz, (4) SPH-OMe-NBz, (5) SPH-CN-NBz, (6) OMe-SPH-NBz and (7) CN-SPH-NBz. ....	164
<b>Figure 5.13</b> Optimized structures of SPH-NBz tetramers (a) symmetric unit and (b) anti-symmetric unit. ....	165
<b>Figure 6.1.1</b> Frequencies of C...O carbon bond donor-acceptor (a) distances ( $d_{C...O}$ ), (b) $\angle Z-C...O$ , (c) $\angle C...O=C$ C-bond angles in proteins. ....	175
<b>Figure 6.1.2</b> Examples of C-C...O=C C-bond in proteins.....	176
<b>Figure 6.1.3</b> Represents the C-bond formation in (a) protein 5JOV, (b) protein 2O7C, (c) & (d) NBO overlap in 5JOV and 2O7C, respectively. (e) & (f) 3D-NCI plot in 5JOV and 2O7C respectively. ....	177
<b>Figure 6.1.4</b> Plot showing the percentage distribution of amino acids involved in C-bonds as donor and acceptor residues.....	178
<b>Figure 6.1.5</b> Histograms representing the percentage distribution of amino acids involved in C-bonds as C-bond acceptor and donor. ....	178
<b>Figure 6.1.6</b> Percentage distribution plot for different type of C-bond donors and acceptors in proteins.....	180
<b>Figure 6.1.7</b> Histogram plot showing percentage location of C-bond acceptor and donor residues in various secondary structures of the proteins.....	181
<b>Figure 6.1.8</b> Ramachandran plots for (a) C-bond donor amino acid residues (b) C-bond acceptor residue.....	181
<b>Figure 6.1.9</b> Representative model compounds of proteins Left: Six different types of C-bond donors, Middle: amide-C=O type of C-bond acceptor, Right: type of C-bond formation. ....	184

- Figure 6.1.10** Represents the bond critical point between O and C along the Z-C···O=C C-bond (a) NNDMA-ACN, (b) NNDMA-NM, (c) NNDMA-ALA, (d) NNDMA-AA, (e) NNDMA-AcetylCl and (f) NNDMA-TFACE. ....186
- Figure 6.1.11** Represents the orbital overlap between oxygen lone pair ( $n_O$ ) and the Z-C antibonding sigma orbital ( $\sigma^*_{Z-C}$ ) of (a) NNDMA-ACN, (b) NNDMA-NM, (c) NNDMA-ALA, (d) NNDMA-AA, (e) NNDMA-AcetylCl and (f) NNDMA-TFACE. ....187
- Figure 6.1.12** Represents the molecular electrostatic potential map of (a) NNDMA-ACN, (b) NNDMA-NM, (c) NNDMA-ALA, (d) NNDMA-AA, (e) NNDMA-AcetylCl and (f) NNDMA-TFACE.....188
- Figure 6.1.13** Represents the colored isosurfaces of reduced electron density gradient in 3D real space for (a) NNDMA-ACN, (b) NNDMA-NM, (c) NNDMA-ALA, (d) NNDMA-AA, (e) NNDMA-AcetylCl and (f) NNDMA-TFACE.....189
- Figure 6.1.14**  $^{13}\text{C}$  NMR spectra for (a) only NNDMA monomer (b) NNDMA-ACN complex .....191
- Figure 6.1.15**  $^{13}\text{C}$  NMR spectra for (a) downfield shift for  $^{13}\text{C}_{\text{CN}}$  (b) upfield shifts for  $^{13}\text{C}_{\text{CH}_3}$  (c)  $^{13}\text{C}$  NMR spectra for ACN only (D)  $^{13}\text{C}$  NMR spectra for NNDMA-ACN complex.....191
- Figure 6.1.16 (a)** Chemical shift of the  $^{13}\text{C}_{\text{CO}}$  peak of NNDMA as a function of concentration of ACN **(b)** Chemical shift of the  $^{13}\text{C}_{\text{CN}}$  peak of ACCN as a function of concentration of NNDMA, **(c)** Chemical shift of the  $^{13}\text{C}_{\text{CH}_3}$  peak of ACN as a function of concentration of NNDMA.....196
- Figure 6.1.17** IR Spectra of vibrational stretching absorption peak for (a) C=O (b) CN with increase of concentration of ACN and NNDMA respectively. ....198
- Figure 6.1.18** Correlation plots between redshifts in IR and downfield chemical shifts in NMR, (a) for C=O (b) for CN in NNMDA-ACN complex.....198
- Figure 6.1.19 (a)** The exponential correlation plot between carbon bond energies ( $D_0$ ) obtained at CCSD-T level and donor-acceptor interaction energies ( $E_{\text{DA}}$ ) of model C-bond complexes. **(b)** The exponential correlation plot between the donor-acceptor energies ( $E_{\text{DA}}$ ) of model C-bond complexes and proteins and C···O bond distances.....200
- Figure 6.1.20** Distribution of different forces (electrostatic (ES), polarization (POL), repulsion (REP), and exchange (EX) and dispersion energy (DISP)) contributing to the intermolecular attraction in NNDMA-ACN C-bond complex.....201
- Figure 6.1.21 (a)** Correlation plot between percentage of dispersion energy contribution and C···O distance in model compounds (b) Distribution of estimated binding energies and

percentage of dispersion energy contribution along the C...O distances at CCSD-T level in proteins. The number in plot represents the model complexes shown in Table 6.1.6. ....202

**Figure 6.1.22** Representative examples of implication of C-bonds in protein structure and function Z-C...O=C C-bonds observed in (a) C-C...O=C C-bond in myoglobin (PDB: 5CNB) (b) N-C...O=C C-bonds in ribosome-inactivating protein (PDB: 1MRJ) (c) Potential energy scan of energy differences ( $E-E_e$ ) over the change in C...O C-bond distances( $r-r_e$ ).....204

**Figure 6.2.1** Top: Represents the C-bond acceptors and Bottom: C-bond donors. ....208

**Figure 6.2.2** Optimized stable structures of C-bond complexes between N-oxides/N-sulfides and acetonitrile and nitromethane at B97D/aug-cc-pVDZ level of theory.....210

**Figure 6.2.3** Left side: Electron density topologies for all the N-oxide complexes, Right side: for all N-Sulfide complexes with ACN and NM.....213

**Figure 6.2.4** Linear correlation plots between X...C C-bond distances and (a) electron density  $\rho(r)$ , (b) Laplacian electron density  $\nabla^2\rho(r)$  for N-oxide complexes. (c) and (d) electron density  $\rho(r)$  and Laplacian of electron density  $\nabla^2\rho(r)$  for N-sulfide complexes, respectively.....215

**Figure 6.2.5** Natural bond orbital overlap diagrams between O or S lone pair orbital ( $n$ ) in N-oxides or N-sulfides and antibonding sigma orbital ( $\sigma^*$ ) of C-C in ACN or C-N in NM complexes. ....216

**Figure 6.2.6** Linear correlation plots between donor-acceptor interaction energies and carbon distances (O/S...C) in (a) N-oxide complexes with ACN and NM (b) N-sulfide complexes with ACN and NM.....217

**Figure 6.2.7** MESP plots represents N-C...O/S-N and C-C...O/S interaction .....217

**Figure 6.2.8** (a) Linear correlation plot between potential energy difference on C atom in ACN C-bond complexes, (b) in NM C-bond complexes with both N-oxides and N-sulfides.....219

**Figure 6.2.9** Linear correlation plot between potential energy difference on O/S atom in acyclic (aliphatic), five membered and six membered C-bond complexes.....220

**Figure 6.2.10** Represents the contribution of different interactions electrostatic (ES), polarization (PL), repulsion (REP), and exchange (EX)) to the stabilization energy (CCSD-T/CBS) for ACN complexes with N-oxides and N-sulfides.. ....221

**Figure 6.2.11** Represents the contribution of different interactions electrostatic (ES), polarization (PL), repulsion (REP), and exchange (EX)) to the stabilization energy (CCSD-T/CBS) for NM complexes with N-oxides and N-sulfides. ....222

## List of Tables

<b>Table 3.1.1</b> Computed binding energy ( $D_0$ in kJ/mol) at CCSD(T)/aug-cc-pVDZ and in parenthesis red shift of N-H stretching frequency ( $\Delta\nu$ in $\text{cm}^{-1}$ ) for N-H $\cdots$ S, N-H $\cdots$ O=C, N-H $\cdots$ O and N-H $\cdots\pi$ H-bond complexes .....	84
<b>Table 3.2.1</b> Donor-Acceptor Interaction Energies ( $E_{DA}$ ) obtained from NBO Aanalysis at MP2/aug-cc-pVDZ level in biomolecules .....	95
<b>Table 3.2.2</b> The geometrical parameters hydrogen bond distance ( $d_{H\cdots O}$ ), angles and hydrogen bond enthalpies for H-Bond complexes optimized at B97D-SMD( $\text{CHCl}_3$ )/aug-cc-pVDZ level..	98
<b>Table 3.2.3.</b> Chemical shift values obtained 2-pyridone and 2-thiopyridone at different concentrations in concentration dependent NMR titration experiments.....	102
<b>Table 3.2.4.</b> Experimental and Computational thermodynamic parameters of 2-pyridone and 2-thiopyridone dimer. Here $\Delta G$ , $\Delta H$ , $\Delta S$ and $\Delta E$ are change in Gibbs free energy, change in enthalpy, change in entropy and change in internal energy of dimer formation respectively. For the concentration dependent studies, the computed entropies are considered to estimate the $\Delta H$ values .....	107
<b>Table 4.1</b> Computed binding energy ( $D_0$ in kJ/mol) at CCSD(T)/aug-cc-pVDZ , red shift of N-H stretching frequency ( $\Delta\nu$ in $\text{cm}^{-1}$ ), and donor-acceptor interaction energies ( $E_{DA}$ in kJ/mol)) for N-H $\cdots$ Y (Y= O, S, Se, and Te) and N-H $\cdots$ O=C H-bond complexes	135
<b>Table 5.1</b> Binding energies and Donor-acceptor interaction energies of -H $\cdots$ O H-bond systems at B3LYP/6-31G* level .....	148
<b>Table 5.2</b> The piezoelectric coefficients at method A and method B, equilibrium H-bond distance, second derivative of potential energy and derivative of dipole moment of different H-bond systems at B3LYP functional with 6-31G* and aug-cc-pVDZ basis sets. ....	152
<b>Table 5.3</b> The piezoelectric coefficients at method A and method B, equilibrium H-bond distance, second derivative of potential energy and derivative of dipole moment of different H-bond systems at PBE0 functional with 6-31G* and aug-cc-pVDZ basis sets. ....	152
<b>Table 5.4</b> The piezoelectric coefficients at method A and method B, equilibrium H-bond distance, second derivative of potential energy and derivative of dipole moment of different H-bond systems at $\omega$ B97XD functional with 6-31G* and aug-cc-pVDZ basis sets. ....	153

<b>Table 5.5</b> The piezoelectric coefficients at method C and Isotropic molecular polarizability for X-H•••O H-bond dimers at B3LYP/6-31G* level of theory. ....	157
<b>Table 5.6</b> Estimated piezoelectric coefficients (pm/V) of different substituents at para position of SPH-NBz dimer. ....	161
<b>Table 5.7</b> Binding energies and donor-acceptor interaction energies of different substituents at para position of SPH-NBz dimer. ....	161
<b>Table 6.1.1</b> Contribution of different type of O-atom as acceptor, type of Z-C bond as donor and different type of secondary structures of C-bond acceptor, donor residues in C-Bond.....	179
<b>Table 6.1.2</b> The values of carbon bond distance (d), the donor-acceptor interaction energies ( $E_{DA}$ ), in kJ/mol at MP2/aug-cc-PVDZ level of theory in proteins. ....	182
<b>Table 6.1.3</b> The values of carbon bond distance (d), the donor-acceptor interaction energies ( $E_{DA}$ ), and Electron density, $\rho(r)$ , and Laplacian of electron density, $\nabla^2\rho(r)$ at MP2/aug-cc-pVDZ level of theory and computed binding energies ( $\Delta E$ ) at CCSD-T/aug-cc-pVDZ level. ....	185
<b>Table 6.1.4</b> The chemical shift ( $\delta$ ) values of $^{13}\text{C}=\text{O}$ of NNDMA and $^{13}\text{CN}$ of ACN at different concentrations of ACN and NNDMA, respectively. [NNDMA] and [ACN] are the concentrations of N,N-dimethylacetamide and acetonitrile, respectively. Titration 1: [NNDMA] kept constant varying the [ACN]. Titration 2: [ACN] kept constant varying the [NNDMA]....	192
<b>Table 6.1.5</b> The vibrational frequency ( $\nu$ ) values for C=O of NNDMA and CN of ACN at different concentrations of ACN and NNDMA, respectively. $\Delta\nu$ values are the red shift values of for for C=O of NNDMA and CN of ACN.....	197
<b>Table 6.1.6</b> The localized molecular orbital energy decomposition analysis (LMOEDA) for Model C-bond complexes The individual components electrostatic (ES), polarization (POL), repulsion (REP), and exchange (EX) are at MP2/aug-acc-pVDZ level and dispersion energy and % of distribution energy contributing to the total binding energy at CCSD-T level. (all values are in kJ/mol). ....	201
<b>Table 6.2.1</b> C-bond stabilization energies at different levels of theory, the geometrical parameters C-bond bond distances, bond angles for all C-bond complexes.....	211
<b>Table 6.2.2</b> Electron density $\rho(r)$ , Laplacian of electron density $\nabla^2\rho(r)$ , Carbon bond energy ( $E_{BCP}$ ) at bond critical point and donor-acceptor interaction energy ( $E_{DA}$ ) of various complexes. ....	214
<b>Table 6.2.3</b> Potential energy differences on C atom ( $\Delta V_C$ ), on O atom ( $\Delta V_O$ ), on S atom ( $\Delta V_S$ ) in all the C-bond complexes in kJ/mol.....	219

## List of abbreviations

AIM	Atoms in molecules
AcetylCl	Acetyl chloride
ACN	Acetonitrile
ALA-	Alanine
au	Atomic units
aug	Augmented
BCP	Bond critical point
BE	Binding energy
BSSE	Basis set superposition error
B97D	Becke 97-D, Grimme's functional including dispersion
B3LYP	Becke, three-parameter, Lee-Yang-Parr
Bz	Benzene
CBS	Complete basis set
cc	Correlation consistent
CCSD	Coupled Cluster Single Double
CCSD(T)	Coupled Cluster Single Double Triple
DEE	Diethyl ether
DFT	Density functional theory
DME	Dimethyl ether
DMF	Dimethyl formamide
DMS	Dimethyl sulfide
DMS <sub>e</sub>	Dimethyl selenide
DMTe	Dimethyl telluride
EDA	Donor-acceptor interaction energy
EDG	Electron donating group
EmNO	N-methylenemethanamine
ES	Electrostatic energy
EtOH	Ethanol
EtSH	Ethane thiol
EWG	Electron withdrawing
EX	Exchange
FC	Franck-Condon
FDIR	Fluorescence dip infrared spectroscopy
HB	Hydrogen bond
HAT	Horizontal attenuated total reflection
HF	Hartee-Fock
IR	Infrared
ImNO	1H-imidazole-3-oxide
LIF	Laser induced fluorescence

LMOEDA	Localized molecular orbital energy decomposition analyses
lp	Lone pair
MeOH	Methanol
MESP	Molecular electrostatic potential
MP2	2nd order Moller–Plesset perturbation theory
NBO	Natural bond orbital
NBz	Nitrobenzene
NCI	Noncovalent interaction
NMA	N-methyl acetamide
NMFA	N-methyl formamide
NNDMA	N,N-dimethyl acetamide
NNDMTA	N,N-dimethyl thioacetamide
NMR	Nuclear Magnetic Resonance
NMTA	N-methyl thioacetamide
NPAA	N-phenylacetamide
OPO	Optical parametric oscillator
PBE	Perdew-Burke-Ernzerhof
PDB	Protein data bank
PH	Phenol
PMT	Photomultiplier tube
PNO	Pyridine-N-oxide
PY	Pyridone
QTAIM	Quantum theory of atoms in molecule
REMPI	Resonantly enhanced multiphoton ionization
RIDIR	Resonant ion depletion by infrared
R2PI	Resonant 2-photon ionization
SCRF	Self-Consistent Reaction Field
SMD	Solvation Model based on Density
THT	Tetrahydrothiophene
TMA	Trimethylamine
TPY	Thiopyridone
TOFMS	Time-of-flight mass spectrometer
YAG	Yttrium aluminum garnet
ZPE	Zero point energy

# Introduction

---

## Chapter 1

### Introduction

This thesis mainly focuses on exploring the unusual non-covalent interactions at the molecular level using a combined experimental and computational approach. The sulfur and selenium-centered hydrogen bonds (SCHB or SeCHB) and carbon bonds (C-bond) in biomolecules are investigated in detail. Hydrogen bond is a class of non-covalent interactions that have been studied for more than a century owing to its importance and implications in almost all fields of sciences, may it be structural biology, medicinal chemistry, material sciences or any branch of chemistry. Non-covalent interactions are the attractive or repulsive interactions between two atoms or molecules. This type of interaction was first discovered by a Dutch scientist van der Waals in 1873. The van der Waals forces are the sum of attractive interactions i.e. dipole-dipole (Keesom interaction), dipole-induced dipole (Debye interaction) and dispersion interactions (London forces) and repulsive interaction. This was experimentally supported by H. Kamerlingh-Onnes in 1908.<sup>2</sup> Later on London,<sup>3</sup> Hellman<sup>4</sup> and Hirschfelder<sup>5</sup> interpreted these interactions in different ways for the sake of basic understanding. These interactions have great importance in supramolecular chemistry,<sup>6</sup> chemical engineering,<sup>7</sup> material chemistry<sup>8</sup> and biological sciences such as molecular recognition,<sup>9</sup> biomolecular ion transport and regulation mechanisms<sup>10</sup>.

The non-covalent interactions are fundamentally different than the covalent bonds in many ways viz. (i) covalent bonds are formed when there is an overlap between two subsystems with unfilled electronic orbital whereas non-covalent interactions are non-bonding interactions; (ii) most of the covalent bond lengths are within 0.74-2.5 Å whereas the noncovalent interactions

## Introduction

---

can be extended to the sum of the van der Waals radii of the interacting atoms. Non-covalent interactions denoted by R-D $\cdots$ A-Z, are defined as the attractive forces between two subunits R-D and A-Z of different (intermolecular) or same (intramolecular) molecules where, D is an electrophilic (electron deficient) atom of the R-D covalent bond and A is the nucleophilic atom (electron rich) of same or different molecular fragment. The non-covalent interactions are pictorially represented by three dots ( $\cdots$ ) whereas the same is given by a short line (-) in case of covalent interactions. The noncovalent interactions are named according the donor atom, e.g. in a D $\cdots$ A bond, if D belongs to hydrogen, halogen, pnicoen, chalcogen and tetrel families then the bond is called hydrogen bond, halogen bond,<sup>11-18</sup> pnicoen bond,<sup>19-21</sup> chalcogen bond<sup>22-26</sup> and tetrel bond<sup>27-30</sup>, respectively. These bonds have found many applications such as protein folding,<sup>31</sup> protein-ligand binding,<sup>32,33</sup> molecular assembly<sup>34,35</sup>, drug discovery<sup>32</sup> and nanotechnology etc.<sup>36</sup>

### 1.1 Hydrogen bonds and their classifications:

In 1912, T. S. Moore and T. F. Winmill found such interactions in the aqueous solution of amines and termed it as “weak union”.<sup>37</sup> Later in 1920 the description of hydrogen bond (H-bond) in water was given by Huggins, Latimer and Rodebush.<sup>38</sup> In 1935, the name ‘hydrogen bond’ was given by Pauling<sup>39</sup> for the first time. In 1960, Pimentel and McClellan<sup>40</sup> came up with a definition of H-bond which states that “*A hydrogen bond is said to exist when (1) there is evidence of a bond and (2) there is evidence that this bond sterically involves a hydrogen atom already bonded to another atom*”. In the year of 2011, the International Union of Pure and Applied Chemistry (IUPAC) Committee recommended a new definition of hydrogen bond based on both experimental and theoretical evidences.<sup>41</sup> The IUPAC definition of Hydrogen bond is “*the hydrogen bond is an attractive interaction between a hydrogen atom from a molecule or a*

## Introduction

---

*molecular fragment X-H in which X is more electronegative than H, and an atom or a group of atoms in the same or a different molecule, in which there is evidence of bond formation.”*

For the formation of X-H $\cdots$ Y H-bond, six criteria are to be satisfied which can be summarized as

(1) The X-H $\cdots$ Y bond angle is usually linear, the more linear it is, the shorter the H $\cdots$ Y distance and the stronger the H-bond.

(2) The length of the X-H bond increases upon hydrogen bond formation leading to a red shift in the X-H stretching frequency and an increase in the infrared absorption cross-section for the X-H stretching vibration. With the formation of the new H $\cdots$ Y contact, new vibrational modes are generated.

(3) X-H $\cdots$ Y hydrogen bond leads to pronounced deshielding of H observed in the X-H bond in NMR, through hydrogen bond spin-spin couplings between X and Y.

(4) The  $pK_a$  of X-H and the  $pK_b$  of Y-Z in a given solvent correlate strongly with the energy of the H-bond formed between them.

(5) The forces involved in the formation of a hydrogen bond may be electrostatic in origin, or dispersive, or may arise from charge transfer between donor and acceptor atoms or groups or a combination of them.

(6) For the formation of hydrogen bond, Gibbs free energy should be greater than the thermal energy of the system for a hydrogen bond to be detected experimentally.

It was believed that H-bond donor, X and acceptor, Y in X-H $\cdots$ Y hydrogen bond, are electronegative atoms such as N, O, F. But it has been proved that the H-bond donor and/or acceptor can be of low electronegativity such as C, P, S, Se, Te. Based on these, H-bond is

## Introduction

---

classified into two groups. The former is called Conventional H-bond whereas the later is called Non-conventional or Unusual H-bond.<sup>42</sup> The conventional hydrogen bonds *viz.* O-H $\cdots$ O, N-H $\cdots$ O, N-H $\cdots$ N, O-H $\cdots$ F, O-H $\cdots$ O=C, N-H $\cdots$ O=C are found to be important in structure determination of proteins, molecular assembly of supramolecular chemistry, designing the drugs in medicinal chemistry, and crystal engineering.<sup>42-50</sup> The weak interactions play a very crucial role in determining the structures of biomolecules and hence their selectivity and functions. The experimental and computational studies over the years were carried out to understand the existence and strengths of the weak hydrogen bonds or non-conventional hydrogen bonds such as C-H $\cdots$ O, C-H $\cdots$ N, C-H $\cdots$  $\pi$ , S-H $\cdots$ O, N-H $\cdots$ S, S-H $\cdots$  $\pi$ , O-H $\cdots$ S and M-H $\cdots$ O.<sup>42,47,51-61</sup>

### 1.1.1 Sulfur centered hydrogen bond (SCHB):

Sulfur centered hydrogen bond (SCHB) is a kind of non-conventional hydrogen bond where sulfur acts as a hydrogen bond donor or acceptor. Sulfur possesses lower electronegativity (2.58 according to Pauling scale) but higher van der Waals radius than those of first row elements. Sulfur is present as thiols, thioether in amino acids, as disulfide bridging between peptide chains, in plants as organic sulfur, in lower living body as inorganic sulfur (in iron-sulfur proteins). It is being used as fertilizer in agricultural field and also being used for medicinal purpose as antibiotics (penicillins, thionucleosides etc.).<sup>62,63</sup> Sulfur has the potential to act as hydrogen bond acceptor as well as donor in the formation of intermolecular and intramolecular hydrogen bonds. The sulfur containing amino acids methionine (Met) and cysteine (Cys) play a crucial role in stabilization of protein structure where Met acts as a H-bond acceptor and Cys acts as both H-bond donor and H-bond acceptor in proteins.<sup>64,65</sup> The intermolecular X-H $\cdots$ S hydrogen bonds (X = O, N and S) have been observed in organic crystals<sup>66-68</sup> and simple

## Introduction

---

molecular complexes<sup>69-75</sup>. A brief review of the previous experimental and computational reports on the SCHB is discussed in the following sections.

### 1.1.1.a Sulfur as a H-bond donor

Water (H<sub>2</sub>O) shows an extensive network of intermolecular hydrogen bonding. The structures of H<sub>2</sub>O and H<sub>2</sub>S are similar and have same symmetry. Computational studies were carried out to investigate the hydrogen bond in hydrogen sulfide (H<sub>2</sub>S) dimer in which S-H can act as hydrogen bond donor as well as acceptor. The S-H···S hydrogen bond energy is 0.71 kcal/mol<sup>76</sup> in H<sub>2</sub>S dimer which is much smaller than O-H···O hydrogen bond energy in water dimer, 5.3 kcal/mol<sup>77</sup>. There are some experimental evidences for the structure and strength of S-H···S hydrogen bond in H<sub>2</sub>S dimer.<sup>78-81</sup> Infrared matrix isolation experimental studies were performed to investigate S-H···S H-bond (SCHB) interaction in H<sub>2</sub>S dimer in solid N<sub>2</sub>, O<sub>2</sub>, and inert gas matrices.<sup>78-81</sup> But S-H stretching frequencies in the H<sub>2</sub>S dimer found from this experiment was not reliable. Later on Bhattacharjee et al<sup>82,83</sup> studied the existence and strength of S-H···X (X = S, O) hydrogen bond in 1:1 complexes of H<sub>2</sub>S dimer, H<sub>2</sub>S-MeOH (MeOH=methanol), H<sub>2</sub>S-DEE (DEE= diethylether), H<sub>2</sub>S-DBE (DBE=dibutylether), and H<sub>2</sub>S-DO (DO=dioxane) using the supersonic expansion method and gas phase IR spectroscopy. They found the binding energies of H<sub>2</sub>S dimer and H<sub>2</sub>O dimer -0.97 kcal/mol, -3.04 kcal/mol at CCSD-T complete basis set limit, respectively.<sup>82</sup> They provided the exact spectral assignment of symmetric stretching and asymmetric stretching frequencies ( $\nu_1$ ,  $\nu_3$ ) of S-H bond in H<sub>2</sub>S dimer. The S-H stretching frequency in H<sub>2</sub>S dimer shifts bathochromically and the shift value increases with the increase of proton affinities of acceptor in the similar way of stronger hydrogen bond donors, O-H and N-H. The acid-base formalism is followed by hydrogen bonds in H<sub>2</sub>S complexes and hydrogen bonds are largely stabilized by dispersion energy. Microwave

## Introduction

---

spectroscopy and quantum chemical calculations were carried out by Cabalciro-Lag et al.<sup>84</sup> to investigate SCHB in methanethiol dimer and trimer. They observed that in methanethiol dimer C-H $\cdots$ S interactions are predominant in strength than S-H $\cdots$ S interactions but in the case of trimer of methanethiol S-H $\cdots$ S hydrogen bond is dominant over the C-H $\cdots$ S interaction. They also noticed that five structures (of same energy) are there on the minima of potential surface while one structure was found in case of methanol dimer and trimer.<sup>85</sup> From matrix isolation-IR spectroscopy and computational studies Grzechnik K. et al. reported<sup>86</sup> that the S-H $\cdots$ N hydrogen bond in CH<sub>3</sub>SH-NH<sub>3</sub> complex is weaker than the O-H $\cdots$ N hydrogen bond in CH<sub>3</sub>OH-NH<sub>3</sub> complex.

The intermolecular and intramolecular X-H $\cdots$  $\pi$  interactions between X-H and aromatic rings play important role in molecular recognition.<sup>87</sup> The statistical survey was done on interaction between S atom and aromatic systems in proteins and lot of interactions were found.<sup>88</sup> Rotational spectroscopic study suggested that S-H $\cdots$  $\pi$  interaction in simple model of H<sub>2</sub>S-benzene complex is stronger than the O-H $\cdots$  $\pi$  interaction in H<sub>2</sub>O-benzene complex.<sup>89</sup> Biswal et al.<sup>90</sup> reported the S-H $\cdots$  $\pi$  interaction in complexes of indole (IND) and 3-methyl indole (3MI) with H<sub>2</sub>S for the first time using the gas phase UV-IR spectroscopy and computational calculations and compared the results with the O-H $\cdots$  $\pi$  interaction. The S-H $\cdots$  $\pi$  interaction was observed in complexes of H<sub>2</sub>S with hydrogen facing towards aromatic ring of indole and 3-methyl indole. It was confirmed by no shift in the N-H stretching frequency of IND and 3MI from their monomer, at the same time ruling out the possible formation of the N-H $\cdots$ S H-bond that is usually accompanied by the red shift of the N-H stretching frequency. But in case of H<sub>2</sub>O, N-H $\cdots$ O hydrogen bond was formed instead of O-H $\cdots$  $\pi$  in IND-H<sub>2</sub>O and 3MI-H<sub>2</sub>O complexes where oxygen acts as hydrogen bond acceptor. The experimental and computational reports

## Introduction

---

revealed S-H $\cdots\pi$  interaction is much stronger than the conventional N-H $\cdots\pi$ , O-H $\cdots\pi$  interactions which is due to significant contribution of dispersion energy. Zondlo N. J. and coworkers<sup>91</sup> investigated the nature of S-H $\cdots\pi$  interaction in the crystal structure of Boc-L-4-thiophenylalanine tert-butyl ester by DFT calculations, in solution state with IR spectroscopy, solid state with solid-state NMR spectroscopy and analysis of the X-ray crystallography. The S-H $\cdots\pi$  H-bond in those is more dispersive than other X-H $\cdots\pi$  (X=N, O) H-bonds. Hydrogen sulfide and thiols are constituents of cysteine amino acid in proteins. Cysteine can act as a hydrogen-bond donor and/or acceptor forming S-H $\cdots\pi$  and N-H $\cdots$ S hydrogen bonds in proteins.<sup>65</sup>

### 1.1.1.b Sulfur as Hydrogen bond acceptor

The sulfur atom is a potential H-bond acceptor, comparable to conventional N, O H-bond acceptors. Methionine is one of the sulfur containing amino acid that can form a variety of X-H $\cdots$ S H-bonds. It forms intermolecular and intramolecular sulfur centered hydrogen bond with back bone amide N-H and side chain of other amino acids in peptides and proteins. From the crystallography data base analysis it has been found that there are abundances of X-H $\cdots$ S (X = N, O atoms) H-bonds in proteins and organic molecules.<sup>92,93</sup> The computational and spectroscopic investigations were performed to understand the nature and the strength of O-H $\cdots$ S hydrogen bonds in 1:1 molecular complex.<sup>94-104</sup> The results obtained show that S forms stronger O-H $\cdots$ S H-bond in some cases and weaker H-bond in other cases. But it did not give any clear information regarding the behavior of S as hydrogen bond acceptor. Further S. Wategaonker and co-workers studied the molecular complexes using the supersonic jet expansion method and resonant ion depletion infrared spectroscopy.<sup>70,72,74,75</sup> They took model

## Introduction

---

molecular complexes of dimethyl sulfide (DMS) as methionine constituent and phenol, p-cresol, and 2-naphthol as tyrosine constituents and proved the existence of O-H $\cdots$ S hydrogen bond in those model compounds. The stretching frequency of O-H in O-H $\cdots$ S hydrogen bond is red shifted with respect to its monomers (hydrogen bond donors) and the magnitude of red shift is comparable to O-H $\cdots$ O hydrogen bonded complexes. This proves that the strength of O-H $\cdots$ S hydrogen bond is as strong as O-H $\cdots$ O hydrogen bond. Similar studies were done to investigate the nature and strength of O-H $\cdots$ S bond in the complexes of p-cresol as a hydrogen bond donor and geometrically similar molecules like H<sub>2</sub>O, H<sub>2</sub>S, DMS, DME, MeOH, MeSH, EtOH, and EtSH as acceptors.<sup>74,75</sup> From these studies they concluded that the O-H stretching frequency in p-CR.DMS is more red shifted from its monomer p-CR than that in p-CR.DME. The more red shift in O-H stretching frequency confirms the stronger O-H $\cdots$ S hydrogen bond in thioether (better H-bond acceptor) complexes than O-H $\cdots$ O hydrogen bond in the ether complexes. The O-H $\cdots$ O interaction energy in alcohols/cyclic ether complexes with p-CR is higher than the O-H $\cdots$ S interaction energy in thiols/cyclic thioether complexes. In alcohols and thiols the H-bond energy is increasing with increasing the chain length of the acceptor. Finally, they revealed that the dispersion energy has more contribution to the total binding energy and is important to sulfur centered hydrogen bond. Bhattacharyya et al. inferred that SCHB follows acid-base formalism like O-H $\cdots$ O hydrogen bond by correlating the gas phase basicity (PA) of several H-bond acceptors (H<sub>2</sub>S, DMS, MeSH, and THT (tetrahydrothiophen)) with the red shifts of O-H stretching frequency of p-fluorophenol (H-bond donor) upon complex formation.<sup>69</sup> Recently Ghosh S. et al.<sup>105</sup> measured the dissociation energy of O-H $\cdots$ S hydrogen bond by zero electron kinetic energy (ZEKE) photoelectron spectroscopy. The dissociation energies of the SCHB in complexes of phenol-H<sub>2</sub>S, p-cresol-H<sub>2</sub>S complexes were 3.15 and 3.31 kcal·mol<sup>-1</sup> in the ground

## Introduction

---

state and 11.97 and 11.28 kcal.mol<sup>-1</sup> in the cationic state, respectively. These are two times weaker in ground state and 1.5 times in the cationic state than the O–H···O hydrogen bond strengths. A few reports of crystal data analysis and *ab initio* calculation explored the existence and strength C–H···S hydrogen bond where sulfur acts as a poor hydrogen bond acceptor than conventional acceptors (O, N).<sup>106,107</sup>

The conventional hydrogen bond donor amide N–H is present in the proteins and nucleotides. Many experimental and computational studies were done on conventional interactions N–H···N, N–H···O and it has been found that the strong H-bonds are formed in all cases.<sup>47,48,59,93,108-111</sup> Sulfur is one of the biological abundant elements and there is a debate whether S acts as a strong H-bond acceptor or not. Biswal et al. studied N–H···S hydrogen bond for the first time with the combination of experimental and computational methods.<sup>73</sup> They recorded the gas phase IR spectra of hydrogen bonded complexes of indole (IND) with different H-bond acceptors such as dimethyl ether (DME), DMS, H<sub>2</sub>O, and benzene. The red shift of N–H frequency of N–H···S hydrogen bond in IND–DMS complex is higher than N–H···O H-bonds formed in the complex of IND with DME, H<sub>2</sub>O and N–H··· $\pi$  H-bond in IND–benzene complex. The higher red shift value indicates stronger N–H···S H-bond than the other interactions. Further they calculated the binding energies of complexes at MP2/CBS level computationally. They accounted the dominating dispersion energy in the total interaction energy for the behavior of a “ $\sigma$ -type” N–H···S H-bond like a “ $\pi$ -type” bond. Later on Michel Mons and coworkers<sup>71</sup> studied the strength of N–H···S H-bonds in peptides using UV-IR double resonance spectroscopy. They have chosen N-acetyl-L-phenylalaninyl-L-methionine-amide (FM) and N-acetyl-L-methioninyl-L-phenylalanine-amide (MF) capped peptides for their experiment and compare the N–H···S H-bonds with other H-bonds present in those peptides. The methionine S can form an intra-residue

## Introduction

---

cyclic six membered ( $C_6$ ) N-H $\cdots$ S H-bond with its own residue or inter  $C_7$ ,  $C_{10}$  N-H $\cdots$ S H-bonds with “i” and “i+1” residues, respectively. The intra-residue N-H $\cdots$ S H-bonds were observed in these two peptides and they were found to be the strongest among all other N-H $\cdots$ O=C, and N-H $\cdots$  $\pi$  H-bonds. Alauddin et al.<sup>112</sup> studied the IR spectra of N-H $\cdots$ S H-bond in two dipeptides containing phenylalanine-cysteine/serine capped dipeptides such as Ac-Phe-Cys-NH<sub>2</sub> (FC), Ac-Cys-Phe-NH<sub>2</sub> (CF), Ac-Phe-Ser-NH<sub>2</sub> (FS) and Ac-Ser-Phe-NH<sub>2</sub> (SF). They have observed from the gas phase IR spectra that the N-H $\cdots$ S H-bond in Cys containing dipeptides are weaker in strength than the O-H $\cdots$ O H-bond in serine containing dipeptides.

Thioamides are analogues of amides and they play crucial roles in structure and function of biomolecules and many other supramolecules.<sup>113-121</sup> The experimental and computational studies were carried out on hydrogen bond formation between the thioamide N-H as hydrogen bond donor and different H-bond acceptors (N, O, and S)<sup>114,117</sup> The results obtained inferred that the thioamide-NH can act as a good hydrogen bond donor than amide-NH but it is a poor hydrogen bond acceptor in the dimer of formamide (FA) and thioformamide (TFA).<sup>117</sup> The IR, near infrared (NIR) and NMR spectroscopy and computational studies<sup>114</sup> were done to investigate the existence and strength of hydrogen bond between simple model compounds like thioacetamide (TA) which acts as a H-bond donor and formamides [e.g; dimethyl formamide (DMF), diethyl formamide (DEF), diisopropylformamide (DIF)], acetamides [e.g; dimethylacetamide (DMA), diethylacetamide (DEA), diisopropylacetamide (DIA)] which act as H-bond acceptors. The enthalpy change of hydrogen bond formation in thioamide-acetamide 1:1 complexes increases with increasing the bulkiness of the alkyl group attached with the amide nitrogen but there is no change in case of thioamide-formamide complexes. It has been found that the hydrogen bond formation is stronger via the H syn to the sulfur atom of TA in the

## Introduction

---

formamide complexes than acetamide complexes. Culik R. M et al. identified the hydrogen bond formation of thioamide with backbone amide-N-H in proteins where the former acts as H-bond acceptor and the latter acts as H-bond donor. However, they found that thioamide is a weaker H-bond acceptor.<sup>118</sup> Recently Raines<sup>121</sup> and co-workers observed that thioproline (Pro<sup>S</sup>) insertion stabilizes the collagen triple helix while incorporation of Gly<sup>S</sup> destabilizes it. These reports seem not to be sufficient to understand the strength of SCHB disputing with conventional H-bonds. The clear understanding of SCHB is needed at molecular level in both isolated and solution states.

### 1.1.2 Selenium Center Hydrogen Bonds (SeCHBs)

Selenium is the fourth row element in the periodic table having electronegativity of 2.55 (Pauling scale) that is similar to that of carbon. It was discovered in 1817 by Swedish chemist Jöns Jacob Berzelius. The review article<sup>122</sup> by Reich and Hondal gives information about the important discoveries in biological processes with the replacement of sulfur with selenium. Selenocysteine is the 21<sup>st</sup> amino acid in mammalian selenoproteins.<sup>123,124</sup> Sunoj and coworkers in a review<sup>125</sup> explained the capability of selenium to form non-covalent bond in organoselenium chemistry. Selenoorganic compounds are frequently used in anti-inflammatory antioxidant drugs.<sup>126</sup> Selenium chemistry is known as selenium paradox because both natural and artificial selenoenzymes have ability to get oxidized and reduced rapidly.<sup>127</sup> The other properties of Se in selenite ions are lower basicity, higher nucleophilicity, better leaving group ability, higher polarizability, greater tolerance for hypervalence, enhanced stability and reversibility in selenyl radicals. Deficiency of selenium causes many diseases like cardiovascular disorder, cancer and HIV.<sup>128,129</sup>

## Introduction

---

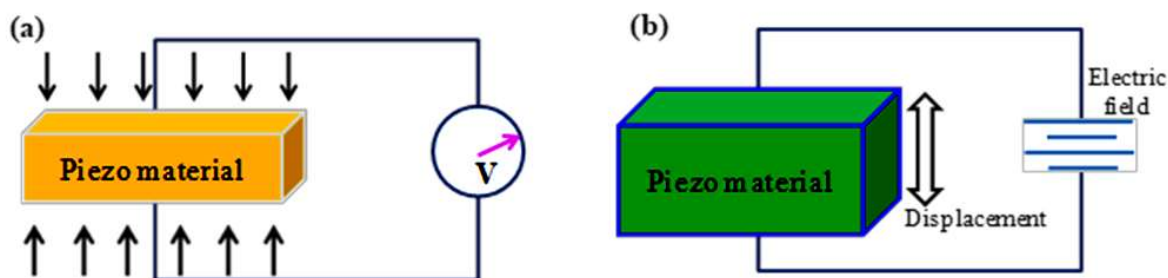
Selenium atom has potential to form H-bond and some of previous reports explained that it form weak H-bond because of its lower electronegativity<sup>130</sup>. There are very few theoretical studies on Selenium Centered Hydrogen Bond (SeCHB) in organoselenium compounds<sup>125,131-139</sup>. Michio Iwaoka et al.<sup>131</sup> observed the intramolecular hydrogen bond C-H $\cdots$ Se formation in diselenocin molecule by single crystal XRD, NMR experimental methods in solid and solution, respectively. They confirmed the C-H $\cdots$ Se interaction with the shorter distance between selenium and benzylic carbon atom ( $r = 2.95 \text{ \AA}$ ). This was further confirmed by solid-state IR spectra recorded in KBr matrix. The C-H vibrational frequency observed at  $2800 \text{ cm}^{-1}$  that is lower than the non-bonded benzylic C-H vibrational frequency ( $2853 \text{ cm}^{-1}$ ). Unlike in solution phase where diselenocin undergoes conformational exchange, the same phenomenon does not occur in solid phase confirmed by the low temperature NMR experiment. Some of computational studies were attempted to explore the existence and the strength of intramolecular selenium hydrogen bond in simple organic molecules competing with the SCHB and conventional hydrogen bonds.<sup>137,139</sup> Madzhidov et al.<sup>134</sup> reported the nature of intermolecular O-H $\cdots$ Se H-bond divalent selenium compounds. The divalent organoselenium compounds are dimethyl selenide, methyl selenocyanate. Dimethyl selenide acts as H-bond acceptor and methanol as an H-bond donor. From their observations of geometrical parameters, binding energies the SeCHB of O-H $\cdots$ Se is weaker compared to traditional H-bonds. In all the complexes charge transfer energy is a main contributing factor to stabilization of O-H $\cdots$ Se interaction. Recently Chakraborty S and his group observed<sup>135,138</sup> computationally that O-H $\cdots$ Se interaction strength is as comparable to SCHB and twice with O containing hydrogen bonds in complexes of para substituted phenols and its cationic form with  $\text{SeH}_2$ . They have characterized the substituent effect on O-H $\cdots$ Se interaction that increases the stabilization energy with increasing the

## Introduction

withdrawing ability at the para position of phenol. The *ab initio* calculations were carried to observe the different stabilizing structures and nature in  $F-H\cdots Y=C$  and  $F-Li\cdots Y=C$  complexes ( $Y=O,S,$  and  $Se$ ). Both in lithium and hydrogen complexes the electrostatic interactions are more dominant and  $Se$  shows similar strengths to sulfur and oxygen.<sup>133</sup> However, we did not find any experimental work reported on  $SeCHB$  in isolated condition. Hence, this encouraged us to investigate the existence and study of the experimental evidence for  $SeCHBs$  in proteins in isolated condition.

### 1.1.3 Applications of Hydrogen Bond Systems as Piezoelectric Materials

The piezoelectric effect is the effect which generates electric charge by applying mechanical stress on material and the reverse of this effect is called inverse piezoelectric effect (see Figure 1(a), and (b)). This stress can be caused by pressure or twisting the material, enough to deform its crystal lattice without fracturing it. This was discovered<sup>140</sup> by two French scientists Jacques Curie and Pierre Curie in 1880. Later, Gabriel Lippmann discovered the inverse piezoelectric effect, a phenomenon of the deformation of materials that results from the application of an external electric field (see Figure 1. (b)). The criteria for material to behave as piezoelectric material is (1) it should contain permanent or induced dipoles (2) it should be non-centrosymmetric.



## Introduction

---

Figure 1.1 (a) Piezoelectric effect: applying mechanical stress on material to generate electricity (b) inverse piezoelectric effect: applying electric field on material and its displacement in the direction of applied electric field.

The behavior of piezoelectric and inverse piezoelectric materials can be represented by the piezoelectric constants. Depending on the measured property of material piezoelectric constants can be classified as i) piezoelectric charge constant (d), ii) piezoelectric voltage constant (g), iii) permittivity constant (e), and iv) electrochemical coupling factor (k). Piezoelectric charge constant is the polarization generated per unit mechanical stress (S) applied to a piezoelectric material or in other words piezoelectric charge constant is the mechanical strain (S) experienced by a piezoelectric material per unit of electric field applied i.e;

$$d_{ij} = \frac{P}{S} \text{ or } d_{ij} = \frac{S}{E} \quad (1)$$

Here "d<sub>ij</sub>" is the piezoelectric coefficient or piezoelectric charge constant; "i" represents the direction of polarization generated in the material when an electric field applied (E), "j" represents the direction of the applied stress or induced strain. According to 176-1987 - IEEE Standard on Piezoelectricity<sup>141</sup>, the piezoelectric coefficient and inverse piezoelectric coefficient can be rearranged in the following matrix form by including the elastic and dielectric coefficients.

$$\{D\} = [e]^T \{S\} + [\alpha^S] \{E\} \quad (2)$$

$$\{T\} = [C^e] \{S\} - [e] \{E\} \quad (3)$$

Here, {D} is the electric displacement vector, {T} is the stress vector, [e] is the dielectric permittivity matrix, [C<sup>e</sup>] is the matrix of elastic coefficients at constant electric field strength,

## Introduction

---

$\{S\}$  is the strain vector,  $[\alpha^S]$  is the dielectric matrix at constant mechanical strain, and  $\{E\}$  is the electric field vector.

The piezoelectric materials are used in many areas of everyday life as home appliances, sensors, actuators, energy harvesting materials<sup>142,143</sup>. The piezoelectric energy harvesting is a conversion of vibration/displacement energy into an electrical energy to power wireless sensors. Most of the piezoelectric materials are inorganic compounds and polymers with high piezoelectric coefficient values. They include quartz ( $\text{SiO}_2$ ), berlinite ( $\text{AlPO}_4$ ), Gallium orthophosphate ( $\text{GaPO}_4$ ), ceramics of lead zirconium titanate (PZT), Barium titanate ( $\text{BaTiO}_3$ ), polyvinylidenedifluoride (PVDF) and polyvinyl fluoride (PVF). But these materials are not suitable or affordable for daily use because of their high stiffness, brittleness, low processability. Hydrogen bonded organic materials could be an alternative choice of piezoelectric material due to the polarized and flexible bonds. Antoine Paturle et al. synthesized organic crystal of hydrogen bonded dimer of 2-methyl-4-nitroaniline and calculated the piezoresponse experimentally using the X-ray diffractometer (XRD) method<sup>144</sup>. Lambrecht and coworkers studied the piezoelectric effect on hydrogen bonded systems by applying electric field using the quantum chemical calculations<sup>145,146</sup>.and demonstrated that the H-bonded systems are indeed potential piezoelectric materials to explore. However, these piezoelectric materials contain conventional H-bonds. In this thesis, we tried to examine the SCHB and SeHB as alternative sources for piezoelectric materials.

### 1.2 Carbon Bonding

#### 1.2.1 Carbon forms a proper non-covalent interaction:

Carbon is the fourth most abundant element in the universe and is the second most essential element in human body. In 2013, Arunan and his group<sup>147,148</sup> found that carbon has

## Introduction

---

similar potential like hydrogen and halogen to form non-covalent bond and they termed it as 'Carbon bond'. They observed the 'carbon bond' while searching for weak hydrogen bonding and van der Waals interactions by Fourier transform microwave spectroscopy of the complexes of methanol with inert gases. They noted that the argon is bound to  $-\text{CH}_3$  of methanol as  $\text{Ar}\cdots\text{C}$  bond in Ar-Methanol complex. The carbon bond bears a penta-coordinate carbon having  $\text{X}-\text{C}\cdots\text{Y}$  interaction in addition to its four covalent bonds. Like H-bond, the carbon bond is represented in a similar fashion i.e.,  $\text{X}-\text{C}\cdots\text{Y}$ , where X and Y denotes carbon bond donor and acceptor respectively. The concept of carbon bond can be understood using sigma-hole concept like halogen bond. The sigma-hole term was first introduced to explain the halogen bonding by Politzer and coworkers<sup>149,150</sup>. In a very short time some computational and experimental studies were carried out to know more details about carbon bonding.<sup>147,148,151-165</sup> Prof. E. Arunan and his group investigated for the first time carbon bond computationally in complexes between electropositive face of  $\text{CH}_3$  in  $\text{CH}_3\text{OH}/\text{CH}_3\text{F}$  and electron rich atoms in  $\text{H}_2\text{O}$ ,  $\text{H}_2\text{S}$ ,  $\text{HX}$ ,  $\text{LiX}$  ( $\text{X}=\text{F}, \text{Cl}$ , and  $\text{Br}$ ),  $\text{ClF}$ ,  $\text{NH}_3$ ,  $\text{PH}_3$  as electron pair donors.<sup>147</sup> The  $\text{X}-\text{C}\cdots\text{Y}$  bond belongs to family of tetrel bond and are found in the intermediate of  $\text{S}_{\text{N}}2$  reactions in organic chemistry. Further Grabowskia<sup>153</sup> and Hai-Bei Li group<sup>162</sup> independently investigated carbon bond by quantum chemical calculations, AIM and NBO analysis. They observed that the strength of C-bond is smaller than that of the other tetrel bonds. The electrostatic interactions are dominated and comparable to polarization interactions in tetrel bond. The main stabilization energy is attributed to the redistribution of charge as similar to the  $\text{S}_{\text{N}}2$  reaction. T. N. Guru Row and coworkers provided the first experimental evidence of carbon bond in solid state by charge density analysis of CSD data. This witnesses the existence of carbon bond in many organic crystals. The charge densities ( $\rho$ ) and laplacian ( $\nabla^2\rho$ ) at the bond critical point (bcp) of  $\text{X}-\text{C}\cdots\text{O}$  bond are comparable

## Introduction

---

to carbon bond of water-methanol system.<sup>147</sup> In addition, Southern et al. investigated the existence of carbon bond with the solid state NMR spectroscopy and computational methods in 2015.<sup>159</sup>

In carbon bond, carbon acts as Lewis acid i.e., as carbon bond donor and electron rich atoms or fragments of molecules act as carbon bond acceptors. Just like hydrogen bond, depending on the C-bond acceptor different types of C-bond interactions viz.  $X-C\cdots O$ ,  $X-C\cdots N$ ,  $X-C\cdots \pi$ ,  $X-C\cdots Y$ , ( $Y =$  anions and radicals) and  $X-C\cdots C$  are possible in supramolecular and biological molecules. The researchers keep on investigating the above mentioned C-bonds thoroughly by different computational methods.<sup>154-156,158,160,162-165</sup> The nature and directionality of carbon bond were explored by combination of computational and CSD by taking small cycloalkane as carbon bond donor.<sup>152,166</sup> Pampi Pal et al. found carbon bond in the 2D cobalt coordinated polymer via  $CH_3\cdots N$  noncovalent interactions with the neighboring chains and it is a weak electrophilic-nucleophilic attraction in nature<sup>167</sup>. These C-bonds are responsible to form novel 2D cobalt complex polymer by connecting different chains.

It is evident that hydrogen bond plays the dominant role in biomolecular structure and function. We would expect C-bonds also contribute in biomolecular structure and function. To investigate the existence of carbon bonding in biological molecules Antonio Bauzá et al performed Protein Data Bank (PDB) survey. They also performed *ab initio* calculations for some model compounds and two retrieved PDBs as representatives. They found that electropositive  $CH_3$  plays a dual role i.e., as H-bond donor as well as C-bond donor with nucleophile O closer and linear to that. The distance between C and O in  $R-CH_3\cdots O-Y$  is shorter than H-bond and the bond angle  $\angle COY$  is close to linear. The electrostatic and dispersion interaction energies contribute maximum to form C-bonds in these compounds. The same group<sup>163</sup> recently

## Introduction

---

investigated the role of carbon-bond involving the participation of  $\text{CF}_3$  group in the inhibition mechanism of a  $\text{NADP}^+$ -dependent isocitrate dehydrogenase (IDH) enzyme that converts isocitrate to  $\alpha$ -ketoglutarate in biomolecules. The close to linear geometry and the NCI analysis confirmed the existence of  $\text{X-F}_3\text{C}\cdots\text{O}$  C-bond complex. Both experimental and theoretical investigations are yet to be performed to ensure the existences, strength, nature and directionality of carbon-bonds in proteins.

### 1.2.2 N-Oxides act as C-bond acceptors:

N-oxides or amine oxides are frequently used in shampoos, detergents, hard surface cleaners<sup>168</sup>. The naturally occurring osmolyte trimethylamine N-oxide (TMAO) creates the basis for a mechanism of protein folding by interaction with backbone peptides and offsets of the destabilizing effects of urea<sup>18,169,170</sup>. The aliphatic N-oxides play a crucial role in catalysis<sup>171</sup>, DNA-affinic agents and act as bioreductive drugs<sup>172-174</sup>, while pyridine N-oxides are used for the anti-HIV activity<sup>175</sup> and n-oxide polymers are used as herbicidal activity<sup>176</sup>. N-oxides have unique properties such as (i) large dipole moment of the functional group, (ii) less basic in nature; (iii) the intermediate products are stabilized by noncovalent interactions and (iv) high solubility in water. N-oxides are potential hydrogen and halogen bond acceptor in supramolecular chemistry, crystal engineering, pharmaceutical areas<sup>168,172,174,176-187</sup>. Hammer and coworkers<sup>181</sup> explored their potential to form hydrogen bond and extended hydrogen bond network of TMAO with water, methanol, ethanol, and ethylene glycol by the combination of Raman spectroscopy and computational methods. Saraswatula et al.<sup>182</sup> suggested that pyridine N-oxide acts as a good hydrogen bond acceptor compare to pyridine compound and acid $\cdots$ pyridine N-oxide is slightly stronger than the acid $\cdots$ pyridine. Rissanen and his group<sup>188,189</sup> established the N-oxides act as halogen bond acceptors from experimental and computational methods and the

## Introduction

---

strength of halogen bond is as strong as hydrogen bond in solid-state while in solution it found to possess higher association constant. The ability of N-oxides to form non-covalent interactions (H-bond/X-bond) aids in the development of drug cocrystals<sup>184,190</sup>. This motivates us to study the N-oxides as carbon bond acceptors in model compounds.

### 1.3 Objectivities of the thesis:

With the help of a combination of gas-phase laser spectroscopy, solution NMR spectroscopy, quantum calculations and PDB analysis we endeavored for the following objectives

- I. Determination of the accurate strength of amide N-H $\cdots$ S H-Bonds (SCHBs) of 1:1 intermolecular complexes of small molecules that are constituents of biomolecules sans environmental and conformational effects in an isolated and jet-cooled condition.
- II. Assessment of the strength of amide-N-H $\cdots$ S H-Bonds (SCHBs) of model compounds of proteins and nucleotides by replacing the amides with thioamides as hydrogen bond acceptors.
- III. Experimental evidences of Selenium centered hydrogen bonds (SeCHBs) (amide-N-H $\cdots$ Se H-Bond) in selenocysteine/Selenomethionine containing proteins.
- IV. Determination of the strength of amide-N-H $\cdots$ Te H-bonds in isolated conditions.
- V. Computational studies of the SCHBs and SeCHBs systems as alternative sources for piezoelectric materials.
- VI. Experimental and computational studies of carbon bonds (C $\cdots$ O=C) in proteins. Experimental determination of C-bond energy and implication of C-bonds in protein structure and function.

## Introduction

---

VII. Quantum chemical calculations on the nature and strength of C-bonds by considering N-Oxides and N-Sulfides as carbon bond acceptors.

### 1.4 Structure of the thesis:

- This thesis is broadly divided into two parts: first part discusses (Chapter 3-5) hydrogen bonds in gas phase and solution phase and their applications. The second part of the thesis (Chapter 6 (part A and part B)) discusses the carbon bond interactions in proteins and organic molecules.
- Chapter 1 includes the introduction of the hydrogen bond, carbon bond, piezoelectric effect and literature review.
- Chapter 2 deals with the detail descriptions of the experimental and computational techniques used to achieve the objectives. The experimental techniques briefly discussed here are supersonic expansion, Laser Induced Fluorescence (LIF) spectroscopy, Resonance Enhanced Multi-photon Ionization spectroscopy (REMPI), IR-UV Double Resonance spectroscopy, NMR Spectroscopy, Infrared Spectroscopy. The LIF, REMPI and IR-UV Double Resonance spectroscopy were used for 1:1 complexes in an isolated condition in gas phase (Chapter-3, part-A and chapter-4).  $^1\text{H}$ ,  $^{13}\text{C}$  NMR and  $^1\text{H}$ -DOSY spectroscopy are discussed in chapter-3, part-B and chapter-6, part-A. They were used to measure H-bond and C-bond strength in solution phase. This chapter also describes the various Quantum Chemical methods used to corroborate the experimental findings.
- Chapter 3 is divided into two parts as part A and part B. Part A discusses the spectroscopic determination of the strength of amide-N-H $\cdots$ S H-bonds of model compounds of cysteine/methionine proteins in isolated condition. Part B provides the

## Introduction

---

experimental evidence of sulfur centered hydrogen bond in solution phase where thioamides act as hydrogen bond acceptors.

- Chapter 4 discusses the existence of amide-N-H $\cdots$ Se H-bonds in proteins. In addition, the strength of amide-N-H $\cdots$ Se H-bonds in model compounds of proteins are determined by spectroscopic techniques and computational calculations.
- Chapter 5 describes the computational methods to design the organic piezoelectric materials with sulfur/selenium centered hydrogen bonded systems and calculations of piezoelectric coefficients.
- Chapter 6 is divided into two parts; Part A of this chapter gives the detailed information of the existence of C $\cdots$ O=C carbon bonds in proteins by PDB analysis. The nature and strength of carbon bonds in model compounds of proteins are examined by the experimental and computational methods. Part B discusses the involvement of N-Oxides and N-Sulfides as acceptors in C-bonds.
- Chapter 7 gives the concluding remarks and future scope of overall thesis.

## Introduction

---

### References:

- (1) van der Waals, J. D. *PhD Thesis, Leiden* **1873**.
- (2) Kamerlingh-Onnes, H. *Proc. Sec. Sci* **1908**, *KNAW, XI*, 68.
- (3) London, F. Z. *Phys. Chem.* **1930**, *B11*, 222.
- (4) Hellmann, H. *Acta Physicochim* **1935**, *URSS 2* 273.
- (5) Joseph O. Hirschfelder, C. F. C., and R. Byron Bird *John Wiley & Sons, Inc., New York* **1954**.
- (6) Michael, P.; O., G. M. *Angew. Chem. Int. Ed.* **1996**, *35*, 806.
- (7) Saha, S.; Desiraju, G. R. *J. Am. Chem. Soc.* **2017**, *139*, 1975.
- (8) Sutton, C.; Risko, C.; Brédas, J.-L. *Chem. Mater.* **2016**, *28*, 3.
- (9) Wodak, S. J.; Janin, J. *Adv. Protein. Chem.*; Academic Press: 2002; Vol. 61, p 9.
- (10) Hruska K., S. J., Moskowitz D., Goligorsky M. *Advances in Experimental Medicine and Biology*, Springer, Boston, MA, 1986; Vol. 208.
- (11) Auffinger, P.; Hays, F. A.; Westhof, E.; Ho, P. S. *Proc. Natl. Acad. Sci. U.S.A.* **2004**, *101*, 16789.
- (12) Wilcken, R.; Zimmermann, M. O.; Lange, A.; Joerger, A. C.; Boeckler, F. M. *J. Med. Chem.* **2013**, *56*, 1363.

## Introduction

---

- (13) Chaudret, R.; de Courcy, B.; Contreras-Garcia, J.; Gloaguen, E.; Zehnacker-Rentien, A.; Mons, M.; Piquemal, J. P. *Phys. Chem. Chem. Phys.* **2014**, *16*, 9876.
- (14) Mahadevi, A. S.; Sastry, G. N. *Chem. Rev.* **2016**, *116*, 2775.
- (15) Suponitsky, K. Y.; Burakov, N. I.; Kanibolotsky, A. L.; Mikhailov, V. A. *J. Phys. Chem. A* **2016**, *120*, 4179.
- (16) Danelius, E.; Andersson, H.; Jarvoll, P.; Lood, K.; Gräfenstein, J.; Erdélyi, M. *Biochemistry* **2017**, *56*, 3265.
- (17) Kolář, M. H.; Tabarrini, O. *J. Med. Chem.* **2017**.
- (18) Liao, Y.-T.; Manson, A. C.; DeLyser, M. R.; Noid, W. G.; Cremer, P. S. *Proc. Natl. Acad. Sci. U.S.A* **2017**, *114*, 2479.
- (19) Zahn, S.; Frank, R.; Hey-Hawkins, E.; Kirchner, B. *Chem. Eur. J* **2011**, *17*, 6034.
- (20) Bauza, A.; Quinonero, D.; Deya, P. M.; Frontera, A. *Phys. Chem. Chem. Phys.* **2012**, *14*, 14061.
- (21) Scheiner, S. *Acc. Chem. Res.* **2013**, *46*, 280.
- (22) Nziko, V. d. P. N.; Scheiner, S. *J. Phys. Chem. A* **2014**, *118*, 10849.
- (23) Fick, R. J.; Kroner, G. M.; Nepal, B.; Magnani, R.; Horowitz, S.; Houtz, R. L.; Scheiner, S.; Trievel, R. C. *ACS Chem. Bio.* **2016**, *11*, 748.
- (24) Menichetti, S.; Amorati, R.; Meoni, V.; Tofani, L.; Caminati, G.; Viglianisi, C. *Org. Lett* **2016**, *18*, 5464.

## Introduction

---

- (25) Bora, P. L.; Novák, M.; Novotný, J.; Foroutan-Nejad, C.; Marek, R. *Chem. Eur. J* **2017**, *23*, 7315.
- (26) Legon, A. C. *Phys. Chem. Chem. Phys.* **2017**, *19*, 14884.
- (27) Bauzá, A.; Mooibroek, T. J.; Frontera, A. *ChemPhysChem* **2015**, *16*, 2496.
- (28) Servati Gargari, M.; Stilinović, V.; Bauzá, A.; Frontera, A.; McArdle, P.; Van Derveer, D.; Ng, S. W.; Mahmoudi, G. *Chem. Eur. J* **2015**, *21*, 17951.
- (29) Marín-Luna, M.; Alkorta, I.; Elguero, J. *J. Phys. Chem. A* **2016**, *120*, 648.
- (30) George, J.; Dronskowski, R. *J. Phys. Chem. A* **2017**, *121*, 1381.
- (31) Michael Gromiha, M.; Saraboji, K.; Ahmad, S.; Ponnuswamy, M. N.; Suwa, M. *Biophys. Chem.* **2004**, *107*, 263.
- (32) Zhou, P.; Huang, J.; Tian, F. *Curr. Med. Chem.* **2012**, *19*, 226.
- (33) Tang, Z.; Roberts, C. C.; Chang, C.-e. A. *Frontiers in bioscience (Landmark edition)* **2017**, *22*, 960.
- (34) MacGillivray, L. R.; Atwood, J. L. *Nature* **1997**, *389*, 469.
- (35) Whitesides, G. M.; Grzybowski, B. *Science* **2002**, *295*, 2418.
- (36) Min, Y.; Akbulut, M.; Kristiansen, K.; Golan, Y.; Israelachvili, J. *Nat. Mater.* **2008**, *7*, 527.
- (37) Moore, T. S.; Winmill, T. F. *J. Chem. Soc. Faraday Trans.* **1912**, *101*, 1635.

## Introduction

---

- (38) Latimer, W. M.; Rodebush, W. H. *J. Am. Chem. Soc.* **1920**, *42*, 1419.
- (39) Pauling, L. *J. Am. Chem. Soc.* **1931**, *53*, 1367.
- (40) G. C. Pimentel, A. L. M. *W. H. Freeman, San Francisco* **1960**.
- (41) E. Arunan, G. R. D., R. A. Klein, J. Sadlej, S. Scheiner, I. Alkorta, D. C. Clary, R. H. Crabtree, J. J. Dannenberg, P. Hobza, H. G. Kjaergaard, A. C. Legon, B. Mennucci, D. J. Nesbitt *Pure Appl. Chem.* **2011**, *83*, 1637.
- (42) G. R. Desiraju, T. S. *Oxford University Press* **1999**.
- (43) Jeffrey GA, S. W. *Spinger-Verlag, Berlin* **1991**.
- (44) A, J. G. *Oxford University Press, New York* **1997**.
- (45) S., S. *Oxford University Press, New York* **1997**.
- (46) Müller-Dethlefs, K.; Hobza, P. *Chem. Rev.* **2000**, *100*, 143.
- (47) Sarkhel, S.; Desiraju, G. R. *Proteins: Struct., Funct., Bioinf.* **2003**, *54*, 247.
- (48) Grabowski, S. J. *Springer, New York* **2006**, 3.
- (49) McClements, D. J. *Biotechnol. Adv.* **2006**, *24*, 621.
- (50) Chakrabarti, P.; Bhattacharyya, R. *Prog. Biophys. Mol. Biol.* **2007**, *95*, 83.
- (51) Jeffrey, G. *Acta Crystallogr., Sect. B: Struct. Sci* **2000**, *56*, 333.
- (52) Manikandan, K.; Ramakumar, S. *Proteins: Struct., Funct., Bioinf.* **2004**, *56*, 768.

## Introduction

---

- (53) Belkova, N. V.; Epstein, L. M.; Shubina, E. S. *Monogr. Ser. Int. Conf. Coord. Chem.* **2007**, 8, 20.
- (54) Kundu, P.; Capitani, J. F.; Mitra, A.; Seaton, P. J.; *Am. Chem. Soc.*: 2007, p COMP.
- (55) Cordier, F.; Nisius, L.; Dingley, A. J.; Grzesiek, S. *Nat. Protocols* **2008**, 3, 235.
- (56) Labadi, I.; Transworld Research Network: 2008, p 227.
- (57) Yagai, S.; Hamamura, S.; Wang, H.; Stepanenko, V.; Seki, T.; Unoike, K.; Kikkawa, Y.; Karatsu, T.; Kitamura, A.; Wurthner, F. *Org. Biomol. Chem.* **2009**, 7, 3926.
- (58) Hobza, P.; Muller-Dethlefs, K.; Editors *Non-Covalent Interactions: Theory and Experiment*; Royal Society Chemistry Publishing, 2010.
- (59) Muller-Dethlefs, K.; *Am. Chem. Soc.*: 2010, p PTC.
- (60) Melandri, S. *Phys. Chem. Chem. Phys.* **2011**, 13, 13901.
- (61) Nishio, M. *Phys. Chem. Chem. Phys.* **2011**, 13, 13873.
- (62) Parcell, S. *Alternative Medicine Review* **2002**, 7, 22.
- (63) Gupta, A. K.; Nicol, K. *J. Drugs Dermatol* **2004**, 3, 427.
- (64) Valley, C. C.; Cembran, A.; Perlmutter, J. D.; Lewis, A. K.; Labello, N. P.; Gao, J.; Sachs, J. N. *J. Biol. Chem.* **2012**, 287, 34979.
- (65) Mazmanian, K.; Sargsyan, K.; Grauffel, C.; Dudev, T.; Lim, C. *J. Phys. Chem. B* **2016**, 120, 10288.

## Introduction

---

- (66) Adman, E.; Watenpaugh, K. D.; Jensen, L. H. *Proc. Natl. Acad. Sci. U.S.A.* **1975**, *72*, 4854.
- (67) Ueyama, N.; Nishikawa, N.; Yamada, Y.; Okamura, T.-a.; Nakamura, A. *J. Am. Chem. Soc.* **1996**, *118*, 12826.
- (68) AlDamen, M. A.; Sinnokrot, M. *J. Struct. Chem.* **2014**, *55*, 53.
- (69) Bhattacharyya, S.; Bhattacharjee, A.; Shirhatti, P. R.; Wategaonkar, S. *J. Phys. Chem. A* **2013**, *117*, 8238.
- (70) Biswal, H. S.; Chakraborty, S.; Wategaonkar, S. *J. Chem. Phys.* **2008**, *129*, 184311.
- (71) Biswal, H. S.; Gloaguen, E.; Loquais, Y.; Tardivel, B.; Mons, M. *J. Phys. Chem. Lett.* **2012**, *3*, 755.
- (72) Biswal, H. S.; Shirhatti, P. R.; Wategaonkar, S. *J. Phys. Chem. A* **2009**, *113*, 5633.
- (73) Biswal, H. S.; Wategaonkar, S. *J. Phys. Chem. A* **2009**, *113*, 12763.
- (74) Biswal, H. S.; Wategaonkar, S. *J. Phys. Chem. A* **2010**, *114*, 5947.
- (75) Biswal, H. S.; Wategaonkar, S. *J. Chem. Phys.* **2011**, *135*, 134306.
- (76) Sabin, J. R. *J. Am. Chem. Soc.* **1971**, *93*, 3613.
- (77) Kollman, P. A.; Allen, L. C. *J. Chem. Phys.* **1969**, *51*, 3286.
- (78) Pacansky, J.; Calder, V. *J. Chem. Phys.* **1970**, *53*, 4519.
- (79) Tursi, A. J.; Nixon, E. R. *J. Chem. Phys.* **1970**, *53*, 518.

## Introduction

---

- (80) Woodbridge, E. L.; Tso, T. L.; McGrath, M. P.; Hehre, W. J.; Lee, E. K. C. *J. Chem. Phys.* **1986**, *85*, 6991.
- (81) Isoniemi, E.; Pettersson, M.; Khriachtchev, L.; Lundell, J.; Räsänen, M. *J. Phys. Chem. A* **1999**, *103*, 679.
- (82) Bhattacharjee, A.; Matsuda, Y.; Fujii, A.; Wategaonkar, S. *ChemPhysChem* **2013**, *14*, 905.
- (83) Bhattacharjee, A.; Matsuda, Y.; Fujii, A.; Wategaonkar, S. *J. Phys. Chem. A* **2015**, *119*, 1117.
- (84) Cabaleiro-Lago, E. M.; Rodríguez-Otero, J. *J. Phys. Chem. A* **2002**, *106*, 7440.
- (85) Masella, M.; Flament, J. P. *J. Chem. Phys.* **1998**, *108*, 7141.
- (86) Grzechnik, K.; Rutkowski, K.; Mielke, Z. *J. Mol. Struct.* **2012**, *1009*, 96.
- (87) Meyer, E. A.; Castellano, R. K.; Diederich, F. *Angew. Chem. Int. Ed.* **2003**, *42*, 1210.
- (88) Zauhar, R. J.; Colbert, C. L.; Morgan, R. S.; Welsh, W. J. *Biopolymers* **2000**, *53*, 233.
- (89) Arunan, E.; Emilsson, T.; Gutowsky, H. S.; Fraser, G. T.; Oliveira, G. d.; Dykstra, C. E. *J. Chem. Phys.* **2002**, *117*, 9766.
- (90) Biswal, H. S.; Wategaonkar, S. *J. Phys. Chem. A* **2009**, *113*, 12774.
- (91) Forbes, C. R.; Sinha, S. K.; Ganguly, H. K.; Bai, S.; Yap, G. P. A.; Patel, S.; Zondlo, N. *J. J. Am. Chem. Soc.* **2017**, *139*, 1842.

## Introduction

---

- (92) Gregoret, L. M.; Rader, S. D.; Fletterick, R. J.; Cohen, F. E. *Proteins: Struct., Funct., Bioinf.* **1991**, *9*, 99.
- (93) Desiraju, G. R. *Acc. Chem. Res.* **2002**, *35*, 565.
- (94) Maes, G.; Graindourze, M. *J. Mol. Spectrosc.* **1985**, *113*, 410.
- (95) Maes, G.; Graindourze, M. *J. Mol. Spectrosc.* **1985**, *114*, 280.
- (96) Jeng, M. L. H.; Ault, B. S. *J. Phys. Chem.* **1990**, *94*, 1323.
- (97) Jeng, M. L. H.; Ault, B. S. *J. Phys. Chem.* **1990**, *94*, 4851.
- (98) Li, S.; Li, Y.-S. *Spectrochim. Acta A* **1991**, *47*, 201.
- (99) Li, S.; Li, Y.-S. *J. Mol. Spectrosc.* **1991**, *248*, 79.
- (100) Platts, J. A.; Howard, S. T.; Bracke, B. R. F. *J. Am. Chem. Soc.* **1996**, *118*, 2726.
- (101) Li, S.; Kurtz, H.; Korambath, P.; Li, Y. S. *J. Mol. Struct.* **2000**, *550*, 235.
- (102) Wierzejewska, M. *Vib. Spectrosc* **2000**, *23*, 253.
- (103) Wierzejewska, M. *J. Mol. Struct.* **2000**, *520*, 199.
- (104) Xu, L.-H.; Liu, Q.; Suenram, R. D.; Lovas, F. J.; Hight Walker, A. R.; Jensen, J. O.; Samuels, A. C. *J. Mol. Spectrosc.* **2004**, *228*, 243.
- (105) Ghosh, S.; Bhattacharyya, S.; Wategaonkar, S. *J. Phys. Chem. A* **2015**, *119*, 10863.

## Introduction

---

- (106) Borrmann, H.; Persson, I.; Sandstrom, M.; Stalhandske, C. M. V. *Journal of the Chemical Society, Perkin Transactions 2* **2000**, 393.
- (107) Afonin, A. V.; Toryashinova, D. S. D.; Schmidt, E. Y. *J. Mol. Struct. THEOCHEM* **2004**, 680, 127.
- (108) Stott, K.; UK . 2001, p 76 pp.
- (109) Sarkhel, S.; Desiraju, G. R. *Proteins: Struct., Funct., Bioinf.* **2004**, 54, 247.
- (110) Battistel, M. D.; Azurmendi, H. F.; Frank, M.; Freedberg, D. I. *J. Am. Chem. Soc.* **2015**, 137, 13444.
- (111) Chen, J.; Zhang, Y.; Kohler, B. *Top. Curr. Chem.* **2015**, 356, 39.
- (112) Alauddin, M.; Biswal, H. S.; Gloaguen, E.; Mons, M. *Phys. Chem. Chem. Phys.* **2015**, 17, 2169.
- (113) Sherman, D. B.; Spatola, A. F. *J. Am. Chem. Soc.* **1990**, 112, 433.
- (114) Kim, N.-K.; Lee, H.-J.; Choi, K.-H.; Yu, J.-A.; Yoon, C.-J.; Park, J.; Choi, Y.-S. *J. Phys. Chem. A* **2000**, 104, 5572.
- (115) Alemán, C. *J. Phys. Chem. A* **2001**, 105, 6717.
- (116) Miwa, J. H.; Patel, A. K.; Vivatrat, N.; Popek, S. M.; Meyer, A. M. *Organic Letters* **2001**, 3, 3373.
- (117) Lee, H.-J.; Choi, Y.-S.; Lee, K.-B.; Park, J.; Yoon, C.-J. *J. Phys. Chem. A* **2002**, 106, 7010.

## Introduction

---

- (118) Culik, R. M.; Jo, H.; DeGrado, W. F.; Gai, F. *J. Am. Chem. Soc.* **2012**, *134*, 8026.
- (119) Mes, T.; Cantekin, S.; Balkenende, D. W. R.; Frissen, M. M. M.; Gillissen, M. A. J.; De Waal, B. F. M.; Voets, I. K.; Meijer, E. W.; Palmans, A. R. A. *Chem. Eur. J* **2013**, *19*, 8642.
- (120) Newberry, R. W.; VanVeller, B.; Raines, R. T. *ChemComm* **2015**, *51*, 9624.
- (121) Walters, C. R.; Szantai-Kis, D. M.; Zhang, Y.; Reinert, Z. E.; Horne, W. S.; Chenoweth, D. M.; Petersson, E. J. *Chem. Sci.* **2017**, *8*, 2868.
- (122) Reich, H. J.; Hondal, R. J. *ACS Chem. Bio.* **2016**, *11*, 821.
- (123) A., B.; K., F.; J., H.; W., L.; G., S.; B., V.; F., Z. *Mol. Microbiol.* **1991**, *5*, 515.
- (124) Gladyshev, V. N.; Hatfield, D. L. *J. Biomed. Sci.* **1999**, *6*, 151.
- (125) Mukherjee, A. J.; Zade, S. S.; Singh, H. B.; Sunoj, R. B. *Chem. Rev.* **2010**, *110*, 4357.
- (126) Schewe, T. *General Pharmacology: The Vascular System* **1995**, *26*, 1153.
- (127) Hondal, R. J.; Ruggles, E. L. *Amino Acids* **2011**, *41*, 73.
- (128) Zhao, L.; Cox, A. G.; Ruzicka, J. A.; Bhat, A. A.; Zhang, W.; Taylor, E. W. *Proc. Natl. Acad. Sci. U.S.A* **2000**, *97*, 6356.
- (129) Flohé, L.; Andreesen, J. R.; Brigelius-Flohé, R.; Maiorino, M.; Ursini, F. *IUBMB Life* **2000**, *49*, 411.
- (130) Luis, M. J. *Pept. Sci* **2005**, *11*, 187.

## Introduction

---

- (131) Iwaoka, M.; Tomoda, S. *J. Am. Chem. Soc.* **1994**, *116*, 4463.
- (132) Michalczyk, R.; Schmidt, J. G.; Moody, E.; Li, Z.; Wu, R.; Dunlap, R. B.; Odom, J. D.; Silks Iii, L. A. P. *Angew. Chem. Int. Ed.* **2000**, *39*, 3067.
- (133) Salai Cheettu Ammal, S.; Venuvanalingam, P. *J. Phys. Chem. A* **2000**, *104*, 10859.
- (134) Madzhidov, T. I.; Chmutova, G. A. *J. Mol. Struct.: THEOCHEM* **2010**, *959*, 1.
- (135) Das, B.; Chakraborty, A.; Chakraborty, S. *Comput. Theor. Chem* **2017**, *1102*, 127.
- (136) Michio, I.; Hiroto, K.; Shuji, T. *Bull. Chem. Soc. Jpn.* **1996**, *69*, 1825.
- (137) Harada, T.; Yoshida, H.; Ohno, K.; Matsuura, H.; Zhang, J.; Iwaoka, M.; Tomoda, S. *J. Phys. Chem. A* **2001**, *105*, 4517.
- (138) Schamnad, S.; Chakraborty, S. *Chem. Phys. Lett.* **2015**, *622*, 28.
- (139) Sanz, P.; Yáñez, M.; Mó, O. *J. Phys. Chem. A* **2002**, *106*, 4661.
- (140) Katzir, S. *Archive for History of Exact Sciences* **2003**, *57*, 61.
- (141) *ANSI/IEEE Std 176-1987* **1988**, 0\_1.
- (142) El-Sayed, A. R.; Tai, K.; Biglarbegian, M.; Mahmud, S. In *2016 IEEE Canadian Conference on Electrical and Computer Engineering (CCECE)* 2016, p 1.
- (143) Zhang, Z.; Xiang, H.; Shi, Z. *Compos. Struct.* **2017**, *179*, 368.
- (144) Paturle, A.; Graafsma, H.; Sheu, H. S.; Coppens, P.; Becker, P. *Phys. Rev. B* **1991**, *43*, 14683.

## Introduction

---

- (145) Werling, K. A.; Hutchison, G. R.; Lambrecht, D. S. *J. Phys. Chem. Lett.* **2013**, *4*, 1365.
- (146) Werling, K. A.; Griffin, M.; Hutchison, G. R.; Lambrecht, D. S. *J. Phys. Chem. A* **2014**, *118*, 7404.
- (147) Mani, D.; Arunan, E. *Phys. Chem. Chem. Phys.* **2013**, *15*, 14377.
- (148) Mani, D.; Arunan, E. *ChemPhysChem* **2013**, *14*, 754.
- (149) Clark, T.; Hennemann, M.; Murray, J. S.; Politzer, P. *J. Mol. Model.* **2007**, *13*, 291.
- (150) Murray, J. S.; Lane, P.; Politzer, P. *J. Mol. Model.* **2009**, *15*, 723.
- (151) Bauzá, A.; Mooibroek, T. J.; Frontera, A. *Angew. Chem.* **2013**, *125*, 12543.
- (152) Bauzá, A.; Mooibroek, T. J.; Frontera, A. *Chem. Eur. J* **2014**, *20*, 10245.
- (153) Grabowski, S. *J. Phys. Chem. Chem. Phys.* **2014**, *16*, 1824.
- (154) Li, Q.; Guo, X.; Yang, X.; Li, W.; Cheng, J.; Li, H.-B. *Phys. Chem. Chem. Phys.* **2014**, *16*, 11617.
- (155) Mani, D.; Arunan, E. *J. Phys. Chem. A* **2014**, *118*, 10081.
- (156) McDowell, S. A. C.; Joseph, J. A. *Phys. Chem. Chem. Phys.* **2014**, *16*, 10854.
- (157) Thomas, S. P.; Pavan, M. S.; Guru Row, T. N. *ChemComm* **2014**, *50*, 49.
- (158) Varadwaj, P. R.; Varadwaj, A.; Jin, B.-Y. *Phys. Chem. Chem. Phys.* **2014**, *16*, 17238.
- (159) Southern, S. A.; Bryce, D. L. *J. Phys. Chem. A* **2015**, *119*, 11891.

## Introduction

---

- (160) Bauzá, A.; Frontera, A. *Crystals* **2016**, *6*, 26.
- (161) Bauzá, A.; Mooibroek, T. J.; Frontera, A. *Chem. Rec.* **2016**, *16*, 473.
- (162) Liu, M.; Li, Q.; Cheng, J.; Li, W.; Li, H.-B. *J. Chem. Phys.* **2016**, *145*, 224310.
- (163) García-Llinás, X.; Bauzá, A.; Seth, S. K.; Frontera, A. *J. Phys. Chem. A* **2017**.
- (164) Quinonero, D. *Phys. Chem. Chem. Phys.* **2017**, *19*, 15530.
- (165) Zhang, Z.; Wang, L.; Xuan, X. *New J. Chem.* **2017**, *41*, 42.
- (166) Escudero-Adán, E. C.; Bauzá, A.; Frontera, A.; Ballester, P. *ChemPhysChem* **2015**, *16*, 2530.
- (167) Pal, P.; Konar, S.; Lama, P.; Das, K.; Bauzá, A.; Frontera, A.; Mukhopadhyay, S. *J. Phys. Chem. B* **2016**, *120*, 6803.
- (168) Sanderson, H.; Tibazarwa, C.; Greggs, W.; Versteeg, D. J.; Kasai, Y.; Stanton, K.; Sedlak, R. I. *Risk Analysis* **2009**, *29*, 857.
- (169) Zou, Q.; Bennion, B. J.; Daggett, V.; Murphy, K. P. *J. Am. Chem. Soc.* **2002**, *124*, 1192.
- (170) Hu, C. Y.; Lynch, G. C.; Kokubo, H.; Pettitt, B. M. *Proteins* **2010**, *78*, 695.
- (171) Fulton, J. R.; Glover, J. E.; Kamara, L.; Rowlands, G. J. *ChemComm* **2011**, *47*, 433.
- (172) LH, P. *Cancer Metastasis Rev.* **1993**, *12*, 119.
- (173) Patterson, L. H. *Cancer Metastasis Rev.* **1993**, *12*, 119.

## Introduction

---

- (174) LH, P.; Craven Mr Fau - Fisher, G. R.; Fisher Gr Fau - Teesdale-Spittle, P.; P, T.-S. *Oncol Res* **1994**, *6*, 533.
- (175) Balzarini, J.; Stevens, M.; De Clercq, E.; Schols, D.; Pannecouque, C. *J. Antimicrob. Chemother.* **2005**, *55*, 135.
- (176) Cerecetto, H.; Dias, E.; Di Maio, R.; González, M.; Pacce, S.; Saenz, P.; Seoane, G.; Suescun, L.; Mombrú, A.; Fernández, G.; Lema, M.; Villalba, J. *J. Agric. Food. Chem.* **2000**, *48*, 2995.
- (177) Malkov, A. V.; Bell, M.; Castelluzzo, F.; Kočovský, P. *Org. Lett.* **2005**, *7*, 3219.
- (178) Balzarini, J.; Keyaerts, E.; Vijgen, L.; Vandermeer, F.; Stevens, M.; De Clercq, E.; Egberink, H.; Van Ranst, M. *J. Antimicrob. Chemother.* **2006**, *57*, 472.
- (179) Stevens, M.; Pannecouque, C.; De Clercq, E.; Balzarini, J. *Biochem. Pharmacol.* **2006**, *71*, 1122.
- (180) Aakeroy, C. B.; Wijethunga, T. K.; Desper, J. *CrystEngComm* **2014**, *16*, 28.
- (181) Cuellar, K. A.; Munroe, K. L.; Magers, D. H.; Hammer, N. I. *J. Phys. Chem. B* **2014**, *118*, 449.
- (182) Saraswatula, V. G.; Bhat, M. A.; Gurunathan, P. K.; Saha, B. K. *CrystEngComm* **2014**, *16*, 4715.
- (183) Puttreddy, R.; Beyeh, N. K.; Rissanen, K. *CrystEngComm* **2016**, *18*, 793.
- (184) Saikia, B.; Khatioda, R.; Bora, P.; Sarma, B. *CrystEngComm* **2016**, *18*, 8454.

## Introduction

---

- (185) Vukotic, V. N.; Loeb, S. J. *Supramol. Chem.* **2016**, *28*, 151.
- (186) Puttreddy, R.; Topić, F.; Valkonen, A.; Rissanen, K. *Crystals* **2017**, *7*, 214.
- (187) Su, Z.; Mahmoudinobar, F.; Dias, C. L. *Phys. Rev. Lett.* **2017**, *119*, 108102.
- (188) Puttreddy, R.; Jurcek, O.; Bhowmik, S.; Makela, T.; Rissanen, K. *ChemComm* **2016**, *52*, 2338.
- (189) Topic, F.; Puttreddy, R.; Rautiainen, J. M.; Tuononen, H. M.; Rissanen, K. *CrystEngComm* **2017**, *19*, 4960.
- (190) Rybarczyk-Pirek, A. J.; Łukomska-Rogala, M.; Wojtulewski, S.; Palusiak, M. *Cryst. Growth Des.* **2015**, *15*, 5802.

### Chapter 2

#### Experimental and Computational Methods

The inter- and intra-molecular non-covalent interactions can be characterized by various experimental and computational techniques. X-ray and neutron diffraction methods are the experimental techniques used to determine the high resolution structures of non-covalent interactions (weak H-bonds)<sup>1</sup>. In these techniques geometrical properties like bond length and bond angles of non-covalent interactions are analyzed. The results obtained in diffraction methods are stored in crystal databases like Cambridge Structural Database (CSD) and the Protein Data Bank (PDB) for references. Many chemical and biological systems are difficult to crystallize especially when they possess high molecular weight and lack symmetry.<sup>2</sup> The disadvantage of diffraction methods is that they cannot be applied to the non-crystalline materials. To overcome this, Infrared (IR), Raman and Nuclear Magnetic Resonance (NMR) spectroscopic methods are used. The vibrational frequency of the covalent bond R-D/A-Z (D = Donor atom, A= Acceptor atom) of complex (R-D···A-Z) is measured by the Infrared (IR) spectroscopy and Raman spectroscopy<sup>3-5</sup>. The rotational constants of molecular complexes are determined from Microwave spectroscopy (MW)<sup>6,7</sup> and Vibration-Rotation-Tunneling spectroscopy (VRT)<sup>8</sup>. Nuclear magnetic resonance (NMR) spectroscopy is one of the best techniques to determine the formation of a non-covalent bond and thermodynamical properties (enthalpy (H), free energy (G)) of a complex in solution and solid state. All the experimental methods considered above account for the interactions with the solvent and hence cannot control and distinguish different conformers of non-covalent complexes. Therefore, other experimental techniques are needed to investigate the monomer and 1:1 complexes and their clusters in

## Experimental and Computational Methods

---

isolated condition. The isolation of molecules in the gas phase not only removes solvent effects but also enables progressive addition of interacting molecules in the complex.

In this thesis, high resolution and mass-selective laser spectroscopy and nuclear magnetic resonance (NMR) spectroscopy were used to determine the existence and strength of non-covalent bonds in gas and solution phase respectively. In addition to experimental techniques quantum chemical methods like *ab initio* (coupled-cluster singles doubles and triples, second order Møller–Plesset perturbation theory) and density functional theory (DFT) methods are used to determine the structure and interaction energies. The aim of this chapter is to briefly describe the experimental and computational methods used to achieve the objectives of this thesis.

### 2.1. Experimental methods

The non-covalent interactions are characterized experimentally by using different spectroscopic techniques. Presence of non-covalent interactions in various systems gives rise to subtle spectral signatures. Hence, getting highly resolved spectra is important to obtain the information about non-covalently bonded complexes. The information obtained from the standard spectroscopic techniques is masked by the complexity of the spectrum due to the experiments in these techniques mostly are performed at room temperature in the condensed phase. At room temperature for aromatic and polyatomic molecules, a large density of states (rotational and vibrational) is populated which results into possibility of large number of transitions leading to the spectral congestion in condensed phase. Moreover, in the condensed phase, the peak that appears for each individual transition gets broadened by the frequent collisions with the surrounding molecules and environment causing perturbations in its transitions. The weak non-covalent interaction (H-bonds) energies are lower than the thermal

## Experimental and Computational Methods

---

energy. Therefore, it is not possible to determine the energetic of non-covalent interactions having energy less than the room temperature energy using these conventional spectroscopic techniques at room temperature. In addition to this difficulty, it is also not possible to reveal the donor acceptor interaction energy avoiding complications from neighboring molecules that are present in the condensed phase. The aforementioned problems can be solved only at lower temperature where higher rotational and vibrational levels are not populated which results in reduction in the spectral congestion. Additionally, the problem of molecular collisions can be reduced by carrying out the spectral measurement in gas phase instead of condensed phase. The gas molecules can be solidified by decreasing the temperature of the systems in a normal process and therefore the study of the isolated molecules is impossible. This problem can be solved to some extent by measuring the spectra of the molecules at lowest concentration of analyte molecules by mixing large number of inert gases like Helium, Neon, Argon at lower temperature. Recording the spectra at low temperature not only helps in narrowing the spectral features but also allow easier interpretation. Of all the methods used so far, supersonic expansion method is the best one which simultaneously solves the problems of cooling down the molecules below their freezing point without condensation and reduces the effect of collisions.

### 2.1.1 Supersonic expansion method

Supersonic jet expansion method was first developed and used by Levy and coworkers in 1980.<sup>9,10</sup> Supersonic expansion technique has traditionally been used by spectroscopists to achieve dual objectives i.e. preparing an isolated gas phase sample and producing low internal temperatures. Since the temperature of the system is very low and collision free environment provided by molecular beams spectrum gets greatly simplified as shown in Figure 2.1. Additionally, collision free condition enables us to study the species bound in 1:1 ratio or as

## Experimental and Computational Methods

clusters by weak intermolecular interaction which may not be stable at ordinary condition. The supersonic expansion spectroscopic data can be directly compared with the *ab initio* calculations. Further, experimental data can be taken as the benchmark data to be utilized in the development and testing new theoretical and computational methods.

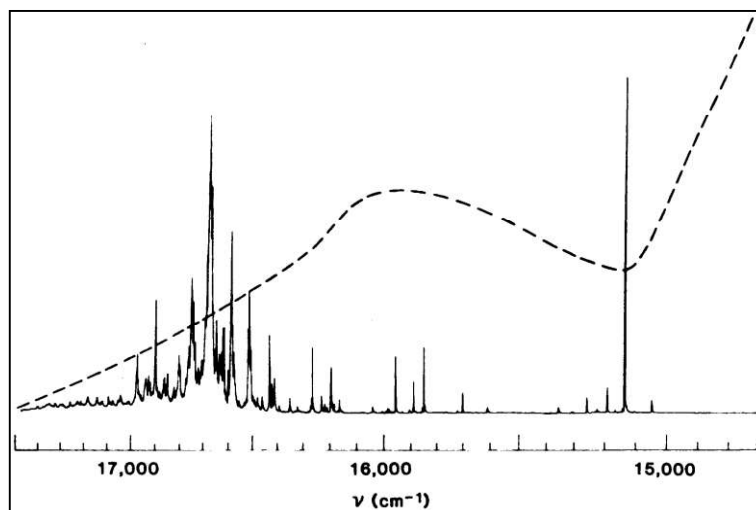


**Figure 2.1** A comparison of the excitation spectra of phthalocyanine measured under static gas room temperature conditions (dashed line) vs jet cooled (solid line), from the ref<sup>9</sup>

A supersonic jet molecular beam is generated by a gas or a mixture of gases expanding from a high pressure region to a low pressure region through a tiny orifice. When required analyte gas is expanded with an inert gas through tiny orifice which has a diameter ( $d$ ), greater than the mean free path of the molecules ( $\lambda$ ) i.e.,  $d \gg \lambda$ , then at trough of orifice the molecules undergo a large number of collisions. Due to these collisions, molecules exchange their kinetic energy (KE) among themselves and the fast moving molecules lose their KE while slow moving molecules gain KE. As a result, the velocity distribution of the analyte molecules becomes narrow. This results in narrow the velocity distribution of analyte molecules and decreases translational temperature among the molecules. After the expansion, the acquired typical

## Experimental and Computational Methods

---

temperatures of molecules are  $\leq 1\text{K}$ ,  $10\text{K}$  and  $50\text{K}$  along the translational, rotational and vibrational degrees of freedom respectively and these vary depending upon molecules and the carrier gas. Figure 2.2 shows schematic representation of the supersonic expansion process and corresponding velocity distribution before and after jet expansion. In this process the flow of molecule is isentropic and the expanding molecules get cooled below their freezing point due to the absence of viscous forces, shock waves and heat conduction.<sup>10</sup> This expansion of molecules converts random thermal motion into directed motion in the expanding gas as shown in Figure 2.2. Therefore the enthalpy for the random motion is reduced in the expansion and the gas is cooled. Under these conditions the temperature, pressure, density, and Mach number (M) are related as shown in the following equations<sup>11,12</sup>. For a perfect gas these relations are

$$\frac{T}{T_0} = \left(1 + \frac{\gamma-1}{2} M^2\right)^{-1} \quad (2.1)$$

$$\frac{P}{P_0} = \left(1 + \frac{\gamma-1}{2} M^2\right)^{\gamma/\gamma-1} \quad (2.2)$$

$$\frac{\rho}{\rho_0} = \left(1 + \frac{\gamma-1}{2} M^2\right)^{1/\gamma-1} \quad (2.3)$$

Where, P = pressure, T = temperature,  $\rho$  = density,  $\gamma$  = ratio of specific heats ( $C_p/C_v$ ) and M=Mach number. The symbols with zero subscript and without zero subscript represent the parameters before and after expansion regions respectively. The Mach number at a distance X from the nozzle of diameter d can be expressed as<sup>13</sup>

## Experimental and Computational Methods

---

$$M = A \left(\frac{X}{d}\right)^{\gamma-1} - \frac{\frac{1}{2}\left(\frac{\gamma+1}{\gamma-1}\right)^{\gamma-1}}{A\left(\frac{X}{d}\right)^{\gamma-1}} \approx A \left(\frac{X}{d}\right)^{\gamma-1} \quad (2.4)$$

Where A is a constant and  $\gamma$  is the ratio of specific heats ( $C_p/C_v$ ). The values of A and  $\gamma$  are (3.26, 5/3) and (3.65, 7/5) for monoatomic and diatomic gases, respectively.

The terminal Mach number can be expressed as

$$M_T = 1.33(P_0 d)^{0.4} \quad (2.5)$$

where,  $P_0$  is the pressure at the nozzle before expansion. By combining equations 2.1 and 2.5 the following equation can be obtained

$$\frac{T}{T_0} = (1 + \varepsilon \times (P_0 d)^{0.8})^{-1}, \quad \varepsilon = \text{constant} \quad (2.6)$$

The above equation gives us the idea of how the temperature changes before and after the expansion with the knowledge of pre-expansion pressure, temperature and nozzle diameter.

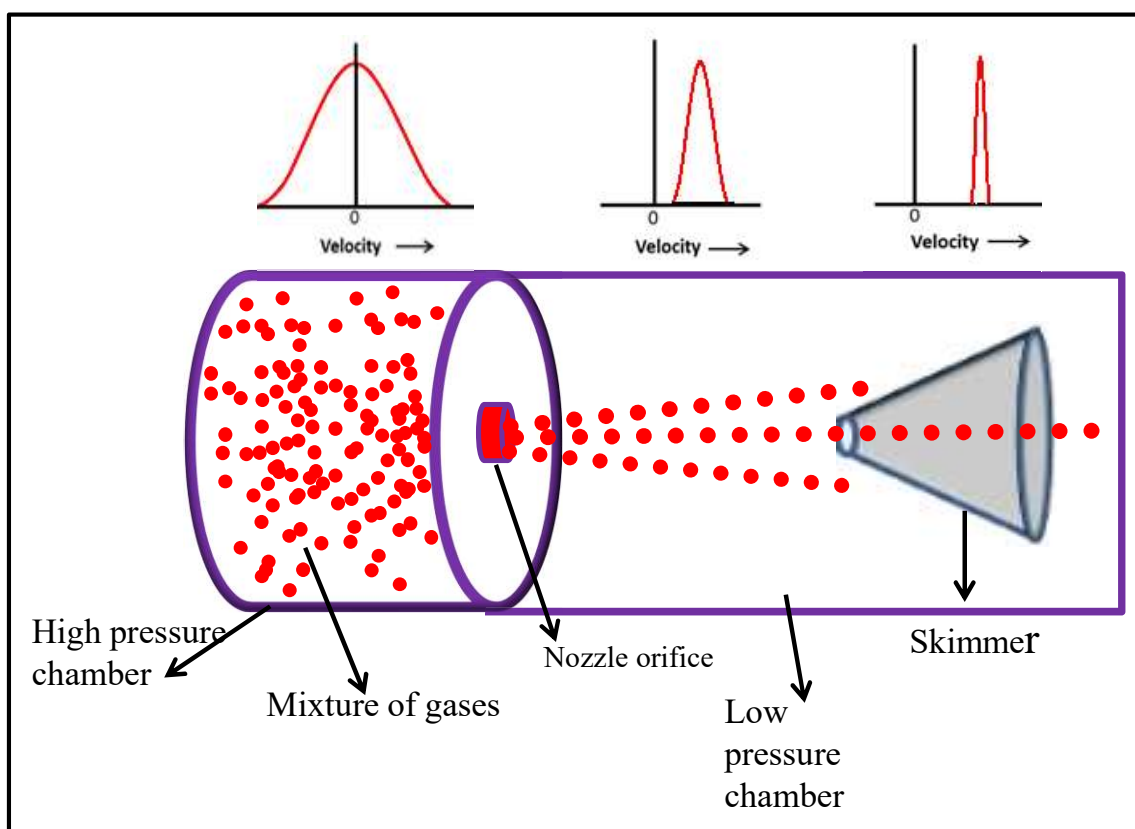


**Figure 2.2** A supersonic jet expansion formed by expansion of a gas from a high pressure chamber to a region of low pressure chamber through an orifice (bottom). The randomly distributed velocities in the pre expansion region get converted into directed flow with a much narrower velocity distribution in the after expansion. (top are the qualitative velocity distribution curves of the molecules in the respective regions).

The velocity distribution of the molecular beam can be expressed in terms of the Mach number (M) by the following equation<sup>13</sup>

$$f(v_x) = \left(\frac{m}{kT_0}\right)^{\frac{3}{2}} \left(1 + \frac{\gamma-1}{2} M^2\right)^{\frac{3}{2}} v_x^2 \exp\left(-\left\{\left(\frac{m}{2kT_0}\right)^{\frac{1}{2}} \left(1 + \frac{\gamma-1}{2} M^2\right)^{\frac{1}{2}} v_x - \left(\frac{\gamma}{2}\right)^{\frac{1}{2}} M\right\}^2\right) \quad (2.7)$$

Here,  $T_0$  is the temperature before expansion.

## Experimental and Computational Methods

The change in velocity distribution of a molecule with respect to the Mach number was represented in the Figure 2.3. It can be seen from the Figure that even with large increase in  $M$ , average velocity does not change significantly.

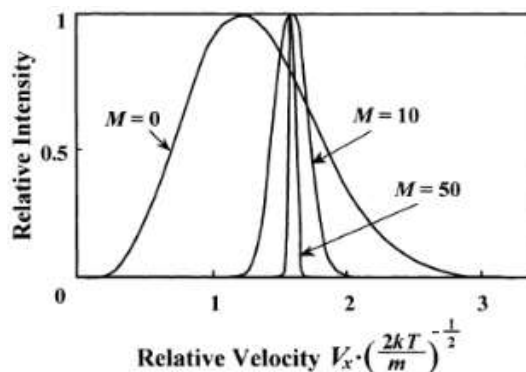


**Figure 2.3** Velocity distributions of monoatomic gases in supersonic jet at different  $M$  values. (Figure is reproduced from the reference (13))

Generation of supersonic beam for different studies of this thesis explained as follow

The vapors of N-phenylacetamide and 2-pyridone are generated by heating at  $\sim 100^\circ\text{C}$ . The nozzle diameter of  $500\ \mu\text{m}$  and operating at 10 Hz by a pulse valve driver (IOTA One, General Valve Corporation). The carrier gas is passed through a sample holder which is positioned before the nozzle where the expansion occurs. In case of solid samples, they were kept in a sample holder and heated appropriately to generate sufficient vapor. Then the sample and Helium were mixed and expanded through nozzle. Helium acts as a carrier gas which was supplied from an ultrapure Helium cylinder through a Teflon tube. In case of liquid and gas samples, premixtures (0.5 % in He) of the sample vapors were prepared in a tank which were then used as carrier gas instead of pure Helium for the supersonic expansion. The schematic of the chamber was shown in the Figure 2.4. The pressures in the vacuum chambers were monitored using ionization gauge. The typical pressures (with the gas pulsing off) were  $2 \times 10^{-6}$

## Experimental and Computational Methods

and  $7 \times 10^{-7}$  Torr in the expansion and ionization chambers, respectively. With the gas pulsing on (300  $\mu$ sec open time, 1-2 atm stagnation pressure) the values of pressure were observed to be  $2-4 \times 10^{-5}$  and  $1-2 \times 10^{-6}$  Torr in the expansion and the ionization chambers respectively.

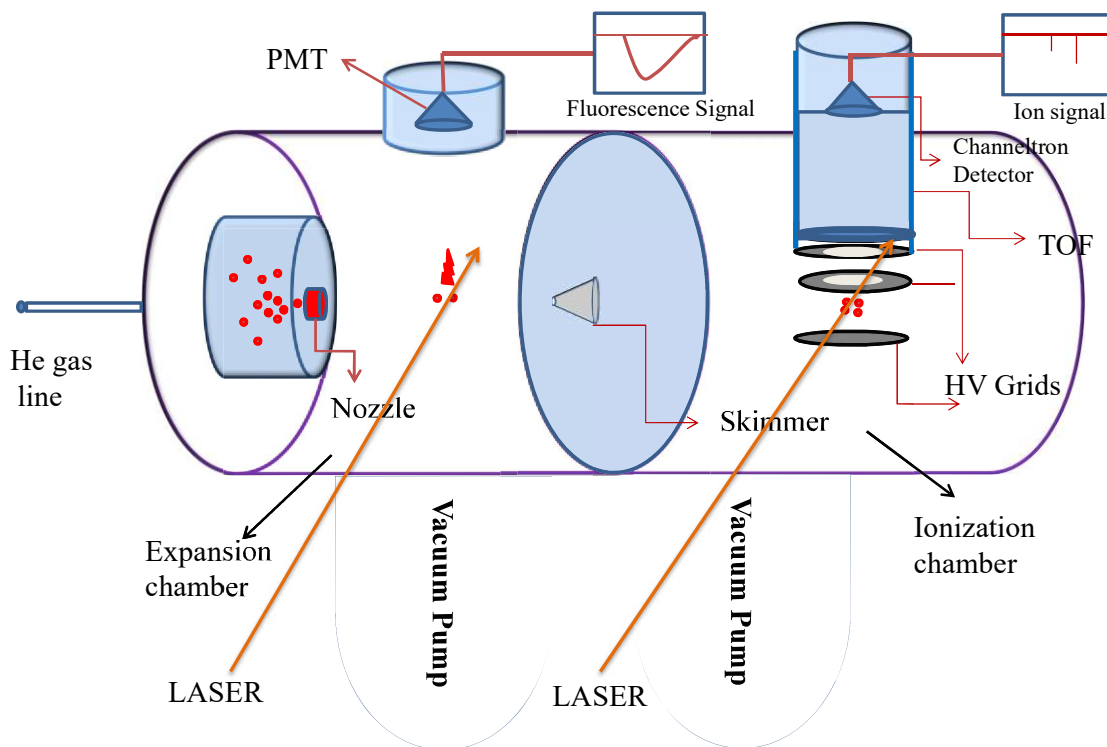


**Figure 2.4** Schematic experimental set-up of High resolution spectroscopy (LIF and REMPI spectroscopy).

### 2.1.2 Electronic excitation spectra of monomers and complexes

The supersonic molecular beam generates less than 1% analyte concentration out of the  $\sim 1 \times 10^{14}/\text{cm}^3$  number density and this molecular beam is probed with the intense light source. Therefore, laser based spectroscopic methods are generally employed to probe the molecular beam. The electronic transitions of the molecules and the complexes were measured by the Laser Induced Fluorescence (LIF) and Resonantly Enhanced Multiphoton Ionization (REMPI) methods.

## Experimental and Computational Methods

---

The LIF and REMPI methods provide the information of the vibronic modes of a molecule in the excited electronic state.

### 2.1.2.1 Laser induced fluorescence (LIF) Spectroscopy

In laser induced fluorescence spectroscopy<sup>14</sup>, the molecules absorb photons from the laser and then excited to the electronic energy as well as its vibrational energy levels. The various levels of vibrational excitation of an electronic excited molecule are called vibronic levels. The excited molecules relax back from its vibronic levels via radiative or non-radiative process. The radiative process called fluorescence and it is monitored by recording total fluorescence as a function of the excitation laser wavelength, see in Figure 2.5. The emission fluorescence collected using a photomultiplier tube (PMT) placed at right angles to both the excitation laser beam direction and the molecular beam direction. Therefore, when the laser energy is in off resonance the molecules would not be excited, thereby no fluorescence will be observed. The obtained electronic spectrum from LIF provides the information of the excited state vibrational levels which are Franck-Condon active with the ground state ( $S_0, v_0$ ). However, in unfavorable cases this is a very sensitive technique for very small quantum yield of molecules. Even in the cases where fluorescence can be detected, not all the excited states of a given molecule can have the same quantum yield. In this case, the peak observed in the spectrum is the product of the absorption strength and quantum yield. However, LIF is limited to some extent due to the fact that fluorescence is not mass selective. Therefore, all the species present in the molecular beam which are fluorescent will show their corresponding transitions in the LIF spectrum. As a result assignment of the individual transition is difficult. This is a major drawback of LIF technique. This problem is overcome by using the mass-selective technique .i.e. REMPI experiment.

## Experimental and Computational Methods

Total fluorescence was detected using a PMT (Hamamatsu IP28) with an appropriate long pass glass filter placed before the PMT detector. A pair of convex lens assembly was kept at the top of the interaction point where laser beam meets the molecular beam. This lens assembly was kept at the perpendicular direction of both the laser beam and the molecular beam direction. Output signal of PMT was digitized on an oscilloscope (Lecroy LT354M) and acquired using homebuilt Labview program via GPIB interface.

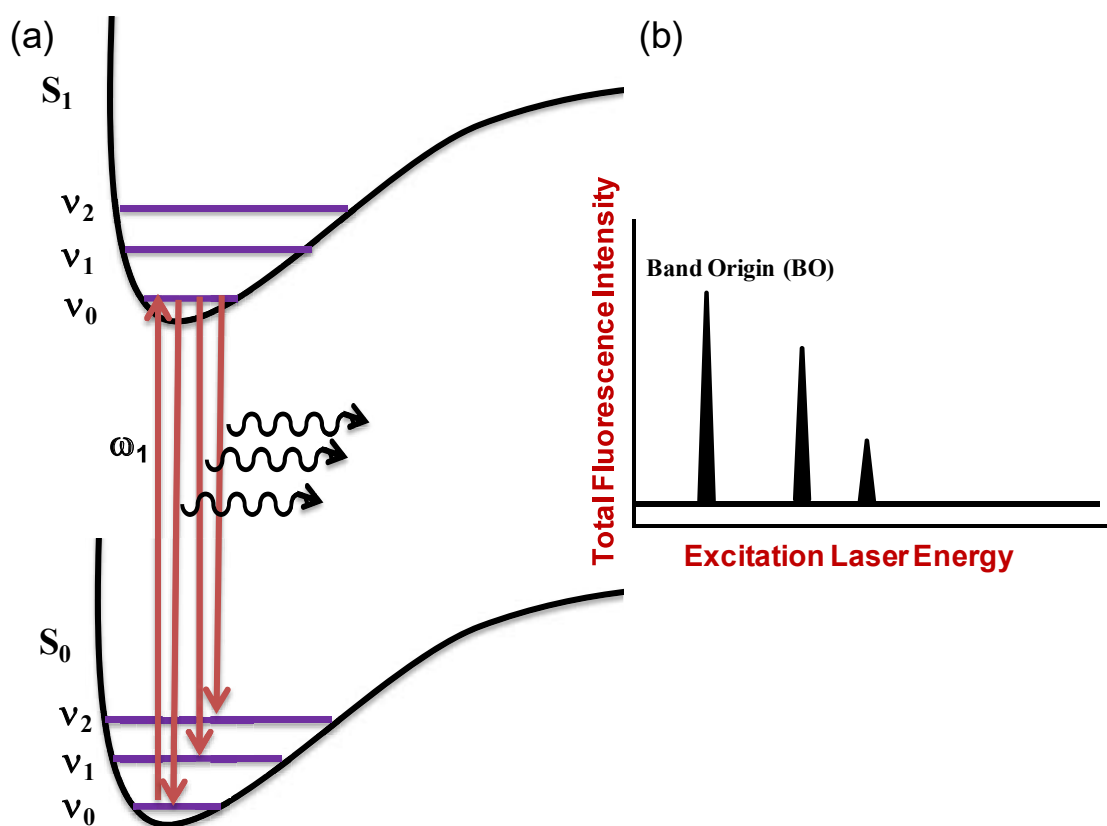


**Figure 2.5** Schematic of a) LIF spectroscopy and b) total fluorescence detection in LIF spectroscopy. In case of LIF spectroscopy total fluorescence is plotted against excitation laser energy ( $\omega_1$ ).

## Experimental and Computational Methods

---

### 2.1.2.2 Resonance enhanced multiphoton ionization (REMPI) or 1-colour (2-colour) resonant two photon ionization (1c or 2c-R2PI)

Resonance enhanced multiphoton ionization (REMPI) technique<sup>15-18</sup> is a mass selective and complementary technique of LIF which also provides the excitation spectra. But in this case the ion signal of a particular mass of monomer or complex is monitored as a function of the excitation laser wavelength. The schematic of REMPI method is shown in Figure 2.6. The  $S_0$ - $S_1$  excitation laser is scanned and chosen the energy ( $\omega_1$ ) of photon to be higher than half way to the ionization potential (IP) to reach higher than IP of the molecule. The resultant spectrum which plots the ion current versus the excitation wavelength is called a resonant two photon ionization (R2PI) spectrum and contains information about the vibrational levels in the excited state (similar to LIF). In this method, like LIF, first the molecules is resonantly excited with its vibronic levels and then probed by second photon of the same laser or of a second laser to ionize the molecule. If the second photon comes from the same source of laser used to excite the molecule, it is called one color two photon ionization (1cR2PI) and if it comes from different source of laser called two color two photon ionization (2cR2PI). In case of 1cR2PI the sum of two photon energy of a single laser is too high than the IP of the complexes, therefore the excess energy can dissociate the complex into its fragments. To avoid fragmentation, soft ionization technique is employed (2cR2PI) where two different laser sources were used which were spatially and temporally overlapped with each other during the interaction with the molecular beam. Intensity of the excitation laser was kept very low so that only single photon absorption can happen and the wavelength of the second photon is chosen in such a way that sum of the two photon energy just exceeded the IP of the complex to be studied. As a result, fragmentation problem is greatly reduced. In this process, the excitation laser is being scanned while the

## Experimental and Computational Methods

ionization laser is kept at a particular wavelength. Whenever, excitation laser will be in resonance with the energy gap between ground and excited state, the ground state molecules will be excited to the excited level, followed by ionization by the absorption of the another photon from ionization laser (Figure 2.6).

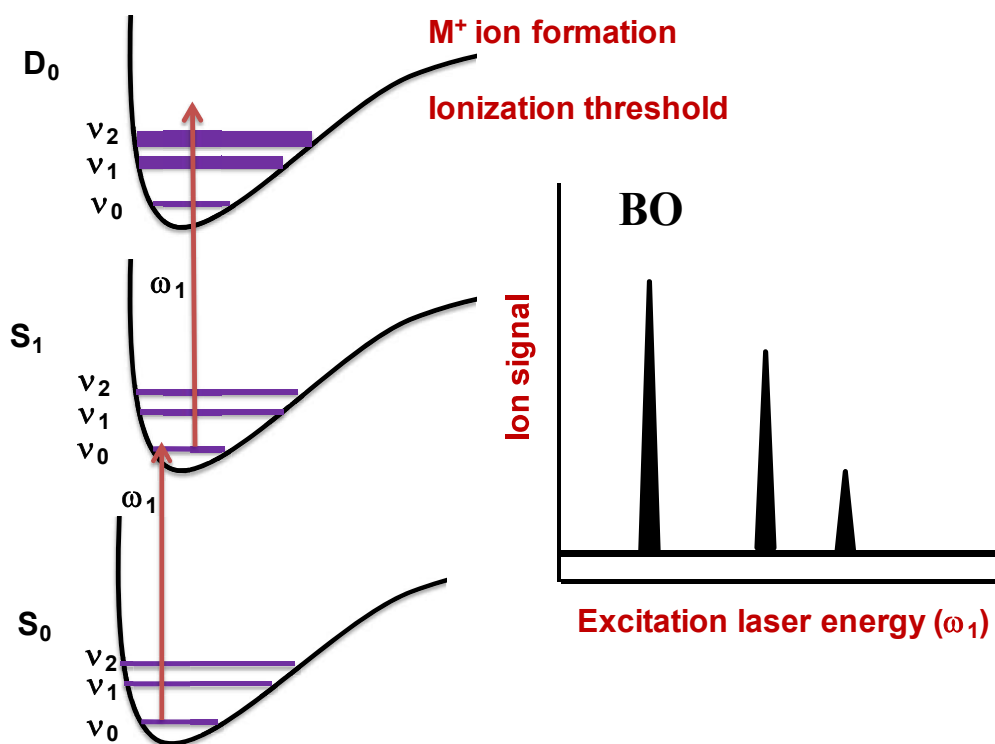


**Figure 2.6** Schematic diagram of the REMPI spectroscopy. The ion signal is plotted against the excitation laser energy ( $\omega_1$ ).

In the above mentioned LIF and REMPI experiments  $\text{Nd}^{+3}$ :YAG pumped dye lasers were employed as the light source. A dye laser (Quantel TDL90), pumped with 532 nm obtained from a second harmonic of  $\text{Nd}^{+3}$ :YAG (Quantel YG 781C, FWHM  $\sim$  6ns, 10 Hz) was used to generate 608 to 732 nm radiation. This light was frequency doubled to produce tunable UV which was used on most occasions as the excitation laser. In the case of two-color REMPI experiments, a second dye laser was used as the ionization laser. The fundamental output (visible range) of the

## Experimental and Computational Methods

---

Molelectron DL18 dye laser pumped with 532nm obtained from the second harmonic of Nd<sup>+3</sup>:YAG (Quantel Brilliant, FWHM ~ 5ns, 10 Hz) was frequency doubled to produce tunable UV to be used as the ionization laser. The typical intensities of the excitation and the ionization UV beams incident on the molecules were of the order of 100 and 500  $\mu$ J per pulse respectively. The temporal synchronization of the lasers and the pulsed valve were controlled by using an electronic delay generator (Stanford Research Systems, DG535). Ions created in REMPI method were detected by using the time-of-flight mass spectrometry.

### 2.1.2.3 Time of flight mass spectrometry

The characterization of different ions of monomers and formation of non-covalent complexes are detected the mass of that particular ion produced by REMPI experiment using time of flight (TOF) mass spectrometry. The time-of-flight detection of ions is based on the principle that electric field is used to accelerate the ions and they get separated temporally according to their  $m/z$  values. Therefore, the ions with different mass  $m/z$  will reach in different time at the detector. By measuring the arrival time of the ions one can get the information of  $m/z$ . The time-of-flight used in our experiment is the Wiley-McLaren<sup>19</sup> type having three grids (dual focusing condition). The typical set-up is shown in the Figure 2.7. The TOF consists of a repeller (bottom grid), accelerator (middle grid), a top grounded grid, field free drift region, electrostatic Einzel lens assembly and an ion detector. The two electric fields i.e.  $E_s$  and  $E_d$  were set in such a way that the initial spatial and velocity distribution of the probed molecules were get minimized and thereby resolution of the mass spectrometer is improved. The ions were produced at the center of the repeller and accelerator where laser beam hits the molecular beam. At this time the time counting on oscilloscope is set at  $T=0$  and when ions fall on the detector, the corresponding

## Experimental and Computational Methods

time is considered as the time of flight. In our experiment intensity of the laser is kept such that single ionization happens i.e.  $z=1$ . For a Wiley-McLaren type TOFMS, it can be shown that

$$T \propto \sqrt{m} \quad (2.8)$$

The above relation can be used as a relative manner i.e. if the time of flight of a reference molecule is known; the mass of the unknown species can be measured using the following equation

$$m_{unknown} = m_{ref} \left( \frac{T_{unknown}}{T_{ref}} \right)^2 \quad (2.9)$$

In our case monomer is considered as a reference mass and the complex is calibrated according to the monomer species.

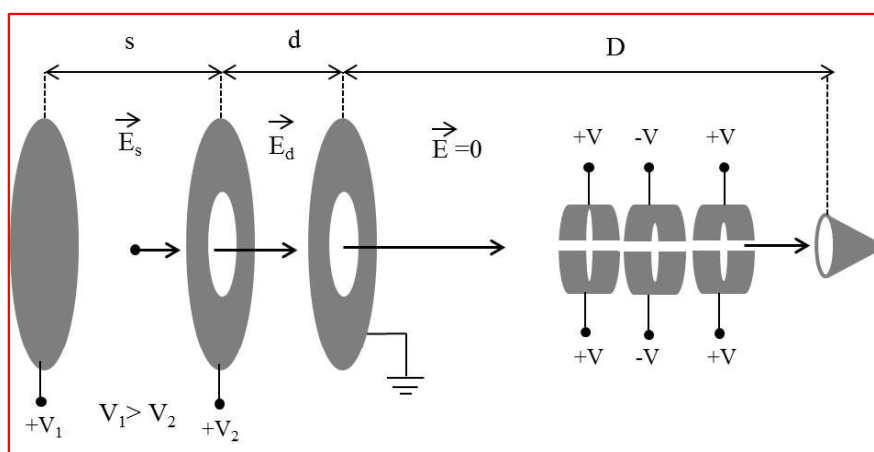


**Figure 2.7** A schematic diagram of the TOF mass spectrometer used for the experiment. The TOF setup is Wiley-McLaren type.

In our set-up the distance between repeller and accelerator grid ( $s$ ) is 32 mm, and that between accelerator and top grounded grid ( $d$ ) is 16 mm. The length of the field free drift

## Experimental and Computational Methods

---

region (D) is 500 mm. The typical voltages applied to the grids were 2900 ( $V_1$ ), 1800 ( $V_2$ ) and 0 volts to the repeller, accelerator and the top grounded grid respectively. The time of flight set-up is also coupled with a set of electrostatic lenses (Einzel lens) in the field free region in order to guide the ionized molecules to the detector. The drawing of the Einzel lens assembly is shown in Figure 2.7. The einzel lens assembly consists of three pairs of stainless steel half cylindrical hollow plates (thickness  $\sim 3$  mm) attached on a Teflon tube for support and insulation. The length of each segment is about 25 mm and they are separated from each other by 5 mm. The plates are held at low voltages supplied by commercially available, 0-200 V adjustable DC power supply through an octal connector mounted on the one of the side ports of the chamber. The voltages on the Einzel lenses 1, 2, 5 and 6 (top and bottom lenses) were kept different positive voltages and 3, 4 (middle lenses) were kept some different negative voltages for the positive ions and opposite for the negative ions.

The detection set-up consists of a single channel electron multiplier (channeltron) as the ion detector (KBL 25 RS Dr. SJUTS Optotechnic GmbH) connected to an oscilloscope via a fast preamplifier. The signal received from the detector was digitized on the oscilloscope and acquired using GPIB interface on to a personal computer. The data acquisition is done by a homebuilt Labview program.

### **2.1.2.4 IR–UV double resonance spectroscopy–Fluorescence depletion by infrared (FDIR)/ Resonant ion depletion by infrared (RIDIR)**

IR-UV double resonance spectroscopy<sup>20-22</sup> is one of the most powerful double-resonance methods for conformational assignment and to get ground state vibrational spectra. Schematic of

## Experimental and Computational Methods

the technique is shown in Figure 2.8. This is a pump-probe method where IR acts as pump beam with the probe being the UV laser. Here, UV laser is fixed to a particular resonance transition of molecule or complex therefore a constant fluorescence signal or ion signal will be observed. Now, approximately, 50 ns prior to the UV laser pulse, an IR laser pulse which is spatially overlapped with the UV laser is made incident with the molecular beam and the IR laser is being scanned. Whenever IR laser will be at resonance with the ground state vibrational levels, population of the ground vibrational state get depleted, therefore total fluorescence signal or ion signal also gets depleted which causes decrease the fluorescence/ion signal through the IR-UV ion-dip spectroscopy. Therefore the dips in the plot of the fluorescence/ion signal vs IR laser frequency will provide the information about the vibrational transitions in the ground electronic state of the probed species.

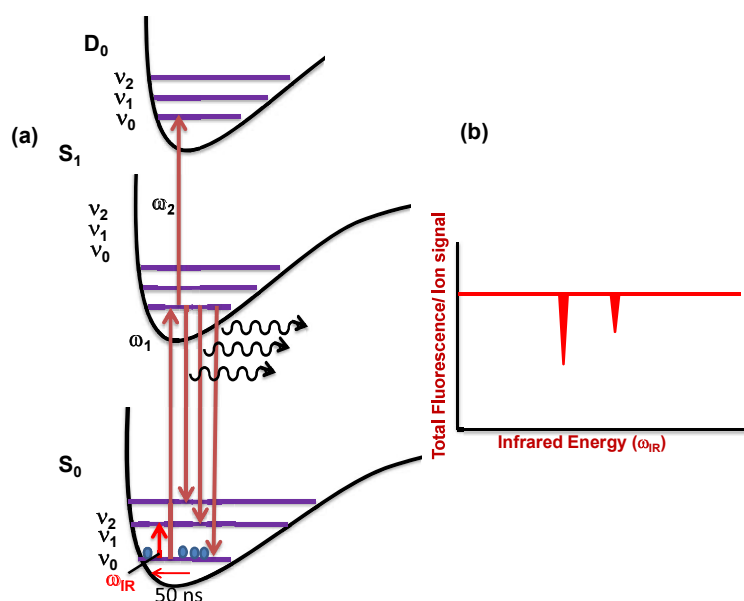


**Figure 2.8** Schematic of the IR-UV double resonance spectroscopy (only FDIR is shown). Total fluorescence signal is plotted against the IR laser energy ( $\omega_{IR}$ ). IR laser pulse comes about 50 ns prior to the UV laser pulse. Whenever, IR laser in resonance in the ground state vibrational levels total fluorescence signal get depleted.

## Experimental and Computational Methods

---

An optical parametric oscillator (LaserSpec) was used for the generation of the tunable IR radiation in the spectral range of 2.6–4.0  $\mu\text{m}$ . The OPO was pumped using an  $\text{Nd}^{3+}$ :YAG pump laser (Quintel Brilliant B, 1064 nm fundamental, FWHM 5ns, 10 Hz, linewidth  $0.06\text{ cm}^{-1}$ ). A  $\text{LiNbO}_3$  crystal was used to generate tunable IR from 2.6 to 4  $\mu\text{m}$  with a line narrowing etalon to limit its bandwidth ( $0.5\text{ cm}^{-1}$ ).  $\text{LiNbO}_3$  crystal has a strong absorption in the spectral region  $\sim 3480\text{--}3510\text{ cm}^{-1}$ ; therefore IR output in this region is insufficient for the experiment. To cover that region a KTP crystal was used without etalon. The UV and IR beams were spatially overlapped in a counter-propagating manner and temporally synchronized such that the IR pulse preceded the excitation pulse by  $\sim 50\text{ ns}$ . The temporal synchronization of the lasers was achieved by a delay generator (SRS DG-535).

Wavelength calibration of IR OPO was done by taking photo-acoustic spectra of water vapor (ambient condition) and  $\text{NH}_3$  ( $\sim 25$  torr of gas with air filled in a gas cell operated at 1 atm). The acquired spectra were compared with the reference lines provided in the HITRAN database. The photo acoustic spectra of water and  $\text{NH}_3$  were used to calibrate O-H ( $4000\text{--}3500\text{ cm}^{-1}$ ), N-H ( $3500\text{--}3200\text{ cm}^{-1}$ ) stretch region, respectively.

### 2.1.3 Spectroscopic Techniques in Solution phase

The above section briefly explained the techniques used to characterize 1:1 non-covalent interaction complexes in gas phase. This section described the standard spectroscopic tools such as nuclear magnetic resonance spectroscopy and vibrational spectroscopy to characterize and finding out the thermodynamic parameter of non-covalent interactions in solution.

### 2.1.3.1 Nuclear Magnetic Resonance Spectroscopy

Nuclear magnetic resonance spectroscopy (NMR)<sup>23</sup> has emerged as a technique that is able to monitor the non-covalent interactions among molecules by measuring the changes of chemical shifts. These different chemical shift values discriminate the nuclei from one another (presence and absence of non-covalent interaction) with their different electronic environments.

In the case of hydrogen bond interactions, we monitored the  $^1\text{H}$  nuclei (chapter-3, part-B) chemical shifts as a function of concentration and temperature. The peak of hydrogen bonded nuclei directly depends on the electron density at  $^1\text{H}$  nuclei which reduces with the formation of hydrogen bond. Then the corresponding average  $^1\text{H}$  nuclei chemical shift moves towards the downfield or high resonance frequency with increasing of H-bond complex formation. The same phenomena are also observed in  $^{13}\text{C}$  nuclei for the formation carbon bond (C-bond). The existence and strength of C-bond were determined by performing the  $^{13}\text{C}$  NMR titration experiments. Formation of C-bond results the change in the chemical shift of  $^{13}\text{C}$  nuclei either downfield or upfield. The strength of non-covalent interactions (H-bond, C-bond) can determine with titration experiments that are monitored by the changes in average chemical shift values with respect to the concentration and temperature. The detailed mathematical expression for calculation of association constant and thermodynamic parameters were explained in the chapter-3, part-B and chapter-6, part-A.

In condensed phase, it is not possible to control the formation of higher clusters instead of hydrogen bond dimers at particular concentration. Therefore, we performed diffusion ordered spectroscopy (DOSY) experiment to verify the existence of monomer and dimer in the solution at lower and higher concentration, respectively. In solution, molecules are in the Brownian molecular motion, shown in Figure 2.9 (a) called as diffusion of the molecule. If the molecule is

## Experimental and Computational Methods

---

spherical, the diffusion coefficient can be written from the Stokes-Einstein equation<sup>24,25</sup> as follows

$$D = \frac{kT}{6\pi\eta r_s} \quad (2.10)$$

Here  $k$  is the Boltzmann constant,  $T$  is the temperature,  $\eta$  is the viscosity of the liquid and  $r_s$  is the radius of the molecule.

Assuming that molecular volume of solute ( $V$ ) corresponds to spherical shape, it can be written as

$$V = \frac{4}{3}\pi r_s^3 \quad (2.11)$$

considering the molecular density of the molecule  $\rho = M_w \cdot V$  (2.12)

$M_w$  is the molecular weight of the molecule or complex

diffusion coefficient can be rearranged from equations (2.10), (2.11), (2.12), then

$$D = \frac{kT}{6\pi\eta} \left( \frac{4\rho\pi}{3M_w} \right)^{\frac{1}{3}} \quad (2.13)$$

So, the diffusion coefficient of a molecule (solute) in a solution is inversely proportional to the cube root of its molecular weight. Calculating the translational diffusion coefficient directly is not possible, so the diffusion coefficient of a molecule in solution can be determined from the pulsed gradient NMR spectroscopy. In this case, when the gradient pulse is applied on the solution (NMR tube), the molecules can be specially labeled i.e. some of molecules differ from other in their position in the sample NMR tube. If the different positioned molecules moves to previous or new position within the diffusion time ( $\Delta$ ) the second gradient decoded the new position. The measured signal is the integral of the whole sample volume and intensity of the NMR signal is attenuated depending on the diffusion time ( $\Delta$ ) and gradient parameters ( $g, \delta$ ). Then, the intensity change can be measured by following equation

## Experimental and Computational Methods

$$I = I_0 e^{-D\gamma^2 g^2 \delta^2 (\Delta - \frac{\delta}{3})} \quad (2.14)$$

where,  $I$  is the observed intensity,  $I_0$  is the reference intensity (unattenuated signal intensity),  $D$  is the diffusion coefficient,  $\gamma$  is the gyromagnetic ratio of the observed nuclei,  $g$  is the gradient strength,  $\delta$  is the length of the gradient,  $\Delta$  is the diffusion time. Diffusion coefficient can be calculated from the slope of the (Stejskal–Tanner plots) linear correlation between the logarithmic normalized signal strength ( $\log_e(I/I_0)$ ) and the squared gradient pulse power ( $G^2$ ) shown in Figure 2.9 (b). Herein, we measured the diffusion coefficient of monomer and complex at lower and higher concentrations, respectively. The ratios of the diffusion coefficient of the monomer ( $D_m$ ) to that of the dimer ( $D_d$ ) in both cases were found and it is close to 1.2. It confirms the formation of dimer through hydrogen bond (chapter-3, part-B).

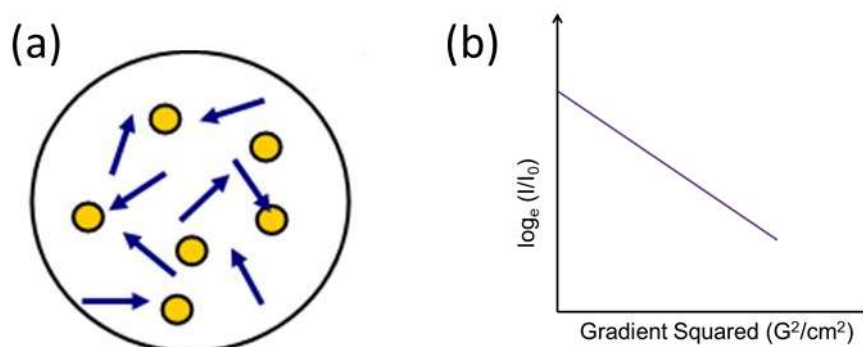


**Figure 2.9** (a) Brownian motion of the solute molecule, (b) Stejskal–Tanner plot

### 2.1.3.2 Horizontal Attenuated Total Reflectance Fourier Infrared Spectroscopy (HATR):

Infrared spectroscopy is a standard technique to investigate the non-covalent interactions presented by their spectral features. Non-covalent interaction has a considerable influence on the stretching vibrational frequency of R-D/A-Z in R-D...A-Z complex. When the non-covalent bond (H-bond) is formed between the two molecules or same molecule the length of the R-H bond usually increases leading to a red shift of the infrared R-H stretching frequency and an increase

## Experimental and Computational Methods

---

in the infrared absorption cross-section for the R-H stretching vibration. The greater the lengthening of the R-H bond the stronger is the H $\cdots$ A bond.

Horizontal attenuated total reflection (HATR) spectroscopy was derived from internal reflection spectroscopy and it was independently pioneered by Fahrenfort<sup>26</sup> and Harrick<sup>27</sup> in the early 1960's. Horizontal attenuated total reflectance (HATR) infrared spectrometer setup is shown in the Figure 2.10. The IR radiation propagating in the optically denser medium (refractive index  $n_1$ ) undergoes total internal reflection at the interface with the optically rarer medium (refractive index  $n_2$ ). The critical angle can be defined as a function of the refractive indices of two media as followed,

$$\theta_c = \sin^{-1} \left( \frac{n_2}{n_1} \right) \quad (2.15)$$

The amplitude of this standing electric wave (E) exponentially decays with distance from the interface in following manner,

$$E = E_0 e^{-\left(\frac{z}{d_p}\right)} \quad (2.16)$$

where  $E_0$  is the amplitude of the electric field at the interface ( $z = 0$ ),  $z$  is the distance from the interface, and  $d_p$  is the penetration depth. The penetration depth ( $d_p$ ) is defined as the distance where the amplitude of the electric field is  $1/e$  of  $E_0$ , which is a function of refractive indices  $n_1$  and  $n_2$ , the incidence angle  $\theta$ , and the wavelength of the IR radiation  $\lambda$ .

$$d_p = \frac{\lambda}{2\pi \sqrt{n_1^2 \sin^2 \theta - n_2^2}} \quad (2.17)$$

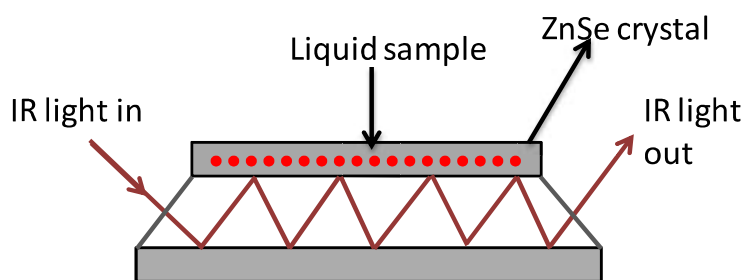


**Figure 2.10** A Horizontal Attenuated Total Reflectance (HATR) experimental setup

The horizontal attenuated total reflectance (HATR) infrared spectroscopy was used to get the vibrational spectra of non-covalent complex and monomers. HATR uses a property of total internal reflection and in this method a solid or liquid sample must be brought near the optical element where a light is totally internally reflected and where the sample interacts with the evanescent wave (Figure 2.10). One advantage of HATR compared to transmission-IR is the limited penetration length into the sample<sup>26</sup>. The advantages of this technique are minimal sample preparation, analysis of samples in their natural states and excellent for thick or strongly absorbing samples.

### 2.2 Computational Methods

The computational methods were used to get the structural parameters and energies of the H-bond and C-bond complexes. The computational methodologies can even probe experimentally inaccessible domains of the energy landscape such as transition states lying on saddle points. These are frequently used in the study of various problems in spectroscopy and molecular dynamics. Moreover, the dissociation energy of a bond, though it has been measured in some cases, is not always experimentally measurable. Hence, even though spectroscopic studies can help elucidate the geometry and mode of bonding in molecular complexes, the energetics of the interaction can only be estimated theoretically. Thus, computations can give interesting insights into the stability of a molecular complex as well as relative ordering of

## Experimental and Computational Methods

---

multiple energy conformers. A brief description of the computational methods used in this thesis is given below.

### 2.2.1 Geometry optimization and frequency calculations:

All the monomers and non-covalent complex geometry optimization and frequency calculations were done using the density functional theory (DFT) methods to compare with experimental results. DFT methods do not describe the London dispersion energy adequately but the computational cost is less with better accuracy.<sup>28</sup> In case of DFT method, the dispersion corrected functional B97-D and Becke, three-parameter, Lee-Yang-Parr B3LYP, exchange correlation PBE0 functional have been used. The B97-D functional belongs to the generalized gradient approximation type. It is based on Becke's power-series ansatz from 1997 that is explicitly represented in terms of parameters including damped atom-pairwise dispersion corrections of the form  $C_6 R^{-6}$  ( $C_6$  = coefficient for atom,  $R$  = atomic vdW radii).<sup>29</sup> The performance of dispersion corrected B97-D functional for noncovalent complex systems including pure van der Waals complexes is good and reaching up to the average CCSD(T) accuracy.<sup>29</sup> However, mostly the optimization structures and frequencies obtained for hydrogen bonded systems and carbon bonded systems at the B97-D levels have been discussed in this thesis. Other DFT functionals B3LYP and PBE0 were also used to optimize and calculate the piezoelectric coefficients of hydrogen bonded systems. We have confirmed the true energy minima by absence of imaginary frequencies for hydrogen bond and carbon bond systems at all levels of theory. Later, the corresponding scaling factors were obtained by matching computed frequencies of the monomers (such as NH of 2-pyridone and N-phenylacetamide) with those experimentally observed. These scaling factors were used for non-covalent complexes. Not only in the isolated condition we also consider the solvation energy to the monomers and hydrogen

## Experimental and Computational Methods

---

bonded complexes in solution. We optimized the structures using the self-consistent reaction field (SCRF) approach<sup>30,31</sup> and Truhlar and co-workers' SMD solvation model<sup>32</sup> taking CHCl<sub>3</sub> as the solvent (in chapter 3 part B).

We have used basis sets developed by Pople<sup>33,34</sup>, Dunning's<sup>35</sup> and Ahlrichs<sup>36,37</sup> which include polarization as well as diffuse functions, Dunning's augmented, correlation consistent basis set. The notation prescribed by Pople for split valence orbitals is X-YZG\*, where the X denotes the number of primitive Gaussians used to construct the core, hyphen separates the core from valence. Y,Z denotes the valence shell is split into two, one is inner shell comprising Y primitive Gaussians and second one an outer comprising Z primitive Gaussians and '\*' indicates that polarization functions have been used for all non-hydrogen atoms. Dunning's augmented basis sets are denoted as aug-cc-pVNZ, where cc is the correlation-consistent and N=D,T,Q...stands for double, triple, quadruple and soon split valence shell. Karlsruhe basis sets were developed by Ahlrich group which is denoted as def2-TZVPP, where as def2 is the second generation of default basis set, TZV stands for valence triple zeta and PP denotes the heavily polarized.

### 2.2.2 Stabilization energy estimation

The binding energies of non-covalent complexes are calculated as the difference in the total energy of the complex and the constituent monomers.<sup>38</sup> This can be represented in Figure 2.12, and the equation is  $X + Y \leftrightarrow X \cdots Y$ . For non-covalent complexes such as hydrogen bond and carbon bond systems  $X \cdots Y$  formed from the monomers X and Y, the binding energy at equilibrium is given as  $\Delta E = D_e = E(X \cdots Y) - [E(X) + E(Y)]$ .

The dissociation energy ( $D_0$ ) is related to the depth of the well ( $D_e$ ) in below schematic representation of potential energy surface shown in Figure 2.11, as

$$D_0 = D_e - \text{ZPE}$$

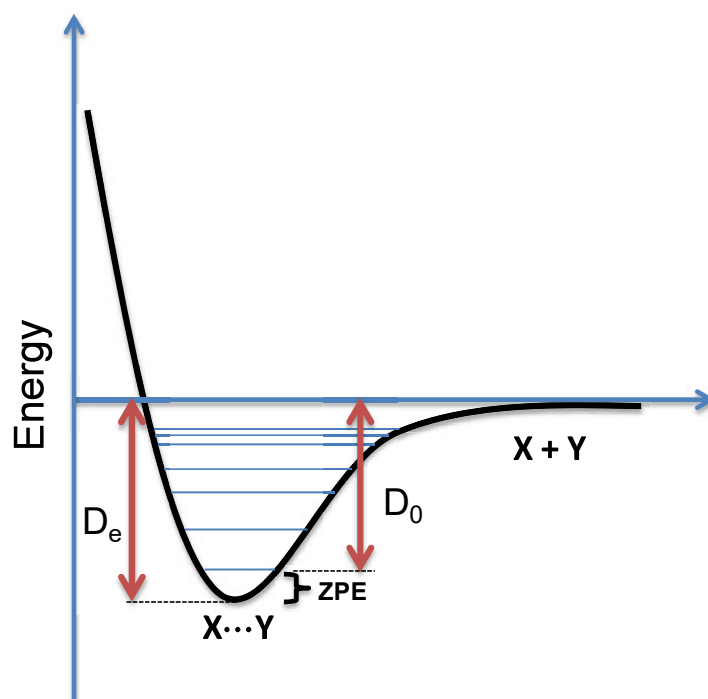


**Figure 2.11** PES of a non-covalent interaction complex ( $X\cdots Y$ ) showing the dissociation energy at equilibrium ( $D_e$ ) the bond dissociation energy ( $D_0$ ) and Zero point energy ( $\text{ZPE} = \frac{1}{2} h\nu$ )

The binding energies of hydrogen bond complexes were estimated at coupled cluster singles doubles and triples CCSD (T) level of method by using the DFT optimized structures. The energy of an oscillator in the ground state is not zero but has some finite value. Thus the binding energy calculated at CCSD (T) level for molecule or complexes must be corrected at the zero point vibrational energy to obtain the true  $D_0$  value. The binding energies and thermodynamic properties of molecules and non-covalent complexes are shown in the following equations

The Electronic energy of molecule or a complex at CCSD (T) with zero vibrational energy corrected can be writing as below

$$E_{Gas}^{CCSD-T} = E_{Gas}^{CCSD-T} + \text{ZPE}_{Gas}^{B97D}$$

## Experimental and Computational Methods

---

$E_{Gas}^{CCSD-T}$  = Electronic energy at CCSD-T in gas phase

$ZPE_{Gas}^{B97D}$  = Zero-point energy correction at B97D/aug-cc-pVDZ level

Binding energy of complexes is given below

$$\Delta E = E'_{Complex} - (E'_{monomer1} + E'_{monomer2})$$

The Enthalpy of molecule or a complex at CCSD(T) with adding zero vibrational energy correction and enthalpy correction can be write as below

$$H'_{Gas}^{CCSD-T} = E_{Gas}^{CCSD-T} + H_{gas}^{B97D}$$

$E_{Gas}^{CCSD-T}$  = Electronic energy at CCSD-T level in gas phase

$H_{gas}^{B97D}$  = Enthalpy correction at DFT level of theory

Change in enthalpy of formation of complex

$$\Delta H = H'_{Complex} - (H'_{monomer1} + H'_{monomer2})$$

The Gibbs free energy of molecule or a complex at CCSD(T) with adding zero vibrational energy correction and Gibbs energy correction can be write as below

$$G'_{Gas}^{CCSD-T} = E_{Gas}^{CCSD-T} + G_{gas}^{B97D}$$

$E_{Gas}^{CCSD-T}$  = Electronic energy at CCSD-T level in gas phase

$G_{gas}^{B97D}$  = Gibbs free energy correction at DFT level of theory

$$\Delta G = G'_{Complex} - (G'_{monomer1} + G'_{monomer2})$$

## Experimental and Computational Methods

In case of weak interactions C-bond complexes (Chapter 6, part B) the single point energies calculations were done at MP2/aug-cc-pVXZ (X=2,3,4) and CCSD and CCSD(T) levels. For a more reliable estimation of the binding, the MP2 interaction energies were extrapolated to the complete basis set (CBS)<sup>39</sup> limit using the two point extrapolation of Helgaker et al<sup>40</sup>.

The energies at CCSD(T)/CBS calculated as followed

$$\Delta E_{CCSD-T/CBS} = E_{HF}^{aug-cc-pVQZ} + E_{MP2/CBS}^{Correlation} + \Delta E_{CCSD-T}^{aug-cc-pVDZ}$$

$$\Delta CCSD(T) = E_{CCSD(T)}^{aug-cc-pVDZ} - E_{MP2}^{aug-cc-pVDZ}$$

$$E_{MP2/CBS}^{Correlation} = \frac{E_{aug-cc-pVQZ}^{MP2-correlation} \times Q^3 - E_{aug-cc-pVTZ}^{MP2-correlation} \times T^3}{Q^3 - T^3}, \text{ Here } Q = 4, T=3.$$

### 2.2.3 Electron density topology and Natural bond orbital analysis of non-covalent interactions:

To confirm the presence of non-covalent interactions in the complexes, Electron density topology maps for the optimized geometries were obtained using Bader's quantum theory of atoms in molecules (QTAIM) theory. The natural bond orbital (NBO) analysis was performed to determine the donor-acceptor pair-wise interaction energy ( $E_{DA}$ ).

The theory of atoms-in-molecules was used to investigate the non-covalent interactions. It helps to characterize the covalent as well as non-covalent interactions in the system with the help of topological parameters, such as the electron density  $\rho(r)$  and its Laplacian  $\rho(\nabla^2\rho)$ .<sup>41,42</sup> It characterizes chemical bonding based on the topology of charge density. A point along the bond path in space at the interatomic surface, where  $\rho(r)$  reaches minimum is called a bond critical

## Experimental and Computational Methods

---

point. At the bond critical point, the second derivative of  $\rho$  ( $\nabla^2\rho$ ) may be positive or negative. The QTAIM criterion for the hydrogen bond was used by Popelier proposed criterion.<sup>43</sup> According to this criterion  $\rho(r)$  has to be between 0.002-0.04 au and ( $\nabla^2\rho$ ) between 0.024-0.139 au at the BCP to qualify the bond as hydrogen bond.

The natural bonding orbital (NBO) analysis<sup>44,45</sup> reduces the multi electron wave function into a set of localized orbitals. Using this approach the electron distribution can be analyzed by the means of familiar concepts such as the occupancy of the bonding and anti-bonding orbitals, orbital overlap, atomic charges, bond order, pair-wise orbital interaction energies. The NBO analysis interpreted in terms of a set of occupied Lewis and a set of unoccupied non-Lewis localized orbitals. Delocalization effects can be identified from the presence of off-diagonal elements of the Fock matrix in the NBO basis. The strengths of these delocalization interactions  $E^{(2)}$  are estimated by second order perturbation theory. In addition, the stabilization energy  $E^{(2)}$  associated with  $i \rightarrow j$  delocalization is estimated by following equation:

$$E^{(2)} = \Delta E_{ij} = q_i \frac{F(i,j)^2}{\epsilon_i - \epsilon_j},$$

where  $q_i$  is the  $i$ th donor orbital occupancy,  $\epsilon_j$ ,  $\epsilon_i$  is the diagonal elements (orbital energies) and  $F(i,j)$  is the off-diagonal element, respectively, associated with the NBO Fock matrix. Therefore, there is a direct relationship between  $F(i,j)$  off-diagonal elements and orbital overlap. We have used NBO 5.0<sup>46</sup> linked with Gaussian09 suite of programs and NBO 6.0<sup>47</sup>.with Gamess suite of programs for this calculation. Donor-acceptor orbital overlap diagram were viewed with Chemcraft software.<sup>48</sup>

## Experimental and Computational Methods

---

Another computational program to assign the non-covalent interactions is the NCI plot, which can examine the non-covalent interaction mapping in real 3D space based on the electron density and their derivatives. The non-covalent interactions can be isolated as regions with low density and low reduced gradient. The sign of Laplacian of the density ( $\nabla^2\rho$ ) is widely used to distinguish between different types of strong interaction<sup>49</sup>. The Laplacian of electron density is the sum of three eigenvalues of the second derivative Hessian matrix such as  $\nabla^2\rho = \lambda_1 + \lambda_2 + \lambda_3$ , ( $\lambda_1 \leq \lambda_2 \leq \lambda_3$ ). The bonding and nonbonding interactions can be identified from the sign of  $\lambda_2$  value. If the  $\lambda_2 < 0$  then it is bonded and if  $\lambda_2 > 0$  then non-bonded interactions, i.e. van der Waal's interaction, hydrogen bonds etc. The density value of this provides the information about their strength. We performed the NCI calculations by using the structures by MP2 wave function file and used NCI-PLOT<sup>50</sup> suite of program. The output files were viewed using the VMD software<sup>51</sup>.

The nature of the different type of non-covalent interactions was identified by the localized molecular orbital-energy decomposition analysis (LMOEDA). This provides information about the contribution of electrostatic, exchange, polarization, charge transfer, repulsive energy and dispersion energies to the total interaction energy. The localized molecular orbital-energy decomposition analysis was carried out using the Gamess suite of program.

### References

- (1) G. R. Desiraju, T. S. *The Weak Hydrogen Bond in Structural Chemistry and Biology*; Oxford University Press., 1999.
- (2) Carpenter, E. P.; Beis, K.; Cameron, A. D.; Iwata, S. *Curr. Opin. Struct. Biol.* **2008**, *18*, 581.
- (3) Ebata, T.; Fujii, A.; Mikami, N. *Int. Rev. Phys. Chem.* **1998**, *17*, 331.
- (4) Munroe, K. L.; Magers, D. H.; Hammer, N. I. *AIP Conf. Proc.* **2010**, *1267*, 854.
- (5) Munroe, K. L.; Magers, D. H.; Hammer, N. I. *J. Phys. Chem. B* **2011**, *115*, 7699.
- (6) Penn, R. E.; Buxton, L. W. *J. Mol. Spectrosc.* **1975**, *56*, 229.
- (7) Warren, I. D.; Wilson, E. B. *J. Chem. Phys.* **1972**, *56*, 2137.
- (8) Dore, L.; Cohen, R. C.; Schmuttenmaer, C. A.; Busarow, K. L.; Elrod, M. J.; Loeser, J. G.; Saykally, R. J. *J. Chem. Phys.* **1994**, *100*, 863.
- (9) Levy, D. H. *Annu. Rev. Phys. Chem.* **1980**, *31*, 197.
- (10) DH, L. *Science* **1981**, *214*, 263.
- (11) Liepmann, H. W., Roshko, A. *Elements of Gas Dynamics*; Wiley: New York, 1957.
- (12) Sanna, G., Tomassetti, G. *Imperial College Press, London* **2005**.
- (13) Imasaka, T.; Moore, D. S.; Vo-Dinh, T. *Pure Appl. Chem.* **2003**, *75*, 975.
- (14) Zare, R. N. *Annu Rev Anal Chem* **2012**, *5*, 1.
- (15) Brutschy, B. *J. Phys. Chem.* **1990**, *94*, 8637.
- (16) Callahan, M. P.; Gengeliczki, Z.; de Vries, M. S. *Anal Chem* **2008**, *80*, 2199.
- (17) Friedrich, D. M.; McClain, W. M. *Annu. Rev. Phys. Chem.* **1980**, *31*, 559.
- (18) Ashfold, M. N. R.; Howe, J. D. *Annu. Rev. Phys. Chem.* **1994**, *45*, 57.
- (19) Wiley, W. C.; McLaren, I. H. *Rev. Sci. Instrum.* **1955**, *26*, 1150.

## Experimental and Computational Methods

---

- (20) Riehn, C.; Lahmann, C.; Wassermann, B.; Brutschy, B. *Chem. Phys. Lett.* **1992**, *197*, 443.
- (21) Ebata, T.; Fujii, A.; Mikami, N. *Int. Rev. Phys. Chem.* **1998**, *17*, 331.
- (22) Anouk M. Rijs, J. O. *Gas-Phase IR Spectroscopy and Structure of Biological Molecules*, 2015.
- (23) Günther, H. *NMR Spectroscopy: Basic Principles, Concepts and Applications in Chemistry*.
- (24) Valencia, D. P.; González, F. J. *Electrochem. Commun.* **2011**, *13*, 129.
- (25) Levine, I. N. *Physical Chemistry*, 2009; Vol. 5th edition, chapter 16.
- (26) Fahrenfort, J. *Spectrochimica Acta* **1961**, *17*, 698.
- (27) Harrick, N. J. *Internal reflection spectroscopy*; Interscience Publishers: New York, 1967.
- (28) Mardirossian, N.; Lambrecht, D. S.; McCaslin, L.; Xantheas, S. S.; Head-Gordon, M. *J. Chem. Theory Comput.* **2013**, *9*, 1368.
- (29) Grimme, S. *J. Comput. Chem.* **2006**, *27*, 1787.
- (30) Curutchet, C.; Orozco, M.; Luque, F. J.; Mennucci, B.; Tomasi, J. *J. Comput. Chem.* **2006**, *27*, 1769.
- (31) Tomasi, J.; Mennucci, B.; Cammi, R. *Chem. Rev.* **2005**, *105*, 2999.
- (32) Marenich, A. V.; Cramer, C. J.; Truhlar, D. G. *J. Phys. Chem. B* **2009**, *113*, 6378.
- (33) Binkley, J. S.; Pople, J. A.; Hehre, W. J. *J. Am. Chem. Soc.* **1980**, *102*, 939.
- (34) Ditchfield, R.; Hehre, W. J.; Pople, J. A. *J. Chem. Phys.* **1971**, *54*, 724.
- (35) Dunning, T. H. *J. Chem. Phys.* **1989**, *90*, 1007.
- (36) Weigend, F.; Ahlrichs, R. *Phys. Chem. Chem. Phys.* **2005**, *7*, 3297.
- (37) Weigend, F.; Furche, F.; Ahlrichs, R. *J. Chem. Phys.* **2003**, *119*, 12753.
- (38) Wendler, K.; Thar, J.; Zahn, S.; Kirchner, B. *J. Phys. Chem. A* **2010**, *114*, 9529.

## Experimental and Computational Methods

---

- (39) Jurecka, P.; Sponer, J.; Cerny, J.; Hobza, P. *Phys. Chem. Chem. Phys.* **2006**, *8*, 1985.
- (40) Helgaker, T.; Klopper, W.; Koch, H.; Noga, J. *J. Chem. Phys.* **1997**, *106*, 9639.
- (41) Bader, R. F. W.; Nguyen-Dang, T. T. In *Advances in Quantum Chemistry*; Löwdin, P.-O., Ed.; Academic Press: 1981; Vol. 14, p 63.
- (42) Bader, R. F. W. *Chem. Rev.* **1991**, *91*, 893.
- (43) Koch, U.; Popelier, P. L. A. *J. Phys. Chem.* **1995**, *99*, 9747.
- (44) Pyykkö, P. *Angew. Chem. Int. Ed.* **2006**, *45*, 28.
- (45) Landis C. Weinhold, F. *Cambridge University Press* **2005**.
- (46) A. E. Reed J. E. Carpenter J. A. Bohmann C. M. E. D. Glendening, J. K. B.-.; hoop, M., and F. Weinhold *Theoretical Chemistry Institute, University of Wisconsin, Madison* **2001**.
- (47) E. D. Glendening, J., K. Badenhoop, A. E. Reed, J. E. Carpenter, J. A. Bohmann, C. M. Morales, C. R. Landis, and F. Weinhold *Theoretical Chemistry Institute, University of Wisconsin, Madison* **2013**.
- (48) <https://www.chemcraftprog.com>
- (49) Bader, R. F. W.; Essén, H. *J. Chem. Phys.* **1984**, *80*, 1943.
- (50) Contreras-García, J.; Johnson, E. R.; Keinan, S.; Chaudret, R.; Piquemal, J.-P.; Beratan, D. N.; Yang, W. *J. Chem. Theory Comput.* **2011**, *7*, 625.
- (51) Humphrey, W., Dalke, A. and Schulten, K. *J. Molec. Graphics*, **1996**, *14*, 33

## Sulfur Centered Hydrogen Bond

---

### Chapter 3

#### Sulfur Centered Hydrogen Bond

Sulfur centered hydrogen bond (SCHB) received proper attention in last 10-15 years due to its importance and existence in biomolecules, viz. amino acids like cysteine and methionine, and in iron-sulfur (Fe-S) proteins<sup>1</sup>. In SCHB the S atom is considered to be poor hydrogen bond acceptor and it forms weak H-bond than conventional H-bond acceptors like O, N, F because of its small electronegativity than O, N, F.<sup>2</sup> The strength of SCHB in crystal structures is also considered as weak from crystallographic structural data analysis.<sup>3</sup> On contrary, recently the combination of high resolution laser spectroscopy and quantum chemical calculations on small molecular complexes revealed that the strength of SCHBs is as strong as conventional N-H...O, O-H...O, O-H...N, H-bonds.<sup>4-8</sup> However the strength of N-H...S H-bonds observed in biomolecules are still unknown and debatable.<sup>6,9-11</sup> Therefore, the determination of the strength of N-H...S H-bond at molecular level is required. Several experimental and computational methods provide evidences in favor of the existence and strength of the N-H...S H-bond in gas phase,<sup>4,5,12-16</sup> but till our work, there was no experimental evidence of SCHB in solution. This chapter is divided into two sections. The first section describes the assessment of the strength of N-H...S hydrogen bond in biomolecules. The second section deals with the H-bond enthalpy for amide/thioamide N-H...S=C-thioamide H-bond in a non-polar solvent.

## Sulfur Centered Hydrogen Bond

---

### 3.1. The Strength of Sulfur Centered Hydrogen Bond (SCHB) in Model Systems of Biomolecules in Isolated Condition

#### 3.1.1 Introduction

Recently, M. Mons et al. have showed that the sulfur atom residing at the side chain of methionine and cysteine is capable of forming amide N-H...S H-bonds in tripeptides<sup>6,16</sup>. In the methionine containing peptides (e.g., Ac-Phe-Met-NH<sub>2</sub>; in short FM) N-H...S H-bonds were surprisingly found to be the strongest among the other H-bonds (N-H...O=C and N-H... $\pi$  H-bonds)<sup>6</sup>. But in case of cysteine containing peptides (e.g. Ac-Phe-Cys-NH<sub>2</sub>; in short FC) the strength of N-H...S H-bonds were similar or even weaker than N-H...O=C H-bonds.<sup>11</sup> It is not clear why S forms stronger H-bond in methionine containing peptides and weaker in cysteine containing peptides. From the geometrical observation, it has been found that the C<sub>6</sub> intraresidue interaction of cysteine (Cys) has a similar bonding pattern as the C<sub>6</sub> intraresidue interaction methionine (Met). In methionine containing peptides, the N-H...S H-bond is formed as C<sub>6</sub> intraresidue H-bond of methionine linking NH<sub>Met</sub> to S atom of Met side chain. It has been observed that the red shift value ( $\Delta\nu = -124 \text{ cm}^{-1}$ ) of N-H stretching frequency is larger in methionine containing peptide than in the cysteine containing peptide ( $\Delta\nu = -46 \text{ cm}^{-1}$ ). The calculated NH...S H-bond distances are  $\sim 245 \text{ pm}$ ,  $277 \text{ pm}$  and the N-H...S H-bond angles are in the range of  $130\text{-}140^\circ$  and  $100\text{-}110^\circ$  in Met and Cys containing peptides, respectively. Hence, the stronger N-H...S H-bond is observed in methionine tripeptide than cysteine tripeptide may be attributed to the conformational constraints. The additional methylene group in the side chain of Met amino acid provides an extra degree of freedom to facilitate the formation of a stronger and shorter H-bond. Hence, it is the intrinsic structural constraints of the peptides, that decide the

## Sulfur Centered Hydrogen Bond

---

strength of the SCHBs. At this point, it is noteworthy to mention that irrespective of their strengths, the N-H...S H-bonds are very important in controlling the conformational landscape of methionine and cysteine containing peptides<sup>11,15</sup>. However, in some cases, the strength of N-H...S H-bonds is regarded as weak in crystal structures and proteins.<sup>2,17</sup> Desiraju et al. classified the N-H...S H-bonds in crystals under the weak hydrogen bond category. Even in proteins, the survey carried out on PDB structures by Zhou et al.<sup>2</sup> revealed that sulfur atom is a very poor H-bond acceptor and the strength of SCHB is as weak as N-H... $\pi$  H-bond. The discrepancies in strength of SCHB in methionine and cysteine containing peptides and proteins put a challenge to the spectroscopists to determine the absolute strength of amide-N-H...S H-bond in peptides and proteins. To determine the strength of SCHB precisely we have used the high resolution gas phase vibrational spectroscopy and benchmark quantum chemical calculations at CCSD(T). In both the cases we studied 1:1 intermolecular complexes of amide and S/O containing small molecules in gas phase isolated conditions, thereby eliminating environmental and conformational effects.

### 3.1.1.1 The small molecules as model compounds of proteins and nucleic acids.

The model compounds used to investigate the strength of N-H...S H-bond are shown in Figure 3.1.1 along with the other types of H-bond donor and acceptor pairs. The model compounds N-phenylacetamide (NPAA), N-methylformamide (NMFA) and 2-pyridone (2-PY) were chosen as H-bond donors consisting of trans and cis amides, representing the amides in peptides and nucleobases, respectively. DME (dimethylether), DMS (dimethylsulfide), DMF (dimethylformamide) and benzene (Bz) were chosen as H-bond acceptors that represent the side chain of serine (O-), methionine/cysteine (S-), backbone/side chain (-C=O) and side chain

## Sulfur Centered Hydrogen Bond

aromatic groups ( $\pi$ -acceptors), respectively. These H-bond acceptors forms four different types of hydrogen bonds with each H-bond donor which are  $\text{N-H}\cdots\text{S}$ ,  $\text{N-H}\cdots\text{O}=\text{C}$ ,  $\text{N-H}\cdots\text{O}$ , and  $\text{N-H}\cdots\pi$  H-bonds as shown in Figure 3.1.1. Electronic spectra of monomers of H-bond donors (NPAA, 2-PY) and their complexes with H-bond acceptors were obtained by Laser Induced Fluorescence (LIF) Spectroscopy, Resonance-Enhanced Multiphoton Ionization (REMPI) Spectroscopy.

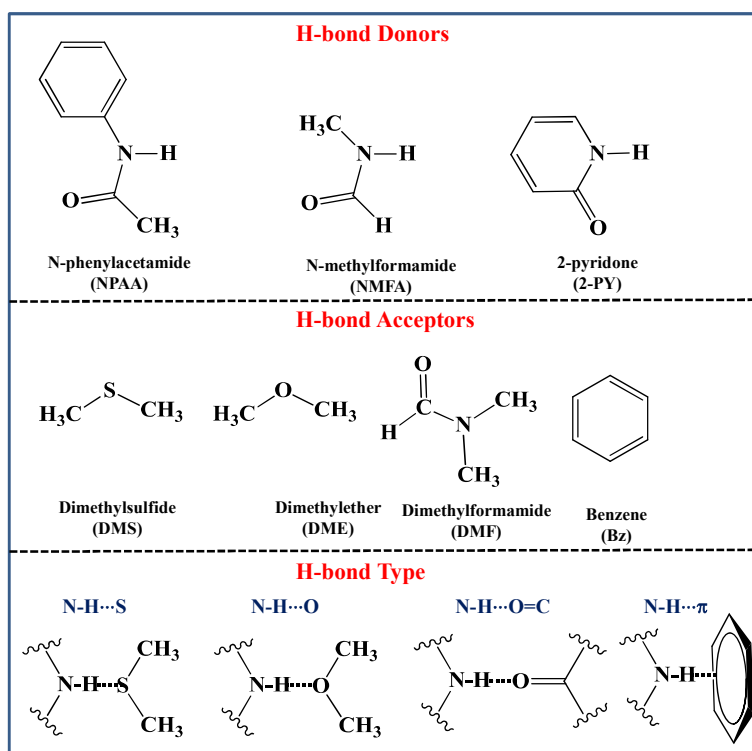


**Figure 3.1.1** Top: Representative *trans* and *cis*-amides as H-bond donors investigated herein. Middle: four different H-bond acceptors. bottom: four different types of H-bonds formed between the donors and acceptors.

## Sulfur Centered Hydrogen Bond

---

### 3.1.2. Experimental and Computational Results

#### 3.1.2.1. Electronic and IR spectra of monomer and H-bond complexes of model compounds

The pre-mixtures of hydrogen bond acceptors DMS, DME, DMF and Bz were prepared about 0.2 to 0.5% in helium gas and used for the complex formation. NPAA and 2-PY were heated to 80-100 °C to obtain sufficient vapor pressure. The cold molecular beam of NPAA, 2-PY and their H-bond complexes were generated by expanding with the passage of helium gas through the H-bond donor vapours and solvent molecules (H-bond acceptors), into vacuum through a pulsed nozzle. The cold monomers and complexes formed in the molecular beam were probed using Laser Induced Fluorescence (LIF) Spectroscopy and Resonance enhanced multi-photon ionization (REMPI) spectroscopy to obtain electronic spectra. Figure 3.1.2 shows the mass selective resonant two-photon ionization (R2PI) spectrum of NPAA and its complexes with DMS, DME, DMF and Bz. An intense peak at 35902 cm<sup>-1</sup> was assigned as the band origin (BO) transition of S<sub>1</sub>-S<sub>0</sub> excitation in NPAA monomer. New peaks were observed for NPAA complexes with DMS, DME, DMF and Bz, which are red shifted by 259, 275, 420, and 401 cm<sup>-1</sup> from monomer BO, respectively, shown in Figure 3.1.2. The observed peaks were assigned as the BO transitions of the S<sub>1</sub>-S<sub>0</sub> state of the NPAA complexes with DMS, DME, DMF and Bz, respectively. The gas phase IR spectrum of NPAA monomer and its complexes were obtained by the IR-UV depletion spectroscopy. The IR spectra obtained by fixing their corresponding UV frequency at BO and probed by scanning the IR laser that was usually introduced ~50 ns prior to the UV pulse. RIDIR spectra of the NPAA and H-bond complexes in the N-H stretch region are shown in Figure 3.1.3. The amide N-H stretching frequency of NPAA was observed at 3472 cm<sup>-1</sup>, while H-bond complexes with DMS, DMF, DME and Bz were observed at 3376, 3399, 3373, and 3460 cm<sup>-1</sup>, respectively. The NPAA amide N-H frequencies were redshifted to 96, 73, 99, 12

## Sulfur Centered Hydrogen Bond

$\text{cm}^{-1}$  in H-bond complexes with DMS, DMF, DME and Bz, respectively. The resulting assignment of the complexes reveals that the amide N-H is involved in H-bonding with different acceptors forming N-H $\cdots$ S, N-H $\cdots$ O=C, N-H $\cdots$ O and N-H $\cdots\pi$  H-bonds. The red shift of the amide N-H stretch for NPAA-DME and NPAA-DMS complexes are similar ( $\Delta\nu \sim 100 \text{ cm}^{-1}$ ) followed by NPAA-DMF and NPPA-Bz complexes. The magnitude of N-H red shift inferred the strength of H-bond. So incase of trans-amide H-bond complexes the strength of N-H $\cdots$ O and N-H $\cdots$ S H-bonds are similar and these are stronger than N-H $\cdots$ O=C and N-H $\cdots\pi$  H-bonds.

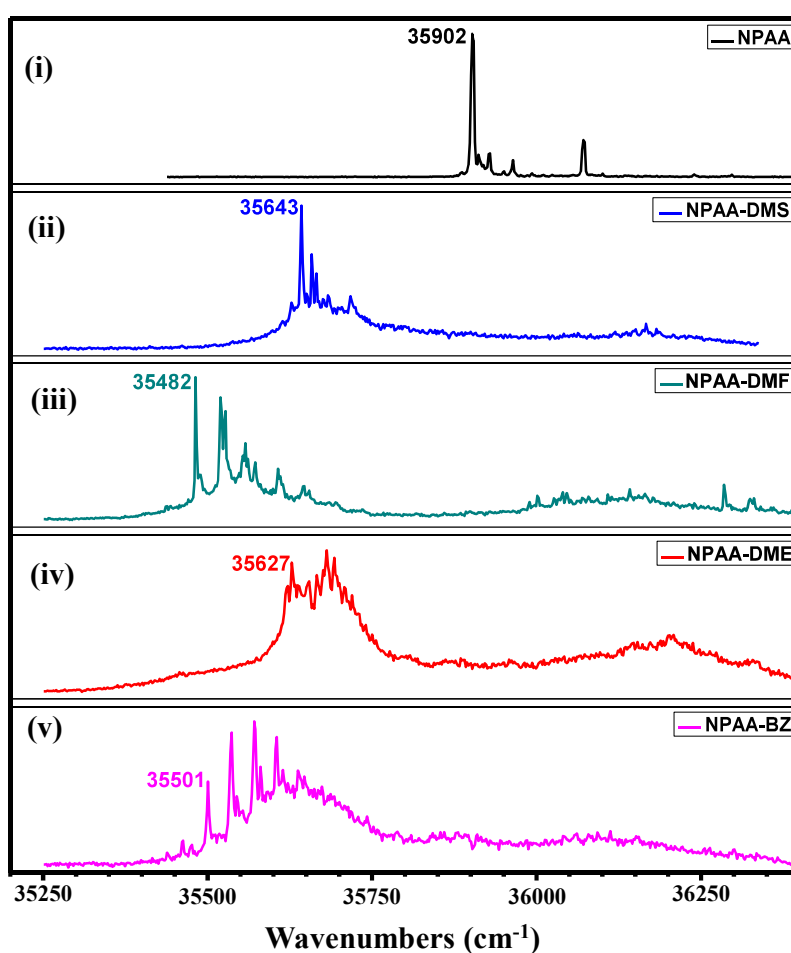


**Figure 3.1.2** The REMPI spectrum of monomer (NPAA) and its H-bond complexes with DMS, DME and DMF and Bz acceptors is assigned as  $S_1$ - $S_0$  band origin (BO). (i) NPAA (ii) NPAA-DMS (iii) NPAA-DMF (iv) NPAA-DME (v) NPAA-Bz

## Sulfur Centered Hydrogen Bond

---

2-pyridone, representing a cis-amide H-bond donor was chosen to mimic amide-N-H...S H-bonds in nucleobase-protein complexes. In this case we have carried out the experiments for 2-PY monomer and its complexes with DMS and DMF. The electronic spectra of 2-PY monomer and its complexes with DMS and DMF were obtained from the LIF spectroscopy, shown in Figure 3.1.4. For 2-PY monomer two intense bands were observed at  $29832\text{ cm}^{-1}$  and  $29930\text{ cm}^{-1}$ . E.R. Bernstein et al and W. Pratt et al assigned these two bands as  $S_1 \leftarrow S_0$  BO transition of keto form. They reported that the appearance of two electronic spectra is due to differ in the nonplanarity at the amine nitrogen of the two separate conformer of lactam in the excited state.<sup>18,19</sup> New peaks were observed in LIF spectrum for 2-PY complexes with DMS, DMF at  $30034\text{ cm}^{-1}$ ,  $30083\text{ cm}^{-1}$ , respectively. The gas phase IR spectra of monomer and complexes with DMS and DMF were obtained from the fluorescence depletion IR (FDIR) spectroscopy. Figure 3.1.5. shows the gas phase FDIR spectra of 2-PY monomer and its complexes with DMS and DMF in the amide N-H frequency range. The stretching frequency of NH was observed at  $3448\text{ cm}^{-1}$  for 2-PY monomer, at  $3157\text{ cm}^{-1}$  for DMS complex and  $3137\text{ cm}^{-1}$  for DMF complex with 2-PY. The 2-PY H-bond complexes with DME and Bz were studied by Mikami et al.<sup>20</sup> and Leutwyler et al.<sup>21</sup> using IR-UV double resonance spectroscopy, respectively. These data were considered to compare amide N-H...S H-bond with other conventional H-bonds. In all the 2-PY complexes the N-H frequencies were red shifted with respect to the 2-PY monomer free N-H.

## Sulfur Centered Hydrogen Bond

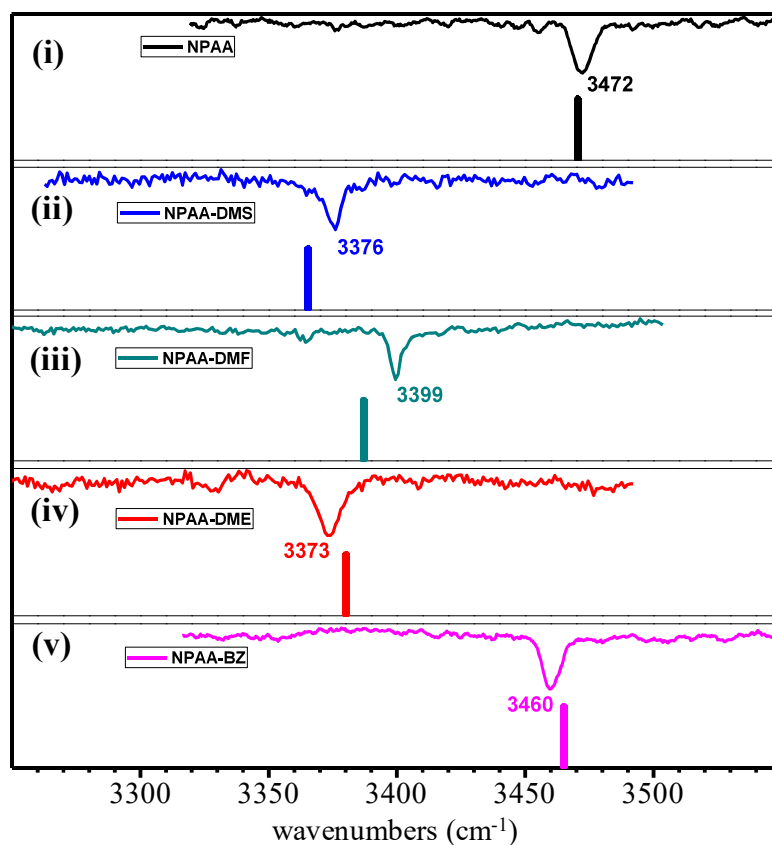


**Figure 3.1.3** Gas phase vibrational spectra of monomer (NPAA) and its H-bond complexes with DMS, DME and Bz acceptors in the N-H stretch region, obtained by IR-UV double resonance spectroscopy. Underneath the experimental spectra, DFT-D calculated stick spectra are presented for the sake of comparison and assignment. The computed vibrational frequencies of the complexes are scaled by 0.9869. (i) NPAA (ii) NPAA-DMS (iii) NPAA-DMF (iv) NPAA-DME (v) NPAA-Bz

## Sulfur Centered Hydrogen Bond

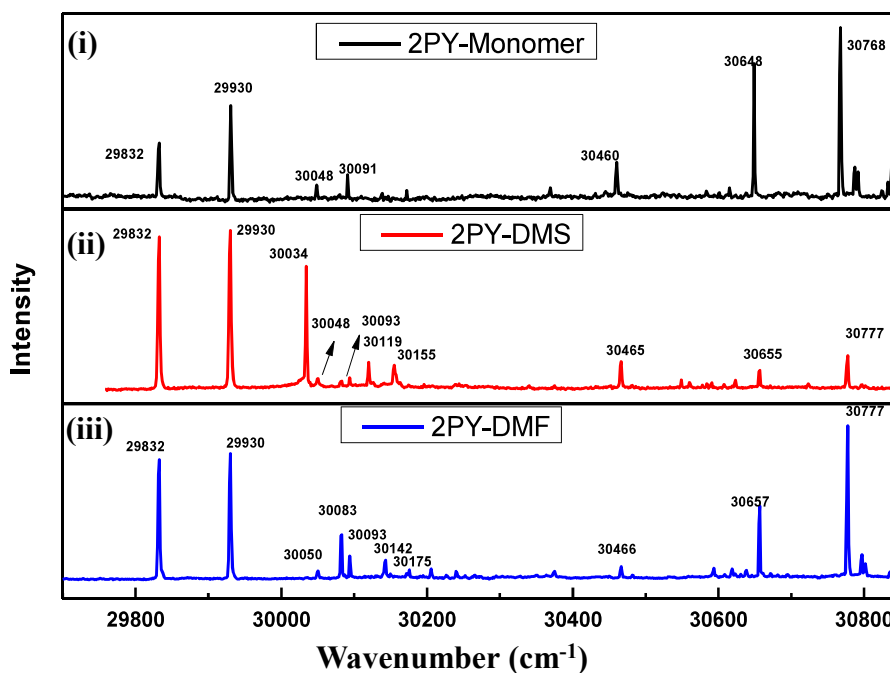


**Figure 3.1.4** The LIF spectra of monomer (2-PY) and its H-bond complexes with DMS and DMF acceptors. (i) 2PY (ii) 2PY-DMS (iii) 2PY-DMF

The red shift values are 291, 311, 250, and 38  $\text{cm}^{-1}$  for  $\text{N-H}\cdots\text{S}$ ,  $\text{N-H}\cdots\text{O}=\text{C}$ ,  $\text{N-H}\cdots\text{O}$  and  $\text{N-H}\cdots\pi$  H-bonds, see Table 3.1.1. The red shift values of N-H stretching frequency of 2-PY complexes were found to be larger than trans amide. In this case, the order of N-H stretching frequency red shift ( $\Delta\nu$ ) follows the order  $\text{N-H}\cdots\text{O}=\text{C} > \text{N-H}\cdots\text{S} > \text{N-H}\cdots\text{O} > \text{N-H}\cdots\pi$ , that is a slight deviation from the trans amide case, the order is  $\text{N-H}\cdots\text{S} \approx \text{N-H}\cdots\text{O} > \text{N-H}\cdots\text{O}=\text{C} > \text{N-H}\cdots\pi$ .

A simple amide N-methylformamide was chosen as trans amide, in this molecule the aromatic ring and extended methyl groups are absent. We have used the computed N-H stretch frequencies of monomer and its complexes with DMS, DME, DMF and Bz which are discussed in next section.

## Sulfur Centered Hydrogen Bond

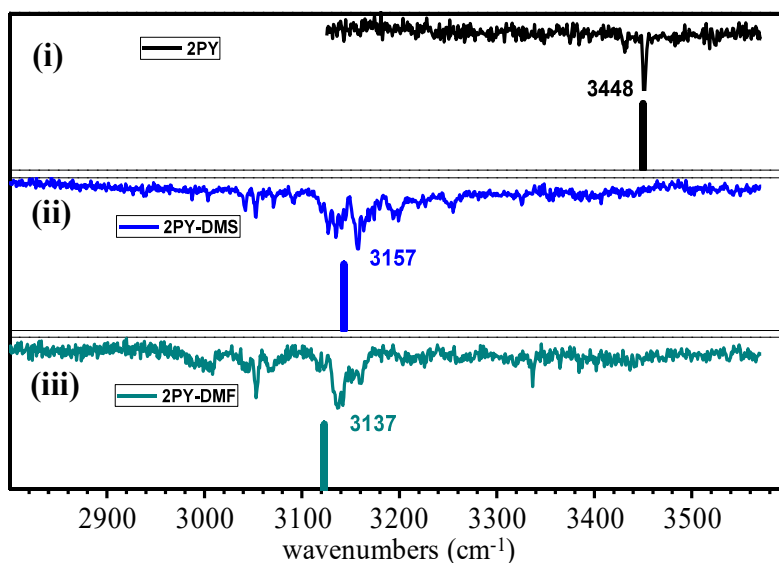


**Figure 3.1.5** Gas phase vibrational spectra of monomer (2PY) and its H-bond complexes with S, and O acceptors in the N-H stretch region, obtained by IR-UV double resonance spectroscopy. Underneath the experimental spectra, DFT-D calculated stick spectra are presented for the sake of comparison and assignment. The computed vibrational frequencies of the complexes are scaled by 0.9869.

### 3.1.2.2. Quantum Chemical Calculations

The experimental N-H frequencies were assigned with the help of density functional theory (DFT). The optimization and frequency calculations for all the monomers and complexes were done using dispersion corrected DFT functional (RI-B97-D3) with def2-TZVPP basis set. We have optimized several H-bond complex conformers and took the global minimum structure for the experimental comparison. The energy and vibrational spectra of global minimum structure were in good agreement with experimental result. Figures 3.1.6 shows the global minimum optimized H-bond complexes. The underneath the experimental IR spectra, Figures 3.1.3 and 3.1.5, represent the computed N-H stretching frequencies of the global minimum structures. From the available experimental and computational NH stretching frequencies we

## Sulfur Centered Hydrogen Bond

have derived the scaling factor which is 0.9869. This is used to estimate the frequencies of NMFA and its complexes, red shift values are shown in Table 3.1.1. The estimated binding energies of monomers and their complexes were calculated at CCSD(T)/aug-cc-pVDZ level of theory. The binding energies ( $D_0$ ) and experimental red shift values of N-H stretches ( $\Delta\nu$ ) are presented in Table 3.1.1. The calculated binding energies of all the complexes are not following the same trend as that of red shift.

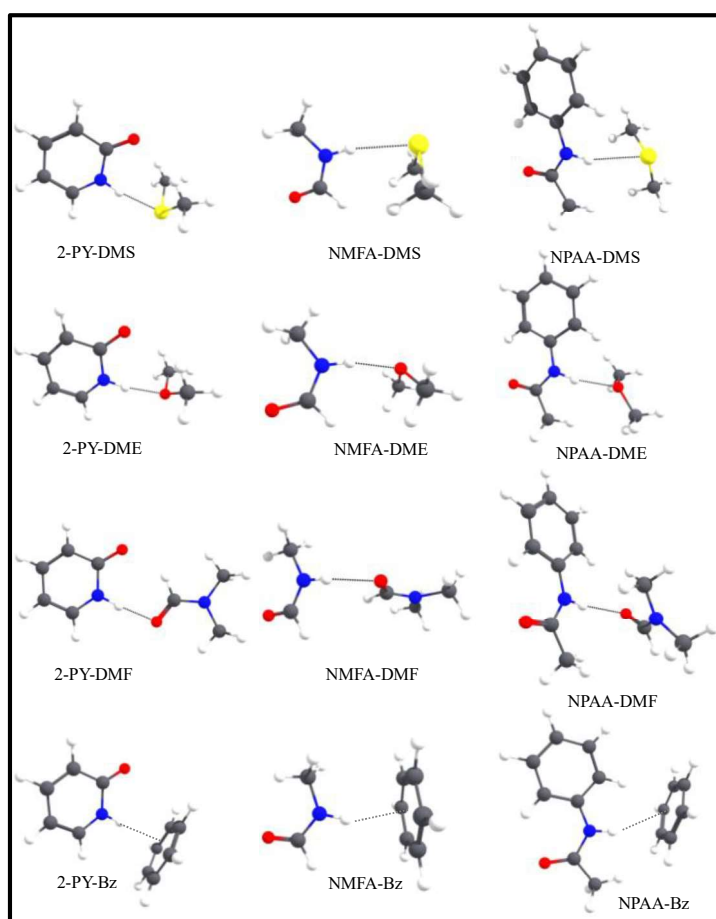


**Figure 3.1.6** The global minimum optimized complexes of NPAA, NMFA and 2-PY with DMS, DME, DMF and Bz obtained at RIB97-D3/def2-TZVPP level

## Sulfur Centered Hydrogen Bond

**Table 3.1.1** Computed binding energy ( $D_0$  in kJ/mol) at CCSD(T)/aug-cc-pVDZ and in parenthesis red shift of N-H stretching frequency ( $\Delta\nu$  in  $\text{cm}^{-1}$ ) for N-H $\cdots$ S, N-H $\cdots$ O=C, N-H $\cdots$ O and N-H $\cdots\pi$  H-bond complexes.

Acceptors Donors	DMS	DMF	DME	BZ
<b>NPAA</b>	40.6 (-96.0)	55.1 (-73.0)	39.2 (-99.0)	40.3 (-12.0)
<b>2-PY</b>	49.0 (-291.0)	57.8 (-311.0)	44.9 (-250.0) <sup>a</sup>	38.1 (-56.0) <sup>b</sup>
<b>NMFA</b>	28.0 (-182.5) <sup>c</sup>	32.1 (-173.7) <sup>c</sup>	27.2 (-147.3) <sup>c</sup>	30.2 (-11.6) <sup>c</sup>

*a, b:* Experimental  $\Delta\nu$  values were taken from references<sup>20,21</sup>, respectively  
*c:* RI-B97-D3/def2-TZVPP computed  $\Delta\nu$  values. Scaling factor: 0.9869

We further confirmed the H-bond existence and their strengths in H-bond complexes computationally by natural bond orbital (NBO) analysis and non-covalent interactions (NCI) analysis. The NBO analysis determines the donor-acceptor interaction energy ( $E_{DA}$ ) of H-bond complexes. This analysis was carried out at MP2/aug-cc-pVDZ level of theory. The orbital overlap between the lone pair (lp) electrons of S/O and the antibonding  $\sigma$  N-H orbital ( $\sigma^*_{N-H}$ ) of trans/cis amides was shown in Figure 3.1.7. From this we infer that the existence of H-bond between N-H and S/O/ $\pi$  and give information of donor-acceptor strength. Non-covalent interaction (NCI) plot for H-bond complexes are shown in Figure 3.1.8., NCI plot shows colored isosurface between donor and acceptor. The blue and green color isosurfaces indicate the attraction between two residues. The blue color represents the stronger attraction between N-H

## Sulfur Centered Hydrogen Bond

and S/O in H-bond complexes. The green color isosurface represents weak attractive interaction in addition to N-H $\cdots$ S H-bond, that means there is small contribution of C-H $\cdots$ S interaction to the total binding energy. In the case of NMFA-Bz complex it seems that the N-H $\cdots$  $\pi$  and C-H $\cdots$  $\pi$  have almost the same contribution to the total binding energy. Because of involvement of C-H $\cdots$ S/O/ $\pi$  interactions the binding energies do not follow the same order of red shift as N-H stretching frequency does.

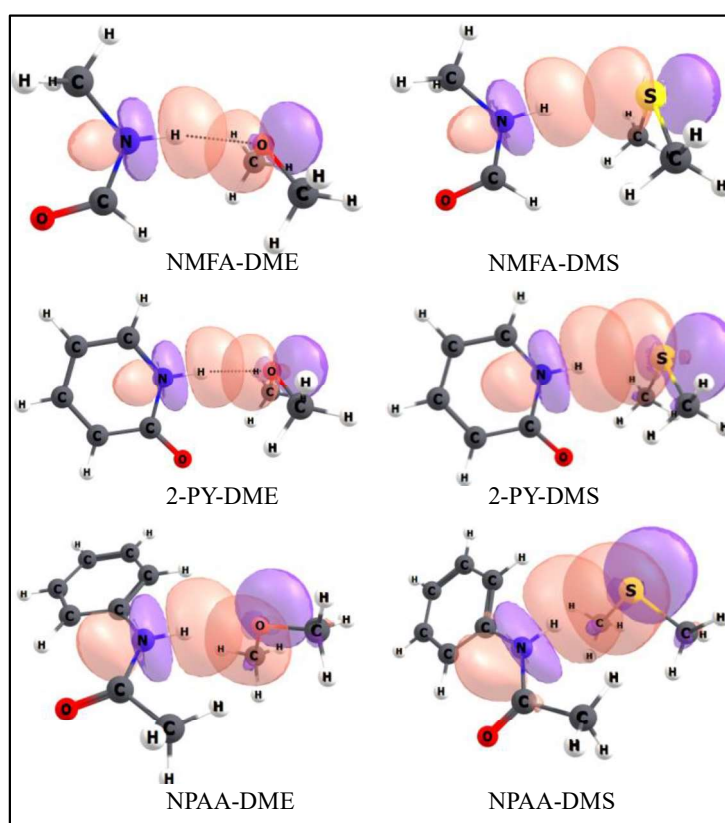


**Figure 3.1.7** The orbital overlap between the lone pair (*lp*) electrons of S/O and the antibonding  $\sigma$  N-H orbital ( $\sigma^*_{N-H}$ ) of *trans/cis* amides

## Sulfur Centered Hydrogen Bond

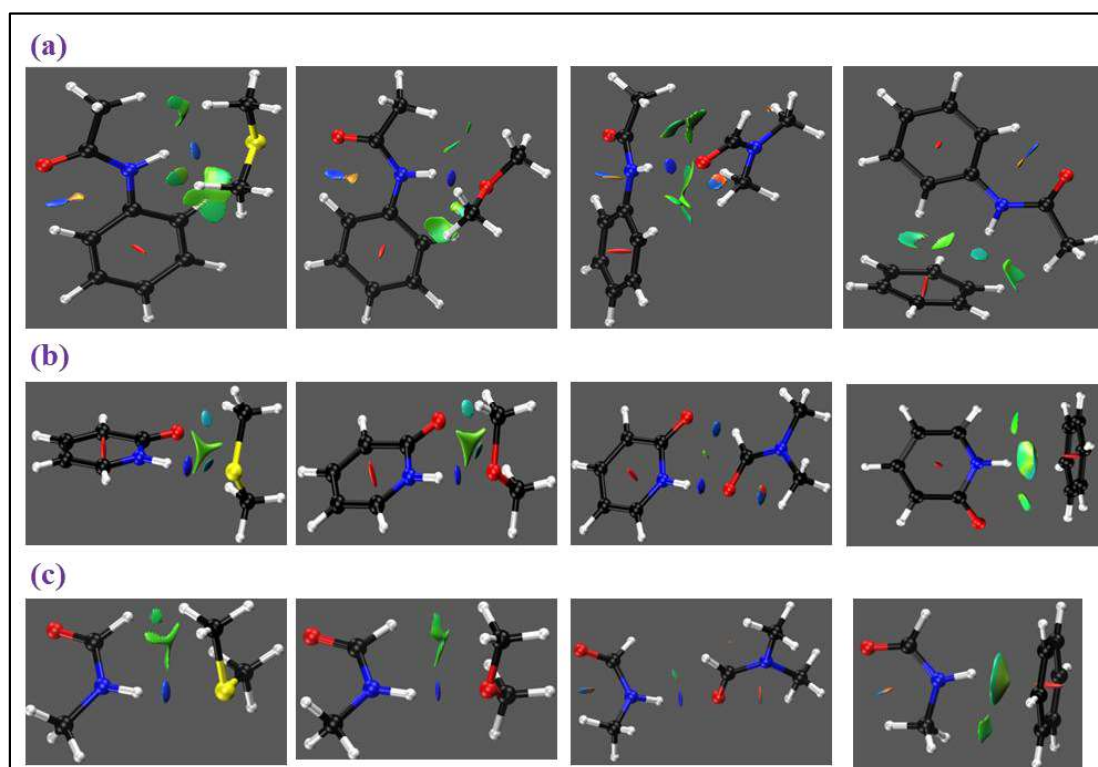


**Figure 3.1.8** Primary N-H...S/O/O=C/π H-bonds and secondary C-H...S/O/π H-bonds in (a) NPAA, (b) 2-PY, (c) NMFA with DMS/DME/DMF/BZ complexes as revealed by colored isosurfaces of the reduced electron density gradient (3D-NCI-plot), following the NCI-plot topological analysis of the electron density at the MP2/aug-cc-pVDZ.

Figure 3.1.9 shows a linear correlation plot between the red shift of N-H and  $E_{DA}$  for all the twelve H-bond complexes. From this study it can be shown that the amide N-H...S H-bond is as strong as classical N-H...O and N-H...O=C H-bonds. The amide N-H...S H-bond energy at the CCSD(T) level is found to be ~30 kJ/mol.

## Sulfur Centered Hydrogen Bond

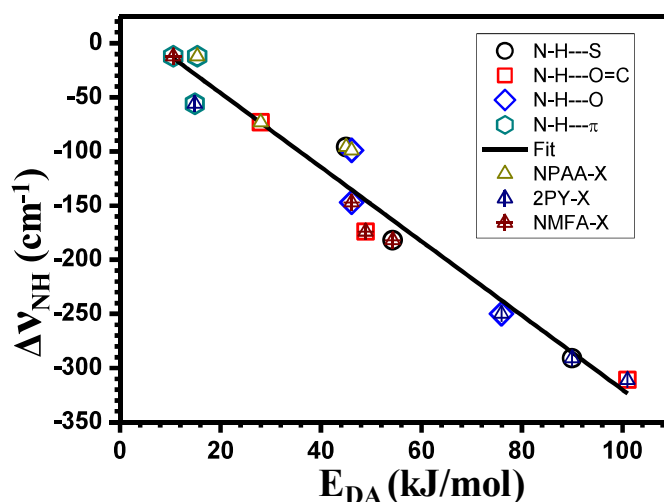


**Figure 3.1.9** Linear correlation plot between donor-acceptor interaction energies and experimental red shift of N-H stretching frequencies in H-bond complexes.

### 3.1.2.3 Comparison with Backbone-amide N-H...S H-Bonds in Peptides and Proteins

The obtained experimental and computational results of model compounds were compared with the work done by M. Mons et al,<sup>6,11</sup> tripeptides that contain methionine and cysteine (FM and FC). The donor-acceptor interaction energy  $E_{DA}$  values were determined for FM and FC and found to be 50.8 kJ/mol and 12.5 kJ/mol, respectively. Figure 3.1.10 shows the orbital overlap between the lone pair orbital of S in methionine side chain and the antibonding  $\sigma$  N-H ( $\sigma_{NH}^*$ ) orbital of backbone amide group, forming an N-H...S H-bond. The obtained  $E_{DA}$  values of FM and FC compared with our model complexes. The  $E_{DA}$  value and experimental red shift ( $124 \text{ cm}^{-1}$ ) of tripeptide FM are similar to that observed model complexes in this work viz NPAA-DMS and NMFA-DMS complexes. The average binding energies of amide N-H...S H-bond complexes computed at CCSD(T)/aug-cc-pVDZ are in the range of 30-40 kJ/mol. This in turn suggests that on relaxing the structural constraints, it is expected that amide N-H...S H-bonds of similar magnitudes should be present in methionine /cysteine containing proteins

## Sulfur Centered Hydrogen Bond

linking the backbone amide N-H and sulfur atom of methionine/cysteine side chains. Figure 3.1.11 shows the intramolecular backbone amide N-H $\cdots$ S H-bonds involving methionine and cysteine as they exist in the two proteins. We took the cartesian coordinates of those amino acid sequences from their protein databank (PDB) structure and added H-atoms manually.

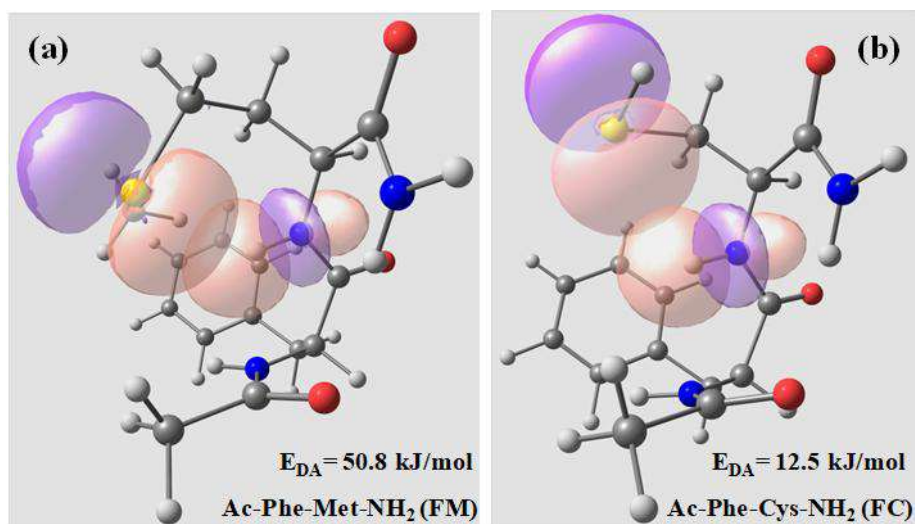


**Figure 3.1.10** NBO 3D overlap diagrams for  $n_S \rightarrow \sigma^*_{NH}$  donor-acceptor interaction in methionine and cysteine containing peptides. The structures presented in (a) and (b) are taken from the gas-phase data<sup>6,11</sup>.

Then they were truncated to only interacting residues and optimized at RI-B97-D/def2-TZVPP level of theory by freezing all the nuclei except the added H-atoms. These optimized structures were used for NBO analysis. The donor-acceptor interaction energies  $E_{DA}$  were found to be 3.9 and 37.5 kJ/mol for amide-N-H $\cdots$ S-methionine and amide-N-H $\cdots$ S-cysteine H-bonds, respectively. These values are very similar to those observed for simple model peptides. This confirms the amide-N-H $\cdots$ S H-bonds in proteins and biomolecules are equally strong H-bonds as their oxygen counterpart. The strength of SCHB in 1:1 intermolecular complex matches well with that of peptides and proteins suggesting amide-N-H $\cdots$ S H-bonds in proteins can be as strong as -N-H $\cdots$ O and -N-H $\cdots$ O=C H-bonds.

## Sulfur Centered Hydrogen Bond

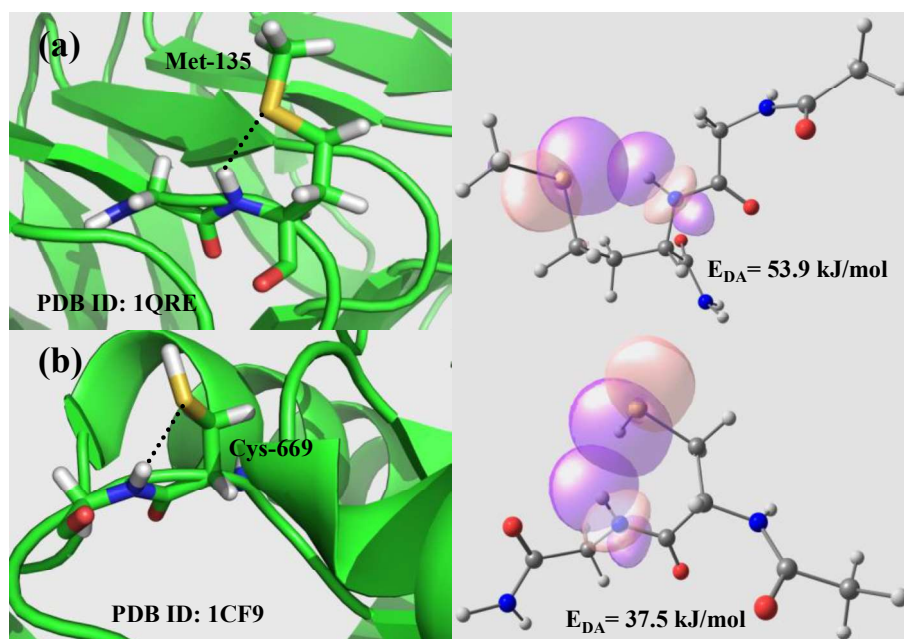


**Figure 3.1.11** (a) Left: Amide-N-H $\cdots$ S hydrogen bond in methionine containing protein, Right NBO 3D overlap diagram for  $n_S \rightarrow \sigma^*_{NH}$  donor-acceptor interaction of same protein (b) Left: Amide-N-H $\cdots$ S hydrogen bond in cysteine containing protein, Right NBO 3D overlap diagram for  $n_S \rightarrow \sigma^*_{NH}$  donor-acceptor interaction of same protein

### 3.1.3 Conclusions

- ❖ The experimental data concludes that amide-NH $\cdots$ S H-bonds in proteins and biomolecules are equally strong H-bonds as their oxygen counterpart, despite lower electronegativity of S compared to O.
- ❖ In the H-bonded complexes of trans-amide, N-H $\cdots$ O or N-H $\cdots$ S H-bonds are found to be stronger in comparison to N-H $\cdots$ O=C and N-H $\cdots$  $\pi$  H-bonds. While in the case of cis-amide the order is N-H $\cdots$ O=C > N-H $\cdots$ S > N-H $\cdots$ O > N-H $\cdots$  $\pi$  H-bonds.
- ❖ A linear correlation between donor-acceptor interaction energies ( $E_{DA}$ ) and red shift of N-H ( $\Delta\nu$ ) is observed.  $E_{DA}$  values for amide-NH $\cdots$ S-methionine and amide-NH $\cdots$ S-cysteine

## Sulfur Centered Hydrogen Bond

---

H-bonds are 53.9 and 37.5 kJ/mol, respectively, are of similar magnitude as those computed for the inter-molecular complexes.

- ❖ The amide-N-H $\cdots$ S H-bond energies obtained at CCSD(T)/aug-cc-pVDZ are  $\sim$ 30 - 40 kJ/mol, suggesting that the amide N-H $\cdots$ S H-bonds are as strong as classical N-H $\cdots$ O and NH $\cdots$ O=C H-bonds.
- ❖ Our findings will help the experimentalists as well as theoreticians to design new force fields for the Protein structure simulation.

## Sulfur Centered Hydrogen Bond

---

### 3.2 Sulfur Centered H-bond Enthalpy in Solution: Thioamides as H-bond Acceptors in Proteins and Nucleic acids

#### 3.2.1 Introduction

The results obtained in the previous section of this chapter revealed that the sulfur centered hydrogen bond i.e. N-H $\cdots$ S H-bond strength is as strong as conventional hydrogen bonds in gas phase without conformational and solvent effects. This high precision gas phase experimental data on SCHB can be useful to chemist and biochemist for estimating the strength of SCHB in gas phase. Recently, F. Biedermann and H. J. Schneider gave a critical summary on essential non-covalent interactions in a review titled "Experimental Binding Energies in Supramolecular Complexes".<sup>22</sup> In this review they enlisted the binding energies of all type of non-covalent interactions like hydrogen bonding, halogen bonding,  $\pi$ - $\pi$ -stacking, cation- $\pi$  and anion- $\pi$  interactions, and hydrophobic interactions in solution phase. But the gas phase binding energies of SCHBs were taken. This is due to till today SCHBs have not been studied in solution. In addition to SCHB H-bond energies in solution phase another problem of SCHB to be addressed, i.e. the hydrogen bond abilities of thioamides are not clear in proteins and nucleic acids.<sup>23,24</sup> Carlos Aleman and Ho-Jin Lee investigated individually the hydrogen bonding strength of thioamides using *ab initio* calculations. These studies led to the finding that the thioamide-N-H is a stronger H-bond donor and the thioamide-C=S is a weaker H-bond acceptor than their corresponding amide counterparts.<sup>24,25</sup> The same trend was observed by Laurence et al. using infrared spectroscopy in hydrogen bond complexes of p-fluorophenol with several thioamides.<sup>26</sup> The opposite trend was also noticed by Byoung K. M. et al. experimentally.<sup>27</sup> They observed that thioamide acts as stronger hydrogen bond acceptor than amide and the strength of H-bond is two times higher than the corresponding amide. This inconsistency of H-bond ability

## Sulfur Centered Hydrogen Bond

---

is not only in model compounds it also extended to biological molecules such as proteins and nucleic acids.<sup>9,28-33</sup> The H-bond ability of thioamides has been used extensively in solution phase to probe the structural disorders in proteins<sup>9,28-33</sup> and nucleic acids<sup>34-40</sup>. With the help of two dimensional NMR spectroscopy and circular dichroism spectroscopy J.H. Miwa et al. studied the stability of secondary structures of proteins by inserting of thioamide linkage into the peptides..<sup>28,29</sup> The incorporation of thioamide linkage into peptides stabilizes II  $\beta$ -turn of peptide and  $\alpha$ -helical secondary structures. They also reported that the  $\beta$ -hairpin conformation is stable at elevated temperatures. Raines and co-workers also have studied the stability of collagen triplex helix by replacing backbone amides with thioamides.<sup>32</sup> In this case they have taken thioamide-substitution within a collagen mimetic peptide (CMP)(Pro-Pro-Gly)<sub>10</sub>. The thermal stability of triple helix was confirmed by circular dichroism spectroscopy and found to be stable with thioamide replacing a central proline (Pro<sup>s</sup>) of CMP. But triple helix of CMP destabilize when thioamide replacing central glycine (Gly<sup>s</sup>). In an extensive work, Petersson and co-workers studied the effect of thioamide backbone substitution in three protein systems (a) calmodulin (CaM), a  $\alpha$ -helical protein; (b)  $\beta$ -sheet and (c) the Polyproline type II helix.<sup>33</sup> They have observed the stabilizing and destabilizing effects of thioamide backbone substitution at different positioning in  $\alpha$ -helix,  $\beta$ -sheet and polyproline type II helix secondary structure motif. This stabilizing and destabilizing of three protein systems are attributed to the stronger H-bond donor ability of thioamide-N-H and weaker H-bond acceptor ability of thioamide-C=S than amide-C=O. It is hard to accept a similar reasoning in proteins where thousands of H-bonds contribute to optimize the protein structure. From the above few examples alone it is not straight forward to conclude that thioamide-C=S is indeed a weaker H-bond acceptor in biomolecules. On the other hand the aforementioned studies<sup>6,11</sup> suggest that sulfur in methionine and cysteine are capable of

## Sulfur Centered Hydrogen Bond

---

forming very strong amide  $\text{N-H}\cdots\text{S}$  H-bonds that encouraged us to further investigate the (thio) amide- $\text{N-H}\cdots\text{S}=\text{C}$ -thio(amide) H-bonds in proteins and nucleic acids in solution.

### 3.2.2 Experimental and Computational Results

#### 3.2.2.1 Computational investigation of strength of SCHB as thioamide H-bond acceptor in proteins and nucleic acids and its model compounds

First, we have taken three PDB structures of proteins (1QX5<sup>41</sup>, 5LPG<sup>42</sup>) and nucleic acids (1KBM<sup>34</sup>) to verify the strength of SCHB in the biomolecules whose coordinates were obtained from the RCSB website<sup>43</sup>. In these structures 10-15 residues around the amide- $\text{N-H}\cdots\text{S}=\text{C}$  H-bonds were chosen and then hydrogen positions were optimized using dispersion-corrected density functional theory (DFT) while freezing all other atomic positions as in the PDB structure. Then we performed the natural bond orbital analysis to find out donor-acceptor interaction energies ( $E_{\text{DA}}$ ) of H-bonds. Figure 3.2.1 depicts structures of proteins, nucleic acids and orbital overlapping between lone pair of S/O/N of acceptor and antibonding N-H ( $\sigma^*_{\text{N-H}}$ ) of donor where thioamide- $\text{C}=\text{S}$  is involved in H-bonding. The  $E_{\text{DA}}$  values along with the H-bonded residues, type of H-bond are provided in Table 3.2.1. The  $E_{\text{DA}}$  values varies from 21 to 77 kJ/mol, suggesting that in some cases conformational constraints imposed by other residues that restrict the N-H and  $\text{S}=\text{C}$  groups to come close enough to have substantial overlap between the lone pair of S and  $\sigma^*_{\text{N-H}}$  to form strong H-bonds. However, the  $\text{N-H}\cdots\text{S}=\text{C}$  H-bond strengths are comparable to those of  $\text{N-H}\cdots\text{O}=\text{C}$  and  $\text{N-H}\cdots\text{N}$  H-bonds in proteins and nucleic acids, (see Table 3.2.1). Since no experimental data of  $\text{N-H}\cdots\text{S}=\text{C}$  H-bond energies are available, it is very difficult to arrive at any conclusion based on the NBO analysis alone. For further confirmation of thioamide forms H-bond and equal in strength with amide carbonyl we screened 23 dimers (see

## Sulfur Centered Hydrogen Bond

Figure 3.2.2) consisting of cis(trans-(thio)amide-N-H $\cdots$ S(O) H-bonds, keeping their relevance in biomolecules in mind. All these dimers and monomers optimization and frequency calculations were carried out at B97D/aug-cc-pVDZ level of theory in solution using the self-consistent reaction field (SCRF)<sup>44</sup> approach and Truhlar and co-workers<sup>45</sup> solvation model based on density (SMD) used by taking CHCl<sub>3</sub> as the solvent. The H-bond enthalpies ( $\Delta H$ ) were calculated at coupled-cluster singles, doubles and triples (CCSD(T)) level for the optimized structures by using CCSD(T)/aug-cc-pVDZ electronic energies and B9D-SMD/aug-cc-pVDZ thermochemistry and solvation energies, the detailed equations are given as below

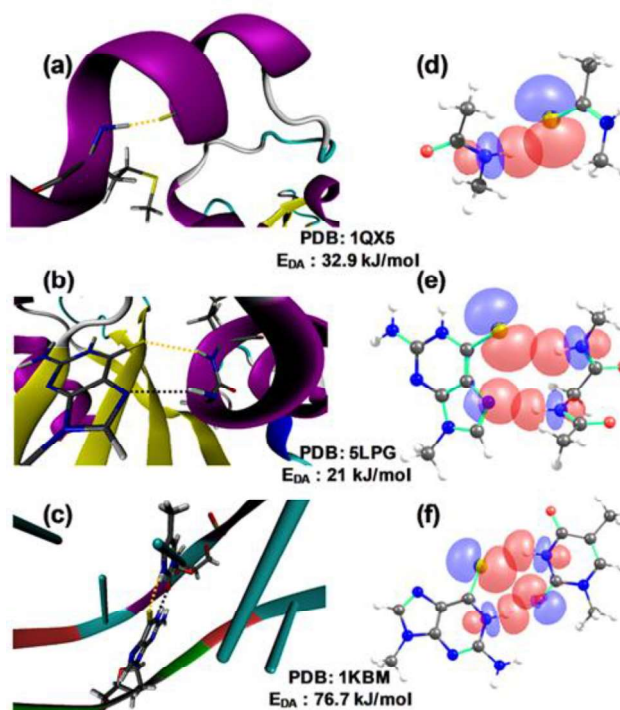


**Figure 3.2.1** Protein and nucleic acid examples of amide-N-H $\cdots$ S=C hydrogen bonds in (a) apoCalmodulin thioamide variant (PDB: 1qx5, Glus1007 substitution)<sup>41</sup>, (b) complex of 6-thioguanosine monophosphate (6-thio-GMP) and NUDT15 ((PDB: 5lpg)<sup>42</sup>, (c) 11-mer DNA duplex containing 6-thioguanine (PDB:1kbn)<sup>34</sup>. The donor-acceptor overlap of p-type sulfur/oxygen/nitrogen lone pair and N-H  $\sigma^*$  orbitals for (d) 1qx5, (e) 5lpg and (f) 1kbn with the donor-acceptor interaction energies for N-H $\cdots$ S=C H-bonds.

## Sulfur Centered Hydrogen Bond

**Table 3.2.1** Donor-Acceptor Interaction Energies ( $E_{DA}$ ) obtained from NBO Analysis at MP2/aug-cc-pVDZ level in biomolecules.

PDB	Donor Residue	Acceptor Residue	H-bond Type	$E_{DA}$ (kJ/mol)
1QX5	1011-MET	1007-GLU <sup>s</sup>	N-H...S=C	32.9
	1011-MET	1007-GLU	N-H...O=C	29.8
1KBM	6-DT(B)	6-S6G(A)	N-H...S=C	76.7
	6-S6G(A)	6-DT(B)	N-H...O=C	70.2
5LPG	138-LEU	1102-71V	N-H...S=C	21.0
	137-GLY	1102-71V	N-H...N-Ar	22.5

The thermodynamic parameters of all the molecules in solution was computed at CCSD (T)/aug-cc-pVDZ as follows

The expression for the Gibbs free energy for the molecule (monomer/dimer) as follow

$$G_{sol}^{CCSD-T} = E_{Gas}^{CCSD-T} + G_{Sol}^{B97D} + ZPE_{Sol}^{B97D} + \Delta E^{Sol}$$

Here  $G' = G_{sol}^{CCSD-T}$  = Gibbs free energy at CCSD-T/aug-cc-pVDZ level in solution

$E_{Gas}^{CCSD-T}$  = Electronic energy at CCSD-T/aug-cc-pVDZ level in gas phase

$G_{Sol}^{B97D}$  = Gibbs free energy correction to electronic energy at B97D(SMD)/aug-cc-pVDZ level

$ZPE_{Sol}^{B97D}$  = Zero-point energy correction at B97D(SMD)/aug-cc-pVDZ level in SMD model

$\Delta E^{Sol}$  = Solvation energy correction at B97D/aug-cc-pVDZ =  $E_{B97D}^{SMD} - E_{B97D}^{Gas}$

Binding energy of dimerization of H-bond dimer

$$\Delta G = G'_{dimer} - 2(G'_{monomer})$$

The expression for the enthalpy for the molecules as follow

## Sulfur Centered Hydrogen Bond

---

$$H' = H_{sol}^{CCSD-T} = E_{Gas}^{CCSD-T} + H_{Sol}^{B97D} + ZPE_{Sol}^{B97D} + \Delta E^{Sol}$$

Here  $H_{sol}^{CCSD-T}$  = Enthalpy at CCSD-T/aug-cc-pVDZ level in solution

$H_{Sol}^{B97D}$  = Enthalpy correction to electronic energy at B97D (SMD)/aug-cc-pVDZ level

Enthalpy change for the dimer is as follow

$$\Delta H = H'_{dimer} - 2(H'_{monomer})$$

Change in entropy for dimerization obtained from the change in Gibbs free energy and change in enthalpy formation. It is given as

$$\Delta G'_{dimer} = \Delta H'_{dimer} - T\Delta S'_{dimer}$$

$$\Delta S'_{dimer} = \frac{1}{T}(\Delta H'_{dimer} - \Delta G'_{dimer})$$

The geometry optimization at lower-level and single point energy calculation at the CCSD(T) level have been regularly employed to get accurate energetics of non-covalent interactions in biomolecules.<sup>46,47</sup> Figure 3.2.2 shows the optimized H-bond dimers of amides and thioamides with their binding enthalpies. The H-bond distances and angles of the optimized structures are provided in Table 3.2.2. In most of the cases, the H-bond angles of N-H $\cdots$ S=C, N-H $\cdots$ O=C are found to be linear, with average of 166 and 171 °C, respectively. The calculated H-bond enthalpies for N-H $\cdots$ S=C H-bonds are in the range of ~-25 to -30 kJ/mol and are close to those of the N-H $\cdots$ O H-bonds. The average H-bond enthalpy ( $\Delta H_{avg}$ ) for the N-H $\cdots$ S H-bond is -25.2 kJ/mol, and that of the N-H $\cdots$ O H-bond is -27.6 kJ/mol.

## Sulfur Centered Hydrogen Bond

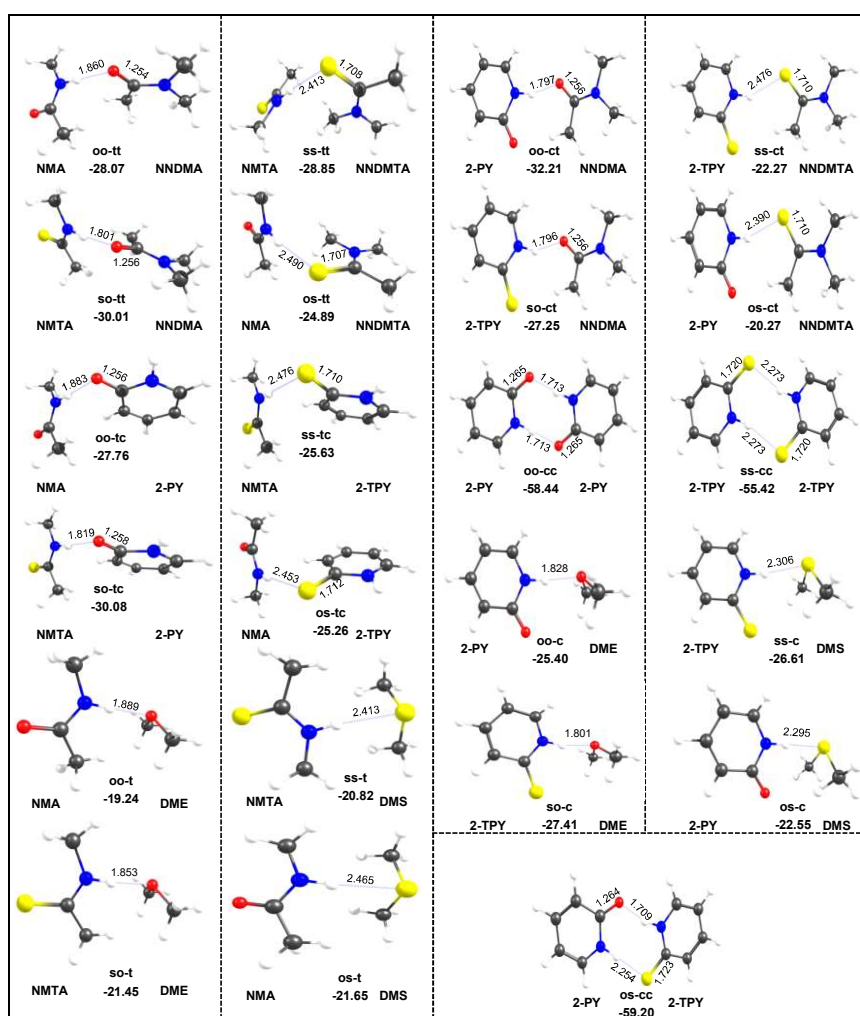


**Figure 3.2.2** Model molecular complexes used to study amide-N-H...S and N-H...O H-bonds in biomolecules. The structures were optimized at B97D-SMD/aug-cc-pvDZ level. The negative values correspond to the H-bond enthalpies in kJ/mol obtained at CCSD(T)-SMD/aug-cc-pVDZ//B97D-SMD/aug-cc-pVDZ level of theory. t: trans (thio)amide, c: cis (thio)amide, oo: amide-N-H...O=C H-bond, so: thioamide-N-H...O=C H-bond, os: amide-N-H...S=C H-bond, ss: thioamide-N-H...S=C H-bond oo: amide-N-H...OMe<sub>2</sub> H-bond, so: thioamide-N-H...OMe<sub>2</sub> H-bond, os: amide-N-H...SMe<sub>2</sub> H-bond, ss: thioamide-N-H...SMe<sub>2</sub> H-bond 2-PY: 2-Pyridone, 2-TPY: 2-Thiopyridone, NMA: N-methylacetamide, NMTA: N-methylthioacetamide, DME: Dimethylether(OMe<sub>2</sub>), DMS: Dimethylsulfide(SMe<sub>2</sub>), NNDMA: N, N-dimethylacetamide, NNDMTA: N, N-dimethylthioacetamide.

## Sulfur Centered Hydrogen Bond

**Table 3.2.2** The geometrical parameters hydrogen bond distance ( $d_{H\cdots O}$ ), angles and hydrogen bond enthalpies for H-Bond complexes optimized at B97D-SMD( $CHCl_3$ )/aug-cc-pVDZ level.

N-H...O				N-H...S			
Complex	$d(H\cdots O)$ (Å)	$\angle(NHO)$ (°)	$\Delta H$ (kJ.mol <sup>-1</sup> )	Complex	$d(H\cdots S)$ (Å)	$\angle(NHS)$ (°)	$\Delta H$ (kJ.mol <sup>-1</sup> )
NMA-NNDMA (oo-tt)	1.860	176.5	-28.07	NMTA-NNDMTA (ss-tt)	2.413	169.4	-28.85
NMTA-NNDMA (so-tt)	1.801	175.5	-30.01	NMA-NNDMTA (os-tt)	2.490	170.5	-24.89
NMA-2PY (oo-tc)	1.883	175.3	-27.76	NMTA-2TPY (ss-tc)	2.375	168.9	-25.63
NMTA-2PY (so-tc)	1.819	175.4	-30.08	NMA-2TPY (os-tc)	2.453	166.9	-25.26
2PY-NNDMA (oo-ct)	1.797	162.9	-32.21	2TPY-NNDMTA (ss-ct)	2.476	148.6	-22.27
2TPY-NNDMA (so-ct)	1.796	154.6	-27.25	2PY-NNDMTA (os-ct)	2.390	160.1	-20.27
2PY-2PY (oo-cc)	1.713	176.4	-58.44	2TPY-2TPY (ss-cc)	2.273	164.4	-55.42
2PY-2TPY (so-cc)	1.709	165.0	-59.20	2PY-2TPY (os-cc)	2.254	176.6	-59.20
2PY-DME(oo-c)	1.828	173.0	-25.44	2TPY-DMS(ss-c)	2.306	170.2	-26.61
2TPY-DME (so-c)	1.801	168.4	-27.41	2PY-DMS(os-c)	2.295	177.5	-22.55
NMA-DME (oo-t)	1.889	175.8	-19.24	NMTA-DMS(ss-t)	2.413	157.7	-20.82
NMTA-DME(so-t)	1.853	172.8	-21.45	NMA-DMS(os-t)	2.465	156.1	-21.65
Avg.	<b>1.812</b>	<b>171.0</b>	<b>-27.61</b>		<b>2.384</b>	<b>165.6</b>	<b>-25.24</b>

These values compared with Desiraju<sup>17</sup> and E.W. Schlag et al. work<sup>48</sup> where the N-H $\cdots$ O=C H-bonds are considered to be strong H-bonds, and their H-bond enthalpies in nonpolar solvents fall in the range of  $\sim$ -20 to -35 kJ/mol. Hence, the N-H $\cdots$ S=C H-bond can also be considered as a strong H-bond. Out of all the dimers the H-bond enthalpies for homo and mixed dimers of 2-pyridone (2-PY) and (2-TPY) are,  $\sim$ -60 kJ/mol as they account for two H-bonds, found to be higher values and strongest H-bonds. We have also calculated the Gibbs free energies and entropies of 2-PY and 2-TPY dimers in solution at CCSD-T/aug-cc-pVDZ level of theory and are provided in Table 3.2.4.

## Sulfur Centered Hydrogen Bond

---

### 3.2.2.2 Experimental investigation of strength of SCHB as thioamide H-bond acceptor in model compounds of proteins and nucleic acids

Solution state nuclear magnetic resonance (NMR) spectroscopic technique was used to determine the strength of SCHBs. This technique is very routinely used by scientists to quantify several non-covalent interactions including H-bonds in solution.<sup>10,49-51</sup> Herein with the help of NMR spectroscopy for the first time we provide very accurate experimental determination of N-H $\cdots$ S=C H-bond energies in solution for model systems without any conformational or structural restrictions. The 2-PY and 2-TPY dimers were chosen as model systems for NMR experiments. The reason for selecting 2-PY and 2-TPY are two-fold: (a) they have very high  $\Delta H$  values and, hence an appreciable amount of their dimers can be formed in solution, enabling easy detection and (b) the  $^1\text{H}$  NMR signal of NH ( $\delta_{\text{NH}} > 10.5$  ppm) is observed in a far lower field than aromatic CH ( $\delta_{\text{CH}} > 6-8$  ppm), (see the Figure 3.2.3 for the 1D  $^1\text{H}$  NMR spectra of 2-PY and Figure 3.2.4 for 2-TPY). Therefore,  $\delta_{\text{NH}}$  can be monitored as function of concentration or temperature without any interference of other  $^1\text{H}$  NMR signals. 2-Pyridone (2-PY), 2-Thiopyridone (2-TPY) and  $\text{CDCl}_3$  were purchased from Sigma-Aldrich. 2-PY and 2-TPY were used directly without purification but  $\text{CDCl}_3$  solvent was dried with molecular sieves before the NMR sample preparation. 2-PY and 2-TPY samples were prepared in  $\text{CDCl}_3$  solvent individually and taken in 5 mm diameter NMR tube separately. We have performed the  $^1\text{H}$  NMR experiments with the initial concentration 0.0005M of 2-PY and 2-TPY in  $\text{CDCl}_3$  separately. The concentration dependent experiment was performed to estimate the association constant of  $2 - \text{PY} \rightleftharpoons [2 - \text{PY}]_2$  and  $2 - \text{TPY} \rightleftharpoons [2 - \text{TPY}]_2$  by monitoring the equilibrium process as a function of concentration because at higher concentration the formation of dimers is favorable. In this case the experiments were done with monitoring the  $^1\text{H}$  NMR signal of NH ( $\delta_{\text{NH}} > 10.5$  ppm) at 16

## Sulfur Centered Hydrogen Bond

different concentrations covering range of 0.0005M to 0.071M. Figure 3.2.5 and 3.2.6 depict the downfield shifts of  $\text{NH}$  peak with an increasing concentration of 2-PY and 2-TPY, respectively. The downfield shift confirms the formation of dimer through  $\text{N-H}\cdots\text{O}$  and  $\text{N-H}\cdots\text{S}$  H-bonds at higher concentrations of 2-PY and 2-TPY, respectively. Table 3.2.3 shows the chemical shift values at different concentrations of 2-PY and 2-TPY.

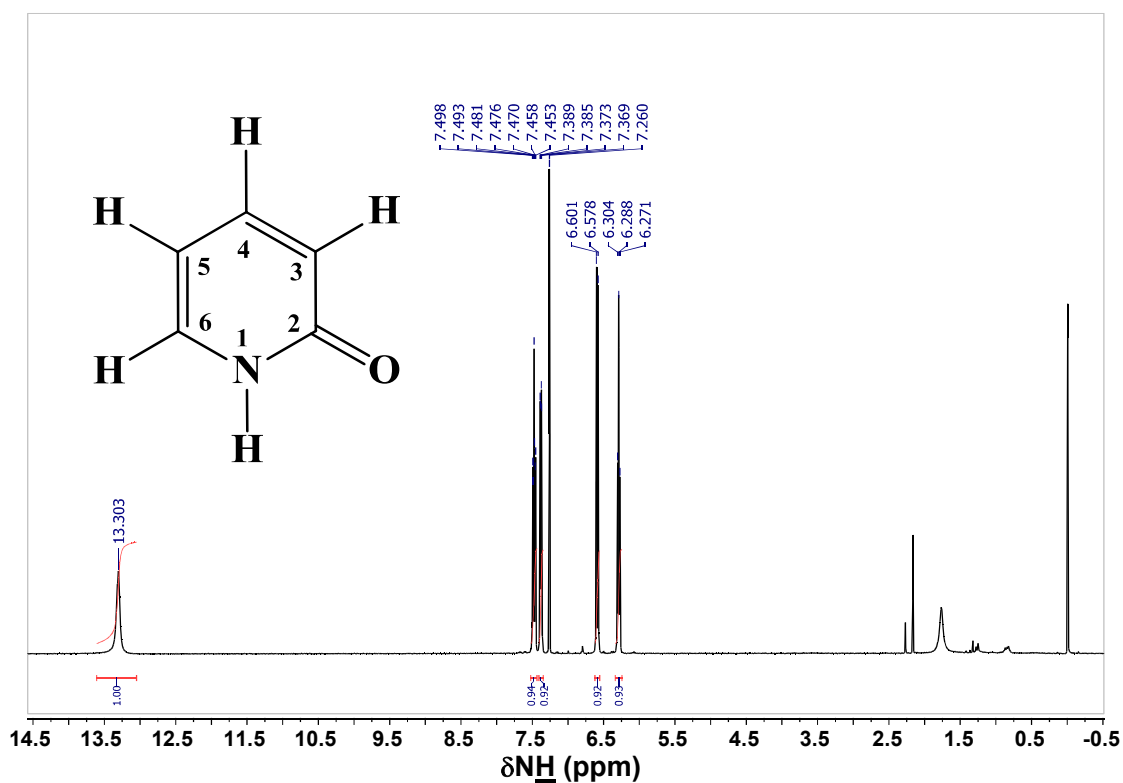


**Figure 3.2.3** 1D  $^1\text{H}$  NMR Spectra of 2-Pyridone at Higher concentration in  $\text{CDCl}_3$  solvent

## Sulfur Centered Hydrogen Bond

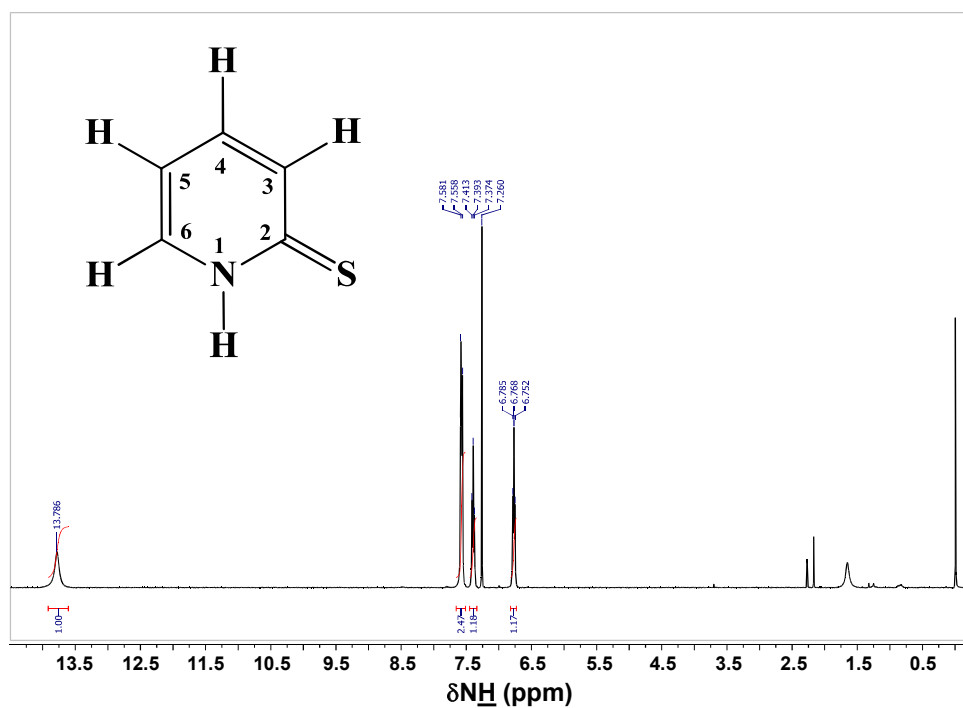


Figure 3.2.4  $1D$   $^1H$  NMR Spectra of 2-thiopyridone at Higher concentration in  $CDCl_3$  solvent

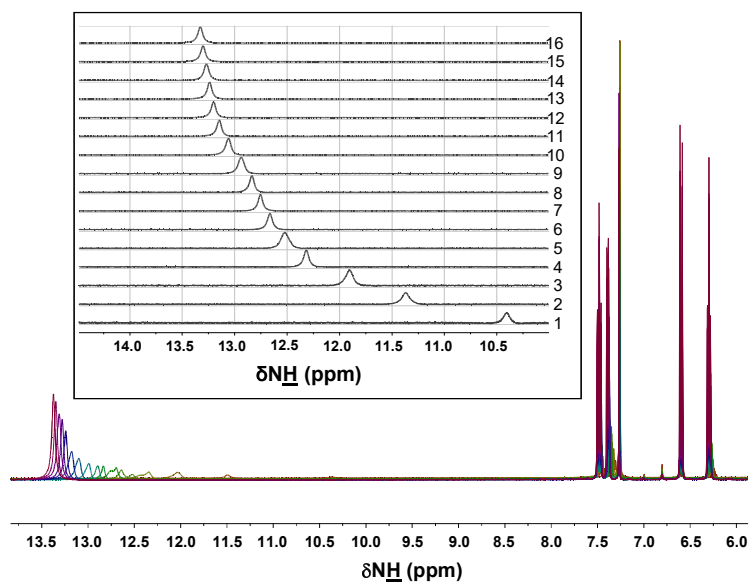
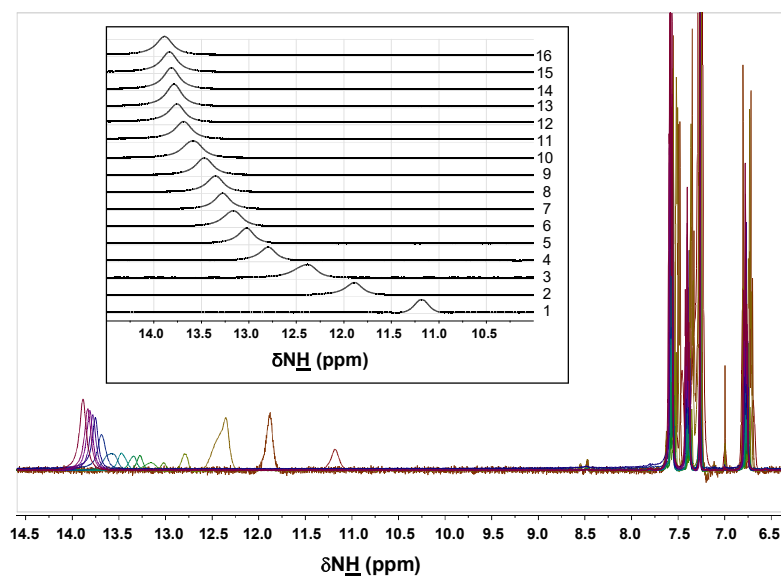


Figure 3.2.5  $^1H$  NMR Spectra of 2-Pyridone with increasing the concentration.(insert the N-H peak with increasing the concentration from bottom to top.

## Sulfur Centered Hydrogen Bond



**Figure 3.2.6**  $^1\text{H}$  NMR Spectra of 2-thiopyridone with increasing the concentration. (insert the N-H peak with increasing the concentration from bottom to top).

**Table 3.2.3** Chemical shift values obtained 2-pyridone and 2-thiopyridone at different concentrations in concentration dependent NMR titration experiments

S.No	Concentration (M)	$\delta$ NH (ppm)	
		2PY	2TPY
1	0.0005	10.39	11.18
2	0.0015	11.37	11.87
3	0.0030	11.91	12.36
4	0.0054	12.32	12.79
5	0.0077	12.52	13.02
6	0.0100	12.66	13.16
7	0.0122	12.75	13.27
8	0.0144	12.84	13.34
9	0.0186	12.94	13.47
10	0.0265	13.06	13.57
11	0.0338	13.15	13.69
12	0.0404	13.2	13.75
13	0.0465	13.24	13.78
14	0.0549	13.27	13.81
15	0.0624	13.3	13.83
16	0.0713	13.33	13.88

## Sulfur Centered Hydrogen Bond

---

To ensure the existence of monomers at lower concentrations and dimers at higher concentration we have performed the diffusion-ordered spectroscopy ( $^1\text{H}$ -DOSY) experiments. This technique is used by many researchers to investigate the aggregation behavior of ionic liquids<sup>52-54</sup>, supramolecular assembly<sup>55</sup> and systems with several non-covalent interactions such as hydrogen and halogen bonds<sup>56,57</sup>. In this case we measured the translational diffusion coefficients at two extreme concentrations by fitting the data to the Stejskal-Tanner equation. Diffusion experiments were carried out by varying the gradient strengths linearly at 16 intervals from 2% to 95% of the maximum gradient strength of  $50 \text{ G}\cdot\text{cm}^{-1}$ . The Stejskal-Tanner plots of 2-PY and 2-TPY was shown in Figure 3.2.7 (a) and 3.2.7 (b), respectively where the slope is proportional to diffusion coefficient in the logarithmic normalized signal strength ( $\log_e(I/I_0)$ ) versus the squared gradient pulse power ( $G^2$ ) plot. The proportional constant depends on the few experimental parameters and can be calculated readily. The diffusion coefficient of a molecule (solute) in a solution is inversely proportional to the cube-root of its molecular mass, if one assumes that the molecule is spherical, and the temperature, density and viscosity of the solvent do not change in presence of the solute (here, 2-PY, 2-TPY and their dimers). The ratios of the diffusion coefficient of the monomer ( $D_m$ ) to that of the dimer ( $D_d$ ) in both cases were found close to 1.2. It confirms that the existence monomer at lower concentration and at higher concentration dimer in both molecules 2-PY and 2-TPY.

## Sulfur Centered Hydrogen Bond

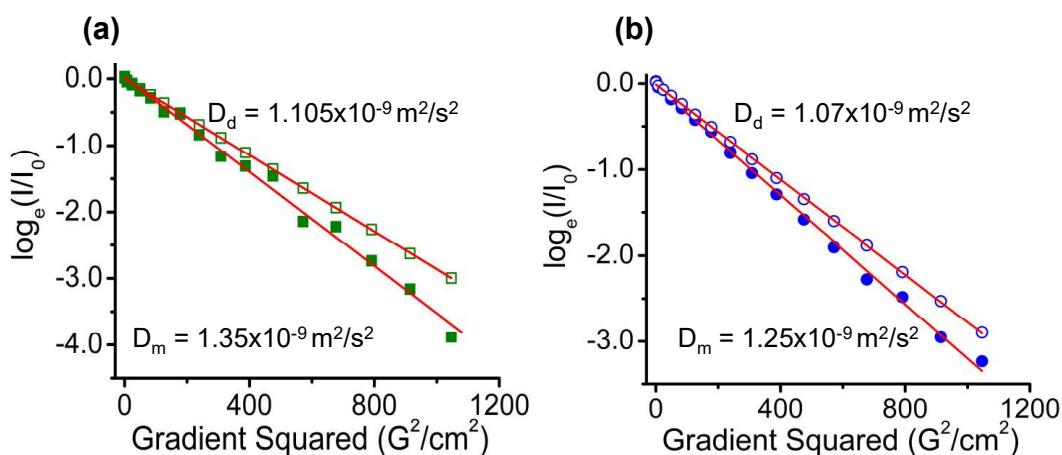
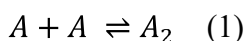


**Figure 3.2.7**  $^1\text{H}$ -DOSY Plot of (a) 2-PY, (b) 2-TPY fitting of Stejskal–Tanner equation to the decay of a spectral peak (NH) of 2-PY at lower concentration and higher concentration.

Thereafter, we have measured the association constant of H-bond complex from the concentration dependent experiments where change of chemical shift ( $\delta_{\text{NH}}$ ) as a function of concentrations of 2-PY and 2-TPY. Figure 3.2.8 (a) and (b) display the fitting to a 1:1 binding isotherm, yielding the association constants and association free energies for 2-PY and 2-TPY, respectively. The fitted equation have been derived to determine association constant/equilibrium constant  $K$  of 2-PY/2-TPY dimer

At room temperature the equilibrium between monomer and dimer as



$A$  is monomer

$A_2$  is dimer

The equilibrium constant for the dimerization given as

## Sulfur Centered Hydrogen Bond

---

$$K = \frac{[A_2]}{[A]^2} \quad (2)$$

The total solution in NMR tube contain monomer and dimer fractions, the concentration of total solution as  $[A]_0 = [A] + 2[A_2]$  (3)

The observed chemical shift is the average of monomer and dimer in total solution given as

$$\delta_{obs} = f_m \delta_m + f_d \delta_d \quad (4)$$

Here  $\delta_m$  is the chemical shift of monomer

$\delta_d$  is the chemical shift of dimer

The mole fraction of monomer in solution as  $f_m = \frac{[A]}{[A]_0} \Rightarrow [A] = f_m [A]_0$  (5)

The mole fraction of dimer in solution as  $f_d = \frac{2[A_2]}{[A]_0} \Rightarrow [A_2] = \frac{f_d [A]_0}{2}$  (6)

$$f_m + f_d = 1 \quad (7)$$

The equilibrium constant K can be expressed in terms of mole fraction of monomer and dimer as

$$K = \frac{f_d}{2f_m^2 [A]_0} \quad (8)$$

From equation (7), the equilibrium constant can be written as

$$K = \frac{1-f_m}{2f_m^2 [A]_0} \quad (9)$$

Equation (9) can be rearrange to a quadratic expression and solved for monomer fraction as follows

$$2K[A]_0 f_m^2 + f_m - 1 = 0$$

## Sulfur Centered Hydrogen Bond

---

$$f_m = \frac{-1 \pm \sqrt{1 + 8K[A]_0}}{4K[A]_0} \quad (10)$$

To measure the equilibrium constant from observable chemical shift and total solution concentration, equation (4) can be written in terms of mole fraction of monomer using equation (7) then

$$\delta_{obs} = f_m \delta_m + (1 - f_m) \delta_d$$

$$\delta_{obs} = (\delta_m - \delta_d) f_m + \delta_d \quad (11)$$

Equation (10) substituted in the above equation then gives

$$\delta_{obs} = \frac{\sqrt{1 + 8K[A]_0} - 1}{4K[A]_0} (\delta_m - \delta_d) + \delta_d \quad (12)$$

The equation (12) was used to measure the equilibrium constant using non-linear fit equation in Origin software.

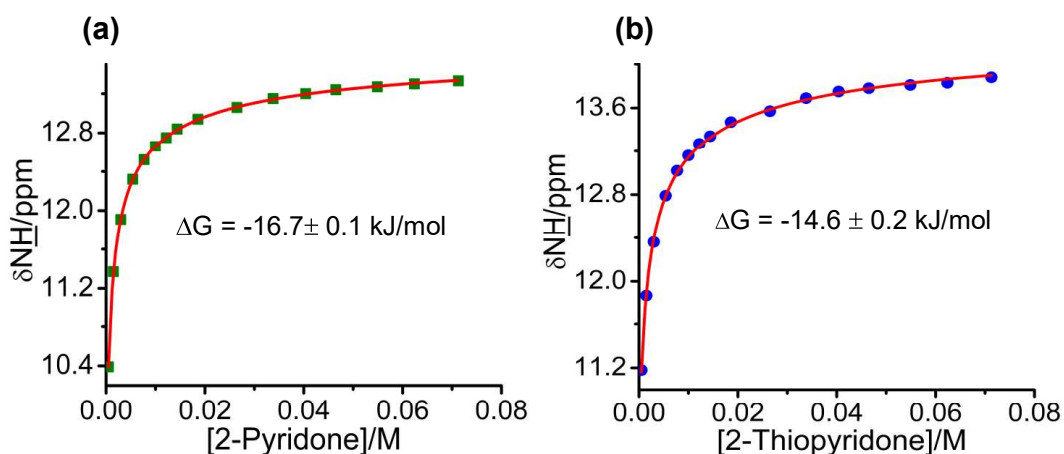


**Figure 3.2.8** (a) 1:1 binding isotherm fitting in concentration dependent NMR experiment for 2-PY (b) for 2-TPY in  $CDCl_3$  solvent.

## Sulfur Centered Hydrogen Bond

**Table 3.2.4.** Experimental and Computational thermodynamic parameters of 2-pyridone and 2-thiopyridone dimer. Here  $\Delta G$ ,  $\Delta H$ ,  $\Delta S$  and  $\Delta E$  are change in Gibbs free energy, change in enthalpy, change in entropy and change in internal energy of dimer formation respectively. For the concentration dependent studies, the computed entropies are considered to estimate the  $\Delta H$  values.

Methods	Thermodynamic Parameters							
	$\Delta G(\text{kJ/mol})$		$\Delta H(\text{kJ/mol})$		$\Delta S(\text{J/mol/K})$		$\Delta E(\text{kJ/mol})$	
	(PY) <sub>2</sub>	(TPY) <sub>2</sub>	(PY) <sub>2</sub>	(TPY) <sub>2</sub>	(PY) <sub>2</sub>	(TPY) <sub>2</sub>	(PY) <sub>2</sub>	(TPY) <sub>2</sub>
NMR-Concentration dependent	-16.7	-14.6	-62.6	-59.8	-153.9	-151.7	-65.0	-62.3
NMR-Temperature dependent	-15.9	-11.7	-31.9	-25.9	-53.8	-47.4	-34.4	-28.3
CCSD(T)/aug-cc-pVDZ	-12.6	-10.2	-58.4	-55.4	-153.9	-151.7	-60.9	-57.9

From the above equation we have determined the association constants (K) 844, 363 M<sup>-1</sup> for 2-PY and 2-TPY, respectively. The change in free energy ( $\Delta G_C$ ) of dimerization can be calculated from the obtained association constants and found to be -16.7 and -14.6 kJ/mol for 2-PY dimer and 2-TPY dimer, respectively. These free energies  $\Delta G_C$  obtained by concentration dependent studies are in good agreement with those benchmark quantum chemical calculations at the CCSD (T) level shown in Table 3.2.4. The results from the concentration dependent and CCSD (T) levels were indicates that the free energies for N-H $\cdots$ O and N-H $\cdots$ S H-bond are very similar. We also estimated the H-bond enthalpies from computed entropy ( $\Delta S$ ) and the  $\Delta H_c$  values are found to be -62.6 and -59.8 kJ/mole for N-H $\cdots$ O and N-H $\cdots$ S H-bond in in concentration dependent experiment respectively. These values are very similar to N-H $\cdots$ O H-bond enthalpies reported by Frey and Lewtwyler for 2-pyridone-uracil and 2-pyridone-thymine Watson-Crick and Wobble isomers.<sup>58</sup> On average the total hydrogen bond enthalpy for N-H $\cdots$ O and N-H $\cdots$ S H-bond is  $\sim$ -30 kJ/mol and the strength of N-H $\cdots$ O and N-H $\cdots$ S H-bond is equal in magnitude.

## Sulfur Centered Hydrogen Bond

---

The temperature dependent NMR studies were also carried out to estimate the H-bond enthalpies. Figures 3.2.9(a) and 3.2.9(b) represent the variation of chemical shift ( $\delta_{\text{NH}}$ ) with temperature.  $^1\text{H}$  NMR Spectra were recorded varying the temperature by 20 K increment from 240 K to 360 K. In this case the peak NH chemical shift ( $\delta_{\text{NH}}$ ) of 2-PY and 2-TPY shifted up field with increasing temperature. The temperature dependence of  $\delta_{\text{NH}}$  is due to the equilibrium between monomer and dimer as  $2 - \text{PY} \rightleftharpoons [2 - \text{PY}]_2$  and  $2 - \text{TPY} \rightleftharpoons [2 - \text{TPY}]_2$ .

Determination of equilibrium constant from the temperature dependent experiment is as below if



The equilibrium constant K between monomer (A) and dimer ( $A_2$ ) is as follows

$$K = \exp\left(-\frac{\Delta H - T\Delta S}{RT}\right) = \frac{[A_2]}{[A]^2} \quad (13)$$

Where  $[A]$ ,  $[A_2]$  are the concentrations of monomer and dimer.

From Eq (3)

$$[A]_0 = [A] + 2[A_2]$$

If  $[A]_0$  is the overall concentration in solution. The observed chemical shift in the fast exchange system is as follow Equation (4) shows

$$\delta_{obs} = \frac{[A]}{[A]_0} \delta_m + \frac{2[A_2]}{[A]_0} \delta_d \quad (14)$$

$$\frac{[A]}{[A]_0} = \frac{\sqrt{1+8K[A]_0}-1}{4K[A]_0}, \frac{2[A_2]}{[A]_0} = 1 - \frac{[A]}{[A]_0} \quad (15)$$

## Sulfur Centered Hydrogen Bond

---

Substituting equation 15 in equation 14 it gives

$$\delta_{obs} = \frac{\sqrt{1+8\exp\left(-\frac{\Delta H-T\Delta S}{RT}\right)[A]_0-1}}{4\exp\left(-\frac{\Delta H-T\Delta S}{RT}\right)[A]_0} \delta_m + \left(1 - \frac{\sqrt{1+8\exp\left(-\frac{\Delta H-T\Delta S}{RT}\right)[A]_0-1}}{4\exp\left(-\frac{\Delta H-T\Delta S}{RT}\right)[A]_0}\right) \delta_d \quad (16)$$

Here  $\Delta H$  is the change in enthalpy of dimer and  $\Delta S$  is entropy change of dimer.  $R$  is the ideal gas constant;  $T$  is the temperature of the sample. The equation 16 was used as a non-linear curve fit equation to calculate the changes in enthalpy and entropy up on dimerization of 2-pyridone and 2-thiopyridone.

Hence the plots 3.2.9(a) and 3.2.9(b) were fitted to a 1:1 binding isotherm yielding in equation (16) in origin, we found the  $\Delta H_T$  (subscript "T" : temperature dependent studies) equals to -31.9 and -25.9 kJ/mol for 2-PY and 2-TPY, respectively. These are huge discrepancies from observed between  $\Delta H_C$  values as obtained from concentration and temperature dependent NMR studies.  $\Delta H_T$  of  $\sim -15$  kJ/mol for a strong amide-N-H $\cdots$ O is too small. It is even less than H-bond energy of Indole-Benzene dimer (-21.8 kJ/mol for an N-H $\cdots$  $\pi$  H-bond)<sup>59</sup> and NH<sub>3</sub>-H<sub>2</sub>O dimers (-18.4 kJ/mol for an O-H $\cdots$ N H-bond)<sup>60</sup> as determined very precisely by gas phase laser spectroscopy experiments. The temperature experimental results were not matching with computational values due to lack of enough data points in for fitting the temperature dependent equation. This is due to infrastructure constraints, we could not perform experiments below 250 K, whereas experiments above 350 K were not possible because of the limitation of the boiling point of the solvent (b. pt. of CHCl<sub>3</sub>  $\sim$  335 K). Therefore, the concentration dependent NMR experiments provided better and precise information about the association free energies ( $\Delta G_C$ ) and H-bond enthalpies ( $\Delta H_C$ ). If one considers  $\Delta H_C$ , the H-bond enthalpy of an (thio)amide-N-H $\cdots$ O and (thio)amide-N-H $\cdots$ S could be  $\sim -25$  to -30 kJ/mol.

## Sulfur Centered Hydrogen Bond

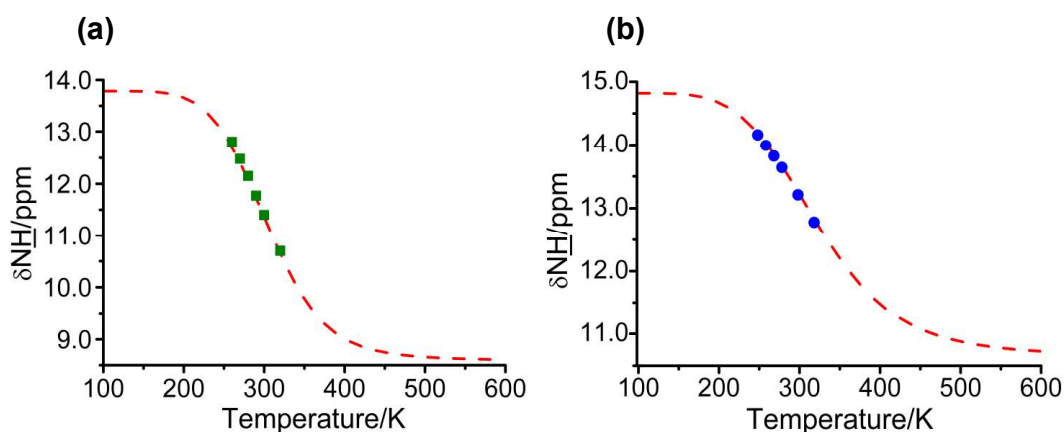


**Figure 3.2.9** (a) Temperature dependent plot of 2-PY and (b) of 2-TPY (red dotted line is the sigmoidal model fitting)

Lastly, we carried out deuterium exchange studies to show that N-H $\cdots$ O and N-H $\cdots$ S H-bond strengths are very similar. The  $^1\text{H}$  NMR experiments were performed at high concentration of 2-PY and 2-TPY (75 mM) to ensure maximum presence of dimers in the solution. Here first we have recorded the  $^1\text{H}$  NMR spectra of 2-PY and 2-TPY in  $\text{CDCl}_3$  solution and then added the 50 $\mu\text{L}$  of  $\text{D}_2\text{O}$  to the solution and monitored the NH peak intensity by recording  $^1\text{H}$  NMR spectra at different time intervals. Figure 3.2.10 (a) shows area under curve of amide-NH peak of 2-PY in reference to different aromatic CH peak (5<sup>th</sup> position) and 3.2.10 (b), CH peak (3<sup>rd</sup> position) in  $\text{CDCl}_3$  solution over time following the addition of  $\text{D}_2\text{O}$  and for the 2-TPY shown in Figure 3.2.11 (a) and (b). The same NMR experimental method amide hydrogen-deuterium exchange (H/D exchange) measurement was used to provide evidence of the intrasidue H-bond in proteins by T. Raines and coworkers.<sup>61</sup> We have fitted the curves with first exponential decay equation and calculated the H/D exchange rate which are found to be  $3.94 \times 10^{-2} \text{ min}^{-1}$  and  $4.18 \times 10^{-2} \text{ min}^{-1}$  for 2-PY and 2-TPY, respectively. Here we have used H/D exchange rates ( $k_{\text{ex}}$ ) to compare the N-H $\cdots$ O and N-H $\cdots$ S H-bonds. The  $k_{\text{ex}}$  ( $3\text{-}4 \times 10^{-2} \text{ min}^{-1}$ ) for 2-PY and 2-TPY

## Sulfur Centered Hydrogen Bond

dimers are of equal order of magnitude; corroborating the CCSD(T) energetics and concentration dependent NMR studies.

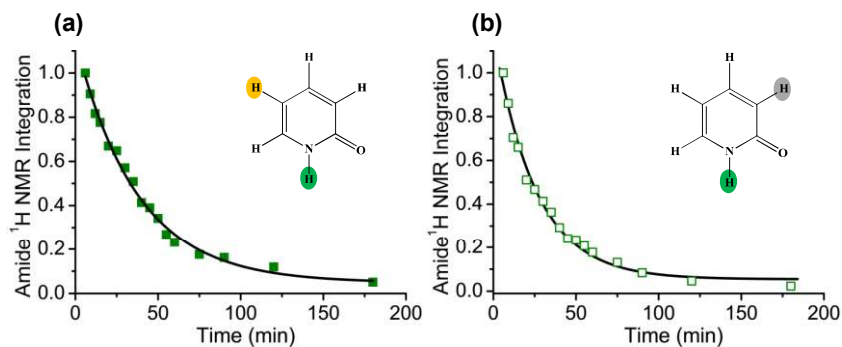


**Figure 3.2.10** (a) Integration of amide (NH)  $^1\text{H}$  NMR peaks of 2-PY with reference of aromatic CH  $^1\text{H}$  NMR peak at 5<sup>th</sup> position and (b) at 3<sup>rd</sup> position in  $\text{CDCl}_3$  over time following the addition of  $\text{D}_2\text{O}$ .

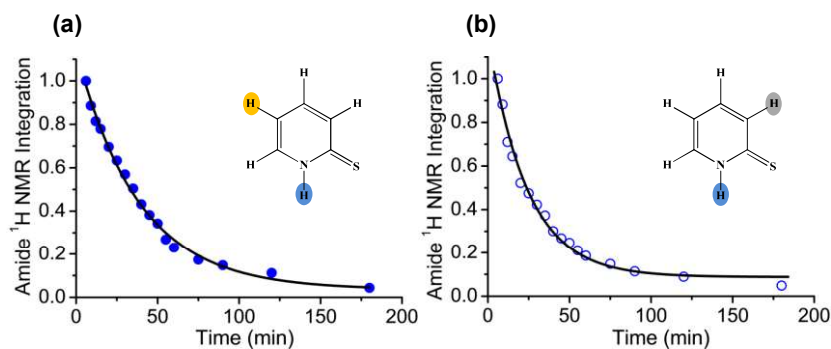


**Figure 3.2.11** (a) Integration of amide (NH)  $^1\text{H}$  NMR peaks of 2-TPY with reference of aromatic CH  $^1\text{H}$  NMR peak at 5<sup>th</sup> position and (b) at 3<sup>rd</sup> position in  $\text{CDCl}_3$  over time following the addition of  $\text{D}_2\text{O}$ .

## Sulfur Centered Hydrogen Bond

---

### 3.2.3. Conclusions

- ❖ The amide-N-H $\cdots$ S H-bonds have been widely studied in gas phase jet cooled condition as relevant contributors to biomolecular structures. However, attesting their existence and strength in solution has been arduous owing to solvent and temperature effects and underestimated H-bond energies. The 2-thiopyridone dimer bestows an appropriate opportunity to detect and measure (thio)amide-N-H $\cdots$ S H-bonds in solution.
- ❖ Several NMR experiments viz. concentration and temperature dependent studies, DOSY and deuterium exchange studies confirm that the (thio)amide-N-H $\cdots$ S H-bonds are as strong as classical amide N-H $\cdots$ O/N-H $\cdots$ O=C H-bonds. The experimental (thio)amide-N-H $\cdots$ S H-bond energy is  $\sim$  -30 kJ/mol, that is appreciably larger than previously observed for a SCHB.
- ❖ The concentration dependent NMR experiments provided precise determination of Gibbs free energy and H-bond enthalpy of amide-N-H $\cdots$ S H-bond that matched well with the bench mark quantum calculations at CCSD(T) level.
- ❖ Only consideration of electronegativity of S is inadequate to explain why amide-N-H $\cdots$ S H-bonds are equally strong as classical amide N-H $\cdots$ O/N-H $\cdots$ O=C H-bonds. It is the combined effect of electronegativity, charge and polarizability of S that determines the strength of amide-N-H $\cdots$ S H-bonds.
- ❖ We hope, this interesting outcome will definitely augment fundamental understanding of non-covalent interactions and to contrive and concede H-bonds beyond the concept of electronegativity.

## Sulfur Centered Hydrogen Bond

---

### References:

- (1) Walters, M. A.; Roche, C. L.; Rheingold, A. L.; Kassel, S. W. *Inorg. Chem.* **2005**, *44*, 3777.
- (2) Zhou, P.; Tian, F.; Lv, F.; Shang, Z. *Proteins: Struct., Funct., Bioinf.* **2009**, *76*, 151.
- (3) Allen, F. H.; Bird, C. M.; Rowland, R. S.; Raithby, P. R. *Acta Crystallogr., Sect. B* **1997**, *53*, 696.
- (4) Biswal, H. S.; Shirhatti, P. R.; Wategaonkar, S. *J. Phys. Chem. A* **2009**, *113*, 5633.
- (5) Biswal, H. S.; Wategaonkar, S. *J. Phys. Chem. A* **2009**, *113*, 12763.
- (6) Biswal, H. S.; Gloaguen, E.; Loquais, Y.; Tardivel, B.; Mons, M. *J. Phys. Chem. Lett.* **2012**, *3*, 755.
- (7) Andersen, C. L.; Jensen, C. S.; Mackeprang, K.; Du, L.; Jørgensen, S.; Kjaergaard, H. G. *J. Phys. Chem. A* **2014**, *118*, 11074.
- (8) Biswal, H. S.; Bhattacharyya, S.; Bhattacharjee, A.; Wategaonkar, S. *Int. Rev. Phys. Chem.* **2015**, *34*, 99.
- (9) Culik, R. M.; Jo, H.; Degrado, W. F.; Gai, F. *J. Am. Chem. Soc.* **2012**, *134*, 8026.
- (10) Nisius, L.; Grzesiek, S. *Nat. Chem.* **2012**, *4*, 711.
- (11) Alauddin, M.; Biswal, H. S.; Gloaguen, E.; Mons, M. *Phys. Chem. Chem. Phys.* **2015**, *17*, 2169.
- (12) Biswal, H. S.; Shirhatti, P. R.; Wategaonkar, S. *J. Phys. Chem. A* **2009**, *113*, 5633.
- (13) Biswal, H. S.; Wategaonkar, S. *J. Phys. Chem. A* **2009**, *113*, 12774.
- (14) Biswal, H. S.; Wategaonkar, S. *J. Phys. Chem. A* **2009**, *113*, 12763.
- (15) Biswal, H. S.; Gloaguen, E.; Loquais, Y.; Tardivel, B.; Mons, M. *J. Phys. Chem. Lett.* **2012**, *3*, 755.

## Sulfur Centered Hydrogen Bond

---

- (16) Alauddin, M.; Biswal, H. S.; Gloaguen, E.; Mons, M. *Phys. Chem. Chem. Phys.* **2015**, *17*, 2169.
- (17) Desiraju, G. R. *Acc. Chem. Res.* **2002**, *35*, 565.
- (18) Held, A.; Champagne, B. B.; Pratt, D. W. *J. Chem. Phys.* **1991**, *95*, 8732.
- (19) Nimlos, M. R.; Kelley, D. F.; Bernstein, E. R. *J. Phys. Chem.* **1989**, *93*, 643.
- (20) Matsuda, Y.; Ebata, T.; Mikami, N. *J. Chem. Phys.* **1999**, *110*, 8397.
- (21) Ottiger, P.; Pfaffen, C.; Leist, R.; Leutwyler, S.; Bachorz, R. A.; Klopffer, W. *J. Phys. Chem. B* **2009**, *113*, 2937.
- (22) Biedermann, F.; Schneider, H.-J. *Chem. Rev.* **2016**, *116*, 5216.
- (23) Alemán, C. *J. Phys. Chem. A* **2001**, *105*, 6717.
- (24) Lee, H. J.; Choi, Y. S.; Lee, K. B.; Park, J.; Yoon, C. J. *J. Phys. Chem. A* **2002**, *106*, 7010.
- (25) Alemán, C. *J. Phys. Chem. A* **2001**, *105*, 6717.
- (26) Laurence, C.; Berthelot, M.; Le Questel, J.-Y.; El Ghomari, M. J. *J. Chem. Soc., Perkin Trans. 2* **1995**, 2075.
- (27) Min, B. K.; Lee, H.-J.; Choi, Y. S.; Park\*, J.; Yoon, C.-J.; Yu, J.-A. *J. Mol. Struct.* **1998**, *471*, 283.
- (28) Miwa, J. H.; Patel, A. K.; Vivatrat, N.; Popek, S. M.; Meyer, A. M. *Org. Lett.* **2001**, *3*, 3373.
- (29) Miwa, J. H.; Pallivathucal, L.; Gowda, S.; Lee, K. E. *Org. Lett.* **2002**, *4*, 4655.
- (30) Wildemann, D.; Schiene-Fischer, C.; Aumüller, T.; Bachmann, A.; Kiefhaber, T.; Lücke, C.; Fischer, G. *J. Am. Chem. Soc.* **2007**, *129*, 4910.

## Sulfur Centered Hydrogen Bond

---

- (31) Bachmann, A.; Wildemann, D.; Praetorius, F.; Fischer, G.; Kiefhaber, T. *Proc. Natl. Acad. Sci. U. S. A.* **2011**, *108*, 3952.
- (32) Newberry, R. W.; VanVeller, B.; Raines, R. T. *Chem. Commun.* **2015**, *51*, 9624.
- (33) Walters, C. R.; Szantai-Kis, D. M.; Zhang, Y.; Reinert, Z. E.; Horne, W. S.; Chenoweth, D. M.; Petersson, E. J. *Chem. Sci.* **2017**, *8*, 2868.
- (34) Bohon, J. *Nucleic Acids Res.* **2003**, *31*, 1331.
- (35) Špačková, N.; Cubero, E.; Šponer, J.; Orozco, M. *J. Am. Chem. Soc.* **2004**, *126*, 14642.
- (36) Bohon, J. *Nucleic Acids Res.* **2005**, *33*, 2880.
- (37) Salon, J.; Jiang, J.; Sheng, J.; Gerlits, O. O.; Huang, Z. *Nucleic Acids Res.* **2008**, *36*, 7009.
- (38) Zhang, F.; Fu, L.; Wang, Y. *Mol. Cell. Proteomics* **2013**, *12*, 3803.
- (39) Faustino, I.; Curutchet, C.; Luque, F. J.; Orozco, M. *Phys. Chem. Chem. Phys.* **2014**, *16*, 1101.
- (40) Kirsanova, O. V.; Sergeev, A. V.; Yasko, I. S.; Gromova, E. S. *Nucleosides, Nucleotides Nucleic Acids* **2017**, *36*, 392.
- (41) Schumacher, M. A.; Crum, M.; Miller, M. C. *Structure* **2004**, *12*, 849.
- (42) Valerie, N. C. K.; Hagenkort, A.; Page, B. D. G.; Masuyer, G.; Rehling, D.; Carter, M.; Bevc, L.; Herr, P.; Homan, E.; Sheppard, N. G.; Stenmark, P.; Jemth, A. S.; Helleday, T. *Cancer Res.* **2016**, *76*, 5501.
- (43) H.M. Berman, J. W., Z. Feng, G. Gilliland, T.N. Bhat, H. Weissig, I.N. Shindyalov, P.E. Bourne. *Nucleic Acids Res.*, ([www.rcsb.org](http://www.rcsb.org)) **2000**, *28*, 235.
- (44) Tomasi, J.; Mennucci, B.; Cammi, R. *Chem.Rev.* **2005**, *105*, 2999.
- (45) Marenich, A. V.; Cramer, C. J.; Truhlar, D. G. *J. Phys. Chem. B* **2009**, *113*, 6378.

## Sulfur Centered Hydrogen Bond

---

- (46) Oliva, R.; Cavallo, L.; Tramontano, A. *Nucleic Acids Res.* **2006**, *34*, 865.
- (47) Hobza, P. *Acc. Chem. Res.* **2012**, *45*, 663.
- (48) Sheu, S. Y.; Yang, D. Y.; Selzle, H. L.; Schlag, E. W. *Proc. Natl. Acad. Sci. U. S. A.* **2003**, *100*, 12683.
- (49) Panman, M. R.; Bakker, B. H.; den Uyl, D.; Kay, E. R.; Leigh, D. A.; Buma, W. J.; Brouwer, A. M.; Geenevasen, J. A. J.; Woutersen, S. *Nat. Chem.* **2013**, *5*, 929.
- (50) Peters, G. M.; Skala, L. P.; Davis, J. T. *J. Am. Chem. Soc.* **2016**, *138*, 134.
- (51) Tsunoda, Y.; Takatsuka, M.; Sekiya, R.; Haino, T. *Angew. Chem., Int. Ed.* **2017**, *56*, 2613.
- (52) Annat, G.; MacFarlane, D. R.; Forsyth, M. *J. Phys. Chem. B* **2007**, *111*, 9018.
- (53) Bayley, P. M.; Best, A. S.; MacFarlane, D. R.; Forsyth, M. *ChemPhysChem* **2011**, *12*, 823.
- (54) Forsyth, M.; Yoon, H.; Chen, F.; Zhu, H.; MacFarlane, D. R.; Armand, M.; Howlett, P. *C. J. Phys. Chem. C* **2016**, *120*, 4276.
- (55) Lamm, J.-H.; Niermeier, P.; Mix, A.; Chmiel, J.; Neumann, B.; Stammler, H.-G.; Mitzel, N. W. *Angew. Chem., Int. Ed.* **2014**, *53*, 7938.
- (56) Johnson, C. S. *Prog. Nucl. Magn. Reson. Spectrosc.* **1999**, *34*, 203.
- (57) Cohen, Y.; Avram, L.; Frish, L. *Angew. Chem., Int. Ed.* **2005**, *44*, 520.
- (58) Frey, J. A.; Leutwyler, S. *Chimia* **2005**, *59*, 511.
- (59) Biswal, H. S.; Gloaguen, E.; Mons, M.; Bhattacharyya, S.; Shirhatti, P. R.; Wategaonkar, S. *J. Phys. Chem. A* **2011**, *115*, 9485.
- (60) Mollner, A. K.; Casterline, B. E.; Ch'ng, L. C.; Reisler, H. *J. Phys. Chem. A* **2009**, *113*, 10174.

## Sulfur Centered Hydrogen Bond

---

- (61) Newberry, R. W.; Raines, R. T. *Nat. Chem. Biol.* **2016**, *12*, 1084.

## Selenium Centered Hydrogen Bond

---

### Chapter 4

#### Selenium Centered Hydrogen Bond (SeCHB) in Selenomethionine Containing Peptides and Proteins

##### 4.1. Introduction:

The results described in chapter 3 revealed that the strength of sulfur centered hydrogen bond is as strong as conventional hydrogen bonds in gas phase and in solution though S is less electronegative than O, N, F. A combination of high-resolution laser spectroscopy and benchmark quantum chemical calculations discerned the strength of sulfur center hydrogen bond<sup>1-6</sup> which is motivate us to re-evaluate the H-bond formation with different low electronegative elements. We have chosen third and fourth elements, selenium (Se) and tellurium (Te) of the 16<sup>th</sup> group in periodic Table as H-bond acceptors. The electronegativity of Se is comparable to that of carbon and lower than S and O. In addition to this, selenium is an important element in chemistry because of its unique properties like lower basicity<sup>7</sup>, higher nucleophilicity<sup>8</sup> of selenolates, better leaving group ability, higher polarizability, greater tolerance for hypervalence<sup>9</sup>, enhanced stability and reversibility of selenyl radicals.<sup>10,11</sup> The detailed description of the importance of selenium in chemistry and biology is provided in the review by Rich and Hondal.<sup>12</sup> Selenium easily replaces the S in cysteine or methionine to form selenocystein<sup>13</sup> (Sec) or selenomethionine (Mse) in proteins, respectively. The Sec and Mse are functionally and structurally almost similar to their natural counterparts Cys and Met. So these can be easily incorporated in protein during translation via Sec and Mse charged t-RNA. Hence, Mse and Sec are widely used in experimental phasing methods for atoms selected in solving the protein crystal structure. L. Moroder reported that selenium easily replaces the S in enzyme-catalyzed reactions which is further more evident by its stoichiometric presence in the active

## Selenium Centered Hydrogen Bond

---

center of various enzymes<sup>14</sup>, e.g. Glutathione peroxidase, thioredoxinreductase and, iodothyroninedeiodinase etc.<sup>15</sup> Selenium not only replaces the S but also the oxygen present in nucleotide and nucleobases which is well established in the literature.<sup>16-18</sup> Se substitution on the nucleobase neither alters the structure nor the H-bonding network in the base pairs.<sup>19-21</sup> In some cases it is mentioned that amide-N-H...Se H-bonds<sup>22,23</sup> are weaker compared to amide-N-H...O H-bonds in nucleobase pairs.

Madzhidov T. I. and Chmutova G. A. studied computationally the intermolecular O-H...Se H-bond in divalent selenium compounds with methanol.<sup>24</sup> They reported that the strength of O-H...Se is weaker than the conventional H-bonds such as O-H...O, O-H...N H-bonds. Recently, Chakraborty S. and co-workers studied using the DFT to explore the existence of O-H...Se H-bonds between substituted phenol and H<sub>2</sub>Se.<sup>25</sup> However, there are no experimental reports on the concrete evidences and assessment of strength of N-H...Se H-bond at the molecular level which encouraged us to study such H-bonds more precisely. As discussed in the following sections we have employed high resolution vibrational spectroscopy, gold standard quantum chemical calculations at Coupled Cluster Doubles Triples (CCSD(T)) level and PDB structure exploration to assess the strength of amide-N-H...Se H-bonds in biomolecules. In addition to Se, we have also studied the existence and strength of H-bond with tellurium which has a electronegativity similar to H.

### 4.2. Existence of amide-N-H...Se H-bonds in proteins: PDB analysis

First we have carried out the protein data bank (PDB) analysis for existence of SeCHBs in proteins. The protein structure coordinates were retrieved from the RCSB<sup>26</sup> website. The criteria given to download the protein structures were 1) structure resolved by X-ray

## Selenium Centered Hydrogen Bond

crystallography at less than 2.5 Å resolution, comprising of Se (Mse: selenomethionine) and 2) with less than 30% sequence identity among the proteins. This parametric selection results total 4472 protein structures (PDBs). REDUCE program<sup>27</sup> was used to optimally compute the hydrogen atom positions in each amino acid for each PDB file. After addition of H atom positions in PDB coordinates, we used in-house program written in C language to identify the hydrogen bonds defined by selenium atom as acceptor. In this case we have defined the distance between H and Se in the range of 2 to 4.5 Å and angle in range  $150^\circ \leq \angle \text{NHS} \leq 180^\circ$ . In our dataset of 4472 protein structures, we have observed 24641 Mse (~6 Mse/protein) which account for 4334 H-bonds i.e. roughly one out of every six Mse is involved in H-bond formation or every protein in this dataset on an average forms at least one Se centered H-bonds (SeCHBs). Out of 4334 H-bond interactions, 2342 are main-chain-N-H...Se H-bonds and 1992 from side-chain-N-H...Se H-bonds. Figure 4.1 (a) depicts the distribution of N-H...Se H-bond interactions with complete H-bond distance ( $d_{\text{H}\cdots\text{Se}}$ ), histogram bar width was used 0.4 Å. Figure 4.1 (b) depicts the distribution within the +0.2 Å of the sum of van der Waal's radii of H and Se ( $r_{\text{H}} = 1.2 \text{ \AA}$ ,  $r_{\text{Se}} = 1.9 \text{ \AA}$ )<sup>28,29</sup>, histogram bar width was used 0.1 Å.

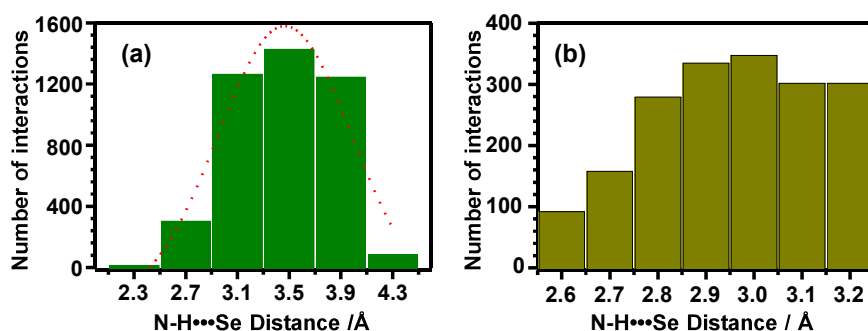


**Figure 4.1** (a) Complete H-bond distance ( $d_{\text{N-H}\cdots\text{Se}}$ ) distribution (b) H-bond distance ( $d_{\text{N-H}\cdots\text{Se}}$ ) distribution within the +0.2 Å of the sum of the van der Waal's radii of H and Se in Selenomethionine (MSe) containing proteins.

## Selenium Centered Hydrogen Bond

Total 2251 N-H...Se H-bond interactions (~52% of total interactions) were found in the distance between Se and H is  $< 3.3 \text{ \AA}$ . It is observed for many cases that the distances between Se and H are within the sum of the van der Waal's radii, suggesting attractive interactions between them.

These interactions further confirmed by natural bond orbital (NBO) analysis and atoms in molecules (AIM) electron density topology analysis. From the NBO analysis we can investigate the donor-acceptor orbital interaction of SeCHBs in the representative amino acids of the proteins. For further confirmation of the existence of backbone amide-N-H...Se H-bonds we have performed quantum chemical calculations on two protein structures from the PDB analysis such as human inositol 1,4,5-trisphosphate 3-kinase (PDB: 1w2f, Resolution:  $1.8 \text{ \AA}$ )<sup>30</sup> and phosphoethanolamine N-methyltransferase (PDB:4krg, Resolution:  $1.8 \text{ \AA}$ )<sup>31</sup>. These interactions are shown in Figure 4.2 (a) and 4.2(b), respectively.

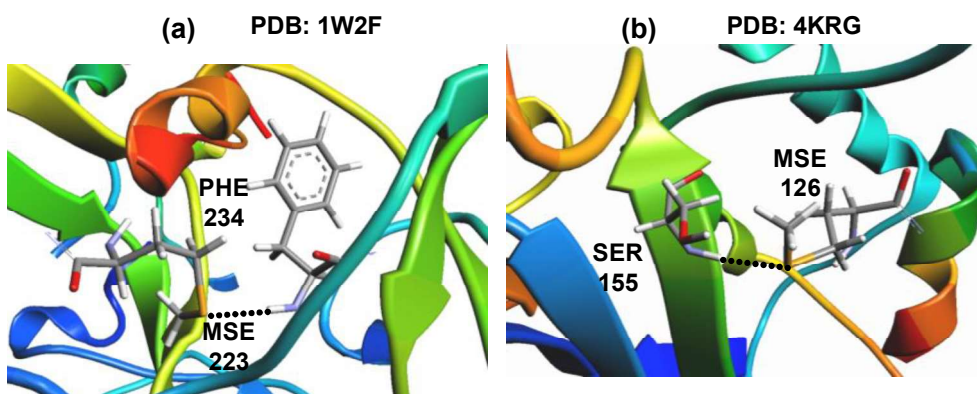


**Figure 4.2** Two representative examples of amide-N-H H...Se hydrogen bond observed in (a) human inositol 1,4,5-trisphosphate 3-kinase (PDB: 1w2f, Resolution:  $1.8 \text{ \AA}$ )<sup>30</sup> (b) phosphoethanolamine N-methyltransferase (PDB: 4krg, Resolution:  $1.8 \text{ \AA}$ )<sup>31</sup>

We have chosen only the interacting peptides in two proteins for density functional theory (DFT) calculations as it is impossible to carry out the calculations of whole protein. In both the cases the H-bond acceptor peptides were AcMseNHMe and the H-bond donor peptides

## Selenium Centered Hydrogen Bond

---

were AcPheNHMe and AcSerNHMe for 1w2f and 4krq, respectively. The positions of H atoms of the selected peptides were further optimized using dispersion-corrected DFT (at RI-B97-D3/def2-TZVPP level) while keeping other atomic coordinates fixed at their crystal structure positions. These optimized structures were used to calculate the donor-acceptor interaction energies ( $E_{DA}$ ) of N-H...Se H-bonds by NBO analysis at MP2/aug-cc-pVDZ level of theory. NBO analysis is very useful in estimating various types of non-covalent interactions in peptides and proteins.<sup>32-33</sup> Figure 4.3 depicts the overlap between two lone pair electrons in s-type orbital ( $s_{n_{Se}}$ ) and in p-type orbital ( $p_{n_{Se}}$ ) of Se ( $LP_{Se}$ ) and antibonding orbital ( $\sigma^*$ ) of amide-N-H ( $\sigma^*_{N-H}$ ) in both proteins. The donor-acceptor interaction energies ( $E_{DA}$ ) are estimated by second order perturbation theory and found to be 175 and 76 kJ/mol in 1w2f and 4krq, respectively. These values are very similar or even more than those estimated for amide-N-H...O and amide-N-H...O=C H-bonds in proteins reported in previous chapter. The higher  $E_{DA}$  value in 1w2f than in 4krq is because of the closer H and Se distance in 1w2f ( $d_{H...Se} = 2.367 \text{ \AA}$ ) than in 4krq ( $d_{H...Se} = 2.676 \text{ \AA}$ ). This suggests that the variable distance between amide-NH and Se is due to the influence of the nearby amides and environments of selenomethionine (Mse). However, from the NBO analysis, it is clearly indicating that Se of Mse has potential to form H-bonds as strong as classical amide-N-H...O and amide-N-H...O=C H-bonds. The strength of the N-H...Se H-bond in proteins depends on the geometrical constraints imposed by other residues in deciding optimum distance between H and Se.

## Selenium Centered Hydrogen Bond

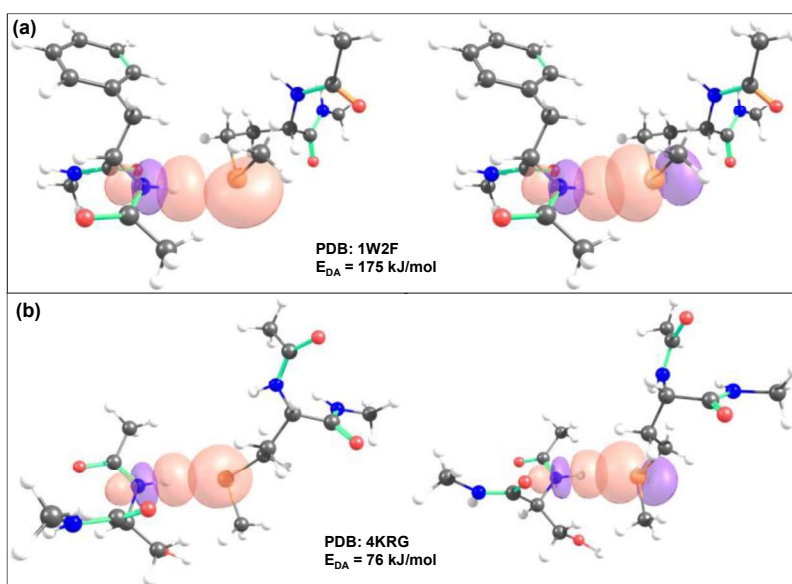


**Figure 4.3** NBO 3D overlap diagram for Left side:  $^s n_{Se} \rightarrow \sigma_{NH}^*$ , Right side:  $^p n_{Se} \rightarrow \sigma_{NH}^*$  donor-acceptor interactions in selenomethionine containing proteins (a) 1W2F (b) 4KRG.

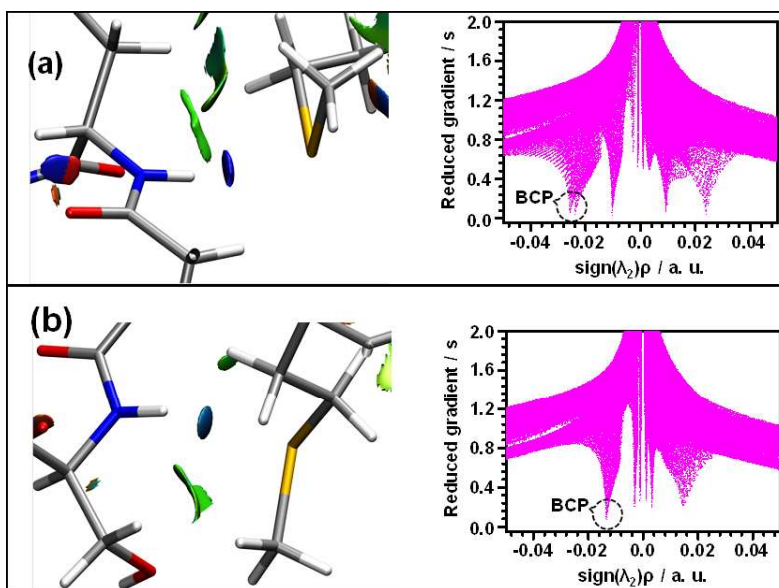


**Figure 4.4** The plots of the reduced density gradient ( $s$ ) versus the sign of the second eigen value of the electron-density Hessian matrix ( $\lambda_2$ ) times electron density ( $\text{sign}(\lambda_2)\rho$ ) for (a) 1w2f and (b) 4krp with the bond critical point (BCP) of amide-N-H...Se hydrogen bond.

## Selenium Centered Hydrogen Bond

---

The N-H...Se H-bond in proteins was further confirmed by Non-Covalent Interaction (NCI)<sup>34</sup> index analysis. Recently, Piquemal and co-workers<sup>35,36</sup> used the NCI analysis tool based on electron density and its derivatives to investigate the formation of H-bonds in biomolecules. Figure 4.4 (a) and (b) shows the plots of the reduced density gradient ( $s$ ) versus the sign of the second eigen value of the electron-density Hessian matrix ( $\lambda_2$ ) times electron density ( $\text{sign}(\lambda_2)\rho$ ) and 3D-NCI colored isosurfaces for 1w2f and 4krq, respectively. In these plots the attractive interaction between amide-N-H and Se of Mse in both proteins were shown at the values of  $\text{sign}(\lambda_2)\rho$  are -0.026 and -0.014 au, respectively. These values are within the range of strong H-bonds ( $-0.01 > \text{sign}(\lambda_2)\rho > -0.06$ )<sup>37,38</sup> and even stronger than N-H...S H-bonds involving cysteine S.<sup>39</sup> The laplacians of the electron densities ( $\nabla^2(\rho(r))$ ) at the bond critical points N-H...Se H-bond are 0.05 and 0.02 in 1w2f and 4krq, respectively which are positive values suggesting that N-H...Se H-bonds are closed shell interactions. The strength of N-H...Se H-bond varies depending on the distance between H and Se and H-bond angle. This is because of conformational constraints of the amino acid residues and several non-covalent interactions at play that lead to an equilibrium N-H...Se H-bond geometry. However, these topological analyses revealed that Se of Mse in proteins has potential to form H-bonds as strong as classical amide-N-H...O and amide-N-H...O=C H-bonds.

PDB structure analysis is not sufficient to get the exact information about the formation of H-bond by selenomethionine in proteins. So, high-resolution laser spectroscopic techniques have been used to study the existence and the strength of amide-N-H...Se H-bonds in proteins in isolated condition by eliminating conformational constraints and solvent effects. In addition to this, quantum chemical calculations have been done to benchmark with the experimental studies.

## Selenium Centered Hydrogen Bond

---

### 4.3. Experimental and Computational studies for -N-H...Se H-bonds in Model Compounds of Biomolecules

#### 4.3.1. High-Resolution Laser Spectroscopy:

The experimental evidence of N-H...Se H-bond (SeCHB) can be revealed with high-resolution IR-UV double resonance spectroscopy in gas phase. The quantitative information of N-H...Se H-bond strength can be obtained by monitoring the red shift in N-H stretching frequency. N-phenylacetamide (NPAA) and 2-pyridone (2PY) were chosen as cis and trans amide-NH H-bond donors, respectively. They also represent the trans and cis amide groups of peptides and nucleobases, respectively. Dimethylselenide (DMSe) and dimethylsulfide (DMS), representing side chains of selenomethionine and methionine, respectively were chosen as H-bond acceptors. The combination of above mentioned H-bond donors and acceptors enabled us to compare N-H...Se and N-H...S H-bonds directly without the interventions of other non-covalent interactions or structural constraints or solvent effects. In Figure 4.5 the model compounds of biomolecules are shown which have been used for the experimental and computational studies. The H-bond donors samples NPAA and 2-PY are solid and vaporized by thermal heating to 80-100 °C. About 0.2 -0.5% pre-mixture of H-bond acceptors (DMSe and DMS) in helium are used for the complex formation. The cold molecular beam was created by passing both H-bond donor and acceptor vapors via a supersonic jet nozzle. The molecular beam was probed using LIF and REMPI spectroscopy to obtain the UV excitation spectra. This UV excitation spectrum helps to record single conformation specific IR spectra which are obtained by IR/UV double resonance spectroscopy. The formation of DMSe complexes with 2-PY and NPAA were identified by LIF and mass-selective resonant two-photon ionisation (R2PI)

## Selenium Centered Hydrogen Bond

spectroscopy, respectively. Bottom trace in Figure 4.6 shows the LIF spectrum of 2-PY and the top trace is the LIF spectrum of 2-PY in presence of DMSe. Two new peaks were observed at 30030 and 30152  $\text{cm}^{-1}$  in hydrogen bonded complex between 2-PY and DMSe. The intense peak at 30030  $\text{cm}^{-1}$  red trace was assigned as the band origin (BO) transition of  $S_1$ - $S_0$  excitation in 2-PY-DMSe complex which is blue shifted by 198  $\text{cm}^{-1}$  from its monomer BO (29832  $\text{cm}^{-1}$ ). On the other hand in the trans amide, the formation of N-H...Se H-bond complex was shown from the resonance enhanced multi-photon ionization (REMPI) spectroscopy. NPAA-DMSe complex was confirmed by the mass spectra appears the peak at  $m/z = 244$ , as shown in the Figure 4.7.

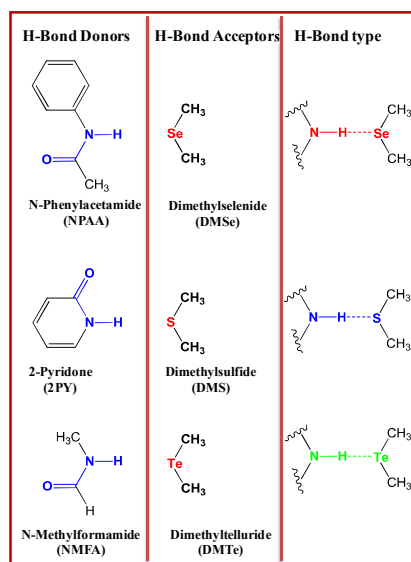


**Figure 4.5** Model compounds of biomolecules, H-bond donors are N-Phenylacetamide (NPAA), 2-pyridone (2-PY) and N-methylformamide (NMFA), H-bond acceptors are dimethyl selenide (DMSe), dimethyl sulfide (DMS) and dimethyl telluride (DMTe).

## Selenium Centered Hydrogen Bond

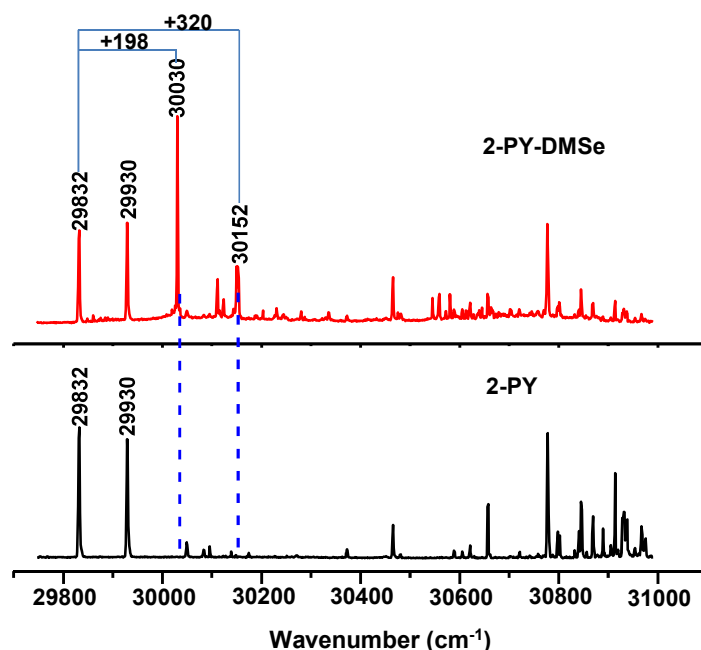


**Figure 4.6** LIF spectra of bare 2-PY and 2-PY in presence of DMSe. The bottom black trace is the LIF spectrum of bare 2-PY. Two peaks at 29832, 29930  $\text{cm}^{-1}$  are assigned as  $S_1$ - $S_0$  band origin (BO) of ground state conformers of 2-PY. The top red trace is the LIF spectrum of 2-PY in presence of DMSe. The numbers indicated by arrows are the red shifts of the corresponding peaks compared to the BO of the monomer.

In Figure 4.7, top box represents the mass spectra of NPAA in presence of DMSe. The peaks appear at  $m/z = 135$  due to the presence of NPAA monomer and at  $m/z = 244$  indicates the presence of NPAA-DMSe complex. The bottom box represents the REMPI spectra of NPAA and its complexes with DMS and DMSe. The intense peak at  $35902 \text{ cm}^{-1}$  was assigned as band origin (BO) of NPAA monomer and  $35643 \text{ cm}^{-1}$  to NPAA-DMS and the maximum in the broad peak at  $35682 \text{ cm}^{-1}$  to NPAA-DMSe complex. The maximum of the peak was observed at  $35682 \text{ cm}^{-1}$  which is red shifted from its monomer BO. The peaks were observed for 2-PY-DMSe is blue shifted while for NPAA-DMSe red shifted from their corresponding monomers respectively. These shifts indicates the formation of H-bond complexes of 2-PY and NPAA with DMSe. The

## Selenium Centered Hydrogen Bond

H-bonded complexes of NPAA and 2-PY with DMSe further confirmed by IR spectra of NH stretching vibration of 2-PY and NPAA using IR-UV double resonance spectroscopy.

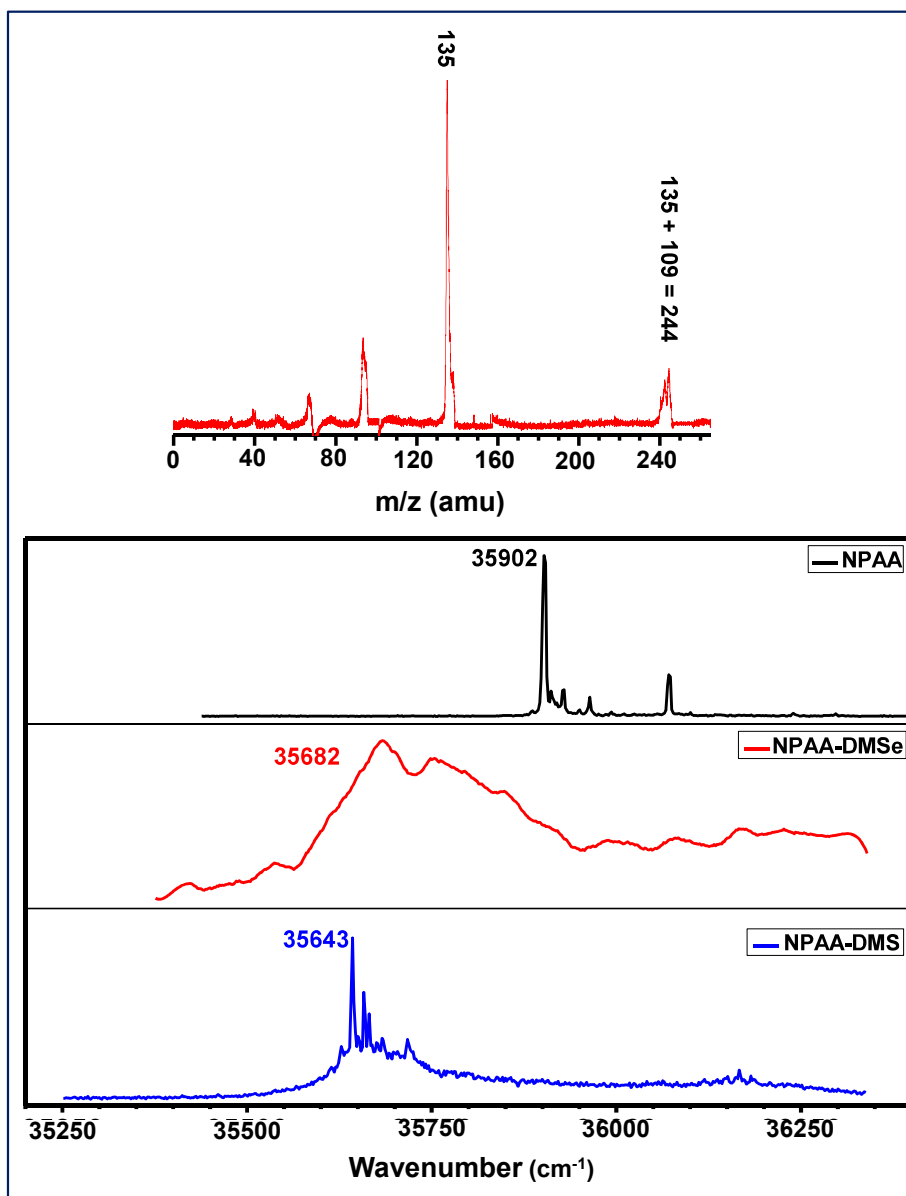


**Figure 4.7** Top red trace represents the mass spectra of NPAA-DMSe, bottom rectangular box represents the 2c-R2PI spectra of NPAA and NPAA in presence of DMS and DMSe.

Figure 4.8, 4.9 are depicted the gas phase IR spectra of NPAA and 2-PY monomers and their complexes with DMSe and DMS, respectively. Underneath stick diagram shows the

## Selenium Centered Hydrogen Bond

computational IR spectra of calculated at RI-B97-D3/def2-TZVPP level of theory in Figure 4.8 and 4.9. The scaled harmonic frequencies obtained from the calculations are helpful to assign experimental IR spectra to specific conformations. The computed NH stretching frequency is an excellent match with the experimentally observed NH stretching frequency. The experimental NH stretching frequency of NPAA monomer is  $3472\text{ cm}^{-1}$ , while  $3381\text{ cm}^{-1}$  for NPAA-DMSe and  $3376\text{ cm}^{-1}$  for NPAA-DMS complexes. The stretching frequencies of N-H for 2-PY monomer is  $3448\text{ cm}^{-1}$  and for its complexes DMSe and DMS were observed at  $3186$  and  $3157\text{ cm}^{-1}$ .

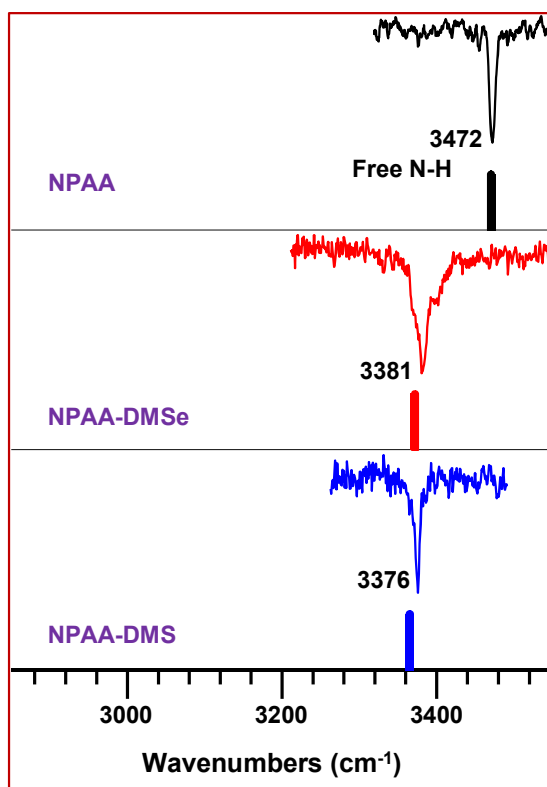


**Figure 4.8** Gas phase vibrational spectra of monomer *N*-phenylacetamide (NPAA) and its H-bond complexes with Selenium and Sulfur acceptors in the N-H stretch region, obtained by IR-UV double resonance spectroscopy. Underneath the experimental spectra, DFT-D calculated stick spectra are presented for the sake of comparison and assignment.

## Selenium Centered Hydrogen Bond

---

Both experimental and computational data suggest that there are red shifts in N-H stretching frequencies ( $\Delta\nu_{\text{NH}}$ ) in N-H...Se and N-H...S H-bonded complexes with respect to those of their corresponding monomer. These red shifts are attributed to the strength of H-bond complexes. In case of NPAA (trans amide) the  $\Delta\nu_{\text{NH}}$  values for N-H...Se and N-H...S H-bond complexes are 91 and 96  $\text{cm}^{-1}$ , respectively, indicating thereby that H-bond strengths are of almost equal magnitude. On the other hand in the cis amide (2PY) the  $\Delta\nu_{\text{NH}}$  is 262  $\text{cm}^{-1}$  for N-H...Se H-bond complex and 291  $\text{cm}^{-1}$  for N-H...S H-bond complex. In cis amide case the N-H...Se H-bond is weaker compared to N-H...S H-bond. However, the substantial red shifts were observed in both cis and trans amide-N-H...Se H-bond complexes and it confirms that Se can be a potential H-bond acceptor in proteins and nucleobases. This is also in excellent agreement with observations made from PDB structure analysis. It should be noted that the cis-amide-N-H...Se H-bonds are stronger than N-H...O H-bonds and N-H... $\pi$  H-bonds which are significantly weaker than both N-H...Se and N-H...S H-bonds. Although red shifts in the N-H stretching frequencies can be used as spectroscopic markers for H-bonds, very recently Steve Scheiner<sup>40</sup> reported that “... IR band shifts will occur even if the two groups experience weak or no attractive force, or if they are drawn in so close together that their interaction is heavily repulsive. The mere presence of a proton-acceptor molecule can affect the chemical shielding of a position occupied by a proton donor by virtue of its electron density, even if there is no H-bond present.” The aforementioned statement is valid a point and needs to be considered carefully while using red shift in vibrational frequencies as the spectroscopic ruler for H-bond strength. Hence, a detailed high level computational study is indispensable to justify our claim and corroborate the experimental observations that N-H...Se H-bonds are as strong as N-H...O and N-H...O=C H-bonds.

## Selenium Centered Hydrogen Bond

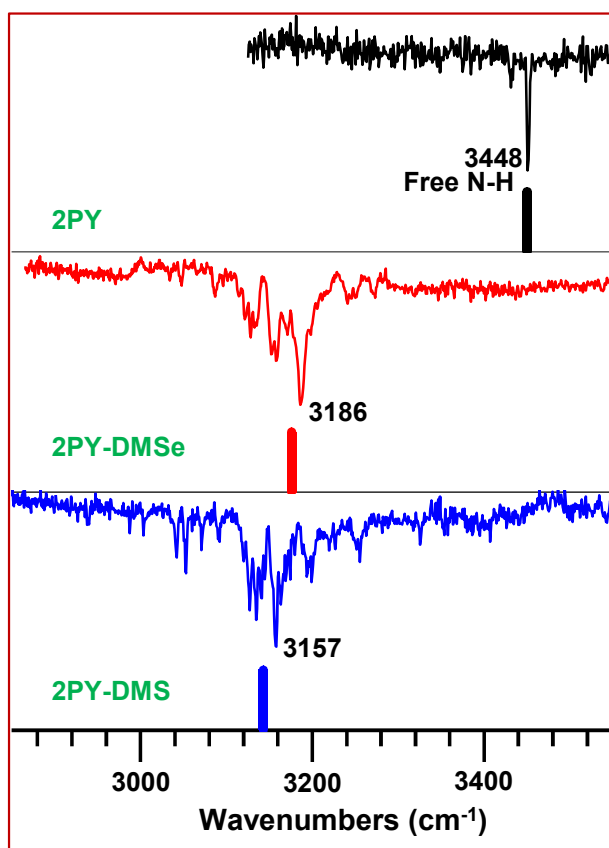


**Figure 4.9** Gas phase vibrational spectra of monomer 2-pyridone (2-PY) and its H-bond complexes with Selenium and Sulfur acceptors in the N-H stretch region, obtained by IR-UV double resonance spectroscopy. Underneath the experimental spectra, DFT-D calculated stick spectra are presented for the sake of comparison and assignment.

### 4.3.2 Quantum Chemical Calculations at CCSD-T level:

To support and assess our experimental outcome, we have carried out high level quantum chemical calculations. Experimental red shifts of N-H stretching frequencies suggest that Se with smaller electronegativity than O can form stronger H-bonds than O. The experimental outcome is surprising and encouraging to go a step further by considering tellurium (Te) (similar electronegative element as hydrogen) as an H-bond acceptor, there by forming N-H...Te H-bonded complexes. So, in addition to DMS, DMSe we have chosen dimethyltelluride (DMTe) as

## Selenium Centered Hydrogen Bond

---

H-bond acceptor for computational studies. The H-bond donor N-methylformamide (NMFA) was chosen, along with NPAA and 2-PY, to avoid the secondary interactions such as C-H...X and CH... $\pi$  because of it does not contain the aromatic ring. Hence, NMFA is the smallest and ideal amide to investigate amide-NH...X (X = O, S, Se, Te) H-bonds.

The optimization and frequency calculations for monomers and H-bonded complexes were done at RI-B97-D3/def2-TZVPP level of theory, shown in Figure 4.10. The H-bond energies are estimated at the CCSD(T)/aug-cc-pVDZ level of theory from the optimized structures. The binding energies at CCSD-T level and red shift values of N-H...Se H-bond complexes and other classical H-bond complexes (obtained from previous chapter) are listed in the Table 4.1. The binding energies observed for N-H...Se H-bonds are comparable to those of N-H...S and N-H...O H-bond complexes. The binding energy for 2PY-DMSe complex is as high as 50 kJmol<sup>-1</sup>. This energy is considerable higher and the N-H...Se H-bond strength is comparable with any classical H-bond energies. Because of unavailability of dimethyl telluride, we could not perform IR-UV spectroscopy of DMTe complexes. However, our experimental IR data of other complexes were very used to estimate the experimental IR data of DMTe complexes from computational IR data. Figure 4.11 shows, a linear correlation between the computed and experimental vibrational frequencies obtained for H-bonded complexes. Then we used the fitted linear equation  $\nu_{NH}(expt) = 0.9868 \times \nu_{NH}(comp.) + 11$  to estimate amide-N-H stretching frequencies of DMTe complexes. The estimated red shift values of N-H...Te H-bonds are listed in the Table 4.1. The estimated red shift values suggest that tellurium is not far behind than oxygen, sulfur and selenium. The  $\Delta\nu_{NH}$  values of DMTe complexes are very similar to those of N-H...X (X= O, S, Se) complexes, suggesting that tellurium can be as strong H-bond acceptor as oxygen despite of having almost same electronegativity as of hydrogen. We would like to

## Selenium Centered Hydrogen Bond

emphasize that the electronegativity concept of atoms (H-bond acceptors) in explaining the strength of H-bonds almost retires here. The red shifts of N-H stretching frequencies are solely because of the interaction of X and N-H, which was further confirmed by two of the most frequently, used H-bond descriptors, those are NBO and NCI analysis.

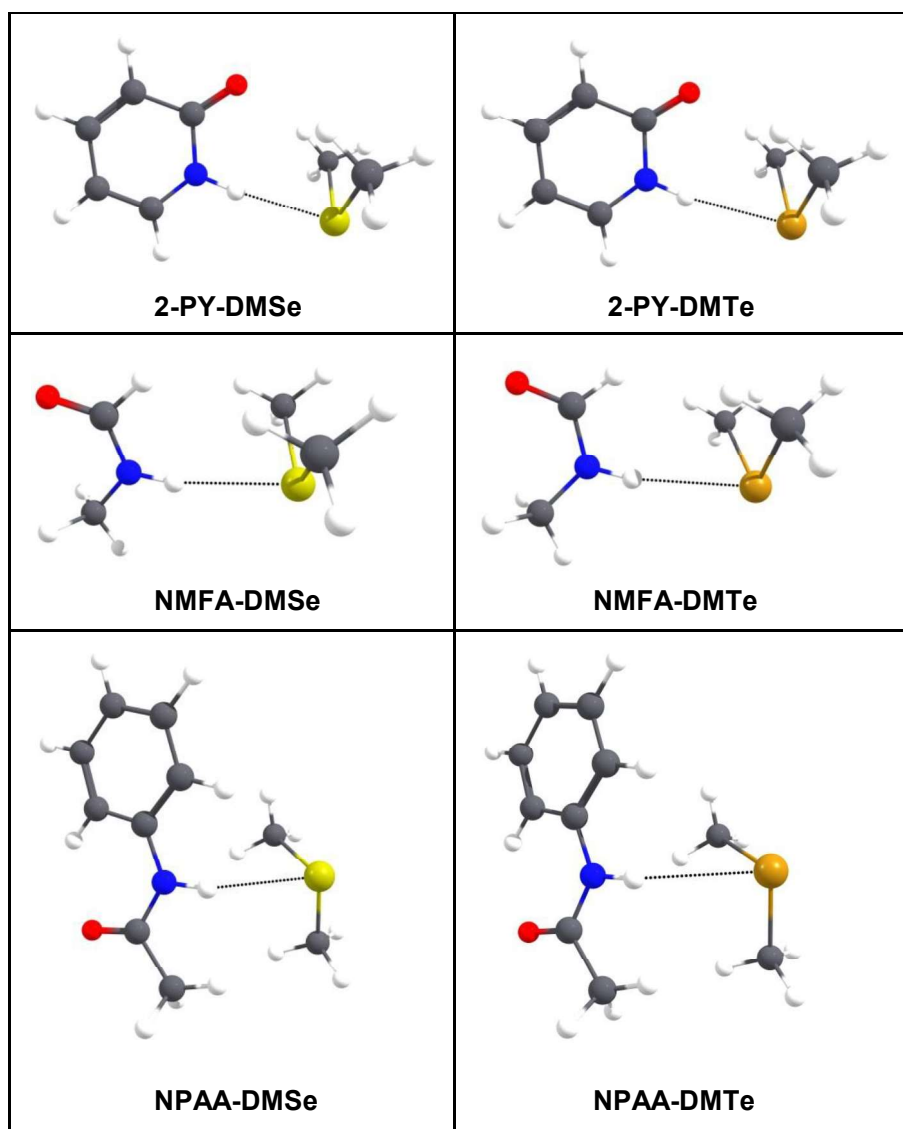


**Figure 4.10** Optimized structures of N-H...Se and N-H...Te H-bond complexes at RI-B97-D/def2-TZVPP level of theory.

## Selenium Centered Hydrogen Bond

**Table 4.1** Computed binding energy ( $D_0$  in kJ/mol) at CCSD(T)/aug-cc-pVDZ, red shift of N-H stretching frequency ( $\Delta\nu$  in  $\text{cm}^{-1}$ ), and donor-acceptor interaction energies ( $E_{DA}$  in kJ/mol) for N-H...Y (Y= O, S, Se, and Te) and N-H...O=C H-bond complexes.

H-bond Type	NPAA-X (trans-amide)			2PY-X (cis-amide)			NMFA-X (trans-amide)		
	$D_0$	$\Delta\nu(\text{NH})$	$E_{DA}$	$D_0$	$\Delta\nu(\text{NH})$	$E_{DA}$	$D_0$	$\Delta\nu(\text{NH})$	$E_{DA}$
N-H...O (X=DME)	39.2	-99	46.1	44.9	-250	75.9	27.2	-97	46.1
N-H...S (X=DMS)	40.6	-96	45.0	49.0	-291	90.0	28.0	-132	54.3
N-H...Se (X=DMSe)	41.2	-91	42.1	50.4	-262	83.0	29.5	-120	51.4
N-H...Te (X=DMTe)	41.7	-80	35.8	46.1	-241	72.4	25.8	-114	49.1
N-H...O=C (X=DMF)	55.1	-73	28.0	57.8	-311	101	32.1	-123	50.0

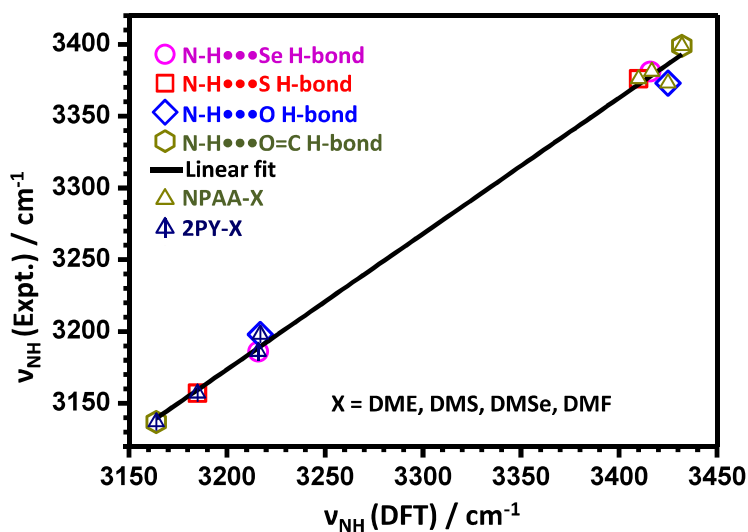


**Figure 4.11:** Linear correlation plot between vibrational frequencies estimated by DFT ( $\nu_{\text{NH}} - \text{DFT}$ ) and experimental N-H stretching frequencies ( $\nu_{\text{NH}} - \text{Expt.}$ ). The fitted equation,  $\nu_{\text{NH}}(\text{Expt.}) = 0.9868 \times \nu_{\text{NH}}(\text{DFT}) + 11$  is used to estimate experimental N-H stretching frequencies ( $\nu_{\text{NH}} - \text{Expt.}$ ) of NPAA-DMTe, 2PY-DMTe and NMFA-DMTe amide-N-H...Te H-bond complexes.

## Selenium Centered Hydrogen Bond

The existence of H-bonds is supported by non-covalent interaction (NCI) analyses using the wave functions of the optimized structures at MP2/aug-cc-pVDZ level of method. Figure 4.12 shows isosurfaces are indicative of attractive interactions between H and Se/Te as green, blue color isosurface in N-H...Se and N-H...Te H-bond complexes.

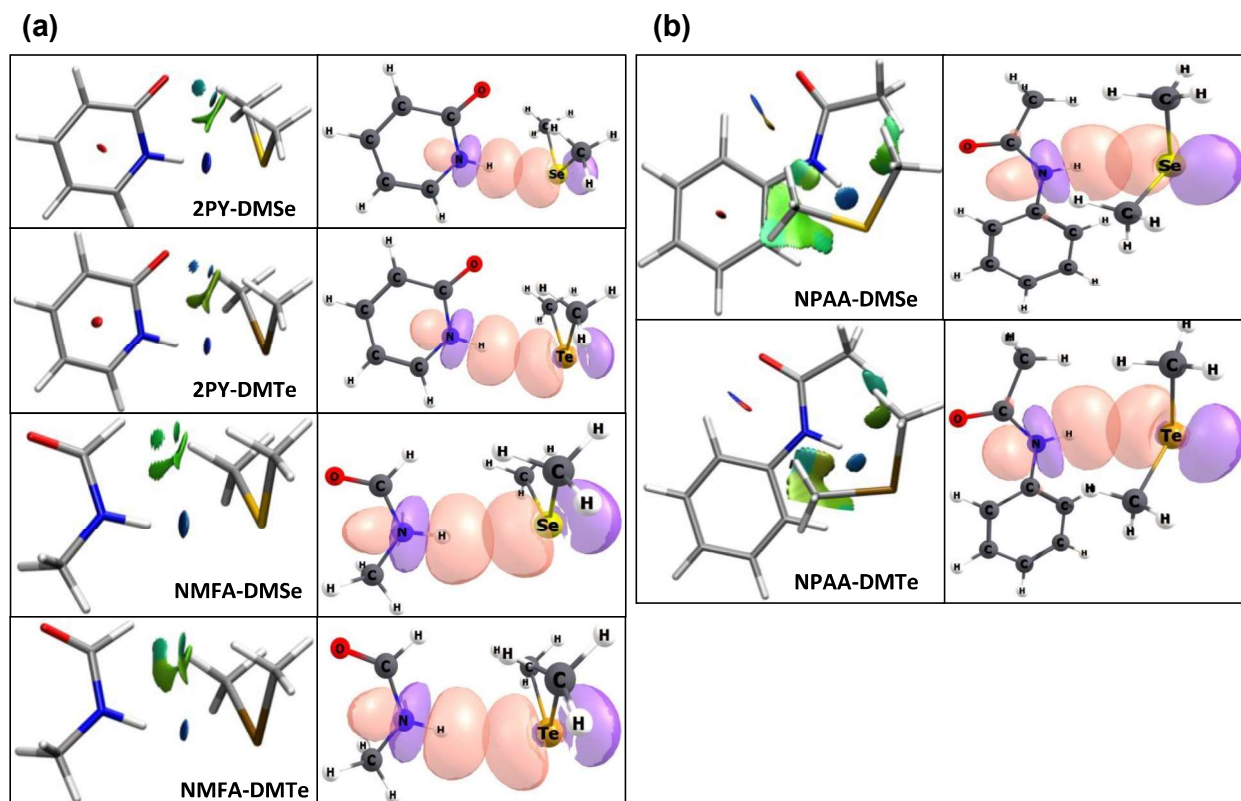


**Figure 4.12** (a) Left panel: 3D-NCI plot, colored isosurfaces of the reduced electron density gradient and Right panel: Orbital overlap of *s*- and *p*-type Se/Te lone pair and N-H  $\sigma^*$  orbitals in N-H...Se and N-H...Te H-bonded complexes of 2-PY, NMFA and (b) NPAA at MP2-aug-cc-pVDZ level of theory.

Further, we carried out the natural bond orbital (NBO) analysis which provides the donor-acceptor pair-wise interaction energies ( $E_{DA}$ ). The donor-acceptor interaction ( $E_{DA}$ ) energies for all the H-bond complexes are computed at MP2/aug-cc-pVDZ level of theory. The orbital overlapping between the lone pair orbital of Se/Te and antibonding orbital  $\sigma$  NH orbital

## Selenium Centered Hydrogen Bond

( $\sigma_{\text{NH}}^*$ ) of N-H...Se and N-H...Te complexes were shown in Figure 4.12 and their values are listed in Table 4.1. The  $E_{\text{DA}}$  values give the strength of H-bonds in the complexes and these were correlated with experimental red shifts. A linear correlation was observed between  $E_{\text{DA}}$  and  $\Delta\nu_{\text{NH}}$ , as shown in Figure 4.13. This concludes that  $\Delta\nu_{\text{NH}}$  can be used as a spectroscopic marker of the H-bond strength of the amide-NH...X complexes.

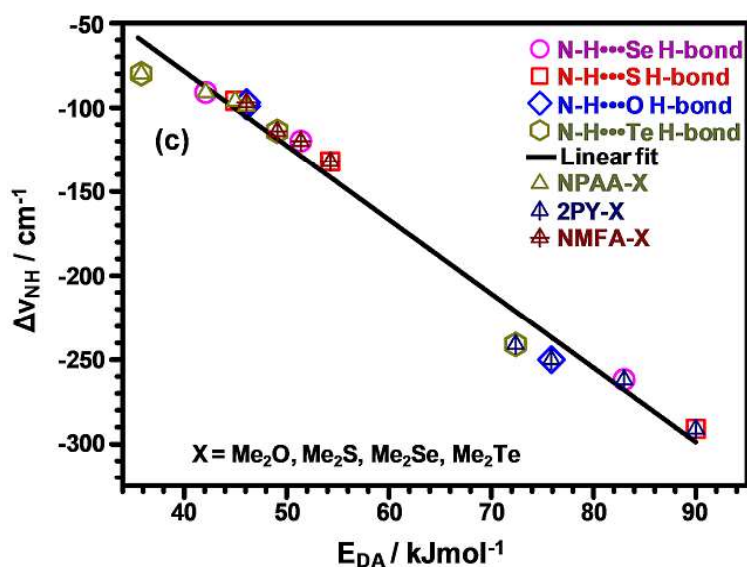


**Figure 4.13** Linear correlation plot between donor-acceptor interaction energies ( $E_{\text{DA}}$ ) and red shift of N-H stretching frequencies.

### 4.3.3. Contribution of Electronegativity, Atomic Charge and Local Polarizability to the strength of H-bond:

The H-bond strength of NMFA-X complexes as observed from  $\Delta\nu_{\text{NH}}$  and  $E_{\text{DA}}$  values follow the order N-H...S > N-H...Se > N-H...Te > N-H...O. On the other hand the electronegativities of O, S, Se and Te follow the order O (3.44) > S (2.58) > Se (2.55) > Te (2.1). One could see there is no

## Selenium Centered Hydrogen Bond

correlation between the H-bond strengths and electronegativities of the H-bond acceptor atoms. Hence, it is no longer a rule that atoms with lower electronegativity will always form

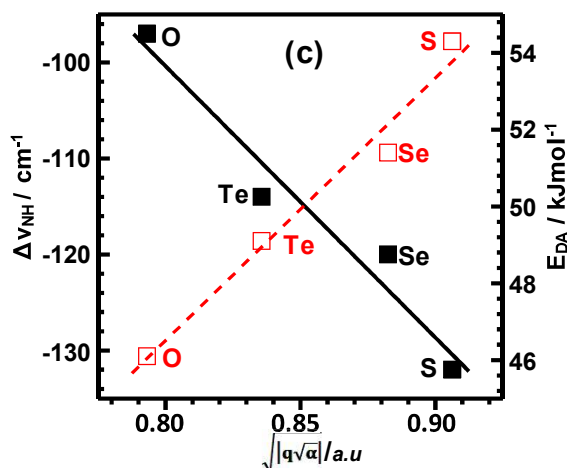


**Figure 4.14** Linear correlation plot between donor-acceptor interaction energies ( $E_{DA}$ ) and red shift of N-H stretching frequencies ( $\Delta v_{NH}$ ) with the geometric mean of atomic charges ( $q$ ) and spherically averaged static square root of polarizability ( $\alpha_{avg}$ ) ( $\sqrt{|q\sqrt{\alpha}|}$ ) of H-bond acceptor atoms.

weak H-bonds. We have seen many exceptions in SCHB systems. Then we calculated atomic charges ( $q$ ) of the H-bond acceptor atoms by using electrostatic potential fitting method (CHarges from ELectrostatic Potentials using a Grid based method, CHELPG<sup>41</sup>). These calculations were performed at M06-2X/aug-cc-pVDZ level of theory. The computed charges of O, S, Se, and Te are -0.3297, -0.2415, -0.2050, and -0.1532 au, respectively. These are exactly the same order of their electronegativities; therefore atomic charges alone may not be sufficient to explain the observed H-bond strengths of the molecular complexes considered in this work. Going down the group in the periodic table not only the electropositive character of the elements enhances but also the atomic polarizability increases. Hence the possible contribution of polarizability of the H-bond acceptor atoms cannot be neglected or overlooked.<sup>4</sup> We calculated

## Selenium Centered Hydrogen Bond

---

spherically averaged static polarizability ( $\alpha_{avg.}$ ) of O, S, Se, and Te in DME, DMS, DMSe, and DMTe, respectively using molecular polarizability partitioning method as described by Donald G. Truhlar and co-authors.<sup>42</sup> The  $\alpha_{avg.}$  values of O, S, Se, and Te in DME, DMS, DMSe, and DMTe are 3.48, 11.87, 14.60, and 20.42 a.u., respectively. Then the geometric mean of atomic charges and polarizabilities of H-bond acceptors ( $\sqrt{|q\sqrt{\alpha_{avg.}}|}$ ) was considered as a possible H-bond descriptor. Figure 4.14 shows a linear correlation between  $\sqrt{|q\sqrt{\alpha_{avg.}}|}$  and  $\Delta v_{NH}$ , and also between  $\sqrt{|q\sqrt{\alpha_{avg.}}|}$  and  $E_{DA}$ . In both the cases the correlation coefficient is more than 0.93. The linear correlation inferred that not only the higher electronegativity or atomic charges of H-bond acceptor atoms are solely responsible for stronger H-bond formation but also polarizability plays a deciding role in determining H-bond strength. It is interestingly observed that  $\sqrt{|q\sqrt{\alpha_{avg.}}|}$  of S is the highest and amide-N-H...S H-bonds are strongest among the others presented here, may be one of the reasons for which nature prefers methionine than its Se/Te/O counterpart.

### 4.4. Conclusions

- The analysis of protein data bank confirmed the existence of Selenium center hydrogen bonds (SeHBs) in selenomethionine containing proteins as amide-N-H...Se H-bond. The donor-acceptor interaction energies suggested that the strength of amide-N-H...Se H-bond is as strong as conventional H-bonds and it is depended on the geometrical constraints.
- The red shifts obtained from the high resolution vibrational spectroscopy evidenced the presence of SeCHBs as amide-N-H...Se in trans- and cis- amide model compounds of peptides and nucleotides respectively. The strength of amide-N-H...Se H-bond in trans-

## Selenium Centered Hydrogen Bond

---

amide as strong as amide-N-H...S H-bond but in the case of cis amide little weaker than amide-N-H...S H-bond and stronger than amide-N-H...O, amide-N-H... $\pi$  H-bonds.

- A combination of experimental and computational studies at CCSD-T level conclude that the strength of amide-NH...Se H-bonds are comparable to that of Sulfur center hydrogen bond (SCHBs) and conventional amide-NH...O and amide-NH...O=C H-bonds.
- The computational studies also suggest that Tellurium can form strong amide-NH...Te H-bonds. The observed red shifts conclude that amide-N-H...Te H-bond is similar to those of amide-N-H...X (X = Se, S, O) H-bonds.
- The strength of amide-NH...Y (Y=O, S, Se and Te) H-bonds are not only governed by the electronegativities and charges of the acceptor atoms (Y) but also by their polarizabilities.
- We would like to emphasize in this work that SeCHBs invoke special attention and critical rethinking of the concept of electronegativity and polarizability in predicting H-bond strength
- This molecular level study on amide-NH...Se H-bond (SeCHBs) is very useful for theoretical and physical chemists while proposing new force field for biomolecular structure simulations and for structural and molecular biologists in de novo designing proteins by replacing methionine and/or other residues with selenomethionine or substituting selenium in place of oxygen in nucleotides.

## Selenium Centered Hydrogen Bond

---

### References:

- (1) Biswal, H. S.; Chakraborty, S.; Wategaonkar, S. *J. Chem. Phys.* **2008**, *129*, 184311.
- (2) Biswal, H. S.; Shirhatti, P. R.; Wategaonkar, S. *J. Phys. Chem. A* **2009**, *113*, 5633.
- (3) Biswal, H. S.; Wategaonkar, S. *J. Phys. Chem. A* **2009**, *113*, 12774.
- (4) Biswal, H. S.; Wategaonkar, S. *J. Phys. Chem. A* **2009**, *113*, 12763.
- (5) Biswal, H. S.; Gloaguen, E.; Loquais, Y.; Tardivel, B.; Mons, M. *J. Phys. Chem. Lett.* **2012**, *3*, 755.
- (6) Alauddin, M.; Biswal, H. S.; Gloaguen, E.; Mons, M. *Phys. Chem. Chem. Phys.* **2015**, *17*, 2169.
- (7) Huber, R. E.; Criddle, R. S. *Arch. Biochem. Biophys.* **1967**, *122*, 164.
- (8) Pearson, R. G.; Sobel, H.; Songstad, J. *J. Am. Chem. Soc.* **1968**, *90*, 319.
- (9) Corey, E. J.; Kim, C. U. *J. Am. Chem. Soc.* **1972**, *94*, 7586.
- (10) Kim, H. Y.; Fomenko, D. E.; Yoon, Y. E.; Gladyshev, V. N. *Biochemistry* **2006**, *45*, 13697.
- (11) Nauser, T.; Steinmann, D.; Grassi, G.; Koppenol, W. H. *Biochemistry* **2014**, *53*, 5017.
- (12) Reich, H. J.; Hondal, R. J. *ACS Chem. Biol.* **2016**, *11*, 821.
- (13) Atkins, J. F.; Gesteland, R. F. *Nature* **2000**, *407*, 463.
- (14) Moroder, L. *J. Peptide Sci.* **2005**, *11*, 187
- (15) Iwaoka, M.; Arai, K. *Curr. Chem. Biol.* **2013**, *7*, 2.
- (16) Carrasco, N.; Buzin, Y.; Tyson, E.; Halpert, E.; Huang, Z. *Nucleic Acids Res.* **2004**, *32*, 1638.
- (17) Höbartner, C.; Rieder, R.; Kreutz, C.; Puffer, B.; Lang, K.; Polonskaia, A.; Serganov, A.; Micura, R. *J. Am. Chem. Soc.* **2005**, *127*, 12035.

## Selenium Centered Hydrogen Bond

---

- (18) Wang, L.; Xie, J.; Schultz, P. G. In *Annu. Rev. Biophys. Biomol. Struct.* 2006; Vol. 35, p 225.
- (19) Salon, J.; Sheng, J.; Jiang, J.; Chen, G.; Caton-Williams, J.; Huang, Z. *J. Am. Chem. Soc.* **2007**, *129*, 4862.
- (20) Salon, J.; Jiang, J.; Sheng, J.; Gerlits, O. O.; Huang, Z. *Nucleic Acids Res.* **2008**, *36*, 7009.
- (21) Sheng, J.; Zhang, W.; Hassan, A. E. A.; Gan, J.; Soares, A. S.; Geng, S.; Ren, Y.; Huang, Z. *Nucleic Acids Res.* **2012**, *40*, 8111.
- (22) Hassan, A. E. A.; Sheng, J.; Zhang, W.; Huang, Z. *J. Am. Chem. Soc.* **2010**, *132*, 2120.
- (23) Sheng, J.; Gan, J.; Soares, A. S.; Salon, J.; Huang, Z. *Nucleic Acids Res.* **2013**, *41*, 10476.
- (24) Madzhidov, T. I.; Chmutova, G. A. *J.Mol.Stru.: THEOCHEM* **2010**, *959*, 1.
- (25) Schamnad, S.; Chakraborty, S. *Chem.Phys. Lett.* **2015**, *622*, 28.
- (26) RCSB 2016.
- (27) REDUCE 2016.
- (28) Bondi, A. *J. Phys. Chem.* **1964**, *68*, 441.
- (29) Rowland, R. S.; Taylor, R. *J. Phys. Chem.* **1996**, *100*, 7384.
- (30) González, B.; Schell, M. J.; Letcher, A. J.; Veprintsev, D. B.; Irvine, R. F.; Williams, R. L. *Mol.Cell.* **2004**, *15*, 689.
- (31) Lee, S. G.; Jez, J. M. *Structure* **2013**, *21*, 1778.
- (32) Weinhold, F.; Landis, C. R. *Valency and Bonding: A Natural Bond Orbital Donor-Acceptor Perspective* **2005**.
- (33) Newberry, R. W.; Raines, R. T. *Nat Chem Biol* **2016**, *12*, 1084.

## Selenium Centered Hydrogen Bond

---

- (34) Contreras-García, J.; Johnson, E. R.; Keinan, S.; Chaudret, R.; Piquemal, J. P.; Beratan, D. N.; Yang, W. *J. Chem. Theory Comput.* **2011**, *7*, 625.
- (35) Fang, D.; Chaudret, R.; Piquemal, J.-P.; Cisneros, G. A. *J. Chem. Theory Comput.* **2013**, *9*, 2156.
- (36) Narth, C.; Maroun, Z.; Boto, R. A.; Chaudret, R.; Bonnet, M.-L.; Piquemal, J.-P.; Contreras-García, J. In *Applications of Topological Methods in Molecular Chemistry*; Chauvin, R., Lepetit, C., Silvi, B., Alikhani, E., Eds.; Springer International Publishing: Cham, 2016, p 491.
- (37) Contreras-García, J.; Boto, R. A.; Izquierdo-Ruiz, F.; Reva, I.; Woller, T.; Alonso, M. *Theor. Chem. Acc.* **2016**, *135*.
- (38) Lane, J. R.; Contreras-García, J.; Piquemal, J.-P.; Miller, B. J.; Kjaergaard, H. G. *J. Chem.The.Comp.* **2013**, *9*, 3263.
- (39) Van Bergen, L. A. H.; Alonso, M.; Palló, A.; Nilsson, L.; De Proft, F.; Messens, J. *Sci. Rep.* **2016**, *6*, 30369.
- (40) Scheiner, S. *ChemPhysChem* **2016**, *17*, 2263.
- (41) Breneman, C. M.; Wiberg, K. B. *J. Comp. Chem.* **1990**, *11*, 361.
- (42) Marenich, A. V.; Cramer, C. J.; Truhlar, D. G. *Chem. Sci.* **2013**, *4*, 2349.

### Chapter 5

#### Applications of SCHBs and SeCHBs in designing Organic Piezoelectric Materials

##### 5.1 Introduction

The applications of hydrogen bonds have been described in many areas of biology and crystal engineering.<sup>1-4</sup> Glowacki *et al.* elucidated the applications of hydrogen bonds in molecular crystals of proteins, DNA, sugars, colorants and electronic conducting materials.<sup>4</sup> In this study they have explained the role of hydrogen bonds in electronic and ionic conducting materials that can be functionalized to form self-assembled supramolecular structures which can support resonant energy transfer. Recently Lambrecht and his coworkers explored the hydrogen bonded systems for potential piezoelectric materials and they can be used as energy harvesters or mechanical sensors.<sup>5,6</sup>

A piezoelectric material is a material which generates the electric charge by applying mechanical stress on it and this phenomenon is called piezoelectric effect. The reverse of this phenomenon is called the inverse piezoelectric effect. Piezoelectric materials are prominently used as energy harvesters.<sup>7</sup> They can convert vibration and movement of a molecular system into the electrical current and vice-versa. Piezoelectric effect is the basis of a mechanical frequency filters, surface acoustic wave devices, bulk acoustic wave devices, sound and ultrasound microphones and speakers, ultrasonic imaging, hydrophones.<sup>8</sup> The reverse effect is basis of an actuators, motors and scientific instrumental techniques with atomic resolution that includes scanning probe microscopes, such as scanning tunneling microscope (STM)<sup>9</sup>, atomic force microscope (AFM)<sup>10</sup> and near field scanning optical microscope (SNOM)<sup>11</sup>. Figure 5.1 represents the piezoelectric materials that are used for several purposes. In all of these microscopes the scanners are made of three piezo crystal and each one is responsible for

## Applications of SCHB and SeCHBs

scanning in the x, y and z directions. Piezoelectric materials are used in daily life such as in lighters and push start propane barbecues, as well as being used as the time reference source in quartz watches. The commercially available piezoelectric materials are ceramics such as lead zirconium titanate (PZT), Barium titanate ( $\text{BaTiO}_3$ ) or polymers such as polyvinylidenedifluoride (PVDF)<sup>7,12-14</sup>, polyvinyl fluoride(PVF)<sup>12</sup>. These materials are conventional and have a high piezo-response. But some of the shortcomings of such piezomaterials are stiffness, brittleness, low processability, decreased piezoelectric response with temperature. Some of these disadvantages have been overcome by using a mixture of two different piezomaterials etc.,<sup>15,16</sup> but this is not enough to meet the constantly growing usage demand.

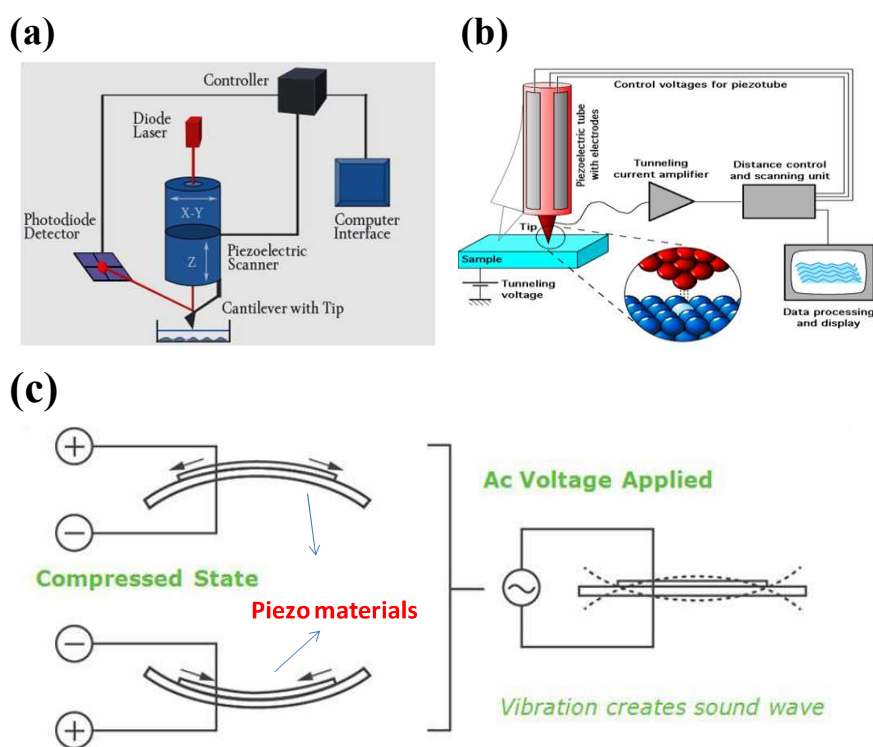


**Figure 5.1** Piezoelectric materials used in different devices (a) Atomic Force Microscope (Precision Mechanics) (b) Scanning Tunneling Microscope (Optics) (c) Buzzers (Industry), Sensors home appliances calling bell.

## Applications of SCHB and SeCHBs

The criteria for a material to be piezoelectric are (a) it should have ionic or partly ionic bonds and (b) it should be non-centrosymmetric. The hydrogen bond is highly directional and polar. The results in the previous chapter explored that the Sulfur/Selenium Center Hydrogen Bonds (SCHB, SeCHB) are as strong as the conventional H-bonds. In addition to these previous works on SCHB complexes suggest that the strength of SCHB falls in weak to moderate range and can be exploited in various applications<sup>17-24</sup>. This encouraged us to explore the possibility of using SCHB complexes as efficient piezo materials. The aim of this chapter is to explore the piezoelectric behavior of SCHB and also SeCHB organic complexes. However, we have chosen nitrobenzene (NBz) as hydrogen bond acceptor and phenol (PH), thiophenol (SPH), selenophenol (SePH) as hydrogen bond donors. The Figure 5.2 represents the H-bond acceptors and donors that are chosen to verify whether the SCHBs, SeCHBs systems can show piezo response or not.

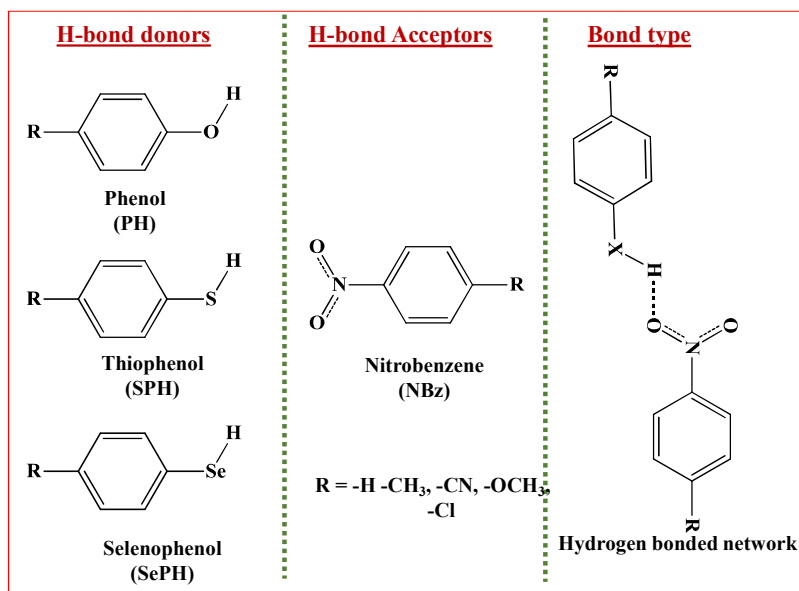


**Figure 5.2** H-bond donors and H-bond acceptors chosen to design Piezoelectric Materials through hydrogen bond

## 5.2 Characterization of Hydrogen bond and binding energies of different H-bond complexes

At first, the geometry optimization and frequency calculations of simple hydrogen bonded systems were carried out at the DFT using B3LYP, PBE0 functionals and 6-31G\*, aug-cc-pVDZ as basis sets. All the computations were performed using Gaussian 09<sup>25, 26</sup>. Figure 5.3 represents the optimized structures of X-H...O (X = O, S and Se) H-bond complexes. These H-bond complex formations were confirmed by atoms in molecule (AIM) analysis and natural bond orbital (NBO) analysis at B3LYP/6-31G\* level of theory. The Figure 5.3 (b, e, h) shows the substantial orbital overlap between the lone pair (lp) of O of nitrobenzene with  $\sigma^*_{X-H}$  orbital of PH, SPH and SePH, leading to the formation of a strong X-H...O H-bonds. In addition to this, atoms in molecule (AIM) analysis confirmed the presence of a BCP between the oxygen of NBz and the hydrogen atom of X-H of PH, SPH and SePH (Figure 3c, f, and 3i). Table 5.1 lists binding energies, Donor-acceptor interaction energies for different type of H-bond systems at B3LYP/6-31G\* level of theory.

**Table 5.1** Binding energies and Donor-acceptor interaction energies of -H...O H-bond systems at B3LYP/6-31G\* level

System	H-bond type	NBO interaction energy (kJ/mol)	Binding energy(kJ/mol)
PH-NBz	O-H...O	46.28	-27.96
SPH-NBz	S-H...O	17.20	-15.85
SePH-NBz	Se-H...O	15.77	-9.84

The strength of hydrogen bond follows the order Se-H...O < S-H...O < O-H...O. The highest binding energy is found for the O-H...O H-bond system. The binding energies and donor-

## Applications of SCHB and SeCHBs

acceptor interaction energies follow the order of the electronegativity of chalcogens Se (2.4) < S (2.5) < (3.5). The AIM and NBO analyses confirm that chosen systems form very strong hydrogen bonds. However, the piezoelectric coefficient can be calculated as mentioned in the following section.

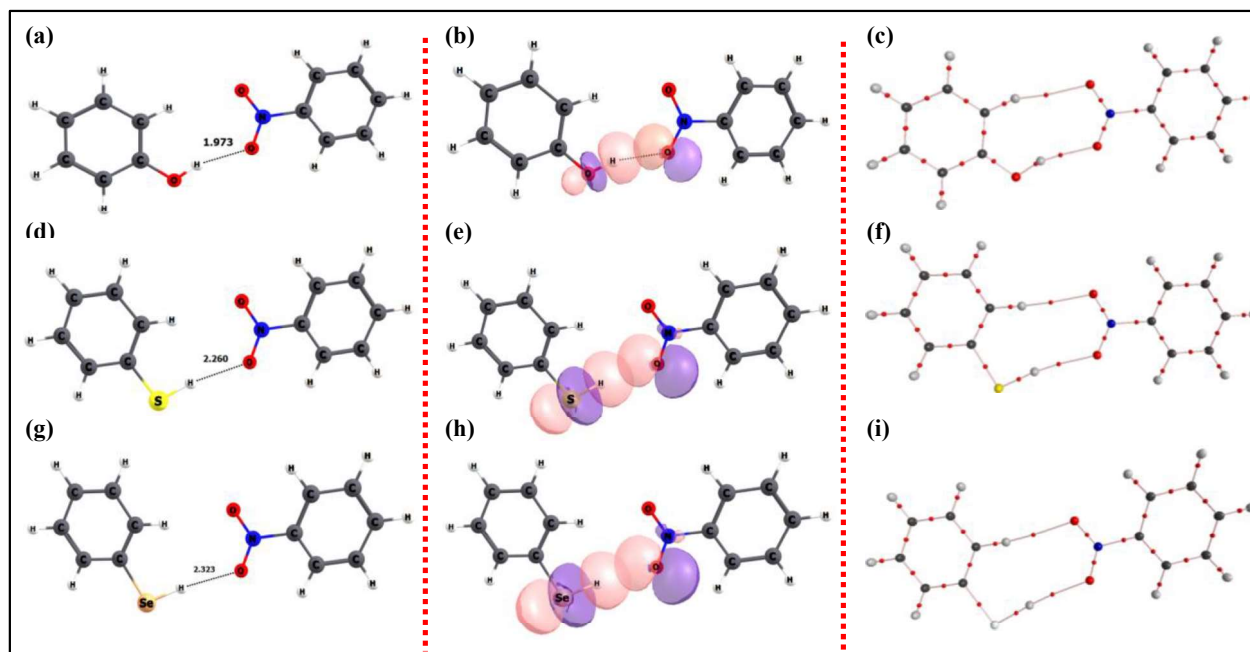


**Figure 5.3** (a, d, g) Optimized geometries, (b, e, h) natural bond orbital overlapping and (c, f, i) electron density topologies for PH...NBz, SPH...NBz and SePH...NBz respectively. Bond critical points are shown in red.

### 5.3 Computational Methods to Calculate the Piezoelectric Coefficients ( $d_{33}$ )

We performed the calculations to determine the piezoelectric coefficients ( $d_{33}$ ) with the two methods used by Daniel S. Lambrecht and co-authors<sup>5,6</sup>. In this work these two methods were followed to screen the SCHB systems as potential piezoelectric materials. In addition to these two methods, one more method including molecular polarizability was also considered. These methods are briefly explained below.

### 5.3.1 Method-A (Estimated Method)

This method is the simplest and computationally less time consuming method. In this method, the optimized structure of H-bond complex was taken for calculating the piezo coefficients with the absence of electric field. No constraints were applied to the geometry optimization and the minimum energy structure was checked by frequency calculation. Hydrogen bond vector was aligned along the direction of z-axis and hydrogen bond length was varied in steps of 0.02 Å, as shown in Figure 5.4. Single point energy for each of the varied hydrogen bond was computed and corresponding z components of dipole moments were taken to calculate piezo-coefficient using the formula outlined in equation 2.<sup>6</sup>

$$d_{33} \approx \frac{1}{z_0} \cdot \left. \frac{\partial^2 E}{\partial \xi^2} \right|_{z_0,0} \mu_0 \quad (1)$$

The expression can further be simplified

$$d_{33} \equiv -\frac{1}{z_0} h_0^{-1} \mu_0 \quad (2)$$

Here,  $z_0$  is the equilibrium hydrogen bond length; E is the potential energy as a function of bond displacement ( $z-z_0$ ).  $\mu$  is the dipole moment of the system and  $h$  represents second derivative of the energy of system. All calculations were done in the absence of electric field.

## Applications of SCHB and SeCHBs

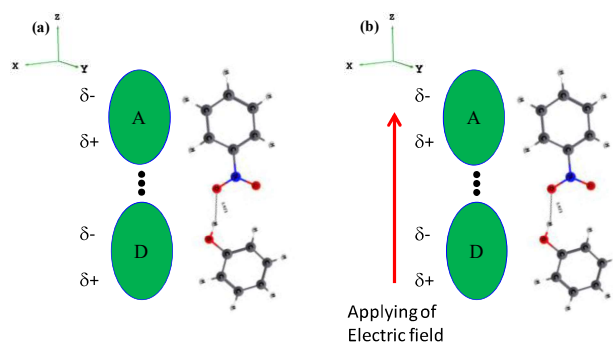


**Figure 5.4** Pictorial representation of H-bond vector in molecule aligned in the direction of applied electric field: In (a), there is no applied electric field ( used in Method A) and in (b) applying the electric field in direction of H-bond vector used in Method B.

Tables 5.2-5.4 lists the piezo electric coefficients and equilibrium H-bond distance and dipole moment of z-component at equilibrium distance at different functionals (B3LYP, PBE0 and  $\omega$ B97xD) with 6-31G\* and aug-cc-pVDZ basis set. In this method the obtained potential energy at different H-bond distances is in atomic units, dipole moment in Debye, distance in Å. All the different units were converted into SI units and the conversions are as followed

$$d_{33} = \frac{1}{10^{-10}m} \frac{10^{-20}m^2}{43.60 \times 10^{-19}N.m} \frac{3.33564 \times 10^{-30}C.m}{10^{-10}m} \quad (3)$$

$$= \frac{3.33564 \times 10^{-11}}{43.60} \left( \frac{C.m}{J} \right) \text{ (Since } N.m = \text{Joule)}$$

$$= 0.7651 \times 10^{-12} \left( \frac{C.m}{J} \right)$$

$$d_{33} = 0.7651 \left( \frac{pm}{V} \right) \text{ (Since } \frac{Joule}{Coulomb} = \text{Volt)} \quad (4)$$

Using this conversion we have calculated the estimated piezo electric coefficients and listed in Tables 5.2 to 5.4 for different level of theory. The order of piezoelectric coefficients of different H-bond systems follows as Se-H•••O > S-H•••O > O-H•••O at all functional and basis set except

## Applications of SCHB and SeCHBs

$\omega$ B97D functional. But the observed  $d_{33}$  values are different with different functional and basis sets used to calculate. The highest piezo electric coefficient is found to be 27.9 pm/V for SePH-NBz H-bond system and 25.2, 19.2 pm/V for SPH-NBz and PH-NBz H-bond systems at B3LYP/aug-cc-pVDZ level, respectively. The lowest piezo coefficient is found to be 13.27 pm/V for PH-NBz system at  $\omega$ B97D/6-31G\* level.

**Table 5.2** The piezoelectric coefficients at method A and method B, equilibrium H-bond distance, second derivative of potential energy and derivative of dipole moment of different H-bond systems at B3LYP functional with 6-31G\* and aug-cc-pVDZ basis sets.

Basis set	Dimer	$z_0$ (Å)	$\left(\frac{dE^2}{dz_0^2}\right)_{z_{0,0}}$ (hartree/Å <sup>2</sup> )	$\left(\frac{d\mu}{dz}\right)_{z_{0,0}}$ (D/Å)	Estimated $d_{33}$ (pm/V)	Slope = $r_{eq}/f$ (Å*nm/V)	Calculated $d_{33}$ (pm/V)
					Method A		Method B
6-31G*	PH-NBz	1.9889	0.055	-2.195	15.45	0.03	14.04
	SPH-NBz	2.3082	0.023	-1.533	22.00	0.05	22.00
	SePH-NBz	2.3767	0.020	-1.515	24.23	0.06	23.57
aug-cc-pVDZ	PH-NBz	2.0115	0.033	-1.655	19.22	0.04	18.89
	SPH-NBz	2.3982	0.015	-1.185	25.20	0.06	25.57
	SePH-NBz	2.4903	0.012	-1.100	27.95	0.07	26.90

**Table 5.3** The piezoelectric coefficients at method A and method B, equilibrium H-bond distance, second derivative of potential energy and derivative of dipole moment of different H-bond systems at PBE0 functional with 6-31G\* and aug-cc-pVDZ basis sets.

Basis set	Dimer	$z_0$ (Å)	$\left(\frac{dE^2}{dz_0^2}\right)_{z_{0,0}}$ (hartree/Å <sup>2</sup> )	$\left(\frac{d\mu}{dz}\right)_{z_{0,0}}$ (D/Å)	Estimated $d_{33}$ (pm/V)	Slope = $r_{eq}/f$ (Å*nm/V)	Calculated $d_{33}$ (pm/V)
					Method A		Method B
6-31G*	PH-NBz	1.9730	0.047	-1.858	15.20	0.03	14.99
	SPH-NBz	2.2593	0.025	-1.565	21.41	0.05	21.71
	SePH-NBz	2.3235	0.021	-1.553	24.01	0.05	23.53
aug-cc-pVDZ	PH-NBz	1.9862	0.036	-1.723	18.48	0.04	17.79
	SPH-NBz	2.3309	0.018	-1.305	24.13	0.06	23.74
	SePH-NBz	2.4211	0.015	-1.233	25.16	0.06	25.36

## Applications of SCHB and SeCHBs

**Table 5.4** The piezoelectric coefficients at method A and method B, equilibrium H-bond distance, second derivative of potential energy and derivative of dipole moment of different H-bond systems at  $\omega$ B97XD functional with 6-31G\* and aug-cc-pVDZ basis sets.

Basis set	Dimer	$z_0$ (Å)	$\left(\frac{dE^2}{dz_0^2}\right)_{z_{0,0}}$ (hartree/Å <sup>2</sup> )	$\left(\frac{d\mu}{dz}\right)_{z_{0,0}}$ (D/Å)	Estimated $d_{33}$ (pm/V)	Slope= $r_{eq}/f$ (Å*nm/V)	Calculated $d_{33}$ (pm/V)
					Method A		Method B
6-31G*	PH-NBz	1.9661	0.045	-1.533	13.27	0.03	12.78
	SPH-NBz	2.3021	0.030	-1.360	14.84	0.03	14.60
	SePH-NBz	2.4516	0.023	-1.093	15.09	0.04	15.76
aug-cc-pVDZ	PH-NBz	1.9720	0.042	-1.505	13.94	0.03	13.62
	SPH-NBz	2.3049	0.022	-1.363	20.77	0.05	19.82
	SePH-NBz	2.3939	0.022	-1.253	18.02	0.04	17.73

### 5.3.2 Method-B (Calculated Method)

This method is simpler than estimated method<sup>6</sup>. In this case, we used the optimized structures of H-bond complexes, the H-bond vector of optimized H-bonded dimer was aligned to Z-direction and then the electric field was applied along the H-bond direction. The external applied electric field was varied from -1 V/nm to +1 V/nm in steps of 0.25 ( $\pm 0.03$ ) V/nm along the z-direction. The H-bond length was changed in steps of 0.02 Å for each of the applied electric field. Single point energies were calculated for each step. We would like to mention here that substantial change of the geometry of the complexes could be possible in the presence of external electric field. In the computational method, this point was also considered. The H-bond length was fixed and all other coordinates of the complexes were relaxed. The H-bond lengths were scanned stepwise to get the equilibrium H-bond length (H-bond length in the minimum energy structure). The geometry optimization was also performed by enforcing the Eckart conditions, but several times SCF convergence failure was noticed. Energy versus hydrogen bond distance was plotted for each of the applied electric field and a polynomial fit of order 6

## Applications of SCHB and SeCHBs

was done. The equilibrium (minimum energy) H-bond length was found from the fit for each of the applied electric field. A linear correlation was observed between the equilibrium H-bond length and an applied electric field. The slope of linear fit was used to calculate the piezo-coefficient. The linear fitting plots were shown in Figure 5.5. The piezo-coefficient was determined using equation 5.6

$$d_{33} \approx \frac{1}{z_0} \times \text{slope} \quad (5)$$

In this method also the piezoelectric coefficients have followed the same order as estimated method and the order is  $\text{Se-H}\cdots\text{O} > \text{S-H}\cdots\text{O} > \text{O-H}\cdots\text{O}$  H-bond systems. The piezoelectric coefficients are found to be 26.9, 25.6, 18.9 pm/V for SePH-NBz, SPH-NBz and PH-NBz H-bond system at B3LYP/aug-cc-pVDZ level, respectively which are larger than other two levels of theory. The lowest piezoelectric coefficients were observed at  $\omega$ B97XD functional. The values of piezoelectric coefficients, slopes are mentioned in Tables 5.2-5.4 at different levels of theory.

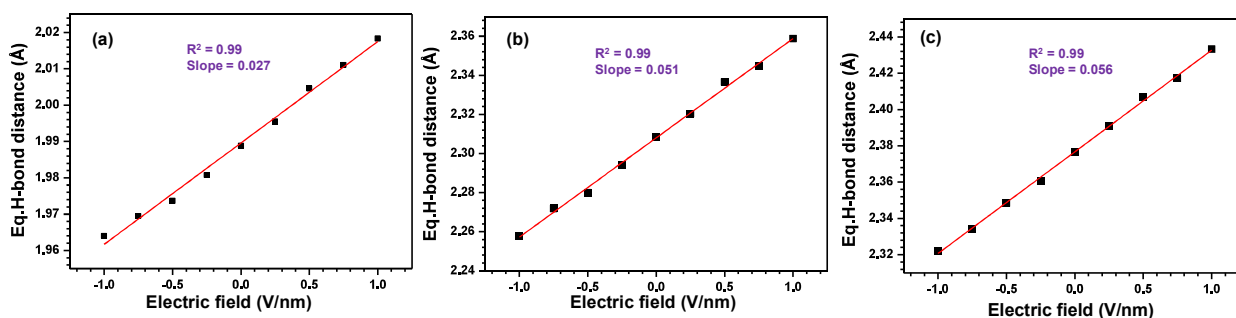


**Figure 5.5** Linear plots applied electric field vs equilibrium H-bond distance (a)PH-NBz dimer, (b) SPH-NBz dimer, (c) SePH-NBz dimer at B3LYP/6-31G\* level of theory.

The piezoelectric coefficients obtained by estimated and calculated methods were compared and showed in Figure 5.6. It was confirmed that the piezoelectric coefficient in the

particular H-bond dimer depends on the basis set and functional employed. But the trend remains same at all the levels of theory and basis set.

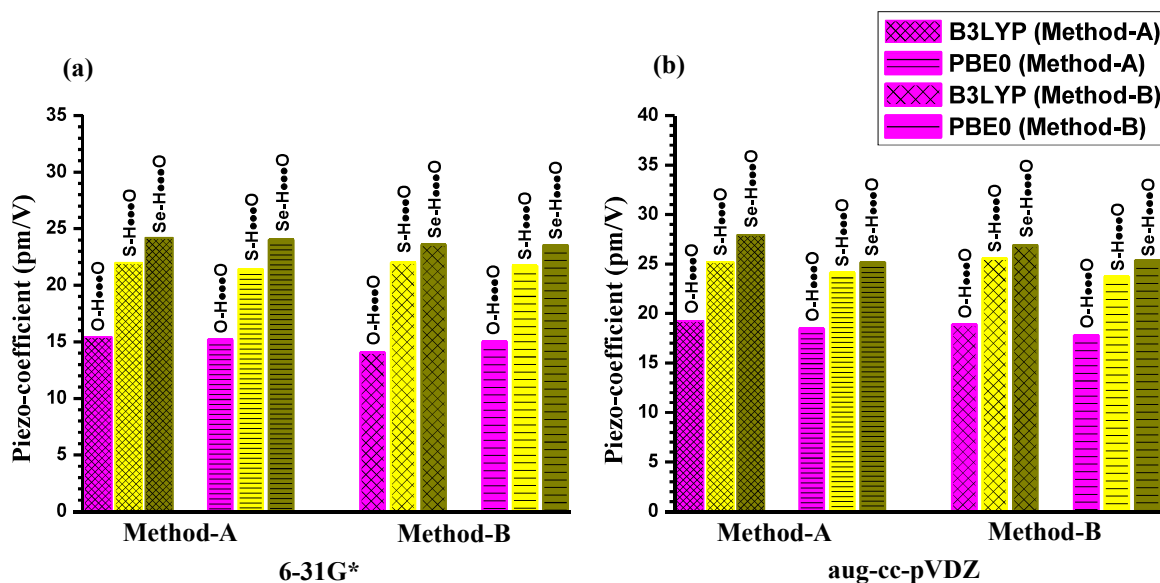


**Figure 5.6** Comparison of piezoelectric coefficients of different hydrogen bonded systems at (a) 6-31G\* (b) aug-cc-pVDZ basis sets using B3LYP and PBE0 functionals in both the methods.

In both the methods irrespective of levels of theory, the piezoelectric coefficient values for sulfur centered hydrogen bond (SCHB) dimer such as SPH-NBz are significantly higher than their oxygen counterpart. The  $d_{33}$  value of PH-NBz is 18.89 pm/V while that of SPH-NBz is 25.57 pm/V at B3LYP/aug-cc-pVDZ level of theory. The piezoelectric coefficient value of SPH-NBz is higher than experimentally observed piezo-response of 2-methyl-4-nitroaniline (14 pm/V)<sup>27</sup>, which is the largest known piezoelectric response in organic crystal. Werling, K. A et al. calculated at B3LYP/6-31G\* level of theory and the value is 23 pm/V.<sup>6</sup> We have calculated the piezoelectric coefficient for same system at B3LYP/aug-cc-pVDZ level of theory and it is 14.93 pm/V which is close to the  $d_{33}$  value of PH-NBz (OH...O) H-bond system. This  $d_{33}$  value is less than value for SPH-NBz H-bond system. This system has the perfect compensation

between hydrogen bond strength and dipole moment derivative as outlined by equation 2 for achieving maximum piezo-response among the systems studied. Apart from the H-bond length and dipole moment derivative, polarizability could affect the piezoelectric coefficient. To verify the polarizability effect we have calculated the piezoelectric coefficient by including the polarizability term. The process of calculation is explained briefly in the following section.

### 5.3.3 Method-C: Effect of Polarizability on piezoelectric coefficient ( $d_{33}$ )

This method is very similar to the method-B; the electric field was applied along the direction of H-bond vector which is aligned along the z-direction of optimized H-bond dimers. Here also the applied electric field was varied from -1 V/nm to +1 V/nm in steps of 0.25 ( $\pm 0.03$ ) V/nm along the z direction. The H-bond length was changed in steps of 0.02 Å for each of the applied electric field. Single point energies were calculated for each step. In this method the polarizability term ( $\alpha = \frac{\partial^2 E}{\partial f^2}$ ) was included by using the following expression for  $d_{33}$ <sup>6</sup>.

$$\begin{aligned} \frac{d\xi}{df} \approx & - \left( \frac{\partial^3 E}{\partial \xi^2 \partial f} f + \frac{\partial^2 E}{\partial \xi^2} \right)^{-1} \left( \frac{\partial^2 E}{\partial \xi \partial f} + \frac{\partial^3 E}{\partial \xi \partial f^2} f \right) \\ & + \left( \frac{\partial^3 E}{\partial \xi^2 \partial f} f + \frac{\partial^2 E}{\partial \xi^2} \right)^{-2} \left( \frac{\partial^2 E}{\partial \xi \partial f} f + \frac{1}{2} \frac{\partial^3 E}{\partial \xi \partial f^2} f^2 \right) \frac{\partial^3 E}{\partial \xi^2 \partial f} \end{aligned} \quad (6)$$

$$d_{33} \approx -\frac{1}{z_0} \times \frac{d\xi}{df} \quad (7)$$

Only the first term in the expression has been considered in the calculation for the sake of simplicity and assuming that the higher order terms have negligible effects (*vide infra*). For all the cases  $d_{33}$  was computed at an applied electric field  $f=0.5$  V/nm.

## Applications of SCHB and SeCHBs

In this method, the isotropic molecular polarizabilities and piezoelectric coefficients were calculated at B3LYP/6-31G\* level of theory. The computed polarizabilities and piezoelectric coefficients were shown in Table 5.5. The polarizability of different H-bond dimers follows the order Se-H...O > S-H...O > O-H...O. This order is follows same in case of piezoelectric coefficients. The higher polarizability is the another reason for higher piezoelectric coefficient for SCHBs and SeCHBs. This evidences the higher piezoelectric coefficients obtained from method-C for SPH-NBz H-bond dimer.

**Table 5.5** The piezoelectric coefficients at method C and Isotropic molecular polarizability for X-H...O H-bond dimers at B3LYP/6-31G\* level of theory.

Method	Dimer	Isotropic molecular Polarizability (a.u)	Calculated $d_{33}$ (pm/V)
			Method C
B3LYP/6-31G*	PH-NBz	138.5	15.05
	SPH-NBz	151.9	24.87
	SePH-NBz	158.6	27.39

Moreover, methods A and B have already been elegantly used by Lambrecht and co-authors<sup>5,6</sup> to compute piezo-response for H-bonded species and validated against the experimental data. The maximum difference in  $d_{33}$  values in these three methods are within 10%. The piezoelectric coefficients obtained from method-B and C are compared with those obtained from method-A as shown in Figure 5.7. In method-C, the piezoelectric coefficient values are higher than the values obtained in method-B and A. These higher values in method-C are because of inclusion of additional term such as polarizability derivatives as shown in equation 6 and 7.

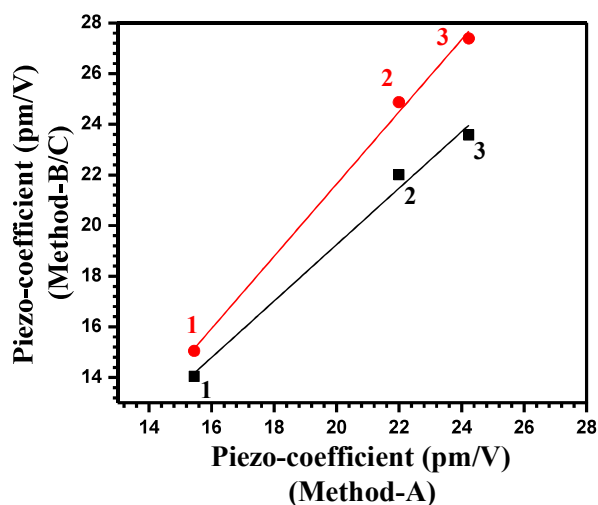


**Figure 5.7** Correlation between piezoelectric coefficients obtained from different methods. Red dots and line indicates method-C vs method-A, black squares and line indicates: method-B vs method-A; 1-PH-NBz dimer, 2-SPH-NBz dimer, 3-SePH-NBz dimer.

The method-A is used to calculate the piezoelectric coefficients of H-bonded piezo organic materials because it is computationally cheaper and faster to do the calculations than method-B as reported by Lambrecht et al. This is also true for method-C. Equation-2 is used for calculating piezoelectric coefficient and it is quite helpful for predicting the piezo-response of H-bonded systems. In method-A, all the calculations were done in the absence of electric field while method-B and C with varying the electric field. Furthermore, in this method, only 13 single point energy calculations have been done whereas 100 calculations are required in case of other two methods. Therefore, we have taken the piezoelectric coefficients obtained in method-A to correlate with dipole moments and its derivative with respect to equilibrium distance. The linear correlation was observed for all these cases and shown in Figure 5.8.

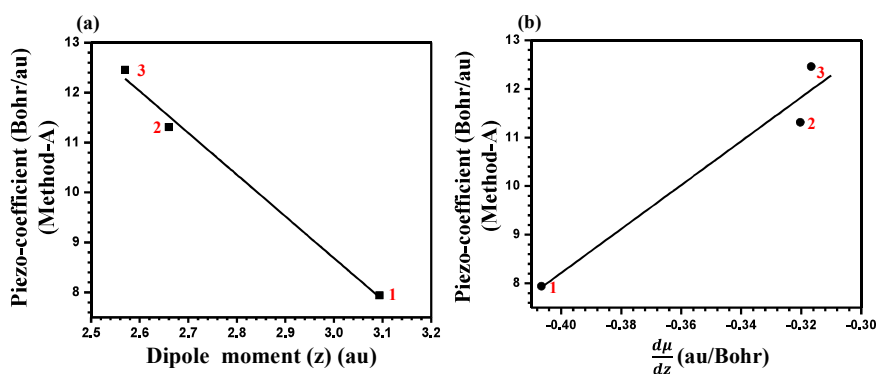


**Figure 5.8** Correlation graphs (a) the linear correlation between piezoelectric coefficient and dipole moment and (b) dipole moment derivative with respect to geometric displacement. 1-PH-NBz, 2-SPH-NBz, 3-SePH-NBz dimers.

The linear correlation was also observed between the piezoelectric coefficients of H-bonded systems obtained in method-A and polarizabilities and derivative of polarizabilities, as shown in Figure 5.9. This indicates that sulfur and selenium centered hydrogen bond systems have higher polarizabilities with higher piezoelectric coefficients. This infers the SCHBs and SeCHBs can be considered as promising organic piezoelectric materials with high piezocoefficients.

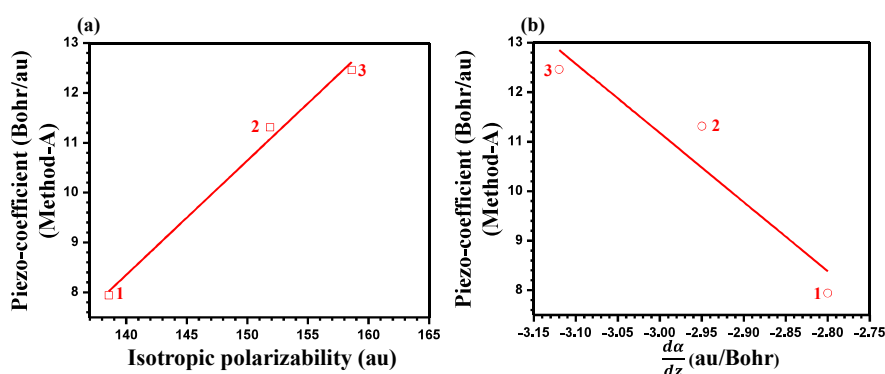


**Figure 5.9** Correlation graphs (a) the linear correlation between piezoelectric coefficient and isotropic polarizability and (b) polarizability derivative with respect to geometric displacement. 1-PH-NBz, 2-SPH-NBz, 3-SePH-NBz dimers.

### 5.4 Substituent effect on $d_{33}$ and Mimicking Crystal Structure

The introduction of substituents in Hydrogen bond dimers is the regular method for fine-tuning the strength and geometry of H-bond interactions which is widely applied in the design of new type of materials with special properties. The strength of hydrogen bond varies with substituents present at para position of aromatic ring of the H-bond donor and H-bond acceptor.<sup>28-30</sup> Herein, we have performed the calculations to determine the effect of substituents on the piezoelectric coefficient with addition of electron donating or electron withdrawing groups to the aromatic systems. To explore this aspect, we have chosen electron withdrawing groups (EWG) such as -Cl, -CN and -OMe and electron donating groups (EDG) such as -CH<sub>3</sub>. These were added at para position of donor benzene ring and acceptor benzene ring of SPH-NBz dimer. First, we have performed the optimization and frequency calculations at B3LYP/6-31G\* level of theory. The formation of H-bond between donor and acceptor was confirmed by NBO and AIM analysis. Later, we have calculated the piezoelectric coefficients of substituted para position of SPH-NBz dimers using the calculated method (method-B). Figure 5.10 and Figure 5.11 show the optimized geometries of substituted SPH-NBz H-bond systems. The calculated piezoelectric coefficient values of all the substituted SPH-NBz dimers were displayed in Table 5.6. The highest piezoelectric coefficient is 24.02 pm/V for Me-SPH-OMe-NBz and the lowest is 21.91 pm/V for CN-SPH-NBz dimer. Table 5.7 shows the binding energies and donor-acceptor interaction energies of some EWD groups like -CN, -OMe substituted para position of donor and acceptor aromatic ring of SPH-NBz dimers. There is a significant change in binding energies and donor-acceptor interaction energies of substituted SPH-NBs dimers. However, the average difference between maximum and minimum  $d_{33}$  values obtained is 2.1 pm/V. This change is not

## Applications of SCHB and SeCHBs

a significant change for EWG and EDG groups on SPH-NBZ dimer. It is confirmed that adding EWG or EDG on SPH-NBz dimer does not change the piezo-coefficient values significantly.

**Table 5.6** Estimated piezoelectric coefficients (pm/V) of different substituents at para position of SPH-NBz dimer.

Donor Acceptor	-CH <sub>3</sub>	H	-OMe	-Cl	-CN
-CH <sub>3</sub>	23.10	22.79	22.63	22.93	22.64
H	22.31	22.00	22.13	22.18	21.91
-OMe	24.02	23.82	23.39	23.49	23.22
-Cl	23.54	23.01	22.50	23.07	23.12
-CN	23.04	22.71	22.47	22.98	23.26

**Table 5.7** Binding energies and donor-acceptor interaction energies of different substituents at para position of SPH-NBz dimer.

System	H-bond type	NBO interaction energy (kJ/mol)	Binding energy (kJ/mol)
SPH-OMe-NBz	O...H-S	19.41	-17.33
SPH-CN-NBz	O...H-S	14.56	-13.22
OMe-SPH-NBz	O...H-S	16.40	-15.14
CN-SPH-NBz	O...H-S	21.46	-22.27



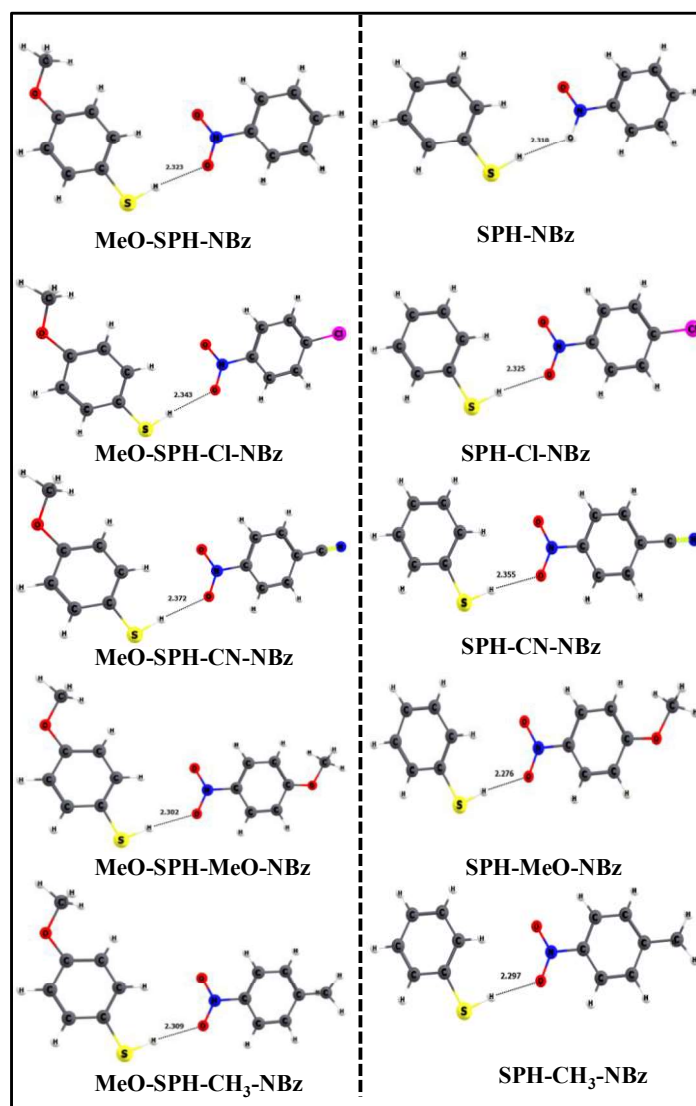


**Figure 5.11** Optimized structure of left panel: MeO-SPH, right panel: SPH with different substituents at para position of NBz dimers at B3LYP/6-31G\* level of theory.

In many crystal lattices of organic compounds, the H-bonds and  $\pi$ - $\pi$  stacking are decisive factors that govern packing.<sup>1,31,32</sup> To determine the piezoelectric coefficient of SCHBs crystal we have extended our calculations to tetramers of SPH-NBz dimer. These tetramer unit consists of a hydrogen bond and  $\pi$ -stacking and represents a system similar to a crystal unit.<sup>5</sup> We considered two kinds of tetramers of SPH-NBz viz. symmetric and anti-symmetric. In symmetric unit, SPH

and NBz were stacked with SPH and NBz, respectively as shown in Figure 5.13 (a). In anti-symmetric unit, SPH units were stacked with NBz units as shown in Figure 5.13(b).

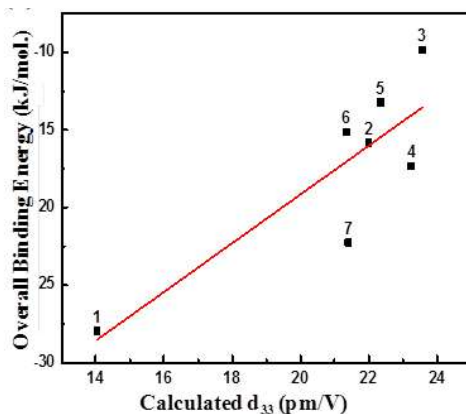


**Figure 5.12** Plot showing dependence of calculated piezo-coefficients,  $d_{33}$  (pm/V) on binding energy (kJ/mol) for (1) PH-NBz, (2) SPH-NBz, (3) SePH-NBz, (4) SPH-OMe-NBz, (5) SPH-CN-NBz, (6) OMe-SPH-NBz and (7) CN-SPH-NBz.

To get the optimized tetramer structures, stacking distance was varied in steps of  $0.05\text{\AA}$ . Single point energies for different distances were calculated at B97D/6-31G\* level of theory by taking dispersion interaction into account for the stacking structures. The equilibrium stacking distance between the two dimer units were found out by a polynomial fit of the plot of energy versus distance. Then, the equilibrium stacking distance between the dimers was fixed and optimization of H-bond distances of SPH-NBz tetramers were done in the similar way as done for dimers, mentioned in method-B. The estimated piezo-coefficients for the symmetric and anti-symmetric SPH-NBz tetramer units were found to be  $20.90\text{ pm/V}$  and  $22.20\text{ pm/V}$  respectively.

## Applications of SCHB and SeCHBs

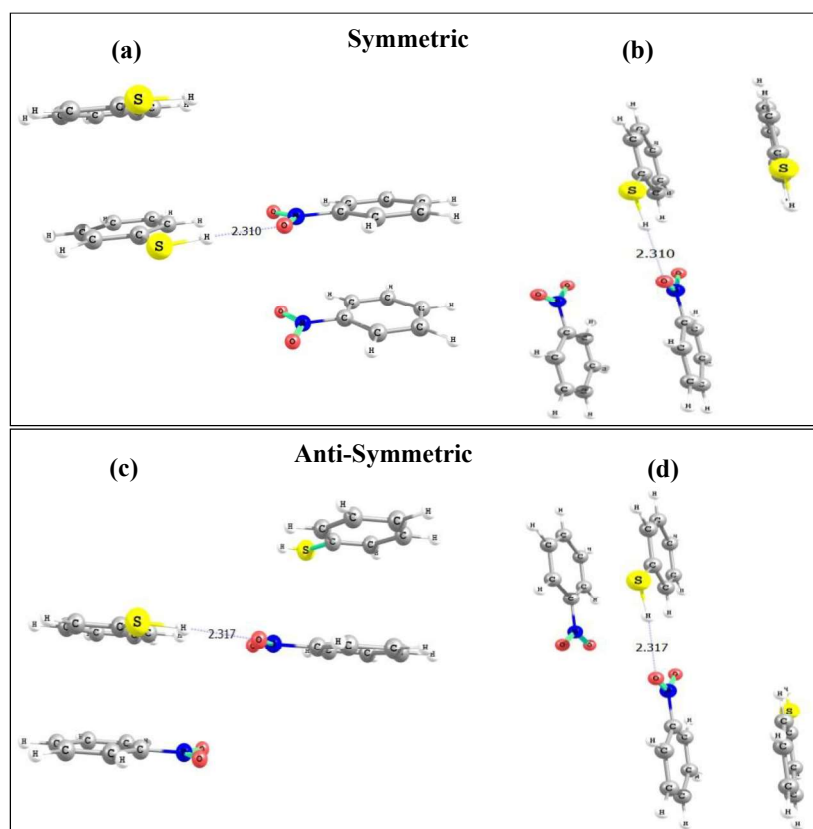


**Figure 5.13** Optimized structures of SPH-NBz tetramers (a) symmetric unit and (b) anti-symmetric unit.

These values are very close to that of the SPH-NBz dimer. It appears that the orientation of dimer units (symmetric and anti-symmetric) does not affect piezo-coefficients. As the present computational method has been validated by the experimental data it is also anticipated that experimental value of piezo-coefficient of SPH-NBz crystal will also be of the same order.

### 5.5 Conclusions

- Piezoelectric coefficients of different H-bonded systems were calculated using the different methods. In estimated method, calculations were performed in the absence of electric field while in calculated methods; piezo-response was calculated at different applied electric field. The estimated method is used for immediate calculation of piezo-response of H-bonded systems.
- We studied the effect of level of theory on piezoelectric coefficients of H-bonded systems and it was confirmed that piezoelectric coefficients values vary with basis sets and with different functionals used but the trend remains same for different levels of theory.
- The H-bond systems such as PH-NBz, SPH-NBz and SePH-NBz dimers, SPH-NBz have the most consistent piezo-coefficient spanning at different levels of theory. This aromatic system is substituted with different EDG groups like CH<sub>3</sub>, OMe and EWG groups like Cl, CN to explore the effect of various substituents on the piezo-coefficient. These infer that there is no significant effect on piezo-response with substitution on H-bond systems.
- We also calculated the piezo-response of tetramer unit of SPH-NBz. Piezoelectric coefficient of tetramer unit of SPH-NBz was also consistent and is equal to SPH-NBz dimer. This is higher  $d_{33}$  piezo-response than 2-methyl-4-nitroaniline (14 pm/V) the organic crystal<sup>5</sup> with the largest known piezoelectric response.
- In this work, correlation between piezo-coefficient with other properties of the system like NBO interaction energy, binding energy and isotropic polarizability were also explored. Isotropic polarizability showed linear correlation with the piezo-coefficient of the investigated systems. NBO interaction energy and binding energy showed no correlation with the piezo-coefficient. Not only the force constant and dipole moment but also the molecular

## **Applications of SCHB and SeCHBs**

---

polarizability of the H-bonded systems plays a crucial role for higher piezo-response. The results are encouraging and many more H-bonded systems could be found with high piezo-response than previously reported ones due to the ubiquity of hydrogen bond in chemistry, materials and biological systems.

### References:

- (1) Desiraju, G. R. *Molecular Crystals and Liquid Crystals Science and Technology. Section A. Mol. Cryst. Liq. Cryst.* **1992**, *211*, 63.
- (2) Aakeroy, C. B.; Seddon, K. R. *Chem. Soc. Rev.* **1993**, *22*, 397.
- (3) Desiraju, G. R. *Cryst. Growth Des.* **2011**, *11*, 896.
- (4) Glowacki, E. D.; Irimia-Vladu, M.; Bauer, S.; Sariciftci, N. S. *J. Mater. Chem. B* **2013**, *1*, 3742.
- (5) Werling, K. A.; Hutchison, G. R.; Lambrecht, D. S. *J. Phys. Chem. Lett.* **2013**, *4*, 1365.
- (6) Werling, K. A.; Griffin, M.; Hutchison, G. R.; Lambrecht, D. S. *J. Phys. Chem. A* **2014**, *118*, 7404.
- (7) Bystrov, V.; Paramonova, E.; Bdikin, I.; Bystrova, A.; Pullar, R.; Kholkin, A. *J. Mol. Model.* **2013**, *19*, 3591.
- (8) Dineva P., G. D., Müller R., Rangelov T. *Springer, Cham* **2014**, 212.
- (9) Binnig, G.; Smith, D. P. E. *Review of Scientific Instruments* **1986**, *57*, 1688.
- (10) Binnig, G.; Quate, C. F.; Gerber, C. *Phys. Rev. Lett.* **1986**, *56*, 930.
- (11) Synge, E. H. *The London, Edinburgh, and Dublin Philosophical Magazine and Journal of Science* **1932**, *13*, 297.
- (12) Janocha, H. **2007**, 221.
- (13) Walter Heywang, K. L., Wolfram Wersing *Springer* **2008**, 4.
- (14) Yu, B.; Fu, Y.; Wang, P.; Zhao, Y.; Xing, L.; Xue, X. *Phys. Chem. Chem. Phys.* **2015**, *17*, 10856.
- (15) Kim, G. H.; Hong, S. M.; Seo, Y. *Phys. Chem. Chem. Phys.* **2009**, *11*, 10506.

## Applications of SCHB and SeCHBs

---

- (16) Cary Baur, D. J. A., Deepam Maurya, Shashank Priya, Walter Voit *ACS Sym. Ser.* **2014**, *In Polymer Composites for Energy Harvesting, Conversion, and Storage.*
- (17) Biswal, H. S.; Shirhatti, P. R.; Wategaonkar, S. *J. Phys. Chem. A* **2009**, *113*, 5633.
- (18) Biswal, H. S.; Wategaonkar, S. *J. Phys. Chem. A* **2009**, *113*, 12774.
- (19) Biswal, H. S.; Wategaonkar, S. *J. Phys. Chem. A* **2009**, *113*, 12763.
- (20) Biswal, H. S.; Wategaonkar, S. *J. Chem. Phys.* **2011**, *135*, 134306.
- (21) Biswal, H. S.; Gloaguen, E.; Loquais, Y.; Tardivel, B.; Mons, M. *J. Phys. Chem. Lett.* **2012**, *3*, 755.
- (22) Biswal, H. S.; Bhattacharyya, S.; Wategaonkar, S. *ChemPhysChem* **2013**, *14*, 4165.
- (23) Biswal, H. S. In *Noncovalent Forces*; Scheiner, S., Ed.; Springer International Publishing: 2015, p 15.
- (24) Biswal, H. S.; Bhattacharyya, S.; Bhattacharjee, A.; Wategaonkar, S. *Int. Rev. Phys. Chem.* **2015**, *34*, 99.
- (25) M.J. Frisch, G. W. T., H.B. Schlegel, G.E. Scuseria, M.A.Robb, J.R.Cheeseman, G.Scalmani, V.Barone, B.Mennucci, G.A.Petersson et al *Gaussian Inc.: Wallingford, CT, 2009* **2009**.
- (26) Kadam, S. A.; Haav, K.; Toom, L.; Haljasorg, T.; Leito, I. *J. Org. Chem.* **2014**, *79*, 2501.
- (27) Paturle, A.; Graafsma, H.; Sheu, H. S.; Coppens, P.; Becker, P. *Phys. Rev. B* **1991**, *43*, 14683.
- (28) Kawahara, S.-i.; Uchimaru, T.; Taira, K.; Sekine, M. *J. Phys. Chem. A* **2001**, *105*, 3894.
- (29) Kawahara, S.-i.; Uchimaru, T. *J. Mol. Struct.: THEOCHEM* **2002**, *588*, 29.
- (30) Nagaraju, M.; Narahari Sastry, G. *J Mol Model* **2011**, *17*, 1801



## Chapter 6

### Carbon Bonding (C-Bonding) in Proteins and Small Organic Molecules

#### 6. Introduction

Last two decades have witnessed a revolution in the field of non-covalent interactions with the emergence of new interactions. These interactions have resulted in a better understanding of many biophysical phenomena such as protein folding and functions.<sup>1,2</sup> Among all the non-covalent interactions, hydrogen bond is being considered as prominent one followed by contributions from other non-covalent interactions such as halogen bonds,<sup>3-6</sup> pnicoen bonds,<sup>7,8</sup> chalcogen bonds,<sup>9-11</sup> aerogen bonds,<sup>12-14</sup> tetrel bonds,<sup>15-19</sup> etc. In this chapter, we have focused on a new type of non-covalent interaction, i.e. ‘carbon bond’(C-bond) which is a subclass of tetrel bonds. The carbon atom is abundant in nature and in synthetic chemistry. Hence, it is expected that carbon bond may play a significant role in protein folding, ligand-protein interactions, and in some other processes of biological importance.

This chapter is divided into two sections. The first section describes the experimental and computational studies for the existence and strength of C-bond in proteins. The second section deals with the computational studies on C-bond formation and strength of C-bonds with N-oxides and N-sulfides as C-bond acceptors.

#### 6.1 Carbon bonding in proteins: NMR, IR Spectroscopy and Quantum Chemical Calculations

##### 6.1.1 Motivation

The carbon bond denoted as X-C...Y for the first by E.Arunan and D Mani in the intermolecular complexes. They studied the C-bond complexes of the electron deficient C atom of substituted methane (CH<sub>3</sub>F, CH<sub>3</sub>OH) and electron rich centers of other molecules (H<sub>2</sub>O, HF,

## Carbon Bonding

---

LiF etc.).<sup>20</sup> They estimated the carbon bond energies at CCSD-T level that varies from  $\sim -2$  to  $-17$  kJ/mol. They suggested that X-C $\cdots$ Y C-bonds have very similar characteristics as observed in X-H $\cdots$ Y hydrogen bond. These could play significant role in numerous chemical and biological processes.<sup>20,21</sup> In a very short time period of discovery of the C-bond, ample of researches have been done to establish the existence and nature of C-bond in crystals and biomolecules. T. N. Guru Row and coauthors provided the experimental evidences of C-bonds through the X-ray charge density analysis. They analyzed CSD crystal structure data base and found 716, 189, 143, 110 and 157 C $\cdots$ O, C $\cdots$ N, C $\cdots$ F, C $\cdots$ S and C $\cdots$ Cl carbon bonded interactions, respectively in the crystal structures of natural products and hormones.<sup>22</sup> These interactions were further confirmed with charge density model i. e. the presence of the (3,-1) bond critical points (bcp). Escudero-Adan E.C. et al. studied the nature of C-bonding in 1,1,2,2-tetracyano cyclopropane crystal structure by X-ray diffraction analysis.<sup>23</sup> They found that C-bond is highly directional and electrostatic in nature. The solid state NMR experimental studies were done by Southern S. A. et al. for existence of C-bond formation between methyl carbon and N or O of other functional groups.<sup>16</sup> They have observed the presence of C-bonds in two sarcosine salts, which have influence on NMR parameters such as coupling constant and chemical shifts. It has been found that the value of chemical shifts increases with decrease of C-bond distance in the solid state. A. Frontera et al. extended the C-bond investigations from small molecules to ligand-protein complexes using combine the high-level *ab initio* calculations and a Protein Data Bank (PDB) analysis.<sup>17,24</sup> They have reported that the formation of C-bond XY<sub>3</sub>C $\cdots$ O (X, Y = H, F) interaction prominent when the methyl protons are located at equidistance to C-bond acceptor atom (electron rich atom or group). In this case the formation of H-bond in the trifurcated binding mode gets poor in protein-ligand binding complexes. In these reports, they suggest that

## Carbon Bonding

---

the calculated interaction energies for C-bond formation vary from  $\sim -1.5$  to  $-80$  kJ/mol from uncharged to charged electron rich atom. Recently, Bani Kanta Sharma et al. demonstrated reciprocal  $C=O \cdots C=O$  interactions i.e. back and forth  $n \rightarrow \pi^*$  and  $\pi \rightarrow \pi^*$  interactions in small organic molecules and PPII helices using crystallographic database analysis and theoretical calculations.<sup>25</sup>

The presence of  $C=O$  groups and aliphatic side chains are ubiquitous in proteins hence, it is expected that the  $C^{sp^3} \cdots O=C$  C-bonds could be present in large numbers that would lead to better understanding of the hydrophobic interactions in proteins. This encouraged us to investigate the  $Z-R_3C \cdots O=C$  C-bonds ( $Z = O, N, C, S, \text{ etc}$ ) through  $n \rightarrow \sigma^*$  electron delocalization in proteins. The objective of this chapter is to explore the occurrence of  $C^{sp^3} \cdots O=C$  C-bonds in proteins and estimate their enthalpic contributions to the stability of protein structures. In addition to this we want to investigate and quantify the role of C-bonds in protein structure and function. First, we carried out structural analysis of protein data bank (PDB) to attest that significant numbers of C-bonds are present in proteins. By using NMR, IR spectroscopic methods on model molecular complexes, we determined C-bond energy very precisely. We then combined quantum chemical calculations and spectroscopic data to formulate an empirical equation that can be adopted to estimate the C-bond energy just by knowing the  $C \cdots O$  distance. Finally we delved into the adoption of the concept of C-bonds in explaining the bio-molecular structures and functions.

### 6.1.2 Protein data base analysis for existence of C-bond in proteins

First we carried out the PDB analysis to check the occurrence of C-bonds in proteins. This PDB analysis was carried out by retrieving the protein structure coordinates from the RCSB website<sup>26</sup> which satisfy the following criteria: structure resolved by X-ray crystallography at less

## Carbon Bonding

---

than 2.0 Å resolution and less than 30% sequence identity among the proteins. With these criteria, we obtained total of 12743 protein structures on 2<sup>nd</sup> July 2018. For simplification, only a single chain i.e. chain A was considered for the identification of Z-C...O=C interactions in all the protein structures. Beforehand, the other chains (B, C, D, etc.) were eliminated by running a shell script generated using sed commands in Linux. Hence, an in-house program written in python 2.7 was used to identify the C-bond interactions between C atom of Z-CR<sub>3</sub> (Z = N, C, O) and O of backbone/side chain carbonyl group in proteins. The python program was written by considering the carbon atom bonded to Z = N, C, O atoms acts as C-bond donor and the carbonyl group acting as C-bond acceptor in Z-R<sub>3</sub>C...O=C interaction. The following criteria were considered to identify the C-bond interaction in our in-house python program:

- i. The minimum and the maximum distances for C=O bond were kept at 1.18 and 1.35 Å respectively. In proteins, the carbonyl groups are either present in the peptide bonds or in the carboxylic acid groups. The distances of C=O bond for the amides is around 1.24 Å. For the carboxylic acids<sup>3</sup>, the conventional distance for C=O is around 1.21 Å but the distance has been lifted to 1.35 Å due to the indistinguishable character of the resonance structures of the carboxylic acids. However, the lower limit is kept 0.03 Å lower than 1.21 Å for the purpose of covering the entire range.
- ii. The minimum and the maximum distances between the O of carbonyl group and the C of C-Z (Z=N, O, and C) bond were kept at 2.5 and 3.6 Å respectively.
- iii. The minimum and the maximum distances of C-Z (Z=N, O and C) bond were kept at 1.41 Å and 1.56 Å respectively. Among C-N, C-O and C-C, conventionally, the highest length is that of the C-C bond followed by C-N bond and C-O bonds respectively. The highest C-C bond length is 1.54 Å. The C-N bond length is around 1.47 Å. The C-O bond length revolves around 1.43 Å. Thus, the upper limit is kept 0.02 Å higher than 1.54 Å and the lower limit is kept at 0.02 Å lower than 1.43 Å to cover the entire range.

## Carbon Bonding

- iv. The bond angles  $\angle Z-C\cdots O$  and  $\angle C\cdots O=C$  were always kept in the range of  $160^\circ$ - $180^\circ$ . Most of the  $C-H\cdots O$  interactions subsume bond angles  $\angle Z-C\cdots O$  and  $\angle C\cdots O=C$  below  $160^\circ$ , thus restricting the value of the bond angle above  $160^\circ$  helps in getting rid of unwanted  $C-H\cdots O$  interactions.

We found about 8358 interactions satisfying these structural criteria and forming C-bonds within the C-bond distance  $\leq 3.6$  Å. Figure 6.1.1 (a) shows the histogram of  $Z-R_3C\cdots O=C$  C-bond distance distribution using 0.1 Å bar width and Figure 6.1.1 (b) & (c) represent the histogram of  $\angle Z-C\cdots O$  and  $\angle C\cdots O=C$  angle distributions with  $2^\circ$  bar width, respectively.

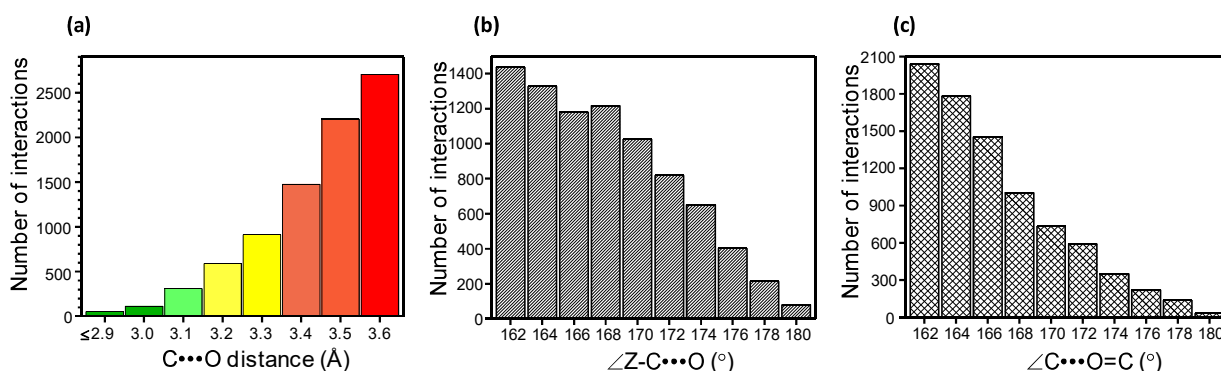


**Figure 6.1.1** Frequencies of  $C\cdots O$  carbon bond donor-acceptor (a) distances ( $d_{C\cdots O}$ ), (b)  $\angle Z-C\cdots O$ , (c)  $\angle C\cdots O=C$  C-bond angles in proteins. Values of the  $C\cdots O$  distances are from protein crystal structures. The histogram represents the distribution of C-bond length within the  $\pm 0.4$  Å of the sum of the van der Waal's radii of O and C ( $r_O = 1.5$  Å,  $r_C = 1.7$  Å)

Several examples of  $Z-R_3C\cdots O=C$  C-bond formation are shown in Figure 6.1.2. The C-bond formation was confirmed in proteins with natural bond orbital (NBO), atoms in molecule (AIM) and non-covalent interaction (NCI) analyses. Herein, to verify the formation of C-bond between donor and acceptor, we have taken the interacting residues and optimized the hydrogen positions only, with other nuclei being fixed at B97D/aug-cc-pVDZ level of theory. The bond

## Carbon Bonding

critical point, electron density surface map and interpenetration of donor acceptor orbitals confirmed the existence of C-bond in proteins, as shown in Figure 6.1.3. Furthermore, we have also analyzed deeply the contribution of the amino acid residues and amino acid donor-acceptor pairing in the formation of C-bond. This analysis results that almost all the amino acids can contribute to the formation of C-bond in proteins. Figure 6.1.4 shows the histogram of the propensity of different amino acids participating in C-bonds. We found that among all the amino acids ALA, LEU, ASP and GLU are contributing 40% of total interactions as potential C-bond acceptors. Among various amino acids, it is observed that LYS involved in the largest number of C-bond interactions in various proteins followed by SER, ASN, ARG as C-bond donors in  $Z\text{-R}_3\text{C}\cdots\text{O}=\text{C}$  C-bond.

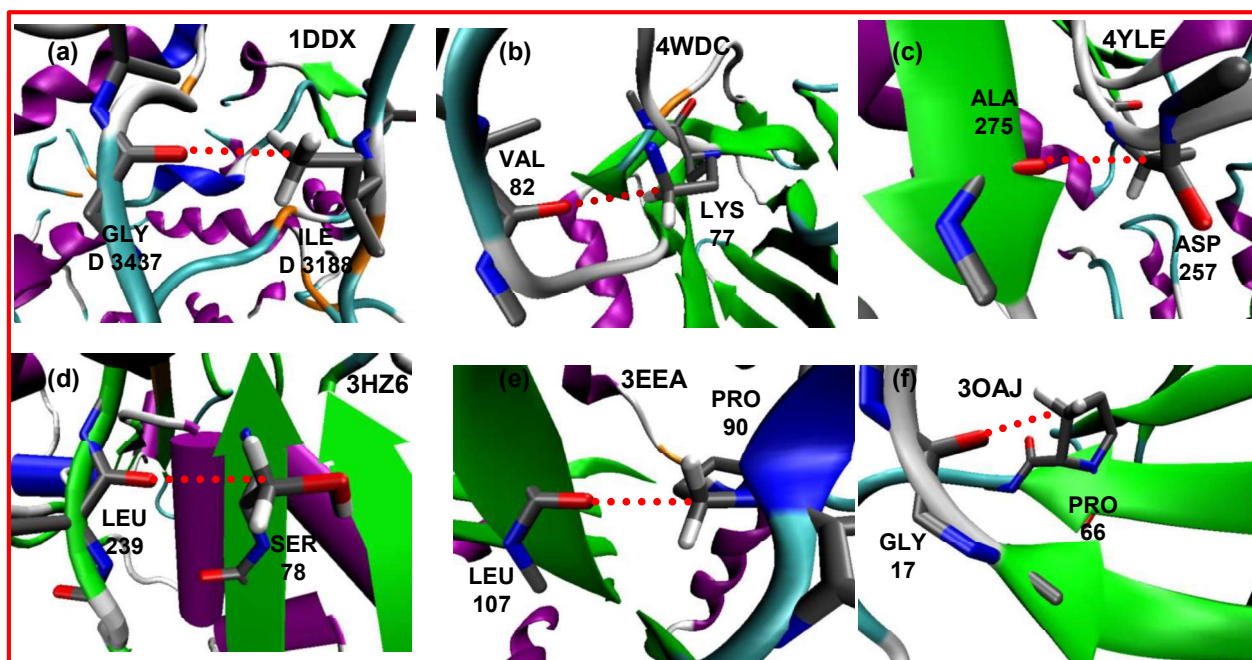
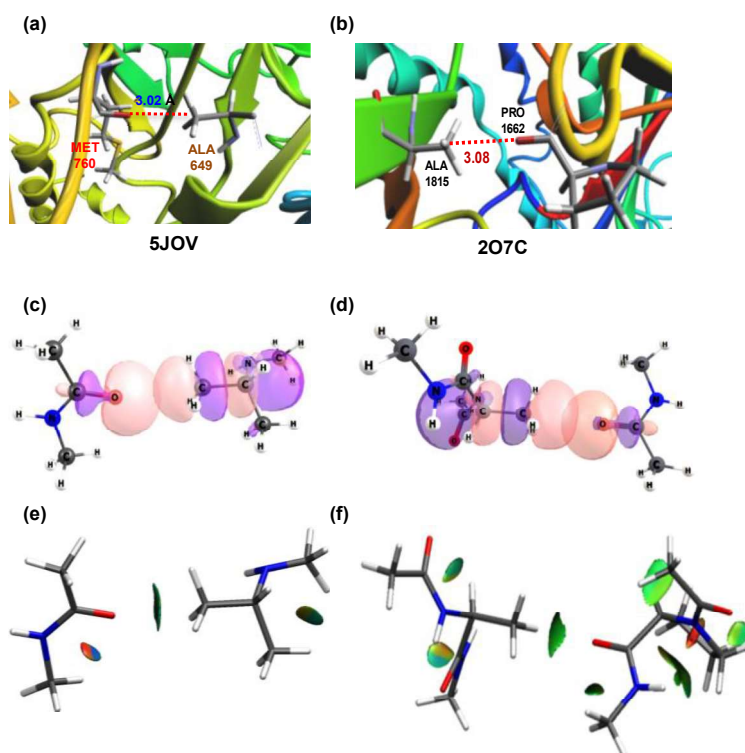


**Figure 6.1.2** (a)  $\text{C}-\text{C}\cdots\text{O}=\text{C}$  C-bond formed by  $\text{C}=\text{O}$  of  $\text{GLY}^{3437}$  with  $\text{CH}_3$  primary carbon of  $\text{ILE}^{3188}$  (PDB: 1DDX). (b)  $\text{C}-\text{C}\cdots\text{O}=\text{C}$  C-bond formed by  $\text{C}=\text{O}$  of  $\text{VAL}^{82}$  with secondary carbon of  $\text{LYS}^{77}$  (PDB: 4WDC). (c)  $\text{C}-\text{C}\cdots\text{O}=\text{C}$  C-bond formed by  $\text{C}=\text{O}$  of  $\text{ALA}^{275}$  with tertiary carbon atom of  $\text{ASP}^{257}$  (PDB: 4YLE). (d)  $\text{O}-\text{C}\cdots\text{O}=\text{C}$  type C-bond formed by  $\text{C}=\text{O}$  of  $\text{LEU}^{239}$  with  $\text{C}-\text{O}$  of

## Carbon Bonding

*SER*<sup>78</sup> in (PDB: 3HZ6) (e) *N-C...O=C* type C-bond formed by *C=O* of *LEU*<sup>107</sup> with *C-N* of *PRO*<sup>90</sup> (PDB:3EEA) (f) *C-C...O=C* type C-bond formed by *C=O* of *GLY*<sup>17</sup> with *C-C* of *PRO*<sup>66</sup> (PDB: 3OAJ).

The representation of C-bond formation between LYS as C-bond donor with VAL as C-bond acceptor and ALA as acceptor with ASP as C-bond donor in 4WDC and 4YLE proteins, respectively, as shown in Figure 6.1.2 (b) and 6.1.2 (c). LYS has long side chain with methyl and amine groups hence it can form C-bond as different C-C and N-C as C-bond donors. The donor-acceptor analysis was done with highest contributing residue LYS as C-bond donor pairing with different amino acids as C-bond acceptors. In another case, donor-acceptor pairing was done with ALA as C-bond acceptor and pairing with different amino acids as C-bond donors. These analyses suggest that LYS-ALA, LYS-ASP and ASN-ALA pairs are prominent one the distribution plot shown in Figure 6.1.5.



## Carbon Bonding

**Figure 6.1.3** Represents the C-bond formation in (a) protein 5JOV, C-C...O=C C-bond formed by C=O of MET<sup>767</sup> with CH<sub>3</sub> primary carbon of ALA<sup>649</sup>, (b) protein 2O7C, C-C...O=C C-bond formed by C=O of PRO<sup>1662</sup> with CH<sub>3</sub> primary carbon of ALA<sup>1815</sup>, (c) & (d) donor-acceptor orbital overlapping between lone pair orbital of O and antibonding orbital of C-C sigma bond in 5JOV and 2O7C, respectively. (e) & (f) 3D-NCI plot, colored isosurfaces of the reduced electron density gradient in 5JOV and 2O7C respectively.

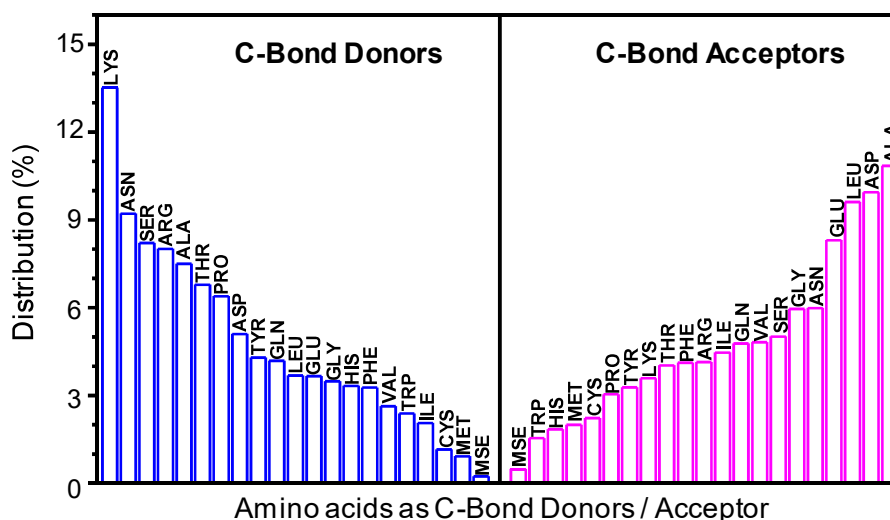
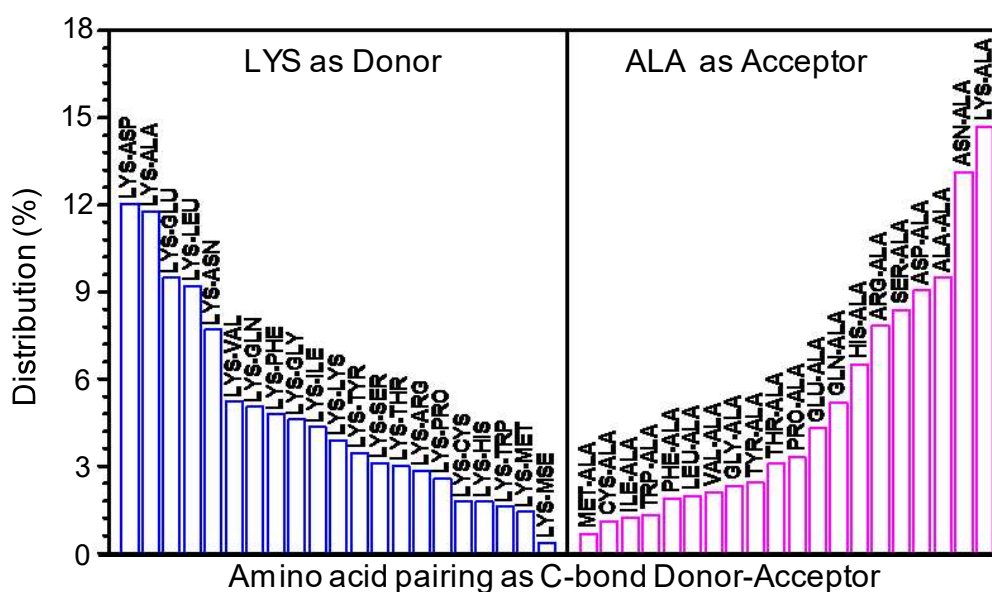


**Figure 6.1.4** Plot showing the percentage distribution of amino acids involved in C-bonds as donor and acceptor residues.



## Carbon Bonding

**Figure 6.1.5 Left Panel:** Histograms representing the percentage distribution of amino acids involved in C-bonds where LYS as C-bond donor pairs with other amino acids. **Right Panel:** Histograms representing the percentage distribution of amino acids involved in C-bonds where ALA as C-bond acceptor pairs with other amino acids.

We also carried out analysis to identify the type of atom participating in C-bond formation as a donor and acceptor. The number of interactions for each type of atom involved in C-bond formation in proteins is shown in Table 6.1.1. Figure 6.1.6 displays different type of C-bond acceptors and donors involved in C-bond formation in proteins. Backbone or side chain carbonyls act as C-bond acceptors in most of the cases whereas in 80.4 % cases C-C bonds are involved as C-bond donor followed by C-N and C-O bonds. Several examples of  $Z-R_3C \cdots O=C$  (R = H & C; Z = C, N, & O) interactions are shown in Figure 6.1.2.

**Table 6.1.1:** Contribution of different type of O-atom as acceptor, type of Z-C bond as donor and different type of secondary structures of C-bond acceptor, donor residues in C-Bond

C-Bond donor		C-Bond Acceptor	
Type	No. of Interaction	Type	No. of Interaction
C-C	6795	Back bone C=O	7086
N-C	1235	Side chain C=O	1261
O-C	328	Side chain C-O	11
Secondary Structures			
Coil	2652	Coil	1287
Turn	1977	Turn	1420
$\alpha$ -Helix	1615	$\alpha$ -Helix	3650
$\beta$ -Strand	1392	$\beta$ -Strand	1361
$3_{10}$ -Helix	433	$3_{10}$ -Helix	328
Bridge	89	Bridge	112

## Carbon Bonding

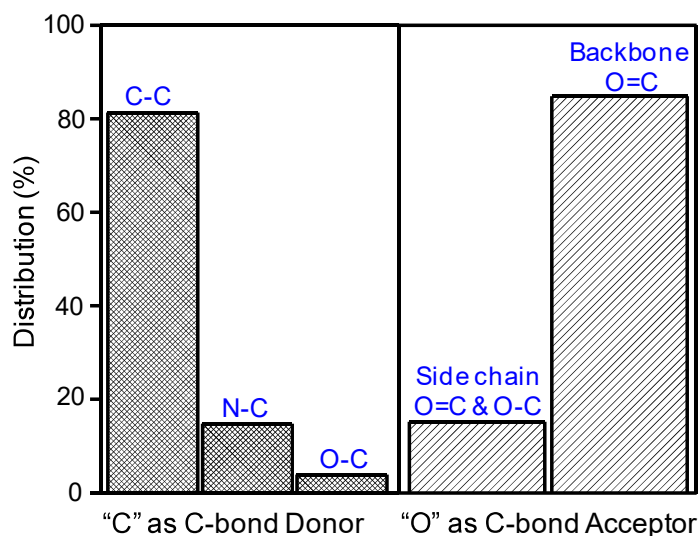


**Figure 6.1.6** Percentage distribution plot for different type of C-bond donors and acceptors in proteins.

To explore the possible location of C-bonds in proteins, we made a secondary structure analysis in detail. The secondary structure information about the C-bond donor and the acceptor residues were obtained using STRIDE<sup>27</sup> software. The obtained data was subsequently assigned by in-house developed python code for particular C-bond donor and acceptor in each protein. Figure 6.1.7 represents the distribution of secondary structures assigned to C-bond donor, C-bond acceptors and combination of both. The C-bond donor and acceptor are located in each secondary structure given in Table 6.1.1. From this analysis, we found C-bond donors are evenly distributed in coils, turns,  $\alpha$ -helix and  $\beta$ -strand, whereas  $\sim 50\%$  of C-bond acceptors are located in  $\alpha$ -helix. The analysis also indicates that the C-bonds are mostly observed in  $\alpha$ -helix, coils, turns, summing up to  $\sim 70\%$  of C-bonds found in proteins. To verify the obtained C-bond interaction are allowed or forbidden ranges we plotted Ramachandran plot from the Ramachandran angles ( $\phi$ ,  $\psi$ , and  $\omega$ ) of the C-bond donor and acceptor residues involved in C-bonds. These Ramachandran angles are measured with the help of a python code that uses the coordinates of

## Carbon Bonding

the donor and acceptor residues. The Ramachandran plots for donor and acceptor amino acid residues are shown in Figure 6.1.8. Both the C-bond donor and acceptor amino acid residues are in the allowed range of different secondary structures range.

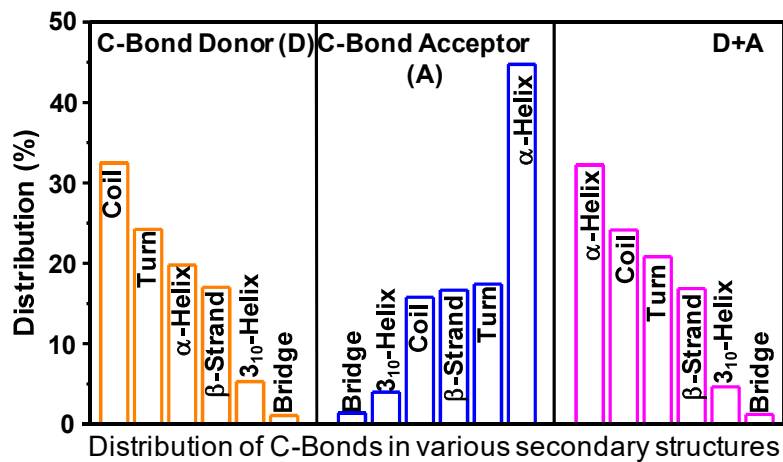


**Figure 6.1.7** Histogram plot showing percentage location of C-bond acceptor and donor residues in various secondary structures of the proteins.

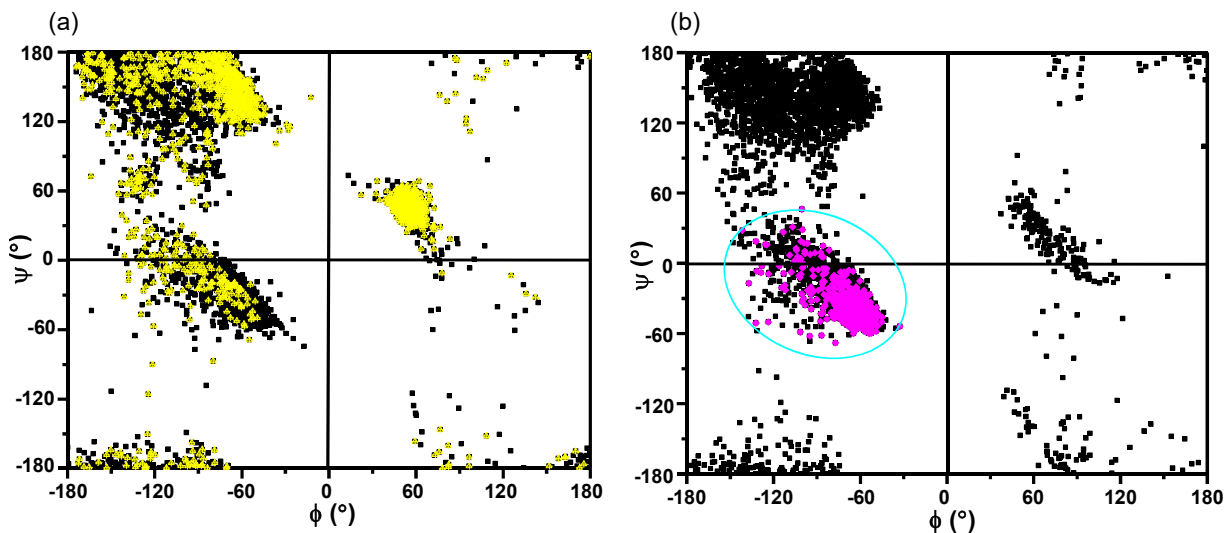


**Figure 6.1.8** Ramachandran plots for (a) C-bond donor amino acid residues (b) C-bond acceptor residue. Each dot on the plot shows the angles for an amino acid. Yellow color dots

## Carbon Bonding

represents in Figure (a) is amino acids in coils. Pink color dots in Figure (b) represents the amino acids in  $\alpha$ -helixes.

We carried out the natural bond orbital (NBO) analysis to determine the donor-acceptor interaction energies and to find out whether the C-bonds are the consequences of  $n \rightarrow \sigma^*$  electron delocalization or not. In this case we have taken 22 amino acid pairs covering complete distance ( $2.75 \text{ \AA} \leq d_{C \cdots O} \leq 3.6 \text{ \AA}$ ) and bond angle range ( $160^\circ \leq \theta_i \leq 180^\circ$ ). Here we have chosen only interacting amino acid donor and acceptor residues and then used dispersion corrected functional B97-D with aug-cc-pVDZ basis set to optimize the H-atom positions around the donor-acceptor by freezing all other atomic positions as in the PDB structure. The donor-acceptor interaction energy ( $E_{DA}$ ) or the  $n \rightarrow \sigma^*$  electron delocalization energy are calculated using second order perturbation theory at MP2/aug-cc-pVDZ level of theory. Table 6.1.2 displays the  $E_{DA}$  values of amino acid pairs in 22 proteins. The substantial donor-acceptor orbital overlap between antibonding orbital of Z-C bond ( $\sigma^*_{Z-C}$ ) and lone pair orbital ( $n$ ) of oxygen of C=O group is shown in Figure 6.1.3.

**Table 6.1.2** The values of carbon bond distance ( $d$ ), the donor-acceptor interaction energies ( $E_{DA}$ ), in kJ/mol at MP2/aug-cc-PVDZ level of theory in proteins.

S.No	PDB/Model compounds	Donor	Acceptor	Distance	$E_{DA}$
				( $\text{\AA}$ )	(kJ/mol)
1	NNDMA-ALA	ALA	NNDMA	3.310	0.711
2	NNDMA-AA	AA	NNDMA	3.130	1.757
3	NNDMA-TFACE	TFACE	NNDMA	3.080	2.259
4	NNDMA-AcetylCl	AcetylCl	NNDMA	3.040	2.678
5	NNDMA-ACN	ACN	NNDMA	3.060	2.929
6	NNDMA-NM	NM	NNDMA	2.940	5.816
7	3EEA	PRO-90	LEU-107	2.790	8.786
8	5NG1	PRO-239	PHE-279	2.833	7.615
9	3DNX	PRO-113	GLU-95	2.870	6.527
10	3A57	ARG-21	GLN-55	2.910	4.226

## Carbon Bonding

11	5A6M	PRO-137	PRO-169	2.958	4.644
12	3DXY	ILE-93	HIS-120	2.960	3.264
13	4JJJ	PRO-102	GLY-126	2.966	4.477
14	4PGM	VAL-51	ASN-79	2.970	3.305
15	3NDS	THR-56	THR-22	2.973	3.180
16	2DHO	PHE-54	ASP-150	2.977	2.678
17	3OAJ	PRO-66	GLY-17	3.020	2.301
18	5JOV	ALA-649	MET-760	3.020	2.678
19	3LGI	PRO-237	ASN-188	3.030	1.841
20	5KAR	PRO-305	ASN-318	3.045	2.092
21	3HZ6	SER-78	LEU-239	3.050	2.552
22	5EL9	ILE-197	GLU-93	3.056	2.678
23	5A0Y	GLY-453	GLN-449	3.063	1.297
24	2O7C	ALA-1815	PRO-1662	3.080	2.845
25	4WDC	LYS-77	VAL-82	3.100	1.046
26	3ZK4	ARG-458	LEU-438	3.130	0.711
27	1RY9	ALA-70	LEU-66	3.150	0.418
28	4IVN	ALA-33	ILE-29	3.150	1.757
29	1DDX	ILE -3188	GLY-3437	3.160	1.464
30	2FAO	ALA-577	HIS-573	3.190	0.460
31	4YLE	ASP-257	ALA-275	3.200	0.293
32	3JQ1	CYS-344	TRP-339	3.210	0.711
33	5JUF	PHE-112	TYR-108	3.210	0.544
34	2QRU	GLN-94	ILE-91	3.250	0.586
35	1M6S	ALA-23	ALA-19	3.360	0.586

The NBO, AIM and NCI analyses confirmed the existence of C-bond in proteins. The  $n \rightarrow \sigma^*$  interaction energies are very similar to those of two  $n \rightarrow \pi^*$  interaction energies observed through reciprocal  $C=O \cdots C=O$  interaction in proteins.

### 6.1.3 Experimental evidences and strength of C-bond in model compounds and proteins

The determination of accurate strength of  $Z-C \cdots O=C$  C-bond in proteins is impossible due to the presence of weak H-bonds. Hence, we have chosen model compounds to determine the strength of C-bonds in proteins. N,N-dimethylacetamide (NNDMA) as the C-bond acceptor mimicking the amide- $C=O$  group in proteins and acetonitrile (ACN), nitromethane (NM), alanine (ALA), acetic acid (AA), acetylchloride (AcetylCl), and trifluoroacetic acid (TFACE) are

## Carbon Bonding

several C-bond donors bearing different functional groups. Figure 6.1.9 shows the model compounds of C-bond acceptor and different C-bond donors.

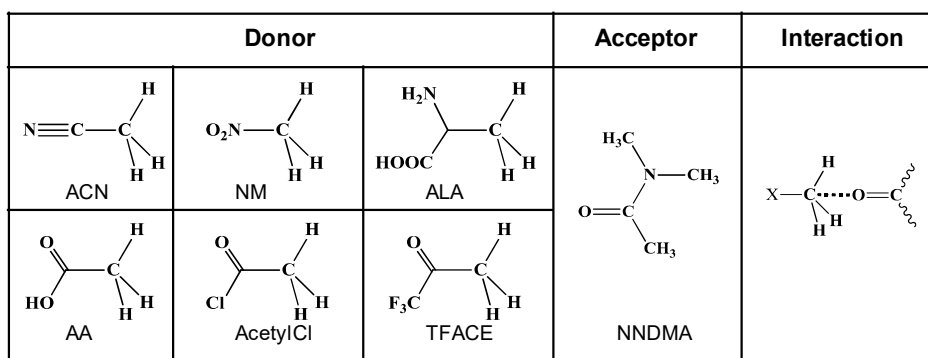


**Figure 6.1.9** Representative model compounds of proteins Left: Six different types of C-bond donors, Middle: amide-C=O type of C-bond acceptor, Right: type of C-bond formation.

Initially, we have carried out the quantum chemical calculations to ensure the formation C-bond in the model C-bond complexes. The geometry optimizations and numerical frequency calculations of all monomers and complexes of model compounds were performed using dispersion corrected functional B97-D3 with aug-cc-pVDZ basis set. The binding energies of carbon bond (C-bond) complexes of model compounds were calculated with gold standard Coupled Cluster Singles Doubles and Triples (CCSD-T) at aug-cc-pVDZ basis set, values are provided in Table 6.1.3. We have also performed the AIM and NBO analysis to confirm the formation C-bond between donors and acceptors in model complexes at MP2/aug-cc-PVDZ level of theory. Figure 6.1.10 shows the bond critical point (BCP) along the Z-C $\cdots$ O=C C-bond. The BCP between C and O in six model complexes confirms the non-covalent bond. The electron density and Laplacian values at BCP are displayed in Table 6.1.3 for six model C-bond complexes.

## Carbon Bonding

**Table 6.1.3** The values of carbon bond distance ( $d$ ), the donor-acceptor interaction energies ( $E_{DA}$ ), and Electron density,  $\rho(r)$ , and Laplacian of electron density,  $\nabla^2\rho(r)$  at MP2/aug-cc-pVDZ level of theory and computed binding energies ( $\Delta E$ ) at CCSD-T/aug-cc-pVDZ level.

S.No	C-bond Complexes	Distance (Å)	$E_{DA}$ (kJ/mol)	$\rho(r)$ (a.u.)	$\nabla^2\rho(r)$ (a.u.)	$\Delta E$ (CCSD-T) (kJ/mol)
1	NNDMA-ALA	3.31	0.711	0.0037	0.0170	-8.41
2	NNDMA-AA	3.13	1.757	0.0056	0.0260	-13.32
3	NNDMA-TFACE	3.08	2.259	0.0060	0.0282	-17.76
4	NNDMA-AcetylCl	3.04	2.678	0.0067	0.0302	-18.18
5	NNDMA-ACN	3.06	2.929	0.0061	0.0301	-18.43
6	NNDMA-NM	2.94	5.816	0.0073	0.0357	-22.11

The natural bond orbital analysis reveals that there is substantial donor-acceptor orbital overlap between lone pair orbital ( $n_O$ ) of O of NNDMA and Z-C antibonding sigma orbital ( $\sigma^*_{Z-C}$ ) bond of different C-bond donors, as shown in Figure 6.1.11. The donor-acceptor interaction energies ( $E_{DA}$ ) are provided in Table 6.1.3 and these values are in the range of  $\sim$ 1-6 kJ/mol. In addition to these analyses we also performed the Non-covalent interaction (NCI) index analysis and molecular electrostatic potential (MESP) calculations to establish that the Z-C $\cdots$ O=C interactions are attractive and involve  $\sigma$ -hole interactions. NCI is a topological analysis tool based on the electron density and its derivatives and used to verify the existence and establish the type of interaction between two molecules in biomolecules. Figure 6.1.12 depicts the reduced density

## Carbon Bonding

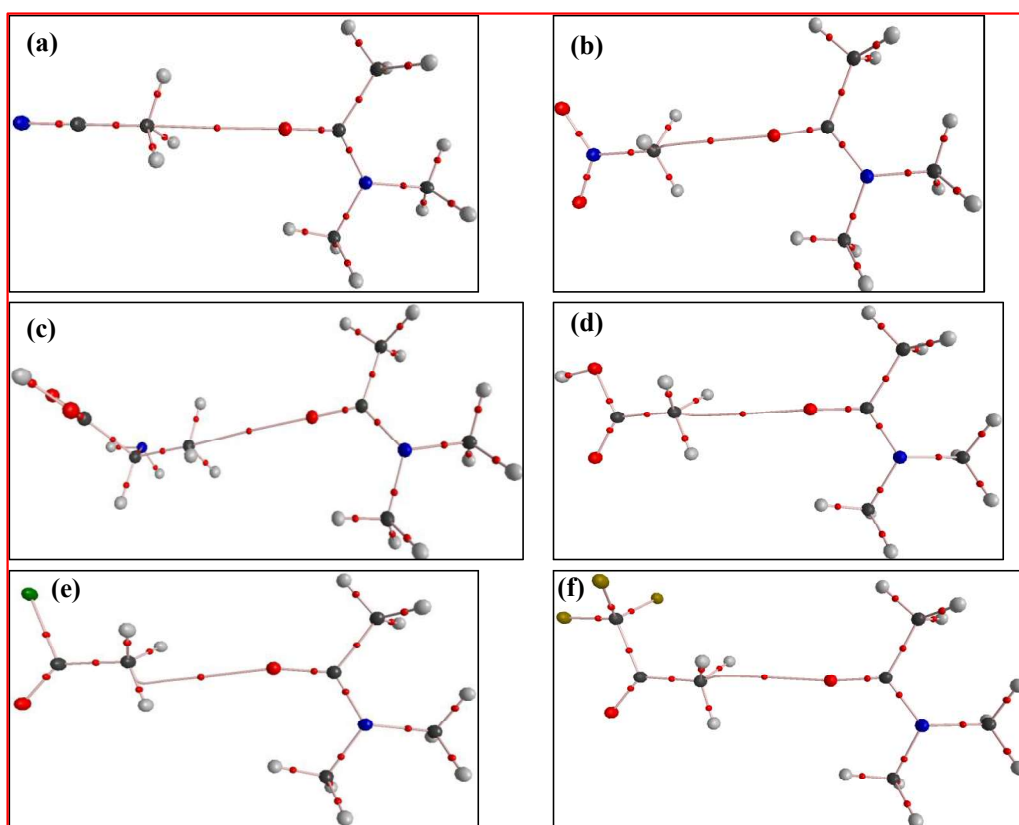


**Figure 6.1.10** Represents the bond critical point between O and C along the Z-C...O=C C-bond (a) NNDMA-ACN, (b) NNDMA-NM, (c) NNDMA-ALA, (d) NNDMA-AA, (e) NNDMA-AcetylCl and (f) NNDMA-TFACE.

gradient isosurfaces in real 3D space for Z-C...O=C C-bond, the green isosurface indicates attractive noncovalent interaction between NNDMA and six different C-bond donors. Figure 6.1.13 displays MESP contours of Z-C...O=C C-bond complexes and it reveals that  $\sigma$ -hole is created on C atom of each C-bond donor and electron rich atom O of NNDMA interacts with that  $\sigma$ -hole.

## Carbon Bonding

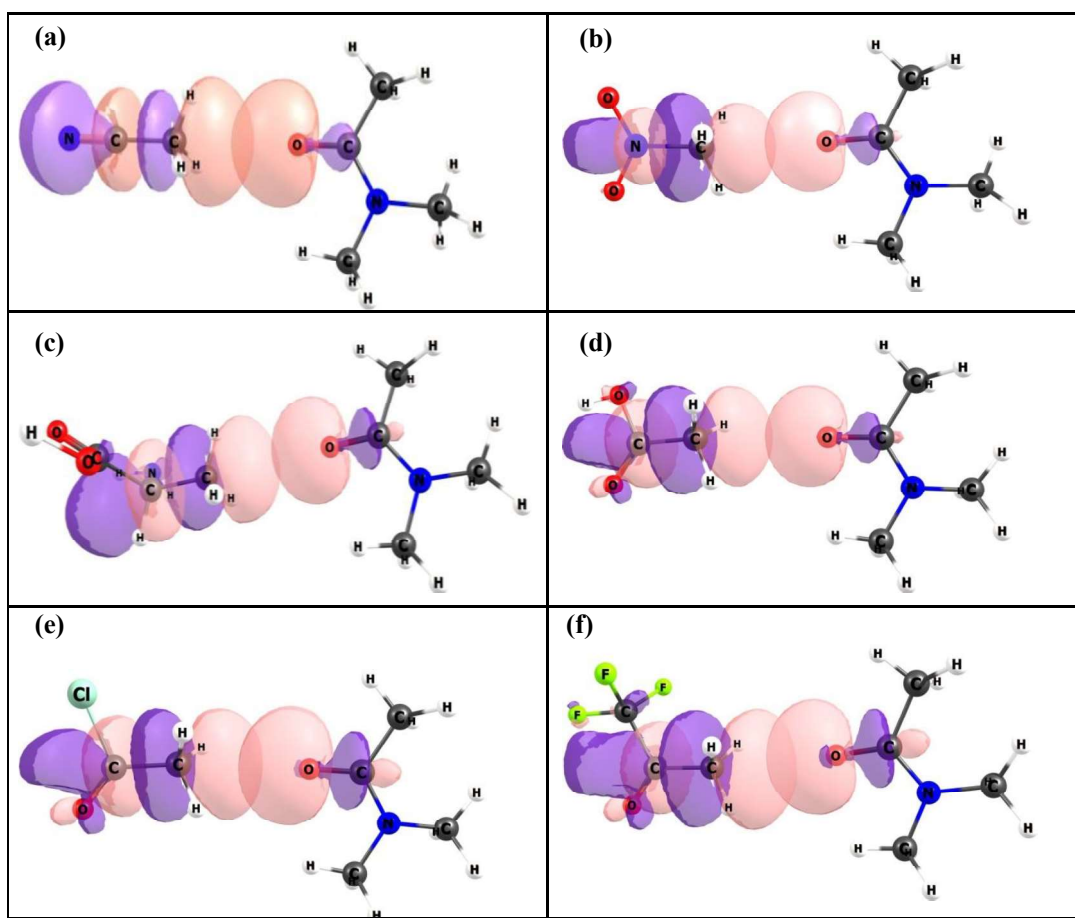


**Figure 6.1.11** Represents the orbital overlap between oxygen lone pair ( $n_O$ ) and the Z-C antibonding sigma orbital ( $\sigma^*_{Z-C}$ ) of (a) NNDMA-ACN, (b) NNDMA-NM, (c) NNDMA-ALA, (d) NNDMA-AA, (e) NNDMA-AcetylCl and (f) NNDMA-TFACE.

## Carbon Bonding

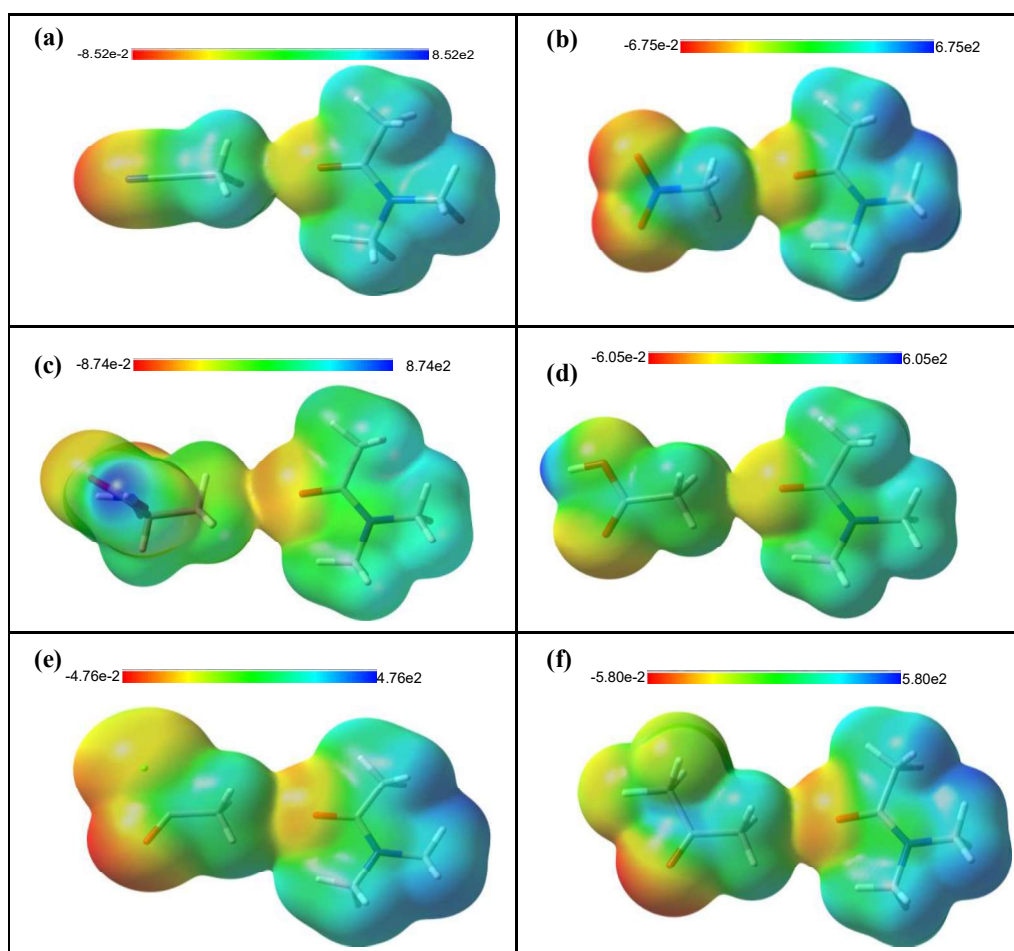


**Figure 6.1.12** Represents the molecular electrostatic potential map of (a) NNDMA-ACN, (b) NNDMA-NM, (c) NNDMA-ALA, (d) NNDMA-AA, (e) NNDMA-AcetylCl and (f) NNDMA-TFACE. Isosurface values at 0.005.

From the six model C-bond complexes we have chosen NNDMA-ACN complex for the experimental purpose to determine the C-bond energy. The reasoning of the choice is many fold: (a) there are two functional groups i.e. C=O in the acceptor and C $\equiv$ N in the donor that are very sensitive probe for NMR and IR spectroscopy. From monomer (NNDMA or ACN) to the complex (NNDMA-ACN) formation we can expect changes in  $^{13}\text{C}$  chemical shift and in the C=O and C $\equiv$ N vibrational stretching frequencies. (b) There are no other non-covalent interactions of measurable magnitude present in between these two molecules. (c) Both the

## Carbon Bonding

molecules are soluble in an inert and non-polar solvent ( $\text{CCl}_4$ ) that helps in avoiding solute-solvent interaction.

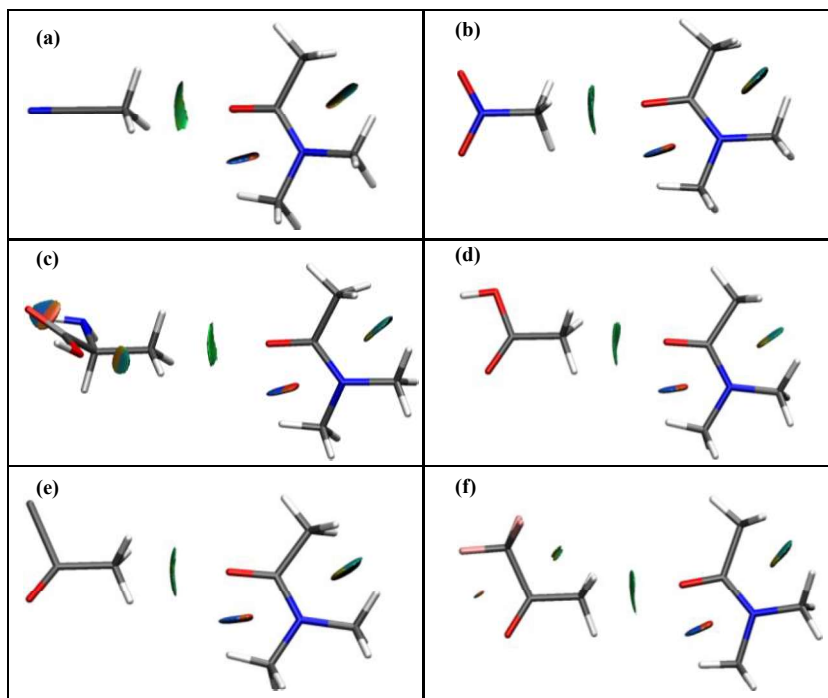


**Figure 6.1.13** Represents the colored isosurfaces of reduced electron density gradient in 3D real space for (a) NNDMA-ACN, (b) NNDMA-NM, (c) NNDMA-ALA, (d) NNDMA-AA, (e) NNDMA-AcetylCl and (f) NNDMA-TFACE, blue and green isosurface indicates attractive non-covalent interaction between O and C atom.

NMR titration is a very conventional experimental method that can be exploited to determine the binding constants between host and guest.<sup>28-31</sup> Hence, we first performed  $^{13}\text{C}$  NMR titration experiments to confirm the existence and strength of NNDMA-ACN C-bond complex.  $^{13}\text{C}$  NMR experiments were carried out using 400MHz (9.41 Tesla) Avance-III Bruker liquid state NMR spectrometer. For NMR experiments, 50  $\mu\text{L}$  of deuterated dimethyl sulfoxide ( $\text{DMSO-d}_6$ ) was taken in capillary tube for locking and external reference. NMR titration experiments were carried out in two ways: (i) keeping NNDMA concentration (0.21M) in  $\text{CCl}_4$

## Carbon Bonding

---

constant and varying the ACN concentration at 17 intervals from 0 M to 3.15 M, and (ii) keeping ACN concentration (1.7M) in  $\text{CCl}_4$  constant and varying the NNDMA concentration at 17 intervals from 0 M to 3 M. The NMR peaks of the host sensitive to the host-guest interactions are monitored. We treated NNDMA as host and ACN as guest in one case and vice-versa in other case. Figure 6.1.14 (a) shows the  $^{13}\text{C}$  NMR spectra for NNDMA monomer and Figure 6.1.14 (b) shows the  $^{13}\text{C}$  NMR spectra of NNDMA in presence of ACN with different concentrations. This results that the  $^{13}\text{C}_{\text{CO}}$  NMR peak of carbonyl of NNDMA is shifted to higher chemical shift value with gradual increase of ACN concentration. In another case, we have monitored the  $^{13}\text{C}_{\text{CN}}$  and  $^{13}\text{C}_{\text{CH}_3}$  peaks of host molecule (ACN) with varying the concentration of (guest) NNDMA. Figure 6.1.15 (a) & (b) show the  $^{13}\text{C}$  NMR spectra for  $^{13}\text{C}_{\text{CN}}$  and  $^{13}\text{C}_{\text{CH}_3}$  peaks shifts of ACN with increased concentration of NNDMA. Table 6.1.4 provides the chemical shift values for both titration cases at particular concentrations of host and guests. It is observed that the chemical shifts for  $^{13}\text{C}_{\text{CN}}$  and  $^{13}\text{C}_{\text{CH}_3}$  peaks are shifted to downfield and upfield with increased NNDMA concentrations, respectively.

## Carbon Bonding

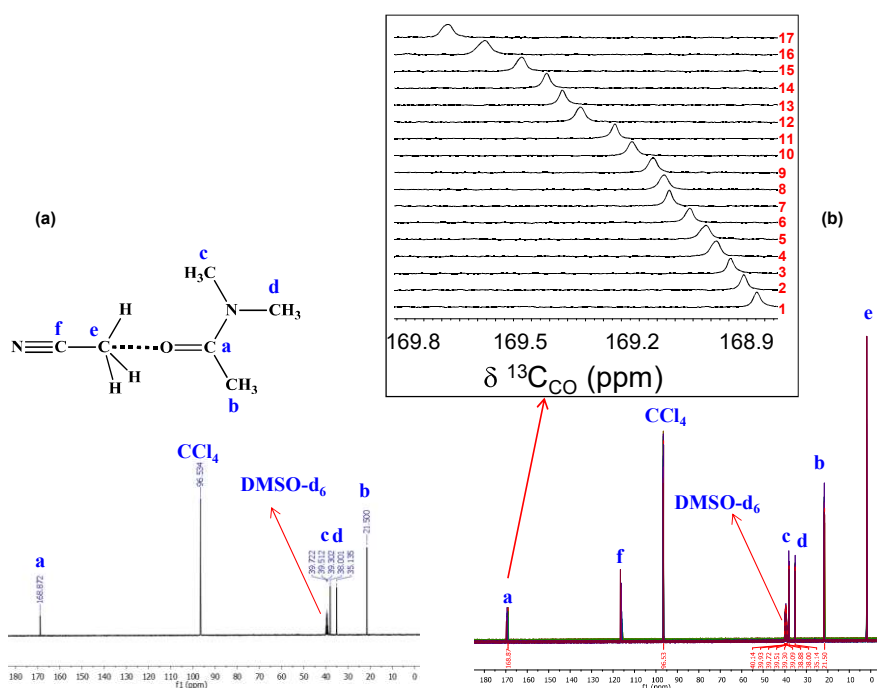


**Figure 6.1.14**  $^{13}\text{C}$  NMR spectra for (a) only NNDMA monomer (b) NNDMA-ACN complex (inset rectangular box downfield shifts of  $\text{C}=\text{O}$  peak).

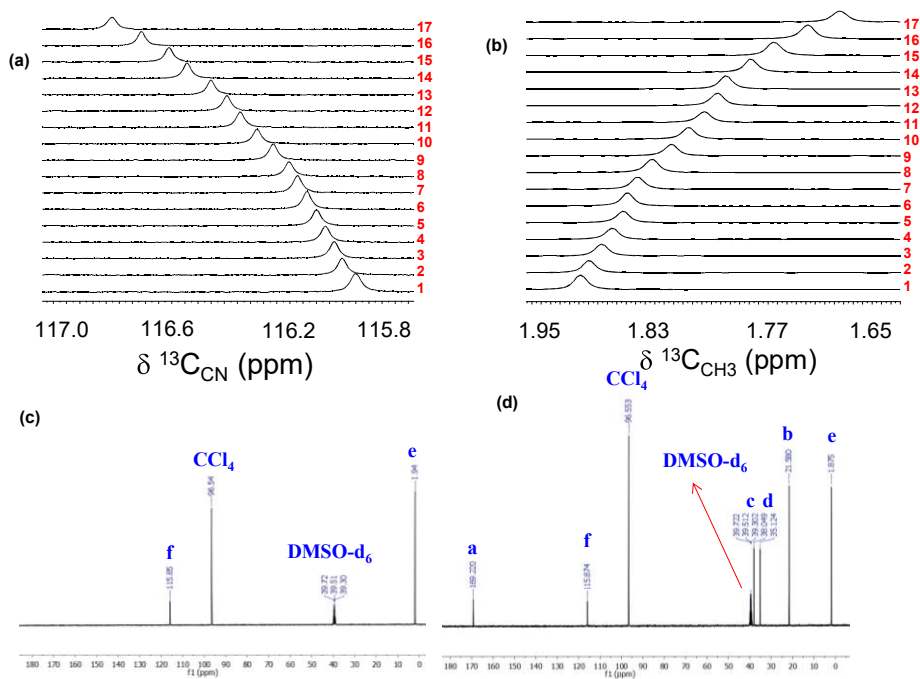


**Figure 6.1.15**  $^{13}\text{C}$  NMR spectra for (a) downfield shift for  $^{13}\text{C}_{\text{CN}}$  (b) upfield shifts for  $^{13}\text{C}_{\text{CH}_3}$  (c)  $^{13}\text{C}$  NMR spectra for ACN only (D)  $^{13}\text{C}$  NMR spectra for NNDMA-ACN complex.

## Carbon Bonding

Table 6.1.4 The chemical shift ( $\delta$ ) values of  $^{13}\text{C}=\text{O}$  of NNDMA and  $^{13}\text{CN}$  of ACN at different concentrations of ACN and NNDMA, respectively. [NNDMA] and [ACN] are the concentrations of N,N-dimethylacetamide and acetonitrile, respectively. Titration 1: [NNDMA] kept constant varying the [ACN]. Titration 2: [ACN] kept constant varying the [NNDMA].

S.No.	[ACN] (M)	[NNDMA] (M)	$^{13}\text{C}$ $\delta(\text{C}=\text{O})$ (ppm)	[NNDMA] (M)	[ACN] (M)	$^{13}\text{C}$ $\delta(\text{CN})$ (ppm)	$^{13}\text{C}$ $\delta(\text{CH}_3)$ (ppm)
Titration 1				Titration 2			
1	0.00	0.21	168.87	0.00	1.70	115.85	1.94
2	0.08	0.21	168.91	0.08	1.70	115.90	1.93
3	0.15	0.21	168.94	0.17	1.70	115.93	1.92
4	0.22	0.21	168.98	0.25	1.70	115.96	1.90
5	0.30	0.21	169.01	0.33	1.70	116.00	1.89
6	0.37	0.21	169.06	0.41	1.70	116.03	1.89
7	0.44	0.21	169.11	0.51	1.70	116.07	1.88
8	0.51	0.21	169.13	0.60	1.70	116.11	1.86
9	0.59	0.21	169.16	0.79	1.70	116.16	1.84
10	0.73	0.21	169.22	0.97	1.70	116.22	1.82
11	0.90	0.21	169.27	1.14	1.70	116.29	1.81
12	1.24	0.21	169.36	1.31	1.70	116.34	1.79
13	1.40	0.21	169.41	1.47	1.70	116.40	1.78
14	1.56	0.21	169.45	1.78	1.70	116.49	1.76
15	2.03	0.21	169.52	2.06	1.70	116.56	1.73
16	2.61	0.21	169.63	2.46	1.70	116.66	1.70
17	3.15	0.21	169.73	3.04	1.70	116.78	1.66

In NNDMA-ACN complex, carbonyl group and cyanide group are very sensitive to the external perturbation hence we have observed the downfield chemical shifts in these. These downfield shifts confirm the formation of C-bond interaction between NNDMA and ACN. Therefore, we can measure the equilibrium constant (K) of C-Bond complex using Host-Guest equilibrium expression which is mentioned in Jonathan R. Nitschke et al.<sup>31</sup> work. The detail expression of the equilibrium constant as a function of guest concentration is provided as follow

## Carbon Bonding

---

The Host-Guest equilibrium is represented as



where H is the Host molecule and G is the Guest molecule

The equilibrium constant (K) for the host-guest complex is given by

$$K = \frac{[HG]}{[H][G]} \quad (2)$$

$$\Rightarrow [HG] = K[H][G] \quad (3)$$

The total concentration of guest  $[G]_0$  and host  $[H]_0$  in the solution is given

$$[G]_0 = [G] + [HG] = [G] + K[H][G] \quad (4)$$

$$[H]_0 = [H] + [HG] = [H] + K[H][G] = [H] \times (1 + K[G]) \quad (5)$$

The fraction of host molecule ( $f_H$ ) forming the H-G complex is given by

$$f_H = \frac{[HG]}{[H]_0} = \frac{K[G]}{1 + K[G]} = y \quad (6),$$

The equilibrium constant or complexation constant or binding constant (K) can be obtained from equation (6) by knowing the guest concentration at equilibrium ( $[G]$ ).  $[G]$  can be expressed in terms of  $[G]_0$ ,  $[H]_0$  and K.

$$[G] = [G]_0 - [HG] = [G]_0 - K[H][G] \quad (7)$$

From equations (5) & (6) it follows that the free host concentration at equilibrium is equal to

$$[H] = (1-y)[H]_0 \quad (8)$$

## Carbon Bonding

---

Combining equation (7) and (8), we have

$$[G] = [G]_0 - K(1-y)[H]_0[G] \quad (9)$$

Rearranging above equation (9) we get

$$(1+K(1-y)[H]_0) \times [G] = [G]_0 \quad (10)$$

From equation (10) it follows that the free guest concentration at equilibrium is equal to

$$[G] = \frac{[G]_0}{1+K(1-y)[H]_0} \quad (11)$$

Equation (6) can be rearranged as

$$y + yK[G] = K[G] \quad (12)$$

Equation (11) substituted in equation (12) gives

$$y + yK\left(\frac{[G]_0}{1+K(1-y)[H]_0}\right) = K\left(\frac{[G]_0}{1+K(1-y)[H]_0}\right) \quad (13)$$

Rearranging the equation (13), we get

$$y(1 + K[H]_0 - Ky[H]_0) + yK[G]_0 - K[G]_0 = 0 \quad (14)$$

Rearranging equation (14), we get

$$-K[H]_0y^2 + (1 + K([H]_0 + [G]_0))y - K[G]_0 = 0 \quad (15)$$

Finally, we can rearrange the equation (15) and get

## Carbon Bonding

---

$$K [H]_0 y^2 - (1 + K([H]_0 + [G]_0))y + K[G]_0 = 0 \quad (16)$$

Equation (16) is a quadratic equation in  $y$  and was solved to give two roots as below

$$y = \frac{[1+K([H]_0+[G]_0)] \pm \sqrt{[1+K([H]_0+[G]_0)]^2 - 4K^2[H]_0[G]_0}}{2K[H]_0} \quad (17)$$

From the two roots of equation (17), it was found that the physically meaningful root is given by:

$$y = \frac{[1+K([H]_0+[G]_0)] - \sqrt{[1+K([H]_0+[G]_0)]^2 - 4K^2[H]_0[G]_0}}{2K[H]_0} \quad (18)$$

Equation (18) was rearranged to the equation (19) as mentioned below and used in origin software to fit the curve obtained from the chemical shifts versus Hosts / Guests concentration.

$$Y = \frac{Y_0 + \Delta Y (K([H]_0 + [G]_0) + 1) - \sqrt{[K([H]_0 + [G]_0) + 1]^2 - 4K^2[H]_0[G]_0}}{2K[H]_0} \quad (19)$$

The unknown parameters  $K$ ,  $Y_0$  and  $\Delta Y$  were obtained from the fitted curve.

Where,  $Y$  is a measured chemical shift,  $Y_0$  is a chemical shift of only host in solution,  $\Delta Y$  is the maximal change in chemical shift i.e. the difference in chemical shift of a fully occupied host and an empty host,  $K$  is the association constant,  $[H]_0$  is a total host concentration in solution,  $[G]_0$  is the total guest concentration in solution.

We have drawn the plot between observed chemical shifts of  $^{13}\text{C}_{\text{CO}}$  as function of concentration of ACN and fitted this in origin using the expression of (19) to determine the equilibrium constant ( $K$ ). Similarly, we have fitted the plots between observed chemical shifts of  $^{13}\text{C}_{\text{CN}}$  and  $^{13}\text{C}_{\text{CH}_3}$  as function of NNMDA concentration. The calculated equilibrium constant ( $K$ ) for three cases are 0.443, 0.283 and 0.26 for NNDMA-ACN complex. The chemical shift versus concentration of the guest plots as shown in Figures 6.1.16 (a), (b), and (c). From the obtained

## Carbon Bonding

equilibrium constant we calculated the free energies of association ( $\Delta G$ ) and subsequently from experimental free energy ( $\Delta G$ ) and computational entropy ( $\Delta S$ ) we could be able to estimate the C-bond energy ( $D_0$ ) by using the expression,

$$(D_0)_{\text{expt.}} = \Delta G_{\text{expt.}} + T(\Delta S - R), \quad R = \text{universal gas constant.} \quad (20)$$

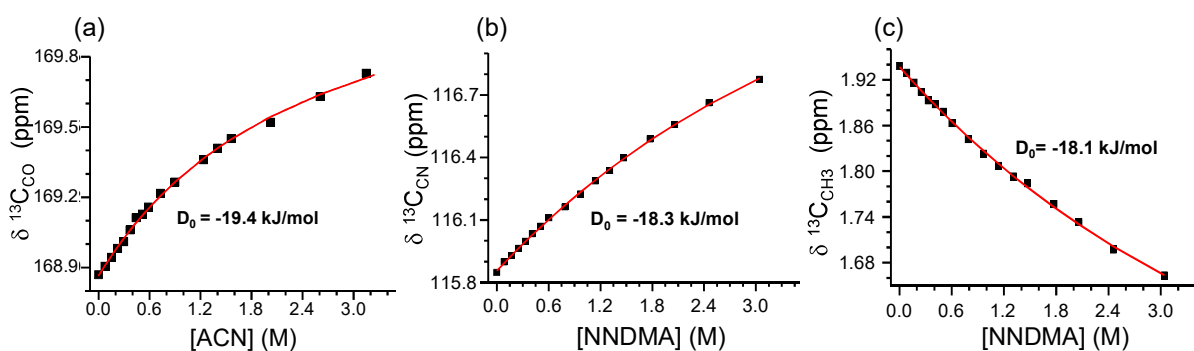


**Figure 6.1.16** (a) Chemical shift of the  $^{13}\text{C}_{\text{CO}}$  peak of NNDMA as a function of concentration of ACN (b) Chemical shift of the  $^{13}\text{C}_{\text{CN}}$  peak of ACCN as a function of concentration of NNDMA, (c) Chemical shift of the  $^{13}\text{C}_{\text{CH}_3}$  peak of ACN as a function of concentration of NNDMA.

The experimental  $D_0$  values for the C-bonded NNDMA-ACN complex for the three experiments are -19.4, -18.3 and 18.1 kJ/mol and the average value is  $\sim$ -18.6 kJ/mol. This value is very close to calculated binding energy of NNDMA-ACN complex at gold standard method CCSD (T)/aug-cc-pVDZ level, see Table 6.1.3. This suggests that our experimental methodology is reliable to determine the C-bond energy very precisely.

Further we confirmed the C-bond formation in the NNDMA-ACN by doing the IR experiments as similar as NMR titrations. We performed the IR experiments to record the vibrational spectra for both monomers (NNDMA, ACN) and NNDMA-ACN complex using the horizontal attenuated total internal reflectance (HATIR) technique. Figure 6.1.17 shows the IR

## Carbon Bonding

spectra for carbonyl peak of NNDMA and cyanide peak of ACN with increasing the guest concentration. It is observed that in both cases, the vibrational stretching frequency of C=O and C≡N shifts to lower frequencies compared to their corresponding monomers in complex formation. These red shifts correlate with change in chemical shifts of corresponding functional group peak at particular concentrations. Hence, we observed a linear correlation between the red shifts of IR frequencies and downfield shifts of <sup>13</sup>C NMR peaks, as shown in Figure 6.1.18. The vibrational stretching frequencies for C=O and C≡N and their red shift values are shown in Table 6.1.5.

**Table 6.1.5** The vibrational frequency ( $\nu$ ) values for C=O of NNDMA and CN of ACN at different concentrations of ACN and NNDMA, respectively.  $\Delta\nu$  values are the red shift values of for for C=O of NNDMA and CN of ACN.

Compound	[ACN] (M)	$\nu_{CO}$ ( $cm^{-1}$ )	$\Delta\nu_{CO}$ ( $cm^{-1}$ )	Compound	[NNDMA] (M)	$\nu_{CN}$ ( $cm^{-1}$ )	$\Delta\nu_{CN}$ ( $cm^{-1}$ )
NNDMA	0.00	1659	0	ACN	0	2254	0
	0.22	1658	-1		0.17	2253.50	-0.50
	0.37	1656	-3		0.35	2253.30	-0.70
	0.90	1655	-4		0.49	2253.00	-1.00
	1.24	1653	-6		0.79	2252.50	-1.50
	1.56	1652	-7		1.05	2252.25	-1.75
	2.61	1650	-9		1.14	2252.00	-2.00
	3.15	1649	-10		1.47	2251.80	-2.20

## Carbon Bonding

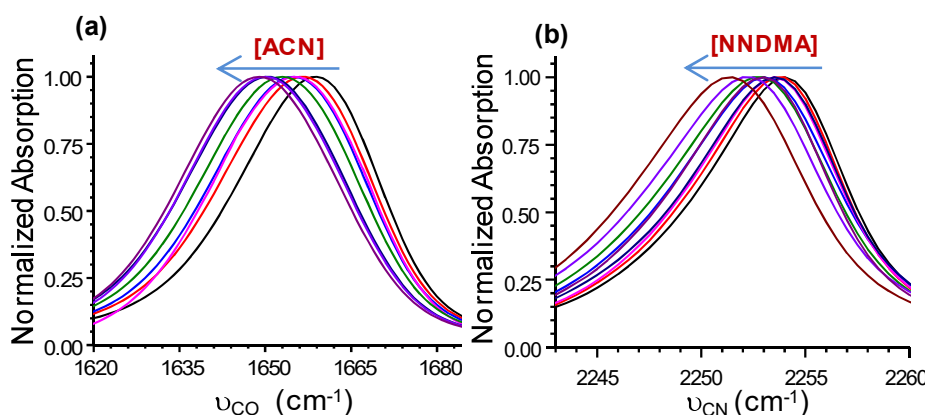


**Figure 6.1.17** IR Spectra of vibrational stretching absorption peak for (a) C=O (b) CN with increase of concentration of ACN and NNDMA respectively.

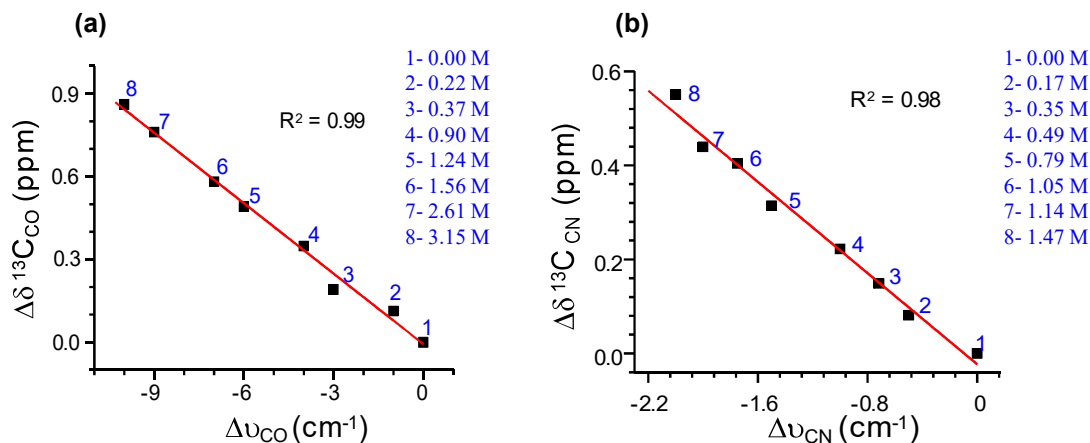


**Figure 6.1.18** Correlation plots between experimental redshifts in IR and downfield chemical shifts in NMR, (a) for C=O (b) for CN in NNMDA-ACN complex.

NMR and IR experiments confirm the formation of Z-C $\cdots$ O=C C-bond in NNDMA-ACN and the binding energy obtained from NMR experiment is comparable to results obtained at CCSD-T method. From the NMR and CCSD-T binding energetics used to extend our calculation to measure the binding energies of C-bond present in proteins. Therefore, we correlated the binding energies with calculated  $n\rightarrow\sigma^*$  interaction energy ( $E_{DA}$ ) for these

## Carbon Bonding

---

complexes. We found an exponential correlation between  $D_0$  and  $E_{DA}$  as shown in Figure 6.1.19(a)  $D_0$  and  $E_{DA}$  are related as

$$D_0 = 22.2 \times e^{-E_{DA}/1.6} - 22.2 \quad (21)$$

Since the calculation of  $E_{DA}$  is not as computationally expensive as CCSD(T), the above expression will be useful in predicting CCSD(T) binding energy with the prior knowledge of  $n \rightarrow \sigma^*$  interaction energy. We, then exploited this expression in predicting CCSD(T) C-bond energetics in proteins. We used computed  $E_{DA}$  values obtained from aforementioned section for 22 amino acid pairs covering complete distance ( $2.75 \text{ \AA} \leq d_{C \cdots O} \leq 3.6 \text{ \AA}$ ) and angle range ( $160^\circ \leq \theta_i \leq 180^\circ$ ), as provided in Table 6.1.2. The  $E_{DA}$  values of PDBs and model compounds were plotted against the distance between interacting O and C atoms and the graph is provided in Figure 6.1.19 (b). An exponential relation between  $E_{DA}$  and  $d_{C \cdots O}$  was deduced as shown in equation 22.

$$E_{DA} = 3.5 \times 10^7 \times e^{(-d_{C \cdots O}/0.184)} \text{ for } 2.75 \text{ \AA} \leq d_{C \cdots O} \leq 3.6 \text{ \AA} \text{ \& } (160^\circ \leq \theta_i \leq 180^\circ) \quad (22)$$

By combining equation (21) and (22), we derived another expression as shown below

$$D_0 \approx e^{(\ln(22.2) - 22.2 \times 10^6 \times (e^{-d_{C \cdots O}/0.184}))} - 22.2 \quad (23)$$

The equation 23 can be used to estimate Z-C $\cdots$ O=C C-bond energy very precisely just by knowing the C $\cdots$ O distances. The estimated  $D_0$  of NNDM-ACN C-bond complex by using the above formula is -17 kJ/mol that is comparable with the experimentally determined binding energy. We are now in a convincing position to use this empirical equation to estimate the C-bond energy in proteins from the C $\cdots$ O distances. Therefore, we applied this empirical equation to estimate the C-bond energies in proteins. We estimated the binding energies of all the 7600

## Carbon Bonding

interaction in proteins and they are in the range of -2 to -22 kJ/mol. We have shown in Figure 6.1.21 (b) the distribution of estimated C-bond energy at CCSD-T levels along the C...O distance in proteins.

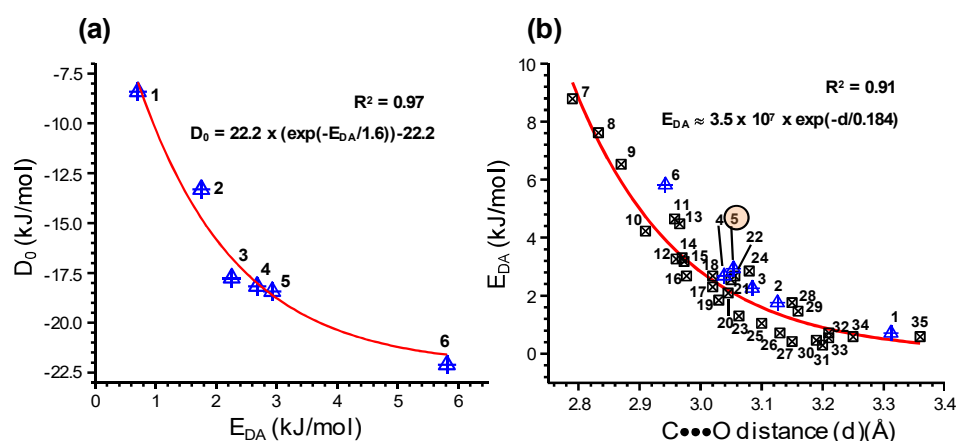


Figure 6.1.19 (a) The exponential correlation plot between carbon bond energies ( $D_0$ ) obtained at CCSD-T level and donor-acceptor interaction energies ( $E_{DA}$ ) of model C-bond complexes. (b) The exponential correlation plot between the donor-acceptor energies ( $E_{DA}$ ) of model C-bond complexes and proteins and C...O bond distances ( $d$ ), 1-NNDMA-ALA, 2-NNDMA-AA, 3-NNDMA-TFACE, 4-NNDMA-AcetylCl, 5-NNDMA-ACN, 6-NNDMA-NM, 7-3EEA, 8-5NG1, 9-3DNX, 10-3A57, 11-5A6M, 12-3DNX, 13-4JJJ, 14-4PGM, 15-3NDS, 16-2DHO, 17-3OAJ, 18-5JOV, 19-3LGI, 20-5KAR, 21-3HZ6, 22-5EL9, 23-5A0Y, 24-2O7C., 25-4WDC, 26-3Zk4, 27-1RY9, 28-4IVN, 29-1DDX, 30-2FAO, 31-4YLE, 32-3JQ1, 33-5JUF, 34-2QRU, 35-1M6S.

### 6.1.4 Nature of C-bond interaction in model compounds and proteins

We have performed the localized molecular orbital energy decomposition analysis (LMOEDA) to better understand the nature and extent of different forces contributing to the intermolecular attraction in these complexes. We have calculated individual energy components

## Carbon Bonding

(electrostatic (ES), polarization (POL), repulsion (REP), and exchange (EX)) at MP2/aug-cc-pVDZ level of theory in C-bond complexes. The values provided in Table 6.1.6 and Figure 6.1.20 displays the distribution of different energies in NNDMA-ACN complex.

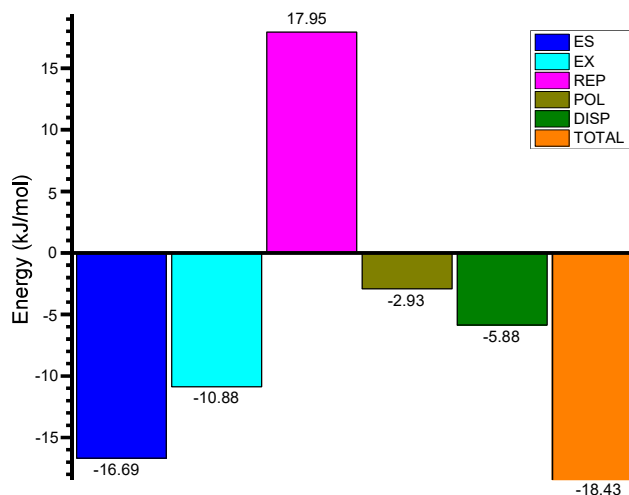


**Figure 6.1.20** Distribution of different forces (electrostatic (ES), polarization (POL), repulsion (REP), and exchange (EX) and dispersion energy (DISP)) contributing to the intermolecular attraction in NNDMA-ACN C-bond complex.

**Table 6.1.6** The localized molecular orbital energy decomposition analysis (LMOEDA) for Model C-bond complexes. The individual components electrostatic (ES), polarization (POL), repulsion (REP), and exchange (EX) are at MP2/aug-acc-pVDZ level and dispersion energy and % of distribution energy contributing to the total binding energy at CCSD-T level. (all values are in kJ/mol).

S.No	Model compounds	$\Delta E_{ES}$	$\Delta E_{EX}$	$\Delta E_{REP}$	$\Delta E_{POL}$	$\Delta E_{DISP}$ (CCSD-T)	% $\Delta E_{DISP}$ (CCSD-T)
1	NNDMA-ALA	-2.26	-5.31	8.37	-1.63	-7.57	90.0
2	NNDMA-AA	-9.79	-9.54	15.56	-2.30	-7.25	54.4
3	NNDMA-TFACE	-18.03	-19.83	33.35	-4.02	-9.22	51.9
4	NNDMA-AcetylCl	-15.61	-12.09	20.00	-3.14	-7.34	40.4
5	NNDMA-ACN	-16.69	-10.88	17.95	-2.93	-5.88	31.9
6	NNDMA-NM	-22.38	-13.56	22.72	-3.93	-4.96	22.4

## Carbon Bonding

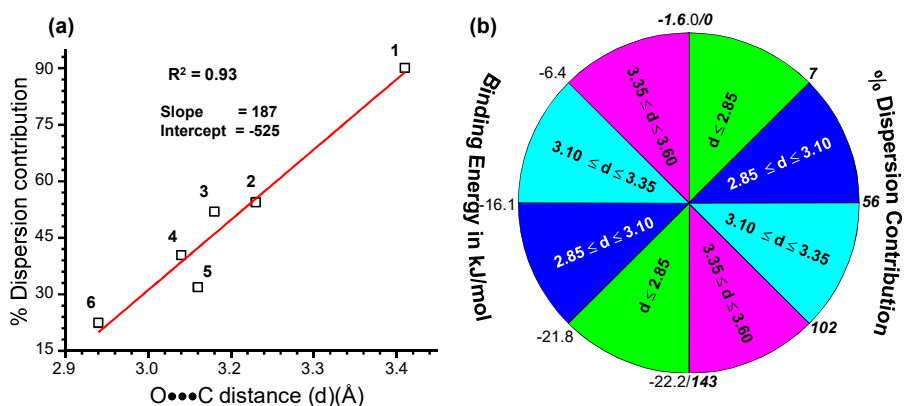


**Figure 6.1.21** (a) Correlation plot between percentage of dispersion energy contribution and C...O distance in model compounds (b) Distribution of estimated binding energies and percentage of dispersion energy contribution along the C...O distances at CCSD-T level in proteins. The number in plot represents the model complexes shown in Table 6.1.6.

Here, we calculated the dispersion energy (DISP) at CCSD-T level of method by subtracting binding energy obtained at CCSD-T/aug-cc-pVDZ from total interaction energy that computed using the LMOEDA method. We correlated the percentage of dispersion energy contributing to the binding energies of model compounds with C...O distances. We found a linear correlation between the C...O distances and dispersion energies of C-bond complexes as shown in Figure 6.1.21 (a). From this linear relation we have estimated the percentage of dispersion energy contribution in proteins. This analysis results that the nature of C-bond depends on the O and C distances ( $d_{O...C}$ ). The C-Bond is electrostatic in nature at shorter distance while purely dispersive at longer distance.

### 6.1.5 Significant role of C-bonds in structural and functional analysis in proteins

Role of C-bonds in protein functions is not reported since its recent discovery. For the first time we provided two examples where the concept of C-bonds can be evoked to explain many biophysical phenomena. In a recent report<sup>32</sup> entitled "Direct observation of ultrafast

## Carbon Bonding

---

collective motions in CO myoglobin upon ligand dissociation", the authors attribute the ultrafast structural changes in the carbonmonoxy myoglobin complex upon photolysis of the Fe-CO bond to the coupling of the ultrafast heme doming mode to the large scale modes of the protein through the low frequency vibrations. They assigned the low frequency modes of the proteins to the H-bonded residues, e.g. Lys<sup>98</sup> O-Lys<sup>42</sup> N<sub>ξ</sub> distance shows oscillations with a period of 500±150 fs through an N-H...O=C H-bond. However these H-bonded residues are remotely located from the heme center and the oscillations are transmitted from residues that are directly bonded to the heme center through multiple H-bonds. A careful structure analysis of the CD corner of CO myoglobin revealed that Lys<sup>42</sup>O is in direct contact with the heme through a C...O=C C-bond (Figure 6.1.22 (a)). Using our aforementioned empirical relation we estimated the C-bond energy from the C...O distance and it is found to be ~15.7 kJ/mol. We performed relaxed potential energy scan as a function  $d_{C...O}$  (Figure 6.1.22(c)) and fitted into a Morse potential to deduce intermolecular stretching frequency ( $\sigma_{C...O}$ ) for NNDMA-ACN that has similar  $d_{C...O}$  distance as in myoglobin. The  $\sigma_{C...O}$  is ~75 cm<sup>-1</sup> (equivalent to 2.25 THz). The corresponding time period for this C-bond is ~450 fs which is highly in synergy with the ultrafast heme doming mode (417-430 fs)<sup>32</sup>. Hence the heme doming oscillation can easily be transmitted directly through Lys<sup>42</sup> to other parts of the protein via a C-bond. However it is not explored in the aforementioned article as the C-bond is yet to be recognized as another important non-covalent interaction that can influence the structures and functions of proteins. One more example as shown in Figure 6.1.22 (b) can be cited where 6-methyladenine (6MA) can be held in the active center of the ribosome-inactivating proteins with a C-bond. In their article Yu Wang and coworkers<sup>33</sup> reported that the ligand (6MA) protein interaction is due to "hydrophobic forces", aromatic stacking and H-bonds. We observed a C-bond between Glu<sup>160</sup>-C=O and 6-MA

## Carbon Bonding

CH<sub>3</sub>. The estimated C-bond energy (using equation 23) in this case is -21.7 kJ/mol. This C-bond energy is strong enough to be considered as a prominent non-covalent interaction to bind 6MA in the active center of the protein. Hence, the concepts of C-bonds can unequivocally be considered to explain a debatable term frequently used in biomolecules called "hydrophobic forces or hydrophobic interactions". These two are just representative examples. We expect the importance of C-bonds would be explored in many more systems in near future.

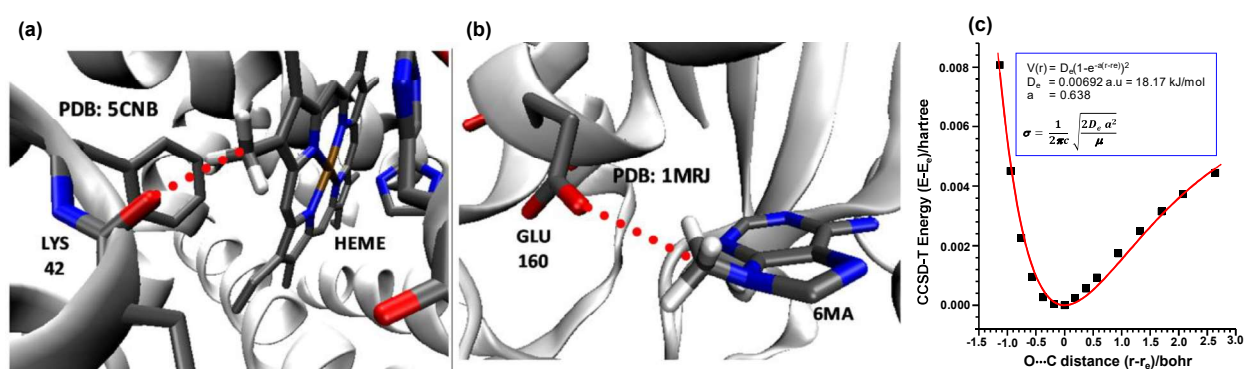


**Figure 6.1.22** Representative examples of implication of C-bonds in protein structure and function Z-C...O=C C-bonds observed in (a) C-C...O=C C-bond in myoglobin (PDB: 5CNB) formed by Lys<sup>42</sup>-C=O and Heme-CH<sub>3</sub>, responsible for the transmission of the heme doming oscillation directly through Lys<sup>42</sup> during CO photolysis in myoglobin to other parts of the protein. (b) N-C...O=C C-bonds in ribosome-inactivating protein (PDB: 1MRJ) formed by Glu<sup>160</sup>-C=O and CH<sub>3</sub> of 6-methyladenine (6MA), contributing significantly to bind 6MA in the active centre of the protein. (c) Potential energy scan of energy differences (E-E<sub>e</sub>) over the change in C...O C-bond distances (r-r<sub>e</sub>). E is the energy for C...O C-bond distance (r) and E<sub>e</sub> is the minimum energy for C...O equilibrium C-bond distance (r<sub>e</sub>) for C-bond interaction. The solid red line represents Morse potential fitted curve.

### 6.1.6 Conclusions

- The analysis of protein data bank confirmed the existence of Carbon Bonds (C-Bond) in proteins as  $Z-C\cdots O=C$  C-bond. This analysis gives detailed information such as involvement of amino acids, secondary structures and type of atoms forming C-bond in proteins.
- LYS-ALA, LYS-ASP and ASN-ALA pairs are dominant contributor to form the C-bonds in proteins. In C-bond formation, LYS and ALA are the dominant participants as C-bond donor and C-bond acceptor in proteins, respectively. The C-bond acceptors are mostly backbone and side chain carbonyl groups and for donor case C atom of C-C bond act as C-bond donor followed by C-N and C-O bonds in side chains of amino acids in proteins.
- The C-bond acceptors are located mostly in  $\alpha$ -helix and C-bond donors present in Coil type of secondary structures in proteins.
- The NMR and FTIR spectroscopy studies evidence the presence of carbon bonding as  $Z-C\cdots O=C$  C-bond in model compounds of proteins in a non-interacting solvent (CCl<sub>4</sub>). The concentration dependent NMR experiments enable us to determine the C-bond energy in NNDMA-ACN complex precisely and found to be -18.6 kJ/mol that can be used to benchmark the CCSD-T binding energy (-18.4 kJ/mol).
- With the combination of experimental and computational studies, we derived empirical functions to estimate the C-bond energy in proteins from C $\cdots$ O distances. The C-bond energies can be in the range of 2-22 kJ/mol.

## Carbon Bonding

---

- Depending on the O and C distances ( $d_{C\cdots O}$ ), the C-Bond can be electrostatic or dispersive in nature; at shorter distance it is electrostatic and at longer distance, it is purely dispersive.
- Finally, we established that the C-bonds can contribute to the functions and structures of proteins i.e. the transmission of the heme doming oscillation in monocarboxy myoglobin can be possible directly through Lys<sup>42</sup> to other parts of the protein via a C-bond. The C-bond was also found to be strong enough to be considered as a prominent non-covalent interaction to bind 6MA in the active centre of ribosome inactivating proteins.

### Part (B)

## 6.2 Computational Assessment of the strength of Carbon bonding: N-Oxides, N-Sulfides as C-Bond Acceptors

### 6.2.1 Introduction

The previous section of this chapter and some of previous reports explains that the C-bond is formed between an electrophilic region of a carbon atom of substituted methyl group and a nucleophilic site in another moiety i.e O, N, F and S atoms.<sup>14,17,18,20,23,24</sup> This chapter describes the C-bond formation between high electron rich atom of N-oxides/N-sulfides and electron deficient C atom of methyl group. N-oxides possess a distinctive common fragment i.e an oxygen atom datively bonded to a nitrogen atom. This dative  $N \rightarrow O/N^- - O^+$  bond shows one of the largest dipole moments of any functional group in organic chemistry. Hence, these are having unique properties due to marked polarity of this functional group such as weak bases than their parent amine, high hygroscopic, soluble in water and hydrogen-bonding acceptor character. The aliphatic N-oxides play significant role in catalysis<sup>34</sup>, DNA-affinic agents and act as bioreductive drugs<sup>35-38</sup>, while pyridine N-oxides are used for the anti-HIV activity<sup>39</sup> and N-oxide polymers are used as herbicidal activity<sup>40</sup>. N-oxides are potential hydrogen and halogen bond acceptor in supramolecular chemistry, crystal engineering, pharmaceutical areas.<sup>35,37,40-52</sup> Saraswatula, V. G et al. suggested that pyridine N-oxide act as good hydrogen bond acceptor than pyridine compound and acid...pyridine N-oxide is slightly stronger than the acid...pyridine.<sup>47</sup> Kari Rissanen and his group<sup>53,54</sup> established, from experimental and computational methods that N-oxides act as halogen bond acceptors and the strength of halogen bond is as strong as hydrogen bond in solid-state while in solution it found to possess higher association constant. The ability of N-oxides to form non-covalent interactions (H-bond/X-bond) aids in the development of drug cocrystals.<sup>49,55</sup> Therefore N-Oxides could be a potential non-covalent bond acceptor. Hence, this

## Carbon Bonding

motivates us to investigate whether the N-oxide can also be a C-bond acceptors or not. Here we have studied the computational studies on C-bond formation between C-atom of methyl and electron rich group such as N-oxides as carbon bond acceptors due to the importance of both the groups in organic and biological molecules. The model compounds chosen as C-bond donors are acetonitrile (ACN) and nitromethane (NM) to mimic the methyl groups which are ubiquitous in proteins and organic compounds. In this study, we have chosen different type of N-oxides for better understanding of N-oxides as C-bond acceptors. The C-bond acceptors are imine N-oxide as aliphatic N-oxide, N-oxide pyridines and N-oxide-imidazoles as aromatic N-oxides which are important in the fields of synthetic chemistry, biochemistry and pharmacology. N-methylenemethanamine (EmNO), 1H-imidazole-3-oxide (ImNO) and pyridine-N-oxide (PNO) as aliphatic N-oxide and imidazole and pyridine N-oxides as aromatic N-oxides, respectively. In addition to these we have also taken corresponding N-sulfides for understanding the N-sulfides as C-bond acceptors. All the C-bond donors and C-bond acceptors are shown in Figure 6.2.1.

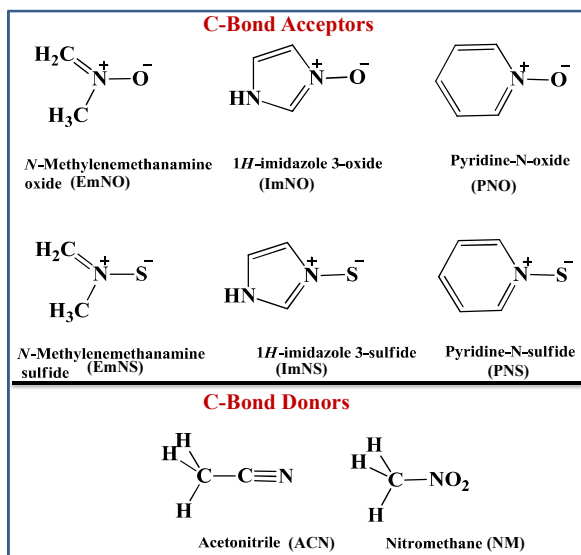


**Figure 6.2.1** Top: Represents the C-bond acceptors and Bottom: C-bond donors.

### 6.2.2 Computational Calculations for evidence of C-bond formation with N-Oxides/N-sulfides

#### 6.2.2.1 Computational methods

The geometries for monomers and Z-C $\cdots$ O/S-N C-bond complexes have been fully optimized at dispersion corrected density functional theory (DFT) B97-D level using aug-cc-pVDZ basis set. Frequency calculations at the same level have been done for all the optimized complex geometries to confirm the nature of the stationary points. All the Z-C $\cdots$ O/S-N C-bond complexes, C-bond bonded structures are the global minimum. The C-bond distances  $d_{C\cdots O/S}$ , angles ( $\angle Z-C\cdots O/S$ ) obtained from these optimized geometries have been provided in Table 6.2.1. The stabilization energy calculations for all the C-bond complexes have been done at B97-D, MP2, and CCSD-T with aug-cc-pVDZ basis set. We also estimated the binding energies for optimized structures of C-bond complexes at CCSD-T/CBS level of theory. The C-bond complex formations were confirmed by natural bond orbital (NBO) and atoms in molecules (AIM) analyses at MP2/aug-cc-pVDZ level on optimized structures. In addition to verify whether the C-bond forms with  $\sigma$ -hole type interaction or not, we performed the molecular electrostatic potential analysis.

Turbomole v 6.5<sup>56</sup> program was used for all the calculations. These calculations were done using the AIM2000 package<sup>57</sup>. NBO calculations were performed using NBO-6.0<sup>58</sup> software suite. Electrostatic potential analysis was done Gaussian 09<sup>59</sup> software. Electrostatic potential maps are viewed by Gaussview v 5.0 software.

## Carbon Bonding

### 6.2.2.2 Geometrical parameters and Stabilization energies for C-bond complexes

The C-bond complexes of N-oxides and N-sulfides with acetonitrile and nitromethane were optimized at B97D/aug-cc-pVDZ level of theory. The structural parameters such as bond length, bond angles of C-bond complexes were obtained from optimized structure at same level of theory. The most stable conformers of C-bond complexes are shown in Figure 6.2.2 and values are provided in Table 6.2.1.

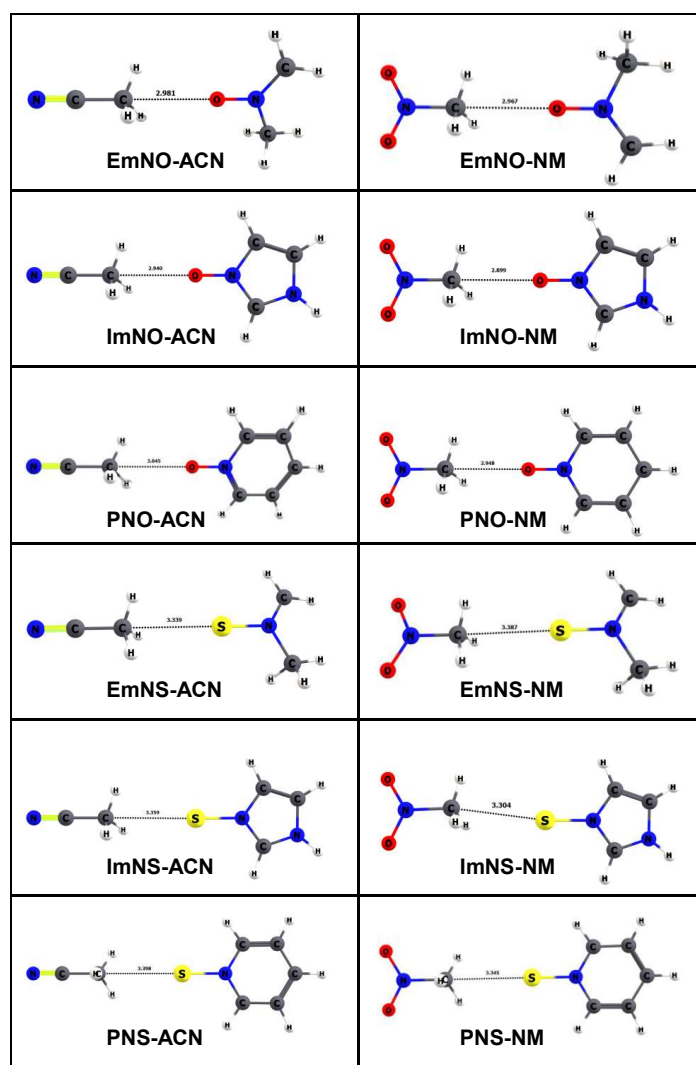


**Figure 6.2.2** Optimized stable structures of C-bond complexes between N-oxides/N-sulfides and acetonitrile and nitromethane at B97D/aug-cc-pVDZ level of theory.

## Carbon Bonding

The C-bond distance between O of N→O and C atom of ACN or NM varied from ~2.8 to 3 Å which is within the sum of van der Waals radii of O and C ( $\leq 3.22$  Å) and the bond angles are close to linear in N-oxides complexes with ACN and NM. The C-bond distance in N-sulfides is approximately found to be on average ~3.3 Å which is also less than the sum of van der Waals radii of S and C ( $\leq 3.5$  Å) and the C-bond angle is  $\sim 177^\circ$ . The binding energies of C-bond complexes were calculated using DFT and *ab initio* methods such as second order Møller–Plesset perturbation theory (MP2) and CCSD-T with aug-cc-pVDZ basis set. In addition, to get full configuration interaction energy, the calculations are done with the complete basis set (CBS) method at CCSD-T level. The binding energies of C-bond complexes with N-oxides and sulfides with ACN and NM as C-bond donors are provided in Table 6.2.1.

**Table 6.2.1** C-bond stabilization energies at different levels of theory, the geometrical parameters C-bond bond distances, bond angles for all C-bond complexes.

Complex	B97D (kJ/mol)	MP2 (kJ/mol)	CCSD-T (kJ/mol)	CCSD-T/CBS (kJ/mol)	d(C···O/S) Å	∠CCX (°)
<b>N-Oxides</b>						
<b>EmNO-ACN</b>	-13.0	-18.2	-17.9	-15.9	2.981	179.99
<b>ImNO-ACN</b>	-16.8	-23.4	-22.4	-20.8	2.940	179.97
<b>PNO-ACN</b>	-13.5	-19.2	-18.9	-16.9	2.942	179.99
<b>EmNO-NM</b>	-14.4	-20.0	-20.6	-19.1	2.967	179.95
<b>ImNO-NM</b>	-18.8	-26.1	-26.1	-24.9	2.899	179.47
<b>PNO-NM</b>	-15.0	-21.0	-21.7	-20.1	2.948	179.00
<b>N-Sulfides</b>						
<b>EmNS-ACN</b>	-11.4	-17.0	-15.1	-12.2	3.339	179.98
<b>ImNS-ACN</b>	-15.5	-20.8	-19.0	-16.5	3.359	179.50
<b>PNS-ACN</b>	-12.4	-18.2	-16.7	-13.4	3.398	179.87
<b>EmNS-NM</b>	-11.9	-16.6	-16.0	-13.3	3.387	176.04
<b>ImNS-NM</b>	-16.1	-21.6	-20.6	-18.5	3.304	169.95
<b>PNS-NM</b>	-13.0	-18.6	-18.1	-15.0	3.345	179.64

## Carbon Bonding

---

The stabilization energies of all C-bond complexes follow the same trend at four levels of theory. The carbon bond stabilization energies of N-oxide complexes with nitromethane are ~3.4 kJ/mol higher than acetonitrile complexes at CCSD-T/CBS method. The stability order of ACN complexes with different type of N-oxides follow ImNO-ACN > PNO-ACN > EmNO-ACN and it is also true for NM complexes. The carbon bond formation of N-sulfides with NM and ACN assumed to be similar due to the stabilization energy differences are close to ~1.4 kJ/mol at CCSD-T/CBS level of method. But in this case also the stability order follow the same order as observed in N-oxide complexes i.e. ImNS-ACN > PNS-ACN > EmNS-ACN. For NM complexes the stability order follow ImNS-NM > PNS-NM > EmNS-NM. Moreover, the binding energies vary from ~-11 to ~-26 kJ/mol for N-oxide/N-sulfide C-bond complexes. This binding energies are higher than C...N C-bond energy (~-8 kJ/mol) for the formation of C-bond between CH<sub>3</sub>F and NH<sub>3</sub> calculated at MP2/aug-cc-pVDZ level by Scheiner<sup>19</sup>. These binding energies are also higher than X-C...Y carbon bond energy (~-15 kJ/mol) mentioned in first report of C-bond by Arunan<sup>20</sup> and Z-C...O=C C-bonds in previous section. Hammer et al. reported the hydrogen bond formation between N-oxide and H<sub>2</sub>O and the binding energies were found to be -26 kJ/mol and this is similar to C-bond energies of N-oxide and N-sulfide C-bond complexes found in this work. This confirms that N-oxides and N-sulfides form C-bonds similar to H-bond and X-bond. For further confirmation C-bond formation we performed NBO and AIM analysis as described in detailed as follow.

### 6.2.2.2 Confirmation of C-bond formation between N-oxides/N-Sulfides and C atom of methyl group with topological analyses

**Atoms in Molecule Analysis:** Quantum theory of atoms in molecules (QTAIM) calculations were used to characterize the topological properties of the electron density and bond critical

## Carbon Bonding

points (BCPs) were located between C and O/S in each of the complexes. All the AIM calculations were carried out using wave function of C-bond complexes generated at MP2/aug-cc-pVDZ level of method. Figure 6.2.3 displays the bond critical points between O/S of N-oxide/N-sulfides and C atom of ACN or NM in C-bond complexes. In all these complexes, a bond critical point is found between the O or S of N-oxide or N-sulfide and the C atom of ACN and NM molecules which confirms the presence of  $X\cdots C$  ( $X = O$  or  $S$ ) C-bonds in these complexes. Electron density values  $\rho(r)$  and Laplacian of electron density values  $\nabla^2\rho(r)$  at the intermolecular BCPs between interacting atoms are listed in Table 6.2.2. The electron density  $\rho(r)$  for all these molecules are in the range of 0.0045 to 0.007 a.u and for all the complexes, the  $\nabla^2\rho(r)$  values are positive, which is characteristic of closed shell interactions.

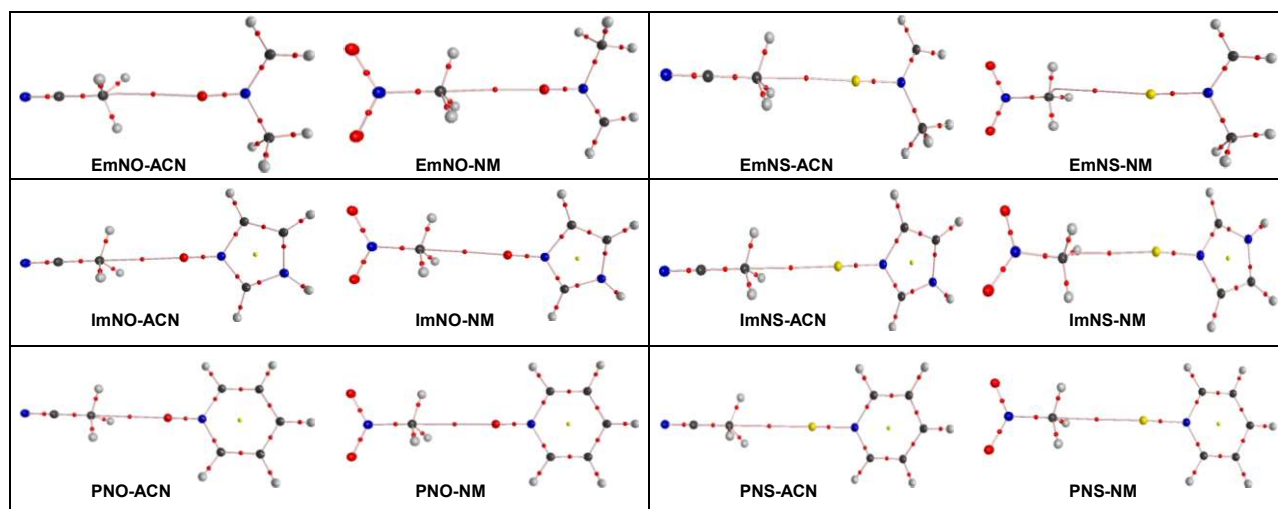


**Figure 6.2.3** Left side: Electron density topologies for all the N-oxide complexes, Right side: for all N-Sulfide complexes with ACN and NM.

## Carbon Bonding

**Table 6.2.2** Electron density  $\rho(r)$ , Laplacian of electron density  $\nabla^2\rho(r)$ , Carbon bond energy ( $E_{BCP}$ ) at bond critical point and donor-acceptor interaction energy ( $E_{DA}$ ) of various complexes.

Complex	$E_{DA}$ (kJ/mol)	$E_{(BCP)}$ (kJ/mol)	$\rho(r)$ (a.u)	$\nabla^2r(r)$ (a.u)
<b>N-Oxide</b>				
EmNO-ACN	2.469	-4.762	0.0055	0.0279
ImNO-ACN	2.971	-6.384	0.0069	0.0364
PNO-ACN	2.887	-6.371	0.0070	0.0362
EmNO-NM	3.138	-5.788	0.0062	0.0313
ImNO-NM	4.142	-6.848	0.0070	0.0367
PNO-NM	3.389	-6.061	0.0064	0.0327
<b>N-Sulfide</b>				
EmNS-ACN	1.464	-3.843	0.0053	0.0225
ImNS-ACN	1.339	-3.660	0.0050	0.0214
PNS-ACN	1.130	-3.378	0.0047	0.0196
EmNS-NM	1.423	-3.405	0.0046	0.0187
ImNS-NM	1.966	-4.137	0.0055	0.0228
PNS-NM	1.715	-3.709	0.0049	0.0203

According to Koch and Popelier criteria<sup>60</sup> for C-H...O H-bonds on the basis of AIM theory, the electron density  $\rho(r)$  and the Laplacian of electron density  $\nabla^2\rho(r)$  should be within the range of 0.002-0.034 a.u. and 0.024–0.139 a.u., respectively. All these values for N-oxides and N-sulfide C-bond complexes lie within these ranges. It indicates that the C-bond formation and strength is similar to weak H-bonds. Figure 6.2.4 shows the correlation plots between electron density  $\rho(r)$  and Laplacian of electron density  $\nabla^2\rho(r)$  at BCPs and X...C (X = O, S) C-bond distances (d). Linear correlations were obtained for individual complexes of N-oxide or N-sulfide with ACN and NM.

## Carbon Bonding

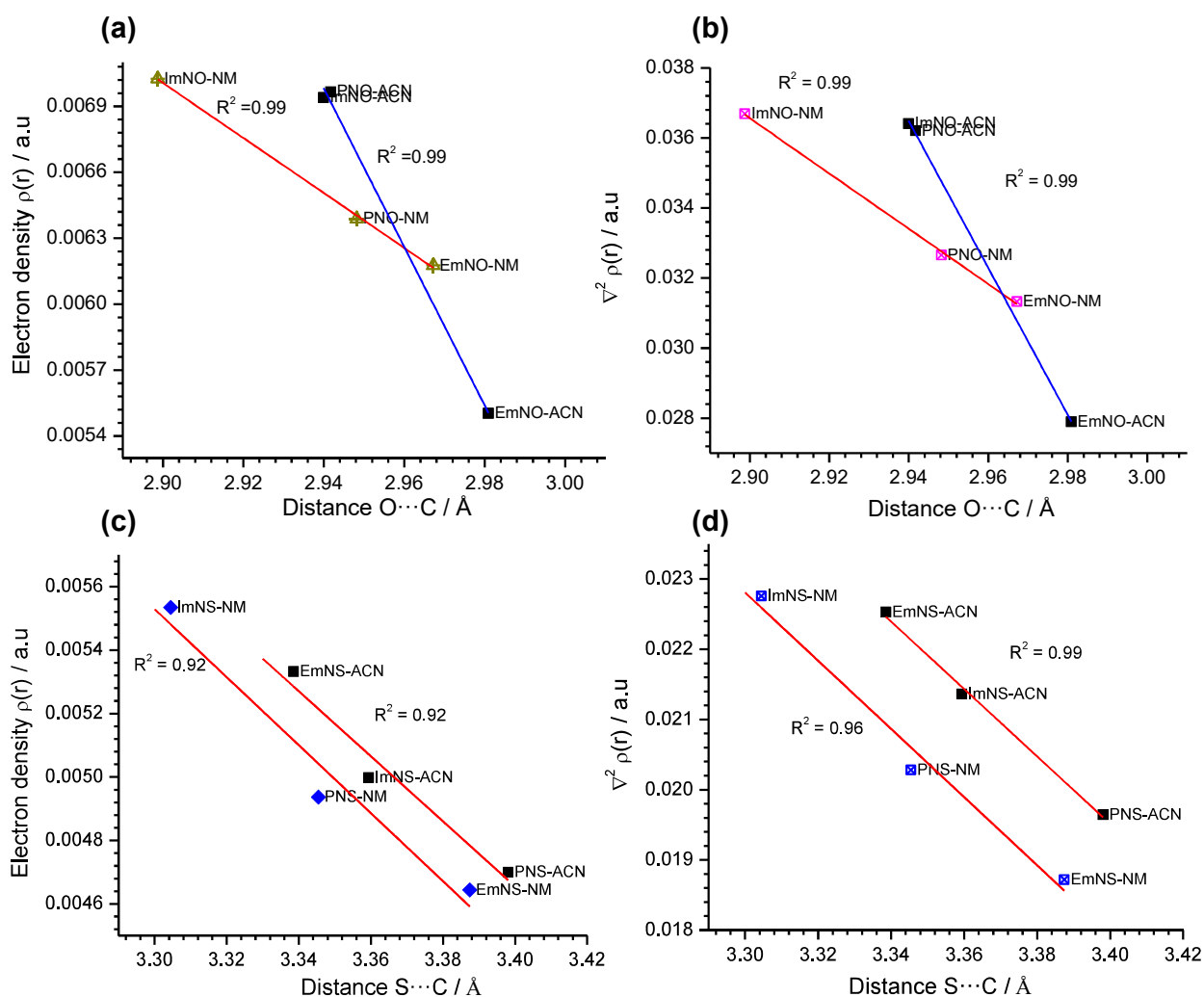


**Figure 6.2.4** Linear correlation plots between  $X \cdots C$  C-bond distances and (a) electron density  $\rho(r)$ , (b) Laplacian electron density  $\nabla^2 \rho(r)$  for N-oxide complexes. (c) and (d) electron density  $\rho(r)$  and Laplacian of electron density  $\nabla^2 \rho(r)$  for N-sulfide complexes, respectively.

**Natural Bond Orbital (NBO) analysis:** To determine the donor-acceptor interaction energies in order to find out the type of electron delocalization, natural bond orbital analysis (NBO) has been performed on all the complexes at MP2/aug-cc-pVDZ level. The donor-acceptor interaction energies ( $E_{DA}$ ) for all these complexes are provided in Table 6.2.2. Figure 6.2.5 represents the orbital overlap ( $n$ ) between the lone pair orbital of O or S with the antibonding sigma orbital ( $\sigma^*$ ) of C-X bond ( $X = N$  or C) in all the C-bond complexes.

## Carbon Bonding

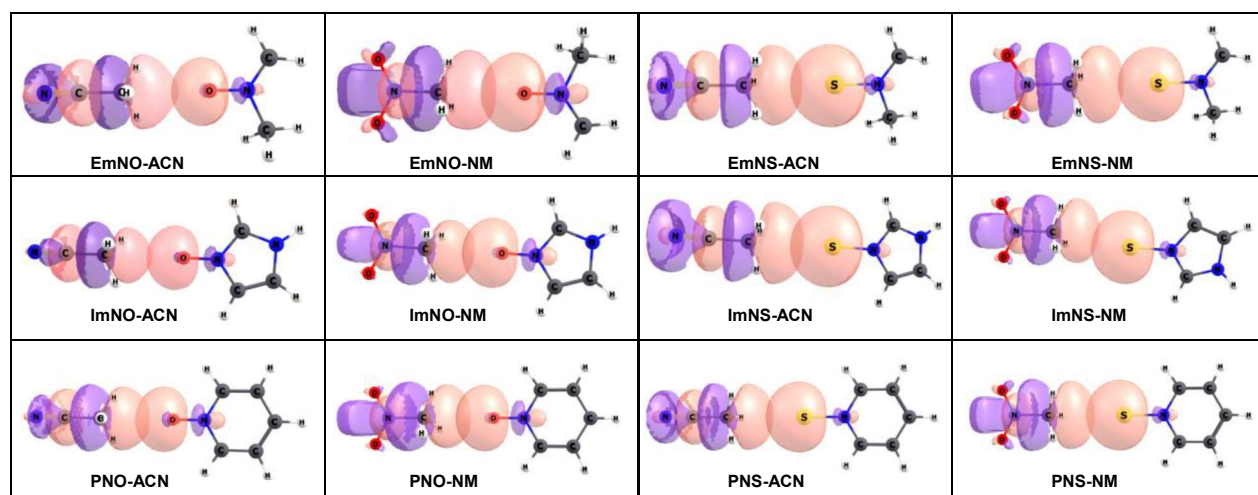


**Figure 6.2.5** Natural bond orbital overlap diagrams between O or S lone pair orbital ( $n$ ) in *N*-oxides or *N*-sulfides and antibonding sigma orbital ( $\sigma^*$ ) of C-C in ACN or C-N in NM complexes.

The donor-acceptor interaction energies ( $E_{DA}$ ) are of the same order as followed by stabilization energies in all the complexes and the  $E_{DA}$  values range from 1 to 4.2 kJ/mol. For all the complexes, the interaction is between lone pair ( $n$ ) of O/S and  $\sigma^*(C-C/C-N)$  antibonding orbitals as  $n \rightarrow \sigma^*$  electron delocalization. Figure 6.2.6 shows the linear dependence of the donor-acceptor interaction energy ( $E_{DA}$ ) on the C-bond distances in both types of complexes. We have also calculated C-bond bond energies at bond critical point for all C-bond complexes using multiwfn software. These energies follow same order of donor-acceptor interaction energies, as shown Table 6.2.2.

## Carbon Bonding

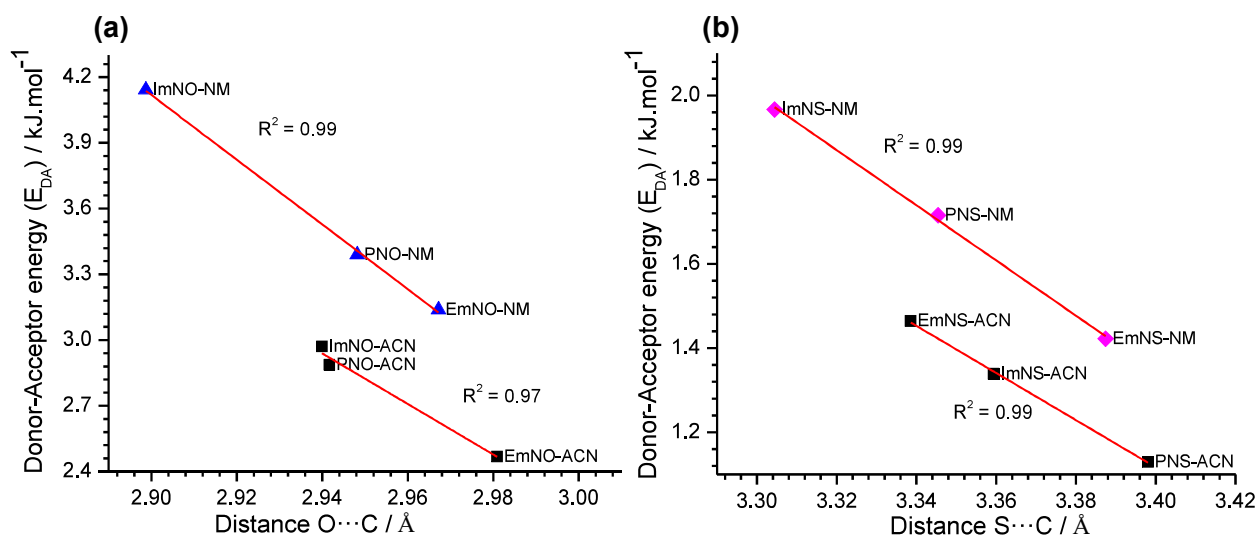


**Figure 6.2.6** Linear correlation plots between donor-acceptor interaction energies and carbon distances (O/S...C) in (a) N-oxide complexes with ACN and NM (b) N-sulfide complexes with ACN and NM.

**Molecular electrostatic potential analysis:** Molecular electrostatic potentials calculations were done with MP2/aug-cc-pVDZ level of theory using Gaussian 09 software. Figure 6.2.7 represents the electrostatic maxima and minima along the C-bond at 0.006 a.u. isosurface of electron density. The electrostatic interaction energies are the energy difference between complex formation and monomer and the potential energy difference values are listed in Table 6.2.3. A positive value for the electrostatic energy indicates a positive surface potential on C atom while a negative value indicates a negative surface potential on O or S of N-oxide and N-sulfides. This inferred that C-bond behaves as  $\sigma$ -hole interaction between the electron rich atoms such as N-oxide and N-sulfides and electron deficient atom of Z-C sigma bond in ACN and NM. We have correlated the positive values on C atom and negative values on O/S with their corresponding binding energies at CCSD-T/CBS level of method. We have observed that a linear correlation for all ACN complexes and NM complexes individually for positive value present in C atom, as shown in Figure 6.2.8.

## Carbon Bonding

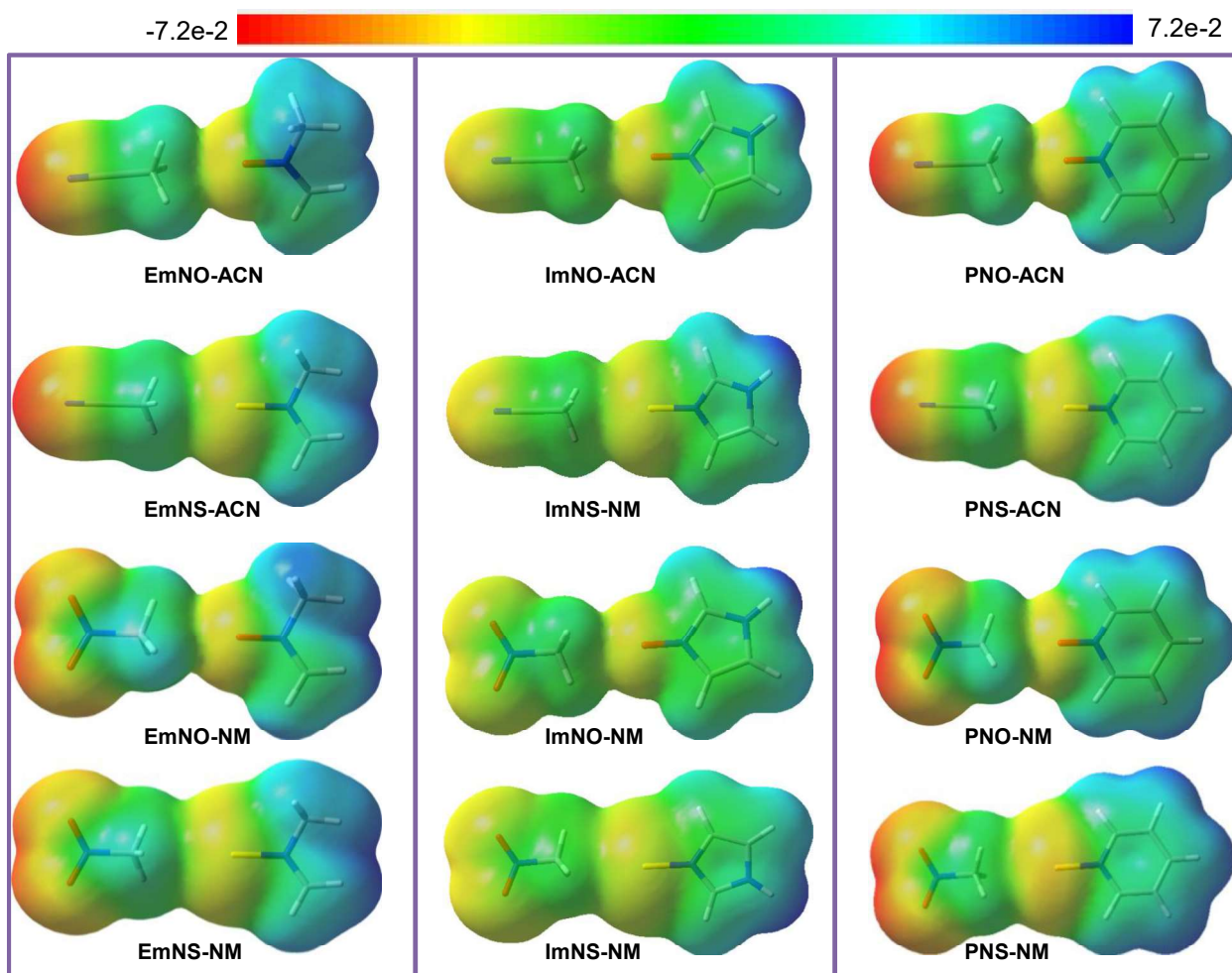


**Figure 6.2.7** MESP plots represents  $N-C\cdots O/S-N$  and  $C-C\cdots O/S$  interaction on isodensity surface of 0.02 au for N-oxide complexes and 0.006 au for N-sulfide complexes. Range: from -0.07 to 0.07, red to blue.

A linear correlation is observed for combination of O and S of different type of N-oxides and N-sulfides, as shown in Figure 6.2.9. All the linear correlation diagrams infer the generation of  $\sigma$ -hole is contributing to the total binding energy in all C-bond complexes and these vary from system to system.

## Carbon Bonding

**Table 6.2.3** Potential energy differences on C atom ( $\Delta V_C$ ), on O atom ( $\Delta V_O$ ), on S atom ( $\Delta V_S$ ) in all the C-bond complexes in kJ/mol.

Complex	$\Delta V_O$ (kJ/mol)	$\Delta V_C$ (kJ/mol)	Complex	$\Delta V_S$ (kJ/mol)	$\Delta V_C$ (kJ/mol)
EmNO-ACN	-38.4	73.9	EmNS-ACN	-35.5	57.9
ImNO-ACN	-41.5	105.5	ImNS-ACN	-39.8	82.3
PNO-ACN	-33.6	82.2	PNS-ACN	-32.2	64.0
EmNO-NM	-41.2	71.7	EmNS-NM	-36.1	54.2
ImNO-NM	-44.1	100.4	ImNS-NM	-41.5	80.5
PNO-NM	-34.9	75.7	PNS-NM	-33.1	62.7

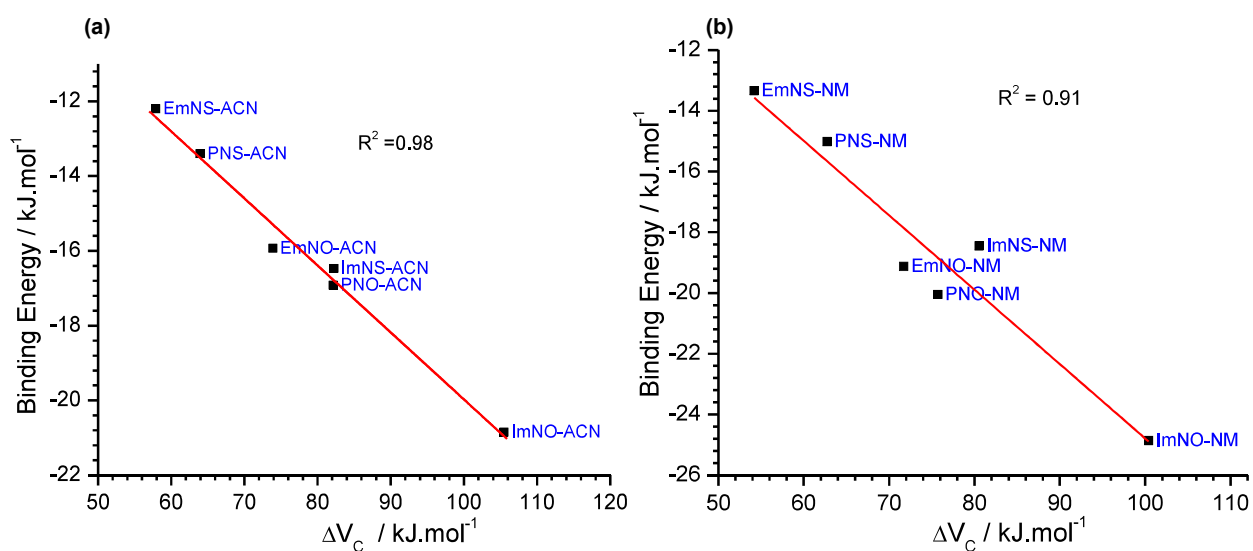


**Figure 6.2.8** (a) Linear correlation plot between potential energy difference on C atom in ACN C-bond complexes, (b) in NM C-bond complexes with both N-oxides and N-sulfides.

## Carbon Bonding

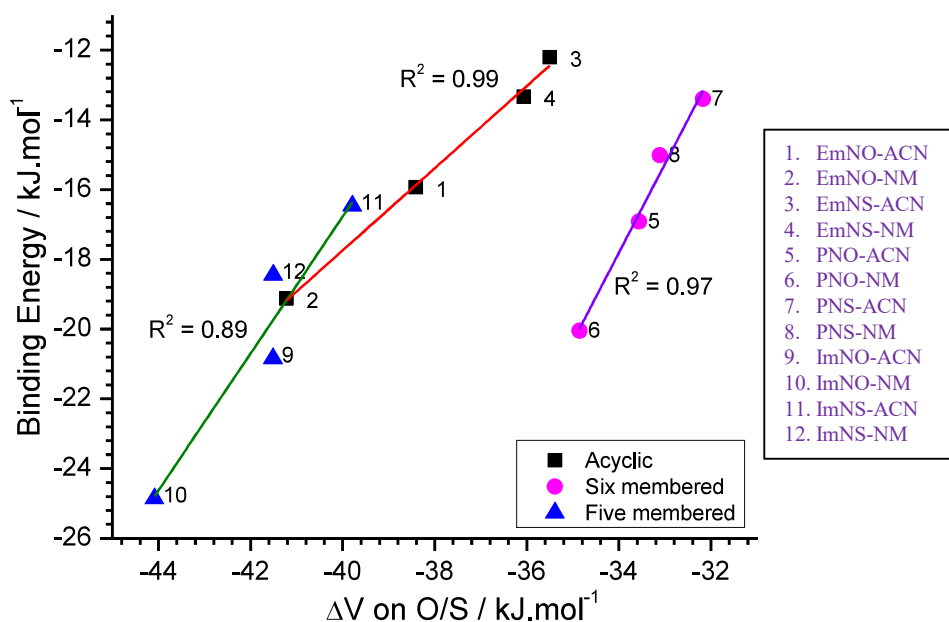


**Figure 6.2.9** Linear correlation plot between potential energy difference on O/S atom in acyclic (aliphatic), five membered and six membered C-bond complexes.

### Localized molecular orbital energy decomposition analysis:

To understand the nature of C-bond formation with n-oxides, we performed localized molecular orbital energy decomposition analysis at MP2/aug-cc-pVDZ level of theory. In this, we have calculated different energy components (electrostatic (ES), polarization (PL), repulsion (REP), and exchange (EX)) at B97D/aug-cc-pVDZ level of theory in C-bond complexes. The distribution of different energies for acetonitrile complexes and nitromethane were shown in Figure 6.2.10 and Figure 6.2.11, respectively. It is observed that in all the cases polarization and dispersion energies play an important role in the stability of the C-bond complexes. LMOEDA analysis shows that the Z-C $\cdots$ O/S-N C-bonds in are electrostatic in nature.

## Carbon Bonding

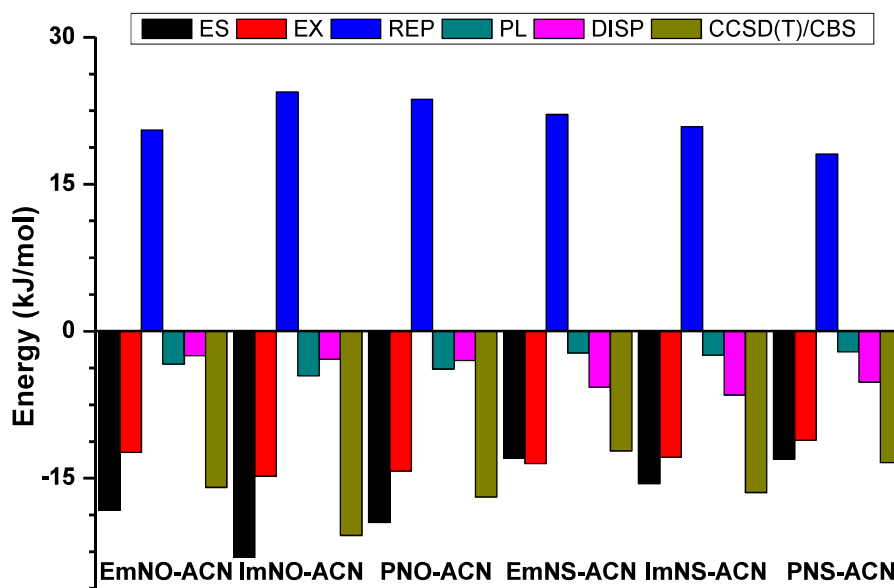


**Figure 6.2.10** Represents the contribution of different interactions electrostatic (ES), polarization (PL), repulsion (REP), and exchange (EX)) to the stabilization energy (CCSD-T/CBS) for ACN complexes with N-oxides and N-sulfides.

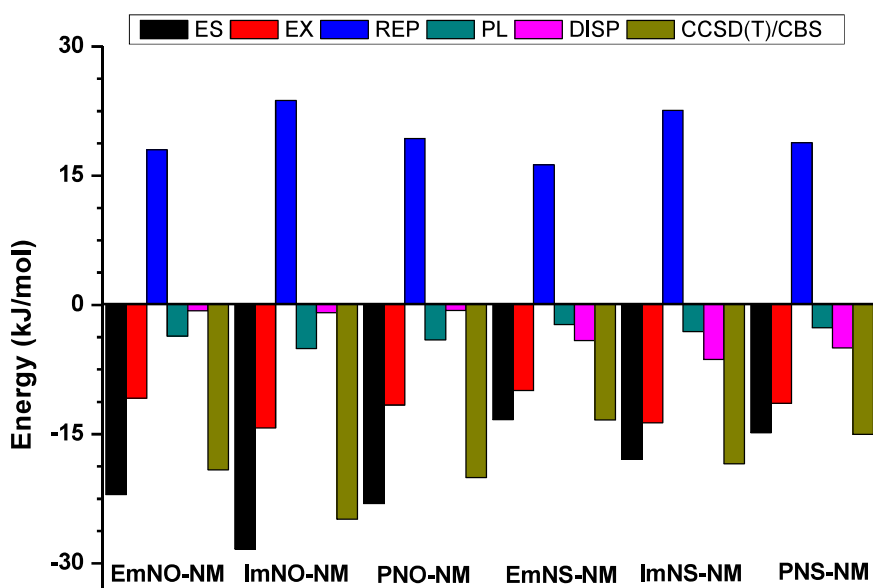


**Figure 6.2.11** Represents the contribution of different interactions electrostatic (ES), polarization (PL), repulsion (REP), and exchange (EX)) to the stabilization energy (CCSD-T/CBS) for NM complexes with N-oxides and N-sulfides.

### 6.2.3 Conclusions

- ❖ We studied the C-bond formation with different types of N-oxides and N-sulfides and it was confirmed that N-oxides and N-sulfides have ability to form C-bond with electron deficient C atom of methyl group.
- ❖ The stabilization energies for N-oxide complexes are greater than N-sulfide complexes. All these energies are found in the range of -13 kJ/mol to -25 kJ/mol at CCSD-T/CBS level. The obtained energies are more than the energy obtained in first report of C-bond. These are also comparable to N-O...X and N-O...H complexes. These inferred that N-oxides and N-sulfide are strong C-bond acceptors like hydrogen bond and halogen bond acceptor.
- ❖ In both C-bond cases Nitromethane complexes are more stable than the acetonitrile complexes.
- ❖ The stability order in N-oxide complexes follow: imidazole N-oxide > pyridine N-oxide > imine N-oxide and this order is also same in N-sulfide complexes.
- ❖ The C-bond complex formation was confirmed with AIM and NBO analyses. The NBO analysis results that C-bond is  $n \rightarrow \sigma^*$  electron delocalization in all the C-bond complexes.
- ❖ Molecular electrostatic potential analysis concluded that the C-bond formation in N-oxide/N-sulfides through the  $\sigma$ -hole and the binding energies are dependent on the strength of  $\sigma$ -hole interaction.
- ❖ The LMOEDA analysis revealed that electrostatic energy contribution is dominant to the Z-C...O/S-N C-bond stabilization energy. It is confirmed that the C-bond is electrostatic in nature.

## Carbon Bonding

---

### References

- (1) Desiraju, G. R., & Steiner T *The Weak Hydrogen Bond: In Structural Chemistry and Biology*; Oxford University Press, 1999.
- (2) Saenger, G. A. J. a. W. *Hydrogen bonding in biological structures*; Springer-Verlag: Berlin, New York, 1994.
- (3) Mukherjee, A.; Tothadi, S.; Desiraju, G. R. *Acc. Chem. Res.* **2014**, *47*, 2514.
- (4) Scholfield, M. R.; Ford, M. C.; Carlsson, A.-C. C.; Butta, H.; Mehl, R. A.; Ho, P. S. *Biochemistry* **2017**, *56*, 2794.
- (5) Danelius, E.; Andersson, H.; Jarvoll, P.; Lood, K.; Gräfenstein, J.; Erdélyi, M. *Biochemistry* **2017**, *56*, 3265.
- (6) Politzer, P.; Murray, J. S.; Clark, T. *Phys. Chem. Chem. Phys.* **2013**, *15*, 11178.
- (7) Scheiner, S. *The J. Chem. Phys.* **2011**, *134*, 094315.
- (8) Scheiner, S. *Acc. Chem. Res.* **2013**, *46*, 280.
- (9) Azofra, L. M.; Scheiner, S. *J. Phys. Chem. A* **2014**, *118*, 3835.
- (10) Fick, R. J.; Kroner, G. M.; Nepal, B.; Magnani, R.; Horowitz, S.; Houtz, R. L.; Scheiner, S.; Trievel, R. C. *ACS Chem. Biol.* **2016**, *11*, 748.
- (11) Nziko, V. d. P. N.; Scheiner, S. *J. Org. Chem.* **2015**, *80*, 2356.
- (12) Zierkiewicz, W.; Michalczyk, M.; Scheiner, S. *Phys. Chem. Chem. Phys.* **2018**, *20*, 4676.
- (13) Antonio, B.; Antonio, F. *Angew. Chem. Int. Ed.* **2015**, *54*, 7340.
- (14) Mani, D.; Arunan, E.; *ChemPhysChem* **2013**, *14*, 754.
- (15) Scheiner, S. *J. Phys. Chem. A* **2015**, *119*, 9189.
- (16) Southern, S. A.; Bryce, D. L. *J. Phys. Chem. A* **2015**, *119*, 11891.
- (17) García-Llinás, X.; Bauzá, A.; Seth, S. K.; Frontera, A. *J. Phys. Chem. A* **2017**, *121*, 5371.
- (18) Scheiner, S. *J. Phys. Chem. A* **2018**, *122*, 2550.

## Carbon Bonding

---

- (19) Scheiner, S. *J. Phys. Chem. A* **2017**, *121*, 5561.
- (20) Mani, D.; Arunan, E. *Phys. Chem. Chem. Phys.* **2013**, *15*, 14377.
- (21) Mani, D.; Arunan, E. *J. Phys. Chem. A* **2014**, *118*, 10081.
- (22) Thomas, S. P.; Pavan, M. S.; Guru Row, T. N. *ChemComm* **2014**, *50*, 49.
- (23) C., E. A. E.; Antonio, B.; Antonio, F.; Pablo, B. *ChemPhysChem* **2015**, *16*, 2530.
- (24) Bauzá, A.; Frontera, A. *Crystals* **2016**, *6*, 26.
- (25) Rahim, A.; Saha, P.; Jha, K. K.; Sukumar, N.; Sarma, B. K. *Nat. Commun.* **2017**, *8*, 78.
- (26) Berman, H. M.; Westbrook, J.; Feng, Z.; Gilliland, G.; Bhat, T. N.; Weissig, H.; Shindyalov, I. N.; Bourne, P. E. *Nucleic Acids Res.* **2000**, *28*, 235.
- (27) Frishman, D.; Argos, P. *Proteins* **1995**, *23*, 566.
- (28) Lowe, A. J.; Pfeffer, F. M.; Thordarson, P. *Supramol. Chem.* **2012**, *24*, 585.
- (29) Kadam, S. A.; Haav, K.; Toom, L.; Haljasorg, T.; Leito, I. *J. Org. Chem.* **2014**, *79*, 2501.
- (30) Thordarson, P. *Chemical Society Reviews* **2011**, *40*, 1305.
- (31) Hristova, Y. R.; Smulders, M. M. J.; Clegg, J. K.; Breiner, B.; Nitschke, J. R. *Chem. Sci.* **2011**, *2*, 638.
- (32) Barends, T. R. M.; Foucar, L.; Ardevol, A.; Nass, K.; Aquila, A.; Botha, S.; Doak, R. B.; Falahati, K.; Hartmann, E.; Hilpert, M.; Heinz, M.; Hoffmann, M. C.; Köfinger, J.; Koglin, J. E.; Kovacsova, G.; Liang, M.; Milathianaki, D.; Lemke, H. T.; Reinstein, J.; Roome, C. M.; Shoeman, R. L.; Williams, G. J.; Burghardt, I.; Hummer, G.; Boutet, S.; Schlichting, I. *Science* **2015**, *350*, 445.
- (33) Huang, Q.; Liu, S.; Tang, Y.; Jin, S.; Wang, Y. *Biochem. J.* **1995**, *309*, 285.
- (34) Fulton, J. R.; Glover, J. E.; Kamara, L.; Rowlands, G. J. *Chem. Commun.* **2011**, *47*, 433.
- (35) LH, P. *Cancer Metastasis Rev* **1993**, *12*, 119.

## Carbon Bonding

---

- (36) Patterson, L. H. *Cancer Metastasis Rev* **1993**, *12*, 119.
- (37) LH, P.; Craven Mr Fau - Fisher, G. R.; Fisher Gr Fau - Teesdale-Spittle, P.; P, T.-S. *Oncol Res* **1994**, *6*, 533.
- (38) Reddy, L. S.; Babu, N. J.; Nangia, A. *Chem. Commun.* **2006**, 1369.
- (39) Balzarini, J.; Stevens, M.; De Clercq, E.; Schols, D.; Pannecouque, C. *J. Antimicrob. Chemother.* **2005**, *55*, 135.
- (40) Cerecetto, H.; Dias, E.; Di Maio, R.; González, M.; Pacce, S.; Saenz, P.; Seoane, G.; Suescun, L.; Mombrú, A.; Fernández, G.; Lema, M.; Villalba, J. *J. Agric. Food. Chem.* **2000**, *48*, 2995.
- (41) Malkov, A. V.; Bell, M.; Castelluzzo, F.; Kočovský, P. *Organic Letters* **2005**, *7*, 3219.
- (42) Balzarini, J.; Keyaerts, E.; Vijgen, L.; Vandermeer, F.; Stevens, M.; De Clercq, E.; Egberink, H.; Van Ranst, M. *J. Antimicrob. Chemother.* **2006**, *57*, 472.
- (43) Stevens, M.; Pannecouque, C.; De Clercq, E.; Balzarini, J. *Biochem. Pharmacol.* **2006**, *71*, 1122.
- (44) Sanderson, H.; Tibazarwa, C.; Greggs, W.; Versteeg, D. J.; Kasai, Y.; Stanton, K.; Sedlak, R. I. *Risk Analysis* **2009**, *29*, 857.
- (45) Aakeroy, C. B.; Wijethunga, T. K.; Desper, J. *CrystEngComm* **2014**, *16*, 28.
- (46) Cuellar, K. A.; Munroe, K. L.; Magers, D. H.; Hammer, N. I. *J. Phys. Chem. B* **2014**, *118*, 449.
- (47) Saraswatula, V. G.; Bhat, M. A.; Gurunathan, P. K.; Saha, B. K. *CrystEngComm* **2014**, *16*, 4715.
- (48) Puttreddy, R.; Beyeh, N. K.; Rissanen, K. *CrystEngComm* **2016**, *18*, 793.
- (49) Saikia, B.; Khatioda, R.; Bora, P.; Sarma, B. *CrystEngComm* **2016**, *18*, 8454.

## Carbon Bonding

---

- (50) Vukotic, V. N.; Loeb, S. J. *Supramol. Chem.* **2016**, *28*, 151.
- (51) Puttreddy, R.; Topić, F.; Valkonen, A.; Rissanen, K. *Crystals* **2017**, *7*, 214.
- (52) Su, Z.; Mahmoudinobar, F.; Dias, C. L. *Phys. Rev. Lett.* **2017**, *119*, 108102.
- (53) Puttreddy, R.; Jurcek, O.; Bhowmik, S.; Makela, T.; Rissanen, K. *ChemComm* **2016**, *52*, 2338.
- (54) Topic, F.; Puttreddy, R.; Rautiainen, J. M.; Tuononen, H. M.; Rissanen, K. *CrystEngComm* **2017**, *19*, 4960.
- (55) Rybarczyk-Pirek, A. J.; Łukomska-Rogala, M.; Wojtulewski, S.; Palusiak, M. *Cryst. Growth Des.* **2015**, *15*, 5802.
- (56) Furche, F.; Ahlrichs, R.; Hättig, C.; Klopper, W.; Sierka, M.; Weigend, F. *Wiley Interdiscip. Rev. Comput. Mol. Sci.* **2014**, *4*, 91.
- (57) AIM 2000 *J. Comput. Chem.* **2001**, *22*, 545.
- (58) Glendening, E. D.; Landis, C. R.; Weinhold, F. *J. Comput. Chem.* **2013**, *34*, 1429.
- (59) Frisch, M. J. et al Gaussian 09, Revision B.01.
- (60) Koch, U.; Popelier, P. L. A. *J. Phys. Chem.* **1995**, *99*, 9747.

## Concluding Remarks and Future Prospective

---

### Chapter 7

#### Concluding Remarks and Future Prospective

##### 7.1 Concluding remarks

This chapter summarizes the work carried out in this thesis into two major findings such as (1) Hydrogen bonds where S, Se and Te act as H-bond acceptors and (2) Carbon bonds in proteins and model compounds. These are investigated with the help of gas phase high resolution laser spectroscopy, solution state NMR spectroscopy and benchmark quantum chemical calculations. Although there are numerous reports on N-H...S hydrogen bonds in gas phase but there is no precise report on accurate strength of amide-N-H...S H-bonds in biomolecules. First, we focused on the determination of absolute strength of amide-N-H...S H-bonds in proteins and peptides in gas phase isolated conditions. In proteins and peptides, it is impossible to study amide-N-H...S H-bond directly due to the environmental and conformational effects. Hence, we have determined the accurate strength of amide-N-H...S H-bond by chosen model compounds of proteins and peptides in gas phase isolated condition. The model compounds, N-phenylacetamide as trans amide in peptides and 2-pyridone as cis amide in nucleobases are chosen as H-bond donors. Dimethyl sulfide as methionine side chain in proteins is chosen as the H-bond acceptor. Dimethyl ether, dimethyl formamide and benzene are chosen as H-bond acceptors which represents in the side chain of serine, backbone/side chain carbonyl group and side chain aromatic groups, respectively. The model compounds chosen give the information and comparative study of different type of interactions i.e. N-H...S, N-H...O=C, N-H...O, and N-H... $\pi$  H-bonds in biomolecules. The gas phase IR experiments were carried out to determine strength of amide N-H...S H-bond in proteins. It is observed that the red shift values of N-H stretch for NPAA-DME and NPAA-DMS complexes are similar ( $\sim 100\text{ cm}^{-1}$ ) whereas for NPAA-DMF and NPAA-Bz are  $75\text{ cm}^{-1}$  and  $15\text{ cm}^{-1}$ , respectively which are found to be less

## Concluding Remarks and Future Prospective

---

than for NPAA-DMS complex. The computational frequency calculations corroborate the experimental red shifts and infer the H-bond strength in complexes. The gas phase IR experiments and computational studies resulted that the N-H $\cdots$ S and N-H $\cdots$ O H-bond strength are similar and these are stronger than N-H $\cdots$ O=C, N-H $\cdots$  $\pi$  H-bonds in trans amide case. In cis amide case, the red shift of N-H stretch was found to follow the order N-H $\cdots$ O=C > N-H $\cdots$ S > N-H $\cdots$ O > N-H $\cdots$  $\pi$ . In all the complexes, the red shifts of N-H stretch are linearly correlated with donor-acceptor orbital interaction energy obtained by NBO analysis. Further, we extended these finds to compare the strength in peptides. We found the donor-acceptor interaction energies in two proteins to be 53.9 and 37.5 kJ/mol for amide-N-H $\cdots$ S-methionine and amide-NH $\cdots$ S-cysteine H-bonds, respectively which are very similar to those observed for model compounds of peptides complexes. The gas phase IR experimentally observed red shift value for amide-N-H $\cdots$ S methionine in FM dipeptide found to be 124 cm<sup>-1</sup> which is comparable to our results for NPAA-DMS and NMFA-DMS complexes. The binding energies for N-H $\cdots$ S H-bond at the CCSD(T)/aug-cc-pVDZ level are in the range of 30-40 kJ/mol. All these results concluded that amide-N-H $\cdots$ S H-bonds are equally strong H-bonds as their oxygen counterpart H-bond complexes in isolated condition.

This gas phase data on strength of amide-N-H $\cdots$ S H-bonds have been exploited extensively by chemists and biochemists. But no one explored the strength of SCHB in solution phase. Hence, we have performed both computational and NMR experimental investigations for existence and strength of sulfur centered hydrogen bond (SCHB) in solution phase. In this case, we have chosen thioamide as the H-bond acceptor due to its importance in biomolecules. The thioamide incorporation in place of amide causes different properties in biomolecules such as functional and structural stability. It is also found that there is an ambiguity on H-bond acceptor

## Concluding Remarks and Future Prospective

---

capability of thioamides whether it behaves as a poor H-bond acceptor or stronger in proteins and some simple molecules.

Therefore first we have investigated the (thio)amide-N-H...S=C-thio(amide) H-bond strengths using NBO analysis in three PDB structures of proteins and nucleic acids. From the NBO analysis, calculated donor-acceptor interaction energies ( $E_{DA}$ ) are varying from 21-77 kJ/mol and observed that the strength of N-H...S=C H-bond is as strong as N-H...O=C H-bond. It is further verified by taking 23 model compound dimers covering all the possible thio(amide)-N-H...S=C-thio(amide) H-bonds which exist in biomolecules. These 23 dimers are optimized at B97-D/aug-cc-pVDZ level of theory in solution phase considering solvation energies (solvent  $CDCl_3$ ). The H-bond enthalpies for all these dimers are estimated at CCSD(T)-SMD/aug-cc-pVDZ level on optimized structures. The N-H...S H-bond enthalpies are in the range of  $\sim$ -25 to -30 kJ/mol which are close to those of the N-H...O H-bonds. The N-H...O=C H-bonds enthalpies are in the range of  $\sim$ -20 to -35 kJ/mol and considered to be strong H-bonds. Hence, the N-H...S=C H-bonds can also be considered as a strong H-bonds in non-polar solvents. Among the 23 dimers, the highest H-bond enthalpies of 2-pyridone dimer (2-PY)<sub>2</sub> and 2-thiopyridone dimer (2-TPY)<sub>2</sub> confirmed stronger H-bond formation in these dimers. So we have used these two systems for experimental H-bond enthalpy determination in  $CDCl_3$  solvent. We have performed the <sup>1</sup>H NMR experiments at different concentrations of 2-PY/2-TPY in solution. We have observed that the N-H peak of 2-PY/2-TPY shifts towards downfield with increasing the concentration. This confirmed that at higher concentrations it is forming H-bond complexes. The <sup>1</sup>H NMR DOSY experiments confirmed that at higher concentration these H-bond dimers are present and there is no other cluster formation. The association constant for H-bond dimer formation was determined from the concentration dependent <sup>1</sup>H NMR experiment. The plots are

## Concluding Remarks and Future Prospective

---

drawn by considering chemical shifts values as a function of concentration and it is fitted to 1:1 binding isotherm. This results in the binding free energies of -16.7 and -14.6 kJ/mol for 2-PY and 2-TPY respectively. These values are in good agreement with those computed at CCSD (T) level (-12.6, -10.2 kJ/mol for 2-PY and 2-TPY, respectively). To obtain the H-bond enthalpies directly from NMR experiments, we performed the temperature dependent experiments and the values obtained did not matching to the computational H-bond enthalpies due to lack of data for fitting. The concentration dependent H-bond enthalpies matched to those obtained for 2-pyridone:uracil and 2-pyridone:thymine Watson-Crick and Wooble isomers. However, the concentration-dependent NMR experiments provided better and more precise information about the association free energies and H-bond enthalpies and inferred that the N-H...O and N-H...S H-bonds are very similar in strength. Finally, to confirm N-H...O and N-H...S H-bond are equal in strength; we performed deuterium exchange studies and determined the H/D exchange rates to compare both H-bonds. The H/D exchange rates are in the range of  $3-4 \times 10^{-2} \text{ min}^{-1}$  for 2-PY and 2-TPY dimers. These are of equal order of magnitude and corroborating the CCSD (T) energetics and concentration dependent NMR studies. All the computational and experimental studies suggested that sulfur centered hydrogen bonds are equally strong as conventional H-bonds though S has less electronegativity. Hence, it is confirmed that electronegativity of S is not only the governing factor for the formation strong H-bonds as conventional H-bonds. This encouraged us to investigate the existence and strength of N-H...Se/Te H-bonds in proteins and model compounds.

We carried out the PDB analysis for the existence of N-H...Se in proteins by retrieving the coordinates of protein structures from RCSB website. We found that total of 4334 N-H...Se H-bonds in selenomethionine containing proteins exist. Out of 4334 H-bond interactions, 2342

## Concluding Remarks and Future Prospective

---

are main-chain N-H...Se H-bonds and 1992 form side-chain N-H...Se H-bonds. The maximum N-H...Se interactions are found within the distance of the sum of van der Waals radii of Se and H atom. These interactions are further confirmed by NBO and AIM analysis carried out on two protein examples (PDBs:1w2f, 4krq). These analyses were done for partial optimization (only H positions optimized and other nuclei kept constant) of interacting residues in two proteins. The NBO analysis confirms the N-H...Se H-bond formation by donor-acceptor orbital overlap and found their interaction energies 175, 76 kJ/mol in 1w2f and 4krq, respectively. This suggested that Se of Mse has potential to form H-bonds with their backbone amide-NH as strong as classical amide N-H...O H-bonds. For experimental evidence and accurate strength of N-H...Se H-bonds, we performed high resolution IR-UV double resonance spectroscopic experiments in gas phase. We have chosen N-Phenylacetamide (NPAA) and 2-Pyridone (2PY) as cis and trans amide-NH H-bond donors which are represent as amide groups in peptides and nucleobases, respectively. Dimethylselenide (DMSe) and dimethylsulfide (DMS) are chosen as H-bond acceptors which are represents side chains of selenomethionine and methionine amino acids in proteins, respectively. Using the above mentioned H-bond donors and acceptors combinations, we have compared the N-H...Se and N-H...S H-bonds in proteins with other conventional H-bonds. The IR spectra of all the monomers and H-bond complexes were obtained by using resonant ion infrared (RIDIR) spectroscopy in gas phase that matched with computed frequency at B97-D/aug-cc-PVDZ level of theory. Both experimental and computational IR spectra suggested that the IR spectra of N-H stretching frequencies are red shifted ( $\Delta\nu$ ) in N-H...Se and N-H...S H-bond complexes and are 91 and 96  $\text{cm}^{-1}$  in NPAA (trans amide) complexes. These red shifts indicated that the H-bond strengths in N-H...Se and N-H...S H-bond complexes are similar. In 2-PY complexes we also observed red shifts 262 and 291  $\text{cm}^{-1}$  for N-H...Se and N-H...S H-

## Concluding Remarks and Future Prospective

---

bond complexes. In this cis amide H-bond complexes, the N-H...Se H-bond is little weaker than N-H...S H-bond complexes. However, the red shifts in trans and cis amide complexes concluded that Se is a potential H-bond acceptor in proteins and nucleobases which is also in excellent match with PDB analysis. The strength of N-H...Se H-bond in trans amide complexes is similar to N-H...S H-bond while it is stronger than N-H...Se H-bond in cis amide complexes. The N-H...Se H-bond strength in cis amide is stronger than N-H...O H-bond and is similar in trans amide. The binding energies of N-H...Se H-bond are comparable to those observed for N-H...S and N-H...O H-bond complexes. We extended our investigation to see whether tellurium (Te) can also form H-bonds.

We could not perform the experiments for dimethyl telluride (DMTe) due to unavailability of DMTe. We estimated their experimental frequencies from computational frequencies by using equation obtained from linear correlation plot between computed and experimental vibrational frequencies. The obtained frequencies are red shifted for DMTe complexes and the values are very similar to those of N-H...Se/S/O complexes. These concluded that tellurium can be as strong as H-bond acceptor as oxygen. All H-bond complex formations were confirmed with NBO and AIM and NCI analyses. We have performed computations to investigate why Se, Te forms a strong H-bond though they have less electronegativities. Hence, we calculated charges from CHELPG method and spherically averaged static polarizability ( $\alpha_{\text{avg.}}$ ) of O, S, Se, and Te in DME, DMS, DMSe, and DMTe, respectively using molecular polarizability partitioning method. The geometric mean of atomic charges and square root of polarizabilities of H-bond acceptors ( $\sqrt{|q\sqrt{\alpha}|}$ ) were considered as a possible H-bond descriptor and plotted with donor-acceptor interaction energies ( $E_{\text{DA}}$ ) and experimental red shift values in

## Concluding Remarks and Future Prospective

---

N-H stretching frequencies. A linear correlations were observed between ( $\sqrt{|q\sqrt{\alpha}|}$ ) and  $E_{DA}$  or red shifts. This results that the polarizability and charge also contribute to form strong N-H...S/Se/Te H-bonds.

In this thesis we have observed that S and Se form H-bonds as strong as conventional H-bonds. Recently, it is observed that N-H...O H-bonded systems used in designing piezoelectrical materials and show high piezo-response. Hence, these results motivated us to explore SCHB and SeCHBs systems in designing piezoelectric materials and their piezo response. We chose phenol, thiophenol and selenophenol as H-bond donors and nitrobenzene as H-bond acceptor. First, we optimized their structures at different DFT functionals (B3LYP, PBE0) with 6-31G\* and aug-cc-pVDZ basis sets and confirmed the H-bond formation between the donors and acceptor by NBO and AIM analysis. Then, we used different methods (estimated method and calculated method) to calculate the piezoelectric coefficients of H-bonded systems at same level of theories. This suggests that the estimated method is computationally cheaper and faster than the calculated method. It is also observed that the level of theory affects the piezoelectric coefficients but the trend remains same. The piezoelectric coefficient for SCHB (SPH-NBz) is 25.57 pm/V which is higher than PH-NBz (18.89 pm/V) H-bonded systems. It is also higher than the organic crystal with the largest known piezoelectric response (14 pm/V) and computationally estimated for Aniline:NBz (15 pm/V) at same level of theory. The piezoelectric response order follow Se-H...O >S-H...O >O-H...O for H-bonded complexes in all the methods and level of theory. We calculated dipole moments and isotropic polarizabilities for H-bond systems to know why SCHB and SeCHBs show higher piezo response. There is a linear correlation observed between dipole moment/polarizability/dipole moment derivative/polarizability derivative with respect to

## Concluding Remarks and Future Prospective

---

geometric displacement and piezoelectric coefficients. Therefore, it can be concluded that sulfur and selenium centered H-bonded systems have higher polarizability and they can be considered as promising organic piezoelectric materials with high piezoelectric coefficients. Further, we studied the substitution effect on piezoelectric coefficients by adding electron donating and electron withdrawing groups to the aromatic systems. We did not observe any significant effect of substitution on piezoelectric coefficients for H-bond systems. The work has been extended to calculate piezoelectric coefficient of SPH-NBz tetramer which is similar to a crystal unit containing H-bonds and  $\pi$ -stacking. Here we considered two types of tetramers of SPH-NBz viz symmetric and anti-symmetric and the piezoelectric coefficients are found to be 20.9 pm/V and 22.2 pm/V, respectively that are higher than the known organic crystal piezo response (2-methyl-4-nitroaniline).

The second part of this thesis describes the C-bond formation in proteins and model compounds. For existence of C-bonds in proteins, we carried out PDB analysis retrieving the protein structures from RCSB website. We have looked for existence of Z-C...O=C C-bond interaction in proteins by using in-build python program and observed that total of 7600 interactions are found in 11501 proteins obtained at given criteria. The Z-C...O=C C-bond interaction was confirmed with NBO, AIM and NCI analyses in 22 amino acid pairs covering complete C...O distance ( $2.75 \text{ \AA} \leq d \leq 3.6 \text{ \AA}$ ). This analysis confirmed that almost all amino acids participate in Z-C...O=C C-bond as C-bond donor and C-bond acceptor. LYS is involved to form large number of C-bond interactions as C-bond donor while ALA, LEU, ASP and GLU as C-bond acceptors and contribute major part of interactions in proteins. LYS-ALA, LYS-ASP pairings are the prominent as Z-C...O=C C-bond interaction residues in proteins. We also analyzed for atom type and secondary structure involvement in C-bond donor residue and C-

## Concluding Remarks and Future Prospective

---

bond acceptor residue. In most of the cases, the carbonyl groups participate in the C-bond interaction as C-bond acceptor and C-C as C-bond donor followed by N-C and O-C. From secondary structure analysis we found that C-bond acceptors are mostly in  $\alpha$ -helix whereas C-bond donors are evenly distributed in coils, turns,  $\beta$ -strand and  $\alpha$ -helix. All these analyses concluded that the Z-C $\cdots$ O=C C-bond interactions prominently occurred and this encouraged us to investigate experimentally for the evidence and strength of C-bonds present in model compounds of proteins.

Therefore, we chose N,N-Dimethylacetamide (NNDMA) as C-bond acceptor whereas acetonitrile (ACN), nitromethane (NM), alanine (ALA), acetyl chloride (AcetylCl) and 1,1,1-trifluoroacetone (TFACE) as different C-bond donors. First computational studies were carried out to know the existence and strength of C-bond formation between NNDMA with different C-bond donors. The amide-Z-C $\cdots$ O=C C-bond formation were confirmed with NBO, AIM, NCI and MESP analyses in six C-bond model complexes. The binding energies obtained at CCSD (T) level of theory vary from -8.41 kJ/mol to -22.1 kJ/mol. These values match to previous reports on C-bond, but there was no experimental evidence for amide-Z-C $\cdots$ O=C C-bond and its strength. For the first time, we determined the existence and strength of Z-C $\cdots$ O=C C-bond experimentally in NNDMA-ACN C-bond complex. We performed  $^{13}\text{C}$  NMR host-guest titration experiments. We treated NNDMA as host and ACN as guest in one case and vice-versa in other case. These resulted that the  $^{13}\text{C}=\text{O}$  peak of NNDMA is shifted towards downfield with increasing concentration of ACN. In other case, downfield shifts of  $^{13}\text{C}\equiv\text{N}$  of ACN and upfield shifts of  $^{13}\text{CH}_3$  of ACN with increasing the concentration of NNDMA was observed. From these titrations we calculated the association constant using the host-guest concentration vs chemical shift plots and fitted into the expression of  $K_{\text{eq}}$  as function of guest concentration. We found the

## Concluding Remarks and Future Prospective

---

association energy for NNDMA-ACN C-bond complex averaged for above three experiments to be  $\sim$ -18.6 kJ/mol which is in excellent match with binding energy at CCSD (T) level (-18.4 kJ/mol). This suggested that the NMR Host-guest titration experiments are reliable to determine the C-bond energy very precisely. The C-bond formation in NNDMA-ACN was confirmed by red shifts of C=O and CN vibrational stretching frequencies. A linear correlation was observed between red shifts and downfield shifts of  $^{13}\text{C}$  NMR peaks. We used computational and experimental data to estimate the C-bond energies in proteins by knowing the C-bond distance. We derived one empirical equation from binding energies and donor-acceptor interaction energies as function of C-bond distance. This equation was used to determine C-bond energies in proteins. The estimated binding energies are observed in the range of -2 kJ/mol to -22 kJ/mol in proteins. We also established the role of C-bonds in the functions and structures of proteins in two examples

Finally, the computational studies were carried out to explore the N-oxides and N-sulfides as a potential C-bond acceptor like H-bond and X-bond acceptor. In this study we took different type of N-oxides and N-sulfides such as aliphatic N-oxide/sulfide, N-oxide/sulfide pyridines and N-oxide/sulfide-imidazoles as aromatic N-oxides and ACN and NM are C-bond donors. The binding energies for N-oxide complexes are greater than N-sulfide complexes and are found in the range of -13 kJ/mol to -25 kJ/mol at CCSD-T/CBS level. These are comparable to N-O $\cdots$ X and N-O $\cdots$ H complexes where N-oxides acts as H-bond and X-bond acceptor, respectively. The LMOEDA analysis suggested that C $\cdots$ O-N C-bond is electrostatic in nature.

## Concluding Remarks and Future Prospective

---

### 7.2 Future prospective

The experimental data on SCHBs and SeCHBs will be useful for theoretical and physical chemists for designing new force fields for biomolecules. The SCHB in solution and SeCHBs in gas phase studies are expected to be studied in more systems and extended to real applications in biology and chemistry. Experimental studies need to be carried out to investigate H-bonded systems as potential alternative for designing piezoelectric materials. More experimental studies are to be carried out on SeCHBs in solution phase to attest and Se as a potential H-bond acceptor in solution in spite of the interference of the solvents. Experimental investigations X–H···Te H-bonds in gas-phase and solution is expected in near future. Experiments are to be carried out for C-bond interactions in gas phase and isolated condition for better understanding of C-bonds in chemistry and biology.

## **Concluding Remarks and Future Prospective**

---